The Dissertation Committee for Jeffrey Wayne Munos Certifies that this is the approved version of the following dissertation:

Mechanistic Studies of HPP Epoxidase and DXP Reductoisomerase:
Applications to Biosynthesis and Antibiotic Development

Committee:

Hung-wen Liu, Supervisor

Walter Fast

Christian P. Whitman

Eric V. Ansyln

Kenneth A. Johnson

Mechanistic Studies of HPP Epoxidase and DXP Reductoisomerase: Applications to Biosynthesis and Antibiotic Development

by

Jeffrey Wayne Munos, B.A.

Dissertation

Presented to the Faculty of the Graduate School of

The University of Texas at Austin

in Partial Fulfillment

of the Requirements

for the Degree of

Doctor of Philosophy

The University of Texas at Austin

May 2008

Dedication

This dissertation is dedicated to my parents Ronald and Martha Munos. They have given

me nothing but encouragement, love and support.

Acknowledgements

I would like to first thank my parents for their continuous encouragement that they have given me. They have allowed me to pave my own path in life and have supported me on all major decisions. I would secondly like to thank my advisor, Prof. Hung-wen (Ben) Liu. Ben has created a stimulating environment to learn and perform science in. He gives his students a great amount of freedom in their research, and allows them to develop their own research style and scientific interest. This is a luxury I know not every lab has. He has produced a serious working environment with rigorous group meetings. The long Monday night meetings can be painful at times, but they have been a valuable factor in my learning experience, and I will miss them.

I would like to also thank the members of the Liu lab, because I have been surrounded by great scientists who are dedicated to their own research. They work hard, long hours in the lab not to please Ben but because they are truly interested in and enjoy their projects. This type of attitude is contagious, and it has kept me motivated even when my research was not going well. In particular I would like to thank Dr. Feng Yan for training my on HppE and for answering all my questions regarding iron, EPR, and general enzymology. I would also like to thank Dr. Kenji Itoh for answering all my questions on Marcus theory and other theoretical areas of chemistry, and for many other stimulating and entertaining conversations. Dr. Steven Mansoorabadi has been a great colleague in the year and half that he has been in the lab. I have learned more from him then any other graduate student or postdoctoral fellow. I am excited to see what he will accomplish in the lab and after he leaves, and I will also miss our routine coffee breaks. I would like to thank the rest of the enzyme mechanisms subgroup that I have had been able to work with for all their ideas and suggestions, which includes Ms. Ping-Hui Szu,

Mechanistic Studies of HPP Epoxidase and DXP Reductoisomerase: Applications to Biosynthesis and Antibiotic Development

Publication No._____

Jeffrey Wayne Munos, Ph.D.

The University of Texas at Austin, 2008

Supervisor: Hung-wen Liu

The focus of this dissertation is the study of two enzymes, DXR and HppE. DXR catalyzes the first committed step in the MEP pathway, which is the pathway most eubacteria, archeabacteria, algae, and the plastids of plants use for the biosynthesis of isoprenoid. Since mammals utilize the mevalonate pathway and isoprenoids are essential for survival, all enzymes in the MEP pathway are excellent antibiotic targets. One antibiotic that has promise in the fight against malaria is the natural product fosmidomycin, whose antibiotic activity is due to its ability to bind and inhibit DXR. With a deeper understanding of DXR's catalyzed reaction, it will be possible to design a more sophisticated and potent antibiotic. To probe the mechanism of DXR, two fluorinated substrate analogues, 3F-DXP and 4F-DXP, and a fluorinated product analogue, FCH_2-MEP were designed and analyzed as possible substrates or inhibitors. To further analyze the mechanism of DXR, a 2° $[^2H]$-KIE study was conducted using the equilibrium perturbation method.

The second enzyme this dissertation examines is HppE, which catalyzes the final step in the biosynthesis of the antibiotic, fosfomycin. Fosfomycin is a clinically useful antibiotic for the treatment of limb-threatening diabetic foot infections and urinary tract infections. Chemically speaking, HppE is unique for two reasons. First, HppE's epoxidation differs from Nature's standard method of epoxide formation by alkene oxidation, where the epoxide oxygen is derived from molecular oxygen. For HppE, the epoxide is formed through the dehydrogenation of a secondary alcohol; thus the epoxide oxygen is derived from the substrate. Second, HppE is a unique member of the mononuclear non-heme iron-dependent family of enzymes. HppE differs from all other mononuclear non-heme iron-dependent enzymes by requiring NADH and an external electron mediator for turnover but not requiring α-KG, pterin, ascorbate, or an internal iron-sulfur cluster. After a study was published on the activity of zinc-reconstituted HppE from *Streptomyces wedmorensis*, the proposed iron and NADH dependent mechanism of HppE was reevaluated and was reconfirmed. The HppE from *Pseudomonas syringae* (*Ps*-HppE) was also purified and was characterized biochemically and spectroscopically. The results of [^{2}H] and [^{18}O]-KIE studies on *Ps*-HppE are also reported.

Table of Contents

List of Tables

List of Figures

Chapter 1: Background and Significance

1.1.   THE IMPORTANCE OF ISOPRENOIDS

Terpenoids are a large family of natural products comprised of over 35,000 distinct compounds.[1] They are widely distributed in nature and are rich in vital biological activities, including light harvesting pigments,[2] growth hormones,[3] and signal transduction.[4] The terpenoid building block is a 5-carbon unit known as isoprene (**1**), which derives from either isopentenyl diphosphate (IPP, **2**) or dimethylallyl diphosphate (DMAPP, **3**), see **Figure 1-1**. Despite the wide variety of terpenoid structures, they all consist of a multiple of five carbons. This allows terpenoids to be classified based on their five carbon multiplicity.   For example, monoterpenes have 10 carbons; sequiterpenes have 15 carbons; diterpenes have 20 carbons; and sesterterpenes have 25 carbons. A few examples of the various types of terpenoid structures are presented in **Figure 1-2**.

Isoprene **(1)**   Isopentenyl diphosphate **(2)**

Dimethylallyl diphosphate **(3)**
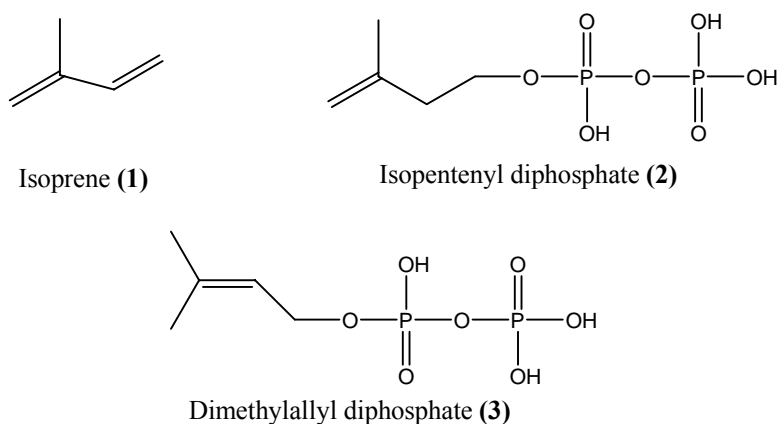
Figure 1-1:   Isoprenoid building blocks.

Camphor **(4)**   Patchouli alcohol **(5)**   Lanosterol **(6)**

β–Carotene **(7)**
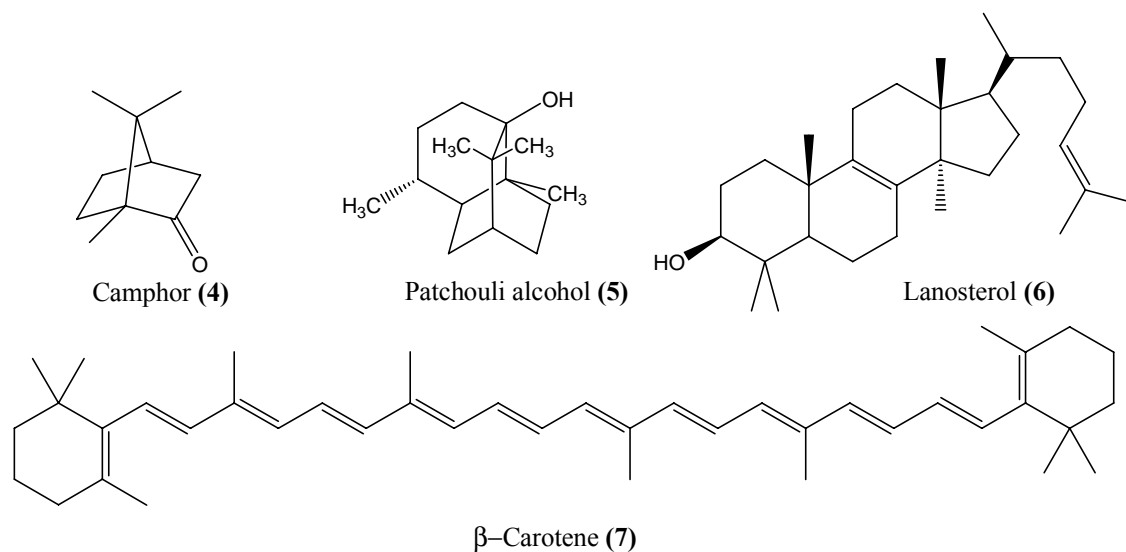
Figure 1-2:   Examples of terpenoids.

1.1.1. Mevalonate Pathway.

While conducting labeling studies in the 1960's to investigate the biosynthesis of cholesterol, Bloch and Lynen discovered the mevalonate pathway for isoprenoid biosynthesis.[5,6] They determined that every carbon of cholesterol is derived from acetate, and after detailed analysis, the biosynthetic pathway shown in **Figure 1-3** was established. The pathway begins with the Claisen condensation of two molecules of acetyl-CoA **(7)** to form acetoacetyl-CoA **(8)**. A third acetyl-CoA reacts with the acetoacetyl-CoA through an aldol condensation reaction, followed by removal of one of the CoA's by hydrolysis to yield (3S)-3-hydroxy-3-methylglutaryl-CoA (HMG-CoA) **(9)**. HMG-CoA is then reduced with NADPH by HMG-CoA reductase to produce mevalonate **(10)**, which in humans is the rate-limiting step in the mevalonate pathway.[7] Inhibitors to HMG-CoA reductase, such as pravastatin, are widely prescribed drugs for lowering cholesterol levels.[8] Mevalonate is then phosphorylated twice at the primary hydroxyl group to add the pyrophosphate functional group, and the secondary hydroxyl

group is activated by phosphorylation. Subsequent dehydration and decarboxylation in a concerted process yields IPP (**2**). The final enzyme in the pathway is IPP isomerase, which catalyzes the isomerization of IPP (**2**) to DMAPP (**3**).
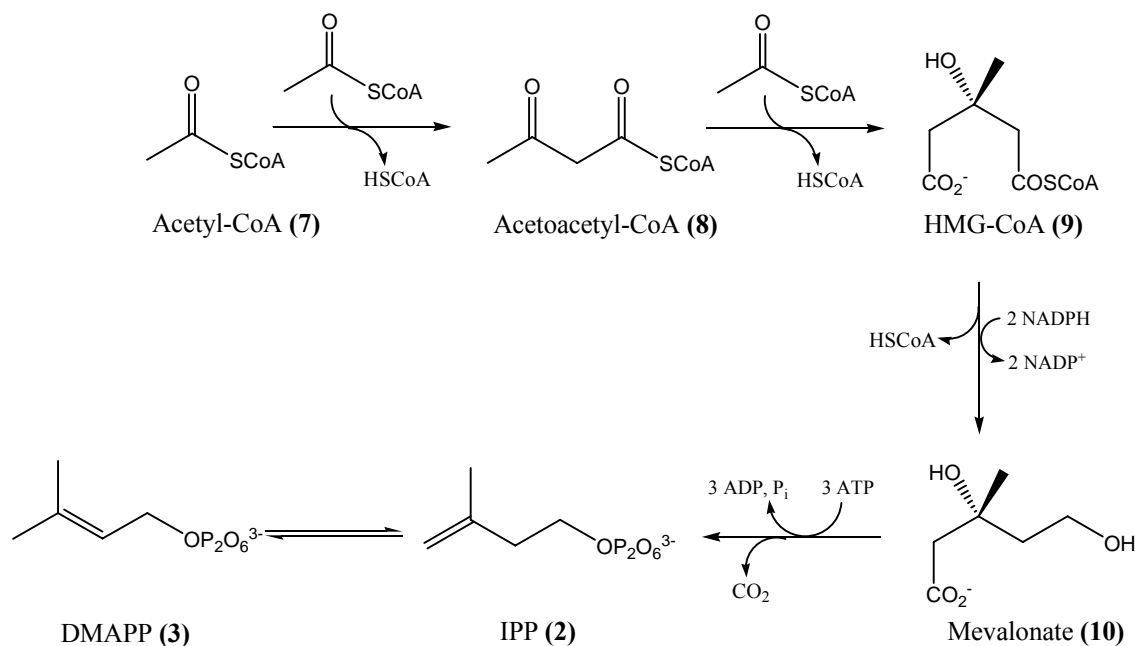
Figure 1-3: **Mevalonate-dependent pathway for isoprenoid biosynthesis.**

1.1.2. Discovery of the MEP Pathway.

For many years, it was believed that all organisms utilize the mevalonate pathway for the biosynthesis of the isoprenoid building blocks, IPP and DMAPP. However, in 1993 a pathway independent of mevalonate was discovered in the labs of Rhomer and Arigoni.[9-11] Rhomer's discovery arose by observing that the labeling pattern in hopanoids using various $[^{13}C_1]$glucose isotopomers and $[^{13}C]$acetate isotopomers as precursors was inconsistent with what the mevalonate dependent pathway predicted.[9] Similar observation was also made by Arigoni and researchers in their labeling studies on ginkgolide formation in seedlings of the *Ginkgo biloba* and on ubiquinone biosynthesis in

3

E. coli.[10,11] After further investigations by them and a few others, the pathway depicted in **Figure 1-4** has been established as the non-mevalonate pathway for the synthesis of IPP (**2**) and DMAPP (**3**) in selected sources. Since 2*C*-methyl-D-erythritol 4-phosphate (**14**, MEP) is the product of the first committed step of the pathway, this pathway is commonly referred as the MEP pathway. Since the MEP pathway is absent in mammals but is essential for many pathogens, including *Plasmodium falciparum*[12] and *Mycobacterium tuberculosis,*[13] all enzymes in this pathway are potential antibiotic targets.[14]
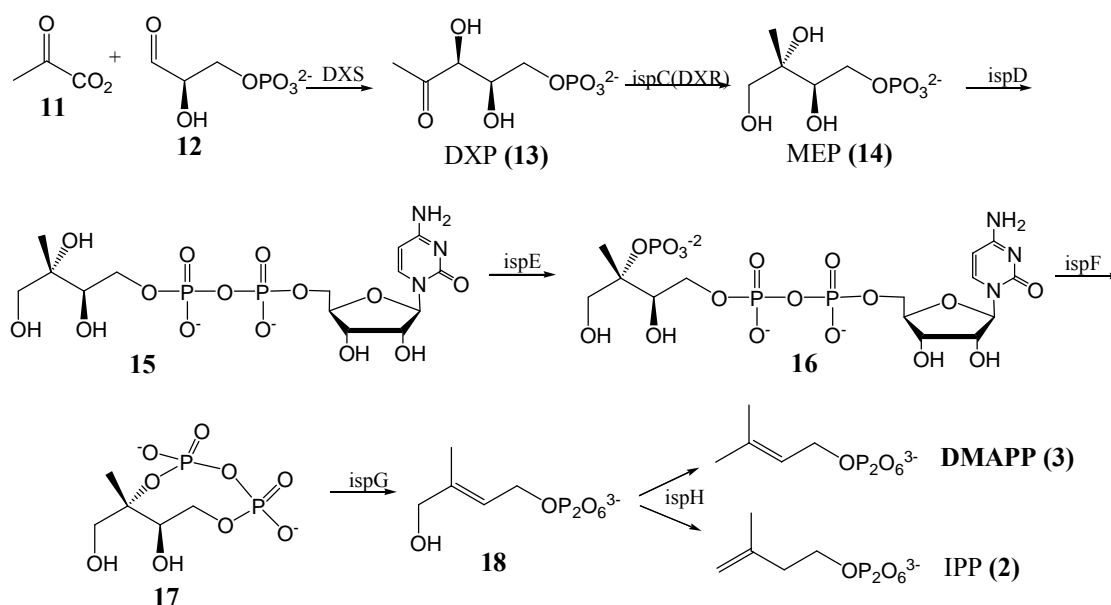
Figure 1-4: **MEP pathway for isoprenoid biosynthesis.**

1.1.2.1. *1-Deoxy-D-Xylulose 5-Phosphate Synthase (DXS).*
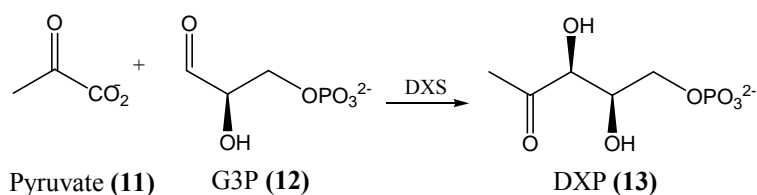
Figure 1-5:   **The DXS reaction.**

The first step in the MEP pathway is catalyzed by 1-deoxy-D-xylulose 5-phosphate (DXP) synthase (DXS).   In the reaction, pyruvate (**11**) condenses with glyceraldehydes-3-phosphate (G3P, **12**) to produce DXP (**13**), see **Figure 1-5**. The DXS reaction is thiamine pyrophosphate (TPP) dependent, and the proposed mechanism is depicted in **Figure 1-6**.
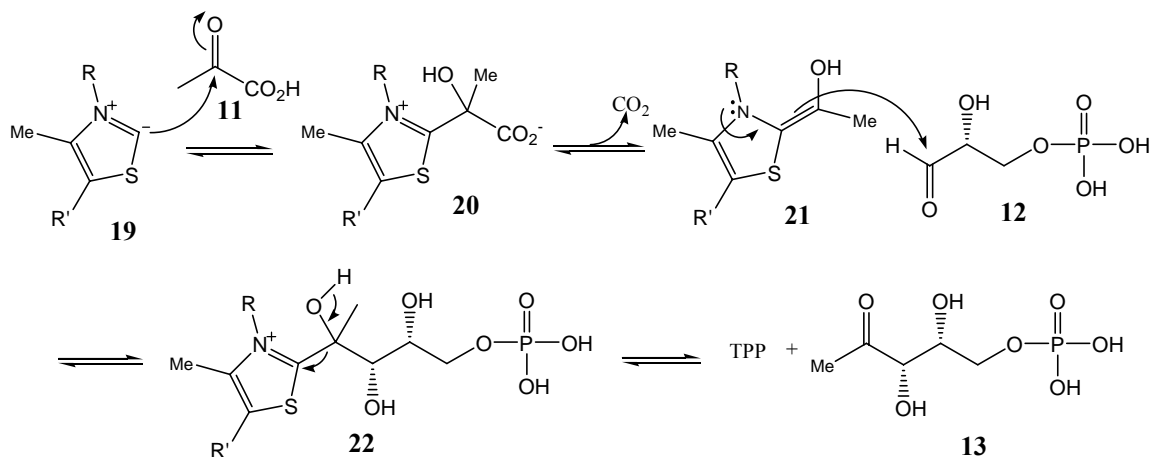
Figure 1-6:   **Mechanism for DXS.**

The reaction begins with the nucleophilic attack of the ylid carbon of the thiazolium ring on to the carbonyl carbon of pyruvate, followed by decarboxylation. The resulting carbanion (**12**), stabilized thought resonance into the thiazolium ring, does nucleophilic addition at the carbonyl of G3P (**12**). The TPP adduct (**22**) is then cleaved

in a retroaldol-like manner to yield DXP (**13**) and TPP. As mentioned above, the first committed product of the pathway is MEP and not DXP, which is due to DXP also being used in the biosynthetic pathways of thiamine and pyridoxal.[15,16]

1.1.2.2.   1-Deoxy-D-Xylulose 5-Phosphate Reductoisomerase (DXR).

DXP (**13**)   MEP (**14**)
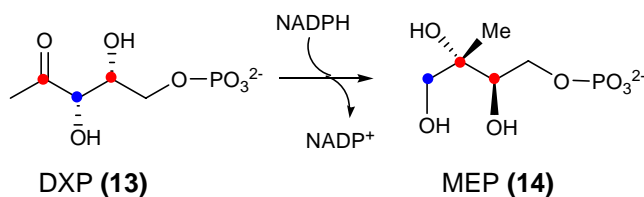
Figure 1-7:   The DXR reaction.

The first committed reaction of the MEP pathway is catalyzed by DXP reductoisomerase (DXR).[17] During this reaction, DXP (**13**) undergoes rearrangement to MEP with the concomitant oxidation of the reduced nicotinamide adenine dinucleotide phosphate (NADPH) to NADP$^+$, see **Figure 1-7**. It is has been shown that DXP first rearranges to an aldehyde intermediate, and the reaction is driven forward by the reduction of the aldehyde intermediate by NADPH.[18] As shown in **Figure 1-8**, there are two proposed mechanisms for the DXR reaction, an α-ketol rearrangement and a retroaldol/aldol rearrangement. The α-ketol rearrangement (route A) is similar to the mechanism catalyzed by ketol acid reductoisomerase, a key enzyme in the biosynthesis of branched chain amino acids.[19] This reaction is initiated by the deprotonation of the C-3 hydroxyl group followed by a 1,2-migration to yield the aldehyde intermediate (**23**). The second mechanism proceeds with a retroaldol/aldol rearrangement to produce the same intermediate, methylerythrose phosphate (**23**, route B). Here the enzyme first catalyzes the cleavage of the C3-C4 bond through a retroaldol mechanism to yield a three-carbon (**24**) and a two-carbon phosphate (**25**) intermediate. These intermediates

then condense through an aldol reaction to form a new C-C bond in **23**, which is subsequently reduced by NADPH. To distinguish between these two proposed mechanisms is a primary focus of this thesis research.

A. *α-Ketol Rearrangement*
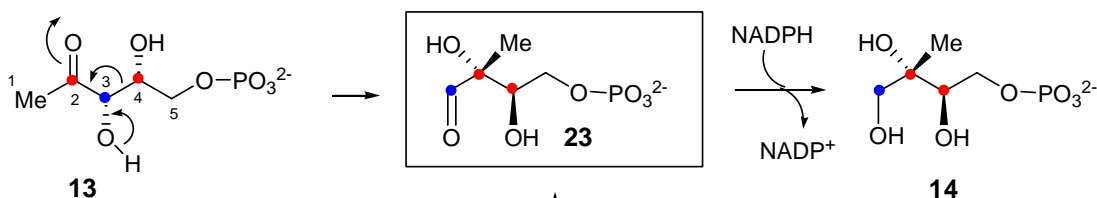
B. *Retroaldol/aldol Rearrangement*
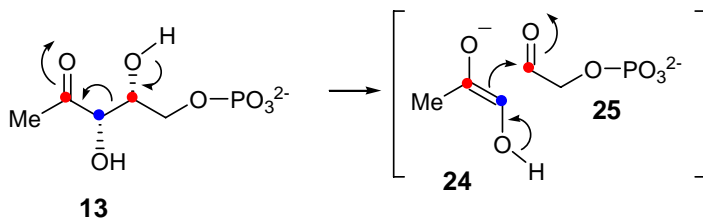
Figure 1- 8:   Proposed mechanisms for DXR.

1.1.2.3.   *IspD, IspE and IspF.*
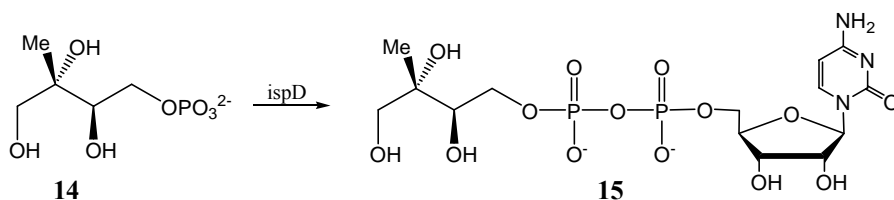
Figure 1-9:   The IspD reaction.

The third step in the pathway is the cytidylynation of MEP (**14**) by IspD to yield 4-(cytidine 5'-diphospho)-2-*C*-methyl-D-erythritol (**15**, CDP-ME), see **Figure 1-9**.[20] The reaction is believed to proceed through an associative mechanism with nucleophilic attack of the phosphate of MEP on the α-phosphate of cytidine 5'-triphosphate (CTP) to yield the pentacoordinate phosphate intermediate (**27**), see **Figure 1-10**. Depending on

the lifetime of this intermediate, it might technically be the transition state in the reaction. Upon the collapse of this pentacoordinate phosphate intermediate, pyrophosphate and CDP-ME (**15**) are formed. However, a disociative mechanism is also possible, where the pyrophosphate group breaks away from CTP before the nucleophilic attack by MEP, leaving the α-phosphate group of CTP as a metaphosphate. The metaphosphate intermediate would then undergo nucleophilic addition by the phosphate of MEP to generate CDP-ME.
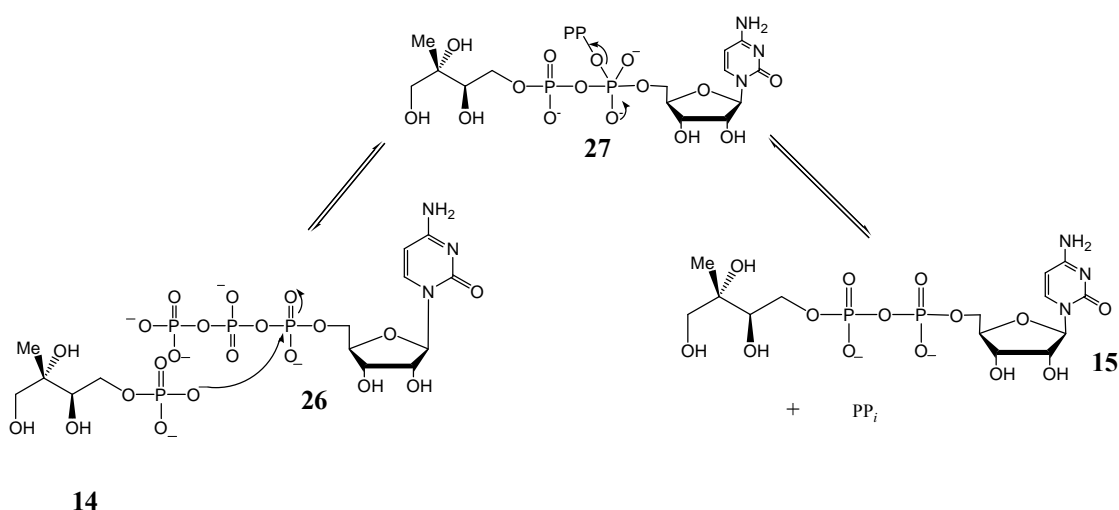
Figure 1-10:   Proposed IspD mechanism.

The forth step in the MEP pathway is the phosphorylation of the C2-hydroxyl group of CDP-ME (**15**) by ATP, catalyzed by IspE, to generate 2-phospho-4-(cytidine 5'diphospho)-2-*C*-methyl-D-erythritol (**16**, CDP-ME2P), see **Figure 1-11**.[21,22]   IspE likely proceeds through a similar associative mechanism as IspD.

8
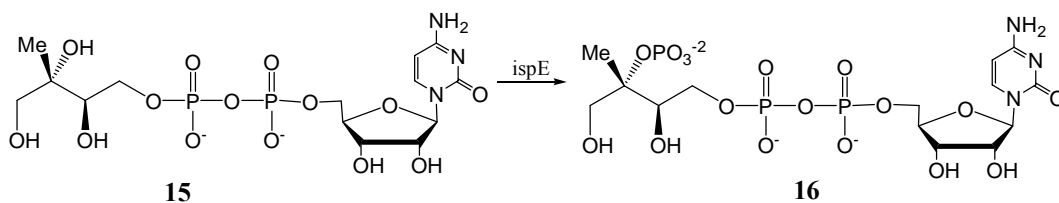
Figure 1-11: The IspE reaction.

The fifth enzyme in the pathway, IspF, catalyzes the cyclization of CDP-ME2P (**16**) to generate 2-C-methyl-d-erythritol 2,4-cyclodiphosphate (**17**, MECDP) and the release of cytidine monophosphate (CMP), see **Figure 1-12**.[23,24] IspF is believed to proceed with an associative mechanism as IspD and IspE.
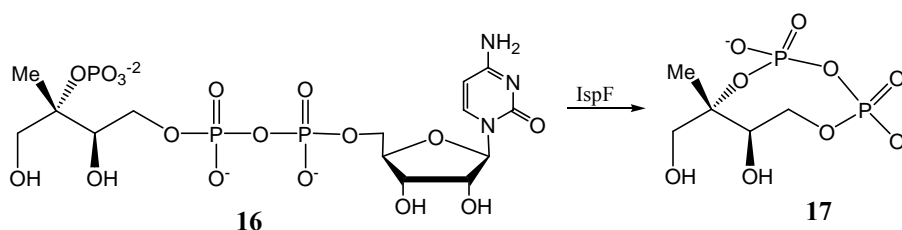
Figure 1-12: The IspF reaction.

1.1.2.4. **IspG.**
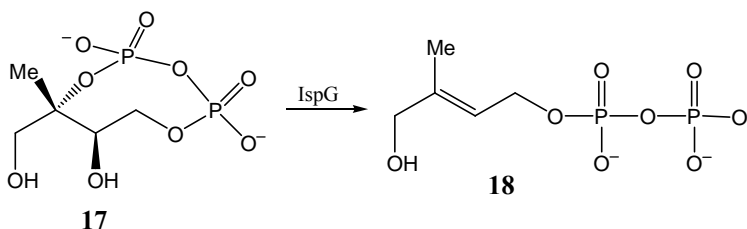
Figure 1-13: The IspG reaction.

The sixth step in the pathway is catalyzed by IspG, and it converts MECDP (**17**) to 4-hydroxy-2-methylbut-2-enyl 1-phosphate (**18**, HMBPP), see **Figure 1-13**.[25]

9

Sequence analysis revealed the presence of three conserved cysteine residues (C270, C273 and C306). When each of these residues were separately mutated to serine, the resulting IspG had no activity.[26] UV/vis and Mössbauer spectroscopy studies showed that these three cysteine residues are ligands of a [4Fe-4S] cluster.[27] Since IspG contains a [4Fe-4S] cluster, several mechanisms involving radical chemistry have been proposed. To date, there is no real experimental evidence to distinguish and/or eliminate any of the proposed mechanisms. However, a theoretical investigation has been performed in which the energies of the proposed intermediates in the different mechanisms were calculated to see which mechanism is most probable.[28] This study best supports the mechanism depicted in **Figure 1-14**. The mechanism begins with the heterolytic cleavage of the C-O bond of MECDP (**17**), probably through the aid of an active site general acid to form the tertiary C3 carbocation intermediate (**28**). An external reductase then channels a single electron through the [4Fe-4S] cluster to reduce the carbocation to a C3-radical (**29**). This is followed by a second single electron transfer through the [4Fe-4S] cluster to reduce **29** to a carbanion (**30**). The carbanion intermediate then undergoes dehydration to yield HMBPP (**18**) as the product.
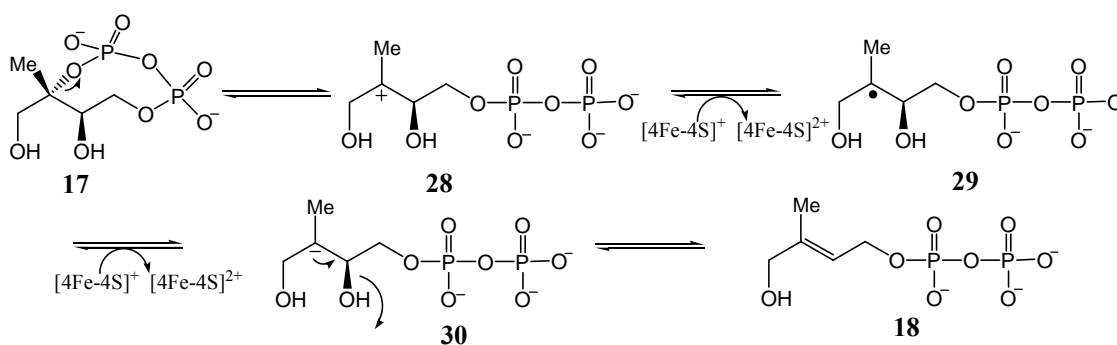
Figure 1-14: **A Proposed IspG mechanism implicated by a theoretical study.**

10

1.1.2.5.   IspH.
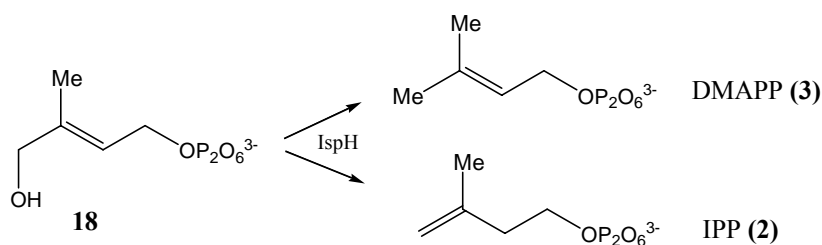
Figure 1-15:   The IspH reaction.

The final reaction in the MEP pathway is the reductive deoxygenation of HMBPP (**18**) catalyzed by IspH to yield IPP (**2**) and DMAPP (**3**), see **Figure 1-15**.[29]   Through characterization by UV/vis and EPR spectroscopy, it was determined that, like IspG, IspH also contains a [4Fe-4S] cluster.[30,31]   Different mechanisms have been proposed for IspH, yet there are no studies to date that can differentiate between the different proposed mechanisms. The mechanism displayed in **Figure 1-16**, which utilizes similar chemistry as IspG, is however the most probable.[30]   The mechanism begins with the elimination of the C4-hydroxyl group, possibly assisted through an iron of the [4Fe-4S] cluster acting as a Lewis acid catalyst, to produce the carbocation intermediate (**31**). Two single electron transfers mediated by the [4Fe-4S], would reduce the carbocation intermediate ultimately to a carbanion species (**33**). This carbanion intermediate can then be protonated at C3 to make IPP (**2**) or at C1 to make DMAPP (**3**) in final ratio of 6:1 (IPP:DMAPP) for the *E. coli* enzyme.[29]

11
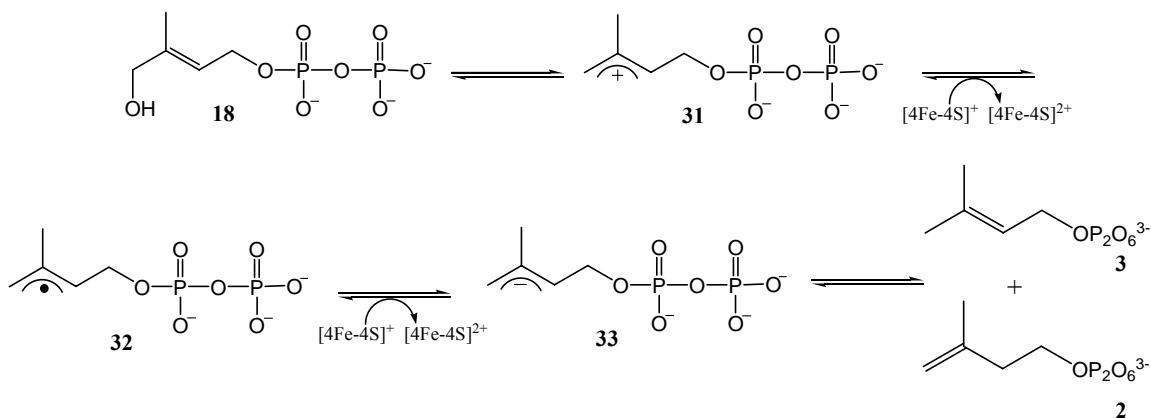
Figure 1-16: Proposed mechanism for IspH.

1.2. FOSFOMYCIN

1.2.1. Antibiotic activity of fosfomycin.

Bacteria live in hypotonic environments. To protect themselves against this enviroment, they are surrounded by rigid cell walls to prevent them from swelling and bursting due to the osmotic pressure. Part of the rigidity of the cell wall derives from the peptidoglycan framework that encases the cell, which consists of covalently linked polysaccharide and polypeptide chains. As seen in **Figure 1-17**, the peptidoglycan is found in Gram-positive and Gram-negative bacteria; however, the exact structure of the peptidoglycan of each differs.
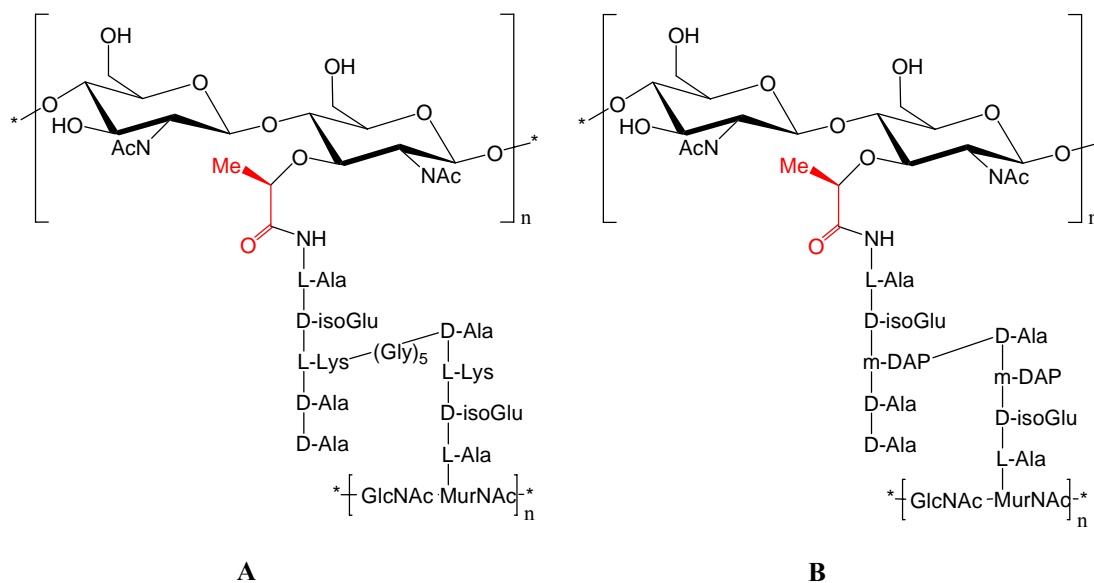
Figure 1-17: **Peptidoglycan structures for Gram-positive (A) and Gram-negative (B) bacteria.**

As can be seen in two peptidoglycan structures in **Figure 1-17**, both Gram-positive **(A)** and Gram-negative **(B)** bacteria have the same three carbon linker, displayed in red, that connects the polysaccharide and polypeptide chains. These three carbons derive from phosphoenolpyruvate (**34**, PEP), and they are transferred to uridine diphosphate-*N*-acetylglucosamine (**35**, UDP-GlcNAc) to form enolpyruvyl-UDP-*N*-acetylglucosamine (**37**, EP-UDP-GlcNAc). This reaction is catalyzed by MurA and is the first committed step of the peptidoglycan biosynthetic pathway.[32] The proposed mechanism of MurA is shown in **Figure 1-18**.[33] The reaction begins with nucleophilic addition of the C3-hydroxyl group of UDP-GlcNAc to the C2 of PEP, which is assisted by the protonation of PEP by Cys115. The resulting tetrahedral (**36**) intermediate breaks down to give the product **37** by the deprotonation of C3 and elimination of inorganic phosphate.
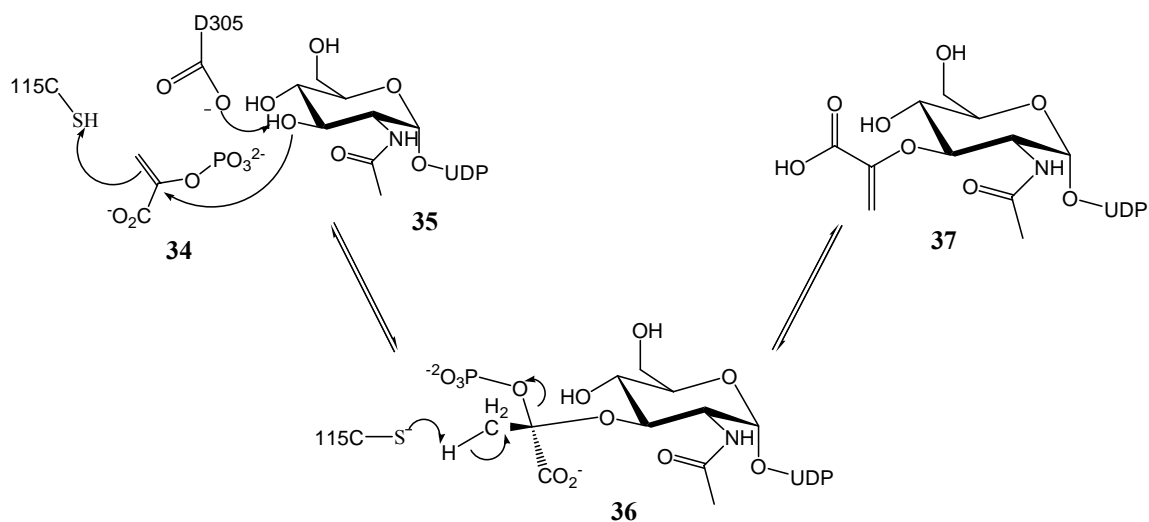
Figure 1-18: **Proposed mechanism for MurA.**
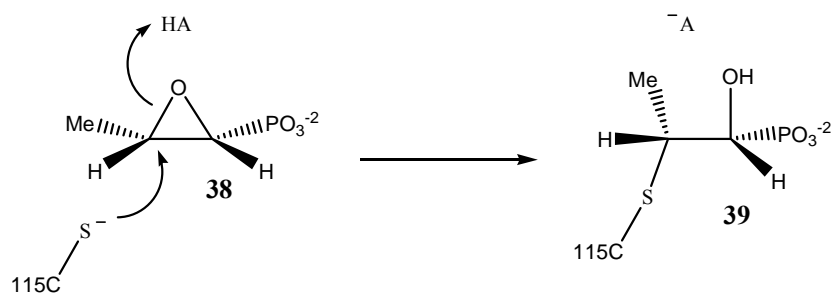
Figure 1-19: **Inactivation mechanism of MurA by fosfomycin.**

The antibiotic fosfomycin (**38**) inactivates MurA by acting as a PEP analogue, and the proposed mechanism for the inactivation is depicted in **Figure 1-19**.[34] MurA catalyzes the nucleophilic ring opening of the epoxide by Cys115, which results in a stable covalent adduct (**39**) and inactive enzyme.

14

1.2.2. Fosfomycin Biosynthetic Pathway.
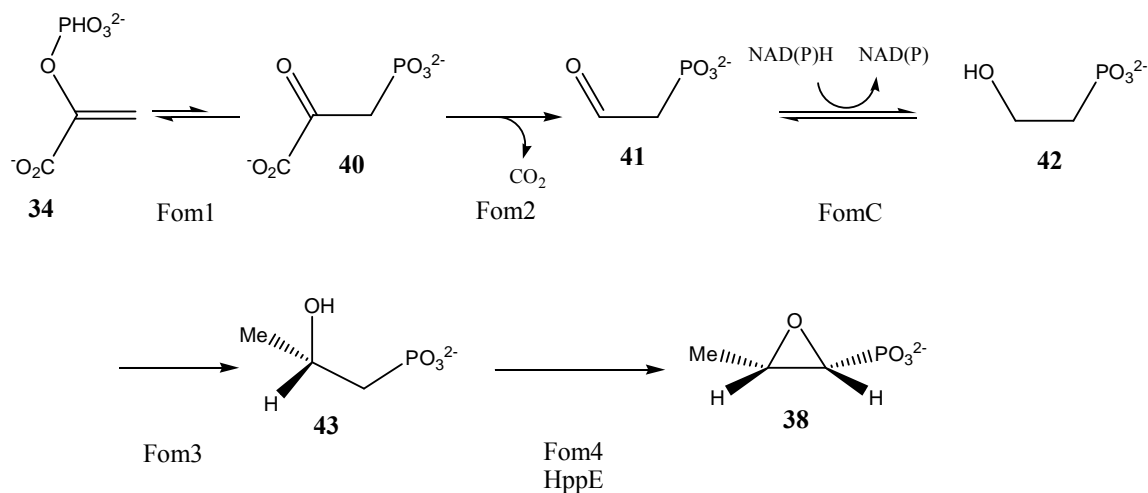
Figure 1-20: Fosfomycin biosynthetic pathway.

1.2.2.1. *The initial steps of the Fosfomycin Biosynthesis: Fom1, Fom2 and FomC.*

Fosfomycin is a natural product that is made by several species of *Pseudomonas* and *Streptomyces*,[35,36] and its biosynthetic gene cluster from *Streptomyces wedmorensis, Streptomyces fradiae* and the partial cluster from *Pseudomonas syringae* have been isolated.[37-39] The entire biosynthetic pathway has been elucidated and is presented in **Figure 1-20**. The pathway begins with Fom1, a PEP mutase, which converts PEP (**34**) to phosphonopyruvic acid (**40**, PnPy) through the proposed mechanism depicted in **Figure 1-21**.[40] This product belongs to a growing family of C-P bond containing natural products, many of which have interesting biological activities.[41] The reaction is believed to proceed through a dissociative mechanism that is initiated by the cleavage of the P-O bond to form a metaphosphate (**44**) and an enolate (**45**) intermediate. The enolate intermediate then rotates around the C1-C2 bond, which aligns C3 to react with the metaphosphate ion to form the new C3-P bond in **40**. This reaction is reversible, with the

15

equilibrium favoring PEP over PnPy greater than 500 to 1.[42] To drive the reaction forward, PnPy (**40**) is decarboxylated to phosphonoacetaldehyde (**41**, PnAA) by the PnPy decarboxylase, Fom2.[43] The third step of the pathway is the reduction of the carbonyl of PnAA (**41**) by the alcohol dehydrogenase, FomC, to hydroxylethylphosphonate (HEP).[44]
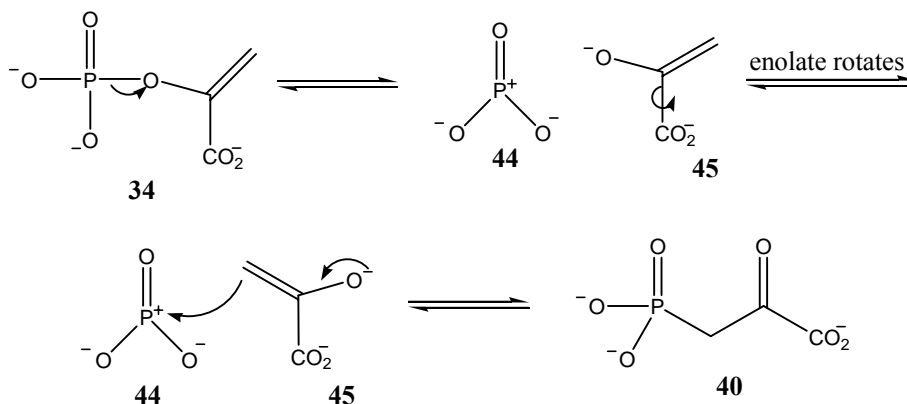
Figure 1-21:   Proposed mechanism for Fom1.

1.2.2.2.   Fom3: A new methyl transferase.

The fourth step in the biosynthetic pathway is the methylation of HEP (**42**) to (*S*)-2-hydroxypropylphosphonic acid (**43**, (*S*)-HPP) by Fom3.[44] Through labeling studies, it is known that the methyl groups is derived from methylcobalamin (MeCbl).[45] Sequence analysis of Fom3 revealed the presence of a cobalamin binding motif and predicted the enzyme to be a member of the radical-SAM (*S*-adenosyl methionine) family of proteins.[39] A mechanism for Fom3 has been proposed based on known chemistry of radical-SAM proteins.[44] The mechanism begins with the reductive cleavage of the C5'-S bond in SAM to generate methionine and 5'-deoxyadenosyl radical (see **48**). The adenosyl radical abstracts a C2 hydrogen atom from HEP (**42**) producing the C2 radical intermediate (see **49**), which would react with the methyl group of MeCbl (see **50**). In order to begin the following turnover, Fom3 has to be reactivated by reducing the [4Fe-4S] cluster,

recharging the cobalamin to MeCbl, and binding a new SAM (see **46**). This does differ from the standard radical-SAM proteins where the [4Fe-4S] and the SAM are regenerated at the end of the reaction cycle so that the enzyme is ready for the following turnover.[46]
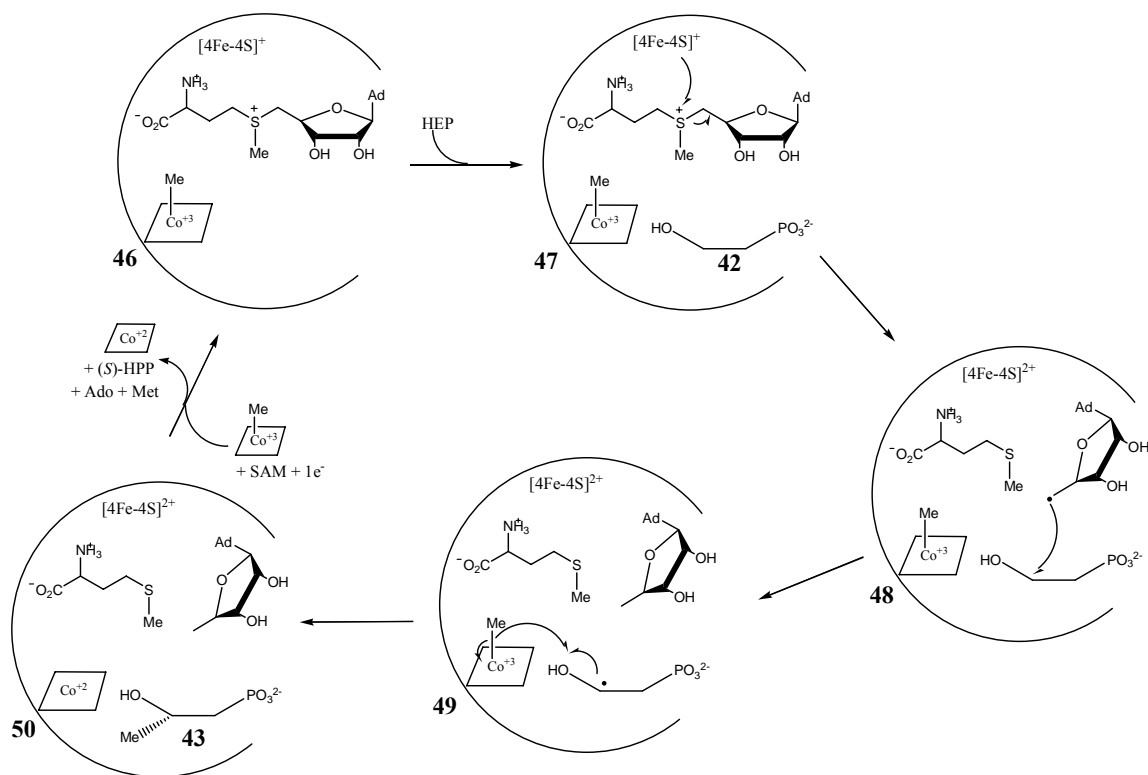
Figure 1- 22:   Proposed mechanism for Fom3.

1.2.2.3.   *HppE: A novel non-heme iron dependent enzyme.*

The final step in the biosynthetic pathway is the epoxidation of (*S*)-HPP (**43**) to fosfomycin (**38**). This reaction is catalyzed by Fom4, which has been named (*S*)-HPP epoxidase (HppE). The mechanistic analysis of HppE is the second primary focus of this dissertation research. The reaction catalyzed by HppE is an epoxidation reaction; however, it differs from Nature's standard strategy for epoxide formation. In nature, most epoxide rings are generated via oxidation of the corresponding alkenes by either

heme-dependent cytochrome P450s[47,48] or non-heme iron-dependent monooxygenases.[49] A general P450 olefin epoxidation mechanism is shown in **Figure 1-23. A** reactive oxygen species known as Compound 1 (**51**) oxidizes the olefin by a single electron to form a new C-O bond (see **52**). The iron-oxygen bond is then cleaved homolytically, and through oxygen rebound the epoxide ring is formed.[50] The non-heme iron dependent olefin epoxidation occurs by the same mechanism, except the reactive species is an iron(IV)-oxo species.[51]

| 51 | 52 | 53 |
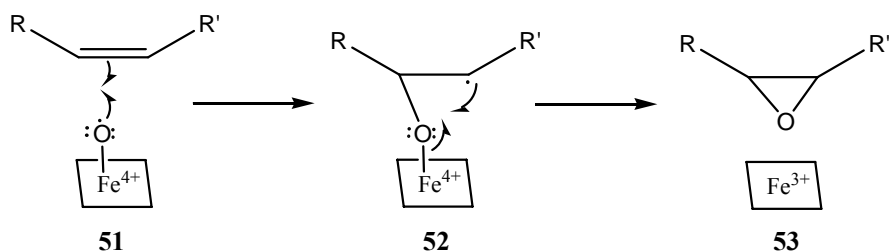
Figure 1-23:   P450 olefin epoxidation.

Previous isotope labeling experiments with HppE demonstrated that no oxygen atom from O_2 is incorporated into fosfomycin. Instead, the oxygen atom of the epoxy ring in fosfomycin (**38**) is derived from the secondary hydroxyl group of (*S*)-HPP (**43**).[52,53] Thus the conversion of (*S*)-HPP to fosfomycin by HppE is effectively a dehydrogenation reaction, not an oxygenation reaction.

HppE is a unique member of the mononuclear non-heme iron dependent enzymes. This family of enzymes is categorized into two groups, iron(II) and iron(III) dependent enzymes.[51] The iron in iron(III) enzymes is ferric in the resting state, while the iron(II) enzyme's iron is ferrous in the resting state of the enzymes. The significance of this difference is that iron(III) can not bind and activate molecular oxygen, while iron(II) can. The role of the iron in iron(III) enzymes is to activate the substrate through a single electron oxidation, generating a substrate radical and ferrous iron. The substrate radical,

18

which now has a doublet spin state, can react with molecular oxygen, which has a triplet spin state. An example of an iron(III) enzyme are lipoxygenases, whose mechanism is depicted in **Figure 1-24**. Lipoxygenases catalyze the oxidation of unsaturated fatty acids to produce fatty acid hydroperoxides at 1,4-pentadienyl positions. The bulk of the mechanistic analysis on lipoxygenases has been conducted on soybean lipoxygenase. The physiological substrate of soybean lipoxygenase is linoleic acid, 9,12-(Z,Z)-octadecadienoic acid (**55**), which is converted to 13-(S)-hydroperoxy-9,11-(Z,E)-octadecadienoic acid (**58**, 13-(S)-HPOD).[54] The reaction proceeds via an initial rate-limiting hydrogen abstraction by the Fe^{III}-OH cofactor to generate a substrate radical (**56**) and Fe^{II}-OH$_2$.[55] The substrate radical rapidly reacts with molecular oxygen and the equivalent of a hydrogen atom is transferred back to the peroxo intermediate (**57**) to produce the hydroperoxide product (**58**) and to regenerate the resting ferric-hydroxide state of the non-heme iron center.
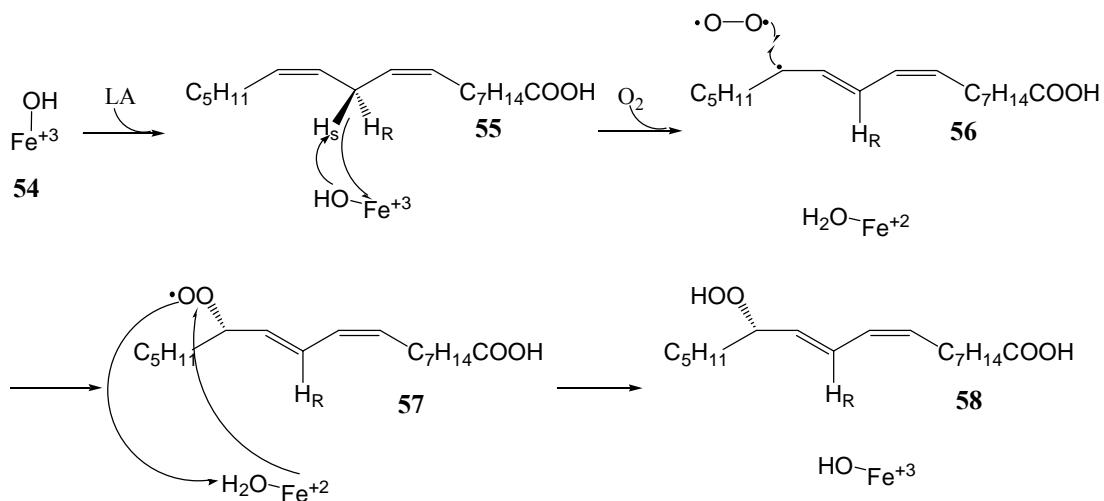
Figure 1-24:   Proposed mechanism for lipoxygenases.

Iron(II) enzymes, which includes HppE, bind and activate oxygen. The reactive oxygen species typically carries out a two electron oxidation of the substrate. Iron(II)

enzymes catalyze a wide variety of reactions, including hydroxylation of aliphatic C-H bonds, epoxidation of C-C double bonds, *cis*-dihydroxylation of arene double bonds, heterocyclic ring formation, and oxidative aromatic ring cleavage.[56] Despite the broad range of reaction types, all iron(II) enzymes share the same structural motif known as the 2-His-1-carboxylate facial triad. The name of this motif derives from the active site iron being bound by three endogenous protein ligands arranged at the vertices of one triangular face of an octahedron. Two of the ligands are histidines, and the other is either an aspartate or a glutamate. The three remaining coordination sites are available for exogenous ligands, such as solvent molecules, the substrate/co-substrate, and molecular oxygen. The iron is usually six-coordinated in the resting state and relatively unreactive towards molecular oxygen. It is after substrate/co-substrate binding that the iron changes to five-coordinated, which provides a coordination site for binding of O_2. The substrate/co-substrate binding generally increases the binding affinity of O_2. With O_2 binding taking place only after the binding of substrate and/or co-substrate also greatly enhances the coupling of the reduction of O_2 to the oxidation of the substrate. This binding event brings together the substrate and activated oxygen together in close proximity for the ensuing reaction.[51]

The reactive oxygen species generated in the reaction can be either Fe(III)-superoxide (Fe(III)-OO•), Fe(III)-hydroperoxide (Fe(III)-OOH) or Fe(IV)-oxo (Fe(IV)=O), with Fe(IV)-oxo being the most reactive and widely used.[51] To date there is no direct evidence of a mononuclear non-heme iron dependent enzyme that utilizes Fe(III)-superoxide as the reactive species; however, it is widely accepted that the reactive species for the first oxidation reaction catalyzed by isopenicillin N synthase (IPNS) is Fe(III)-superoxide.[57] There are no reported mononuclear non-heme iron dependent enzymes which use Fe(III)-hydroperoxide as the reactive species despite its involvement

in flavin-dependent hydroxylases.[58] In contrast, it is well documented for mononuclear non-heme iron dependent enzymes that utilize Fe(IV)-oxo as the reactive species. The list includes the α-ketoglutarate (α-KG) dependent TauD[59] and CytC3,[60] tyrosine hydroxylase,[61] and 1-aminocyclopropane-1-carboxylic acid (ACC) oxidase (ACCO).[62]

The IPNS reaction begins with the binding of the substrate, δ-(L-α-aminoadipoyl)-L-cysteinyl-D-valine (**60**, ACV).[63,64] The thiolate group of ACV coordinates to the iron to produce a five-coordinate iron site, leaving the sixth site open for oxygen binding. Molecular oxygen then binds to the iron(II) at the vacant coordination site, where it is reduced by an inner-sphere electron transfer from iron(II) to yield Fe(III)-superoxide (see **61**). It also has been demonstrated through calculations that the coordination of the thiolate enhances the binding of O_2 by stabilizing Fe(III)-superoxide.[57] The reactive species for the first oxidative ring closure to form the β-lactam ring is believed to be Fe(III)-superoxide; however, this has not been experimentally verified. The Fe(III)-superoxide is proposed to abstract a hydrogen atom from the cysteine β-carbon to form the substrate radical (**62**) and Fe(III)-hydroperoxide. The intermediate is further oxidized by a second single electron transfer to the iron to form the thioketone (**63**) and Fe(II)-hydroperoxide. The O-O bond of the peroxide is then cleaved heterolytically to generate Fe(IV)-oxo and hydroxide, which abstracts the valine N-H proton. Concerted with Fe(IV)-oxo formation, the valine nitrogen performs a nucleophilic attack on the cysteine β-carbon to form the β-lactam ring (**64**). The strong oxidant, Fe(IV)-oxo, can now abstract the unactivated hydrogen atom from the valine β-carbon (see **64**). Similar in fashion to the oxygen rebound mechanism of cytochrome P450 reaction, the resulting substrate radical (**65**) reacts with the thiolate to close the thiazolidine ring (**66**) with concurrent homolytic cleavage of the Fe-S bond.
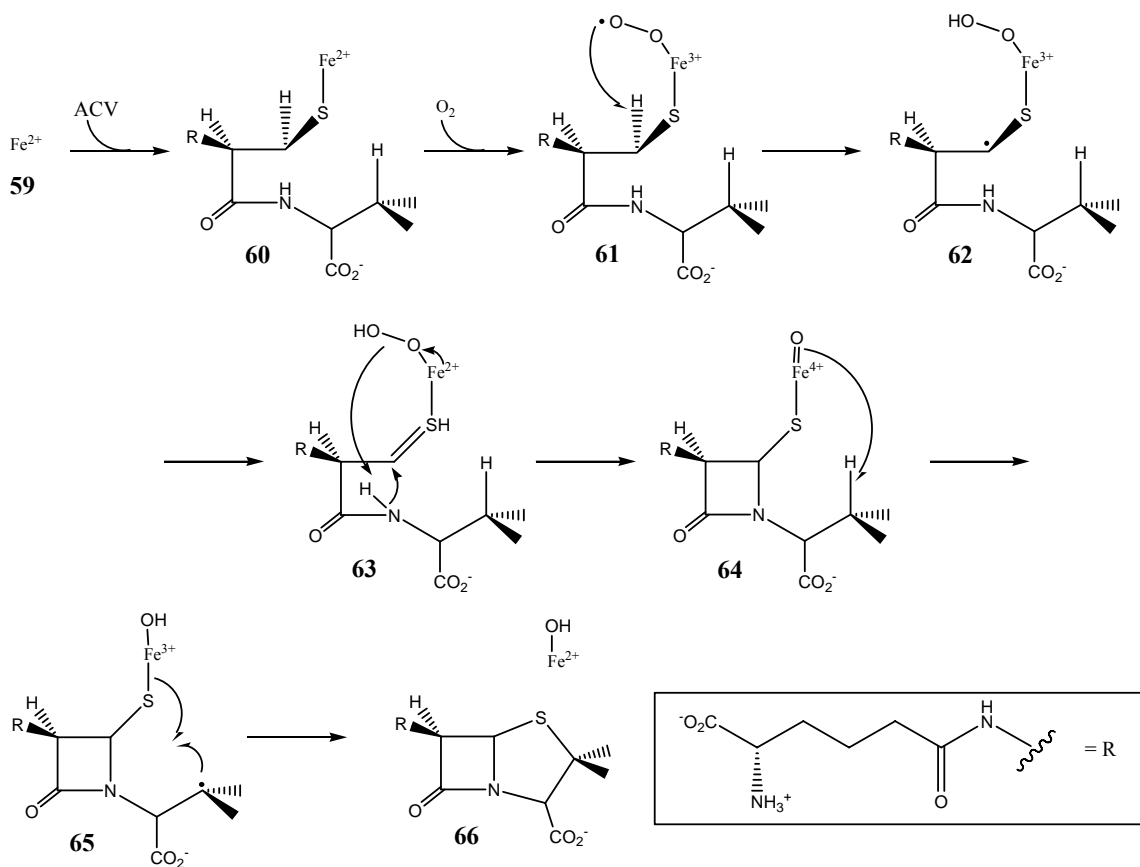
Figure 1-25: **Proposed mechanism for IPNS.**

The oxygen activation mechanism depicted in **Figure 1-26** to generate the reactive Fe(IV)-oxo is shared by believed all known α-KG dependent enzymes.[51] The six coordinated Fe(II) center begins the reaction to bind α-KG by displacing two ligands (see **68**). At this stage, the iron is still six coordinated and is relatively unreactive toward molecular oxygen. The substrate then binds to the active site but does not coordinate to the iron (see **69**). When this occurs, a water ligand dissociates leaving a coordination site open for oxygen binding. By limiting oxygen binding to after the substrate binds reduces the uncoupled reactions. Once molecular oxygen now binds to the open coordination site, it is reduced to Fe(III)-superoxide (**70**). This activates the distal oxygen for nucleophilic attack at the α-keto carbon. The resulting bridged intermediate (**71**) is

22

believed to undergo a concerted decarboxylation of α-KG and a heterolytic cleavage of the O-O bond, forming the Fe(IV)-oxo reactive species (**72**). The reactive Fe(IV)-oxo abstracts a hydrogen atom from the substrate (see **73**), and the substrate radical is either then hydroxylated, as in TauD, or chlorinated, as in CytC3, in a rebound mechanism (see **74**).[51,60]
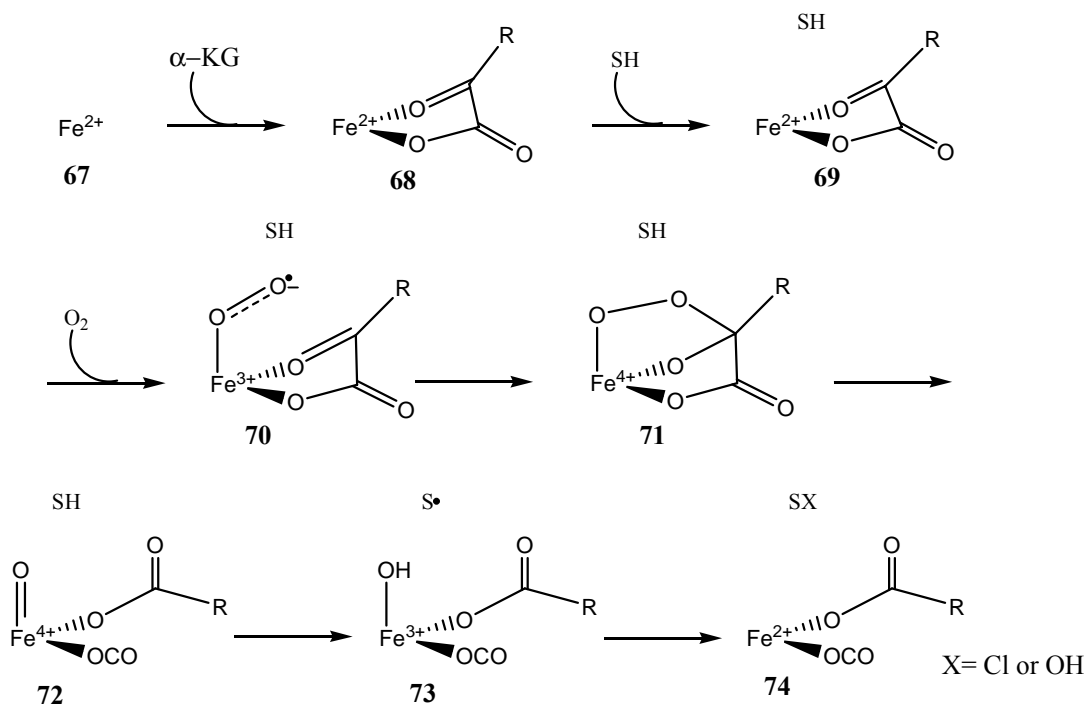
Figure 1-26: **Proposed mechanism for α-KG dependent enzymes.**

A second type of iron(II) enzymes whose reactive species has been verified to be Fe(IV)-oxo are the pterin-dependent aromatic amino acid hydroxylases, specifically tyrosine hydroxylase.[61] As the case for the α-KG enzymes, when tyrosine binds to the active site of tyrosine hydroxylase (**75**), it does not coordinate to the iron (see **76**). However, binding of tyrosine triggers the release of a water ligand to change the iron from six coordinated to five coordinated, which produces a vacant coordination site for binding of molecular oxygen. When oxygen binds in the active site, it first reacts with

the iron to form Fe(III)-superoxide before forming a putative Fe(II)-O-O-pterin adduct (**77**).[65] The peroxy-adduct then cleaves heterolytically to form 4a-hydroxypterin and Fe(IV)-oxo (see **78**).[61] The Fe(IV)-oxo does not perform hydrogen atom abstraction, but instead facilitates the electrophilic attack of the aromatic ring to generate a carbocation intermediate (**79**), which is then deprotonated to give the hydroxylated product.
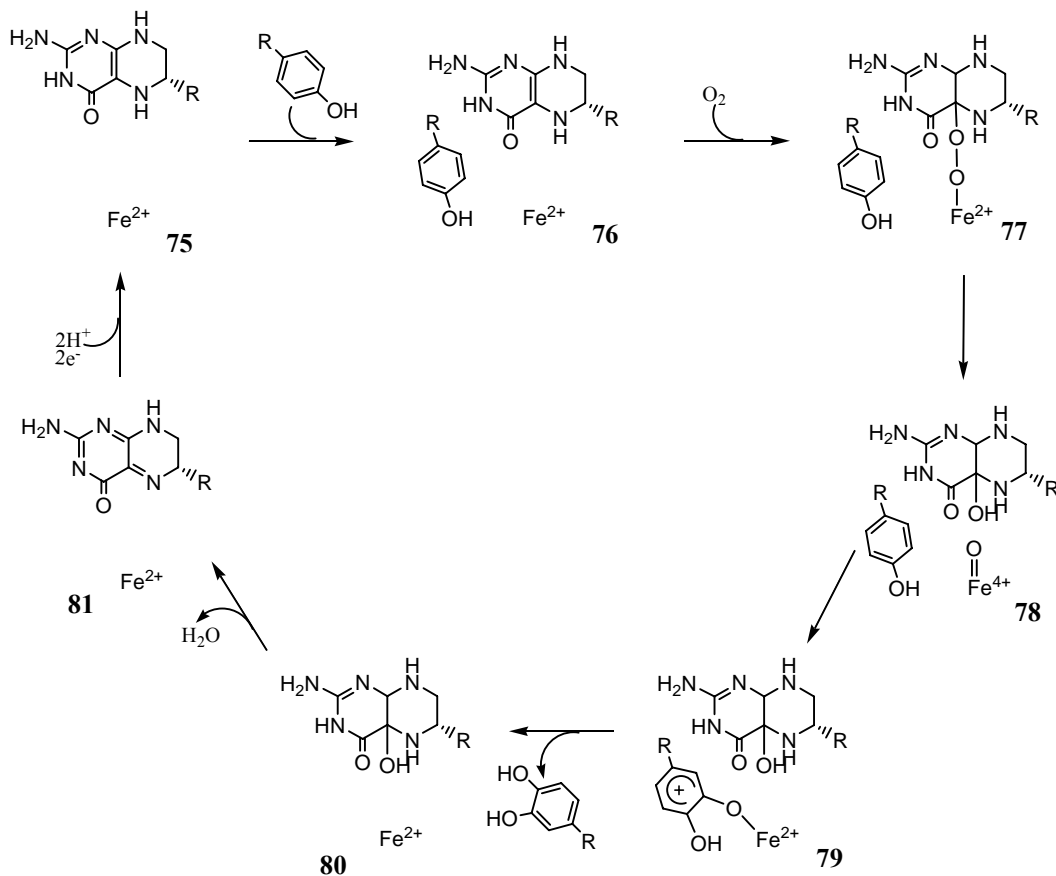
Figure 1-27:   Proposed mechanism for tyrosine hydroxylase.

A third type of iron(II) enzyme where the reactive species has been determined to be Fe(IV)-oxo is ACCO, which oxidatively breaks down ACC into ethylene, hydrogen cyanide and CO_2.[66] ACCO does not utilize α-KG or reduced pterin for the reductive activation of O_2; instead, ascorbate plays the reductant role. The substrate binding order

24

has not been fully deduced, but it is believed that ascorbate and ACC bind before O_2 (see **82** and **83**).[67] When O_2 binds to the ferrous center, Fe(III)-superoxide forms (see **84**), which is reduced by a single electron transfer from ascorbate to generate Fe(III)-hydroperoxide (see **85**). A second single electron transfer from ascorbate and cleavage of the O-O bond produces the reactive species, Fe(IV)-oxo (see **86**).[62] The Fe(IV)-oxo then performs a single electron oxidation of the amine to form a cation amine radical (**87**), which subsequently breaks down in a manner yet to be determined to yield ethylene, HCN and CO_2 (see **88**).
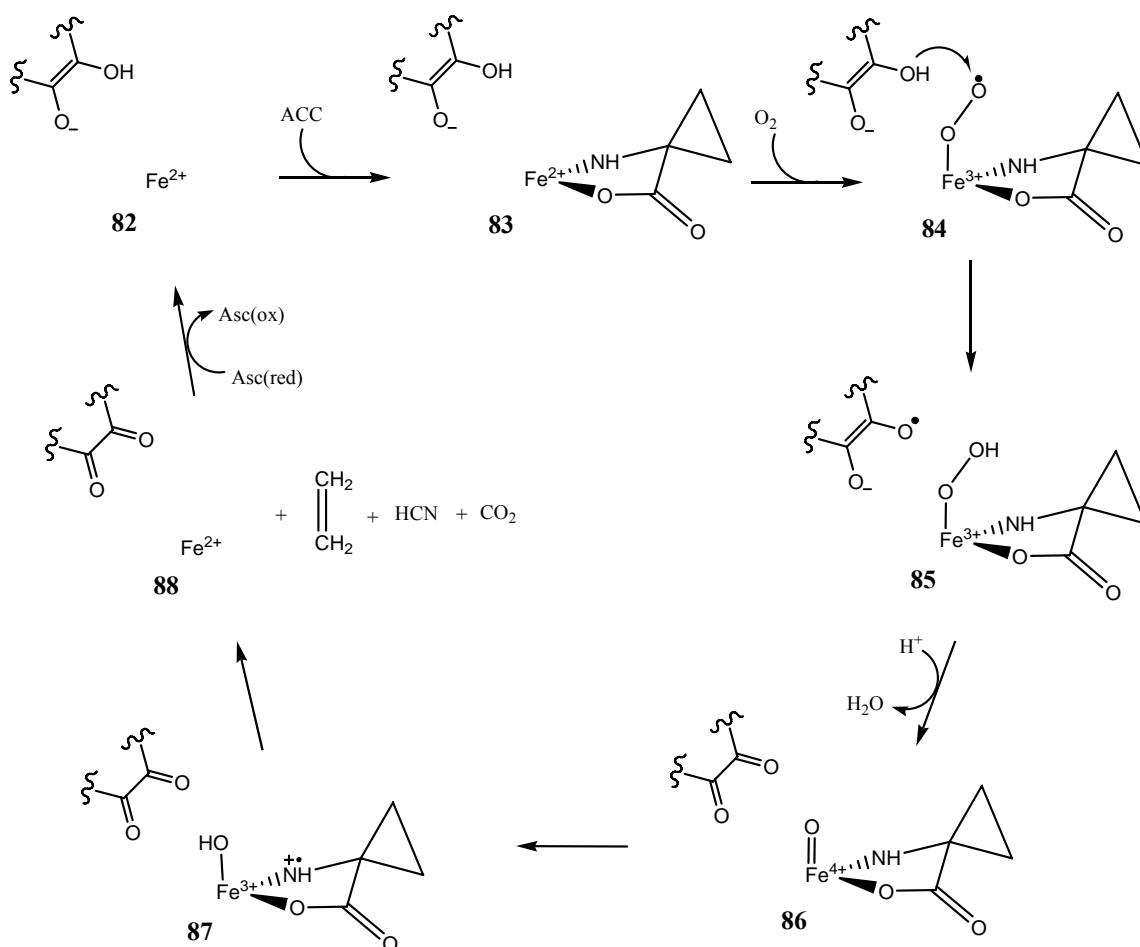
Figure 1-28: **Proposed mechanism of ACCO.**

25

HppE is unique with respect to all other mononuclear non-heme iron-dependent enzymes regarding the required components for activity. The HppE reaction is independent of ascorbate, α-KG, pterin, or an internal iron-sulfur cluster. Instead, the HppE reaction requires two external electrons from NAD(P)H to complete the four electron reduction/activation of O_2 ; the other two electrons are supplied by (*S*)-HPP (**43**). An external reductase is required to mediate single electron transfer into the iron active site; however, a putative HppE reductase is yet to be discovered. For *in vitro* activity assays of HppE, a promiscuous reductase from a separate biosynthetic pathway, such as CDP-6-deoxy-L-*threo*-D-*glycero*-4-hexulose-3-dehydrase reductase (E3), or a chemical electron mediator, such as flavin mononucleotide (FMN), are substituted for the putative HppE reductase.

The mechanism of HppE epoxidation has been proposed to parallel the alkane hydroxylation catalyzed by cytochrome P450[48] and non-heme iron-dependent oxygenases.[51,68] The reaction likely begins with hydrogen abstraction from the C-1 position of **43** by an activated oxygen species. In a manner similar to the oxygen rebound mechanism for cytochrome P450s, the C-1 centered radical intermediate can then cyclize to form fosfomycin (**38**) and the reduced iron center. As shown in **Figure 1-29**, the reactive oxygen species can be one of three species. One of them is Fe(III)-superoxide (**91**), which forms upon dioxygen binding to the ferrous iron center (**90**), similar to what has been proposed for the initial H-atom abstraction in isopenicillin N synthase (IPNS).[57,64] The Fe(III)-superoxide species can be reduced by one electron and protonated to form Fe(III)-hydroperoxide (**93**), which can also abstract the C-1 hydrogen atom. The Fe(III)-hydroperoxide species can be further reduced by a second single electron transfer with concurrent cleavage of the O-O bond to form Fe(IV)-oxo (**94**), as

described above for the α-KG dependent enzymes[59,60] and for ACCO.[62] This reactive species clearly can abstract the hydrogen atom.
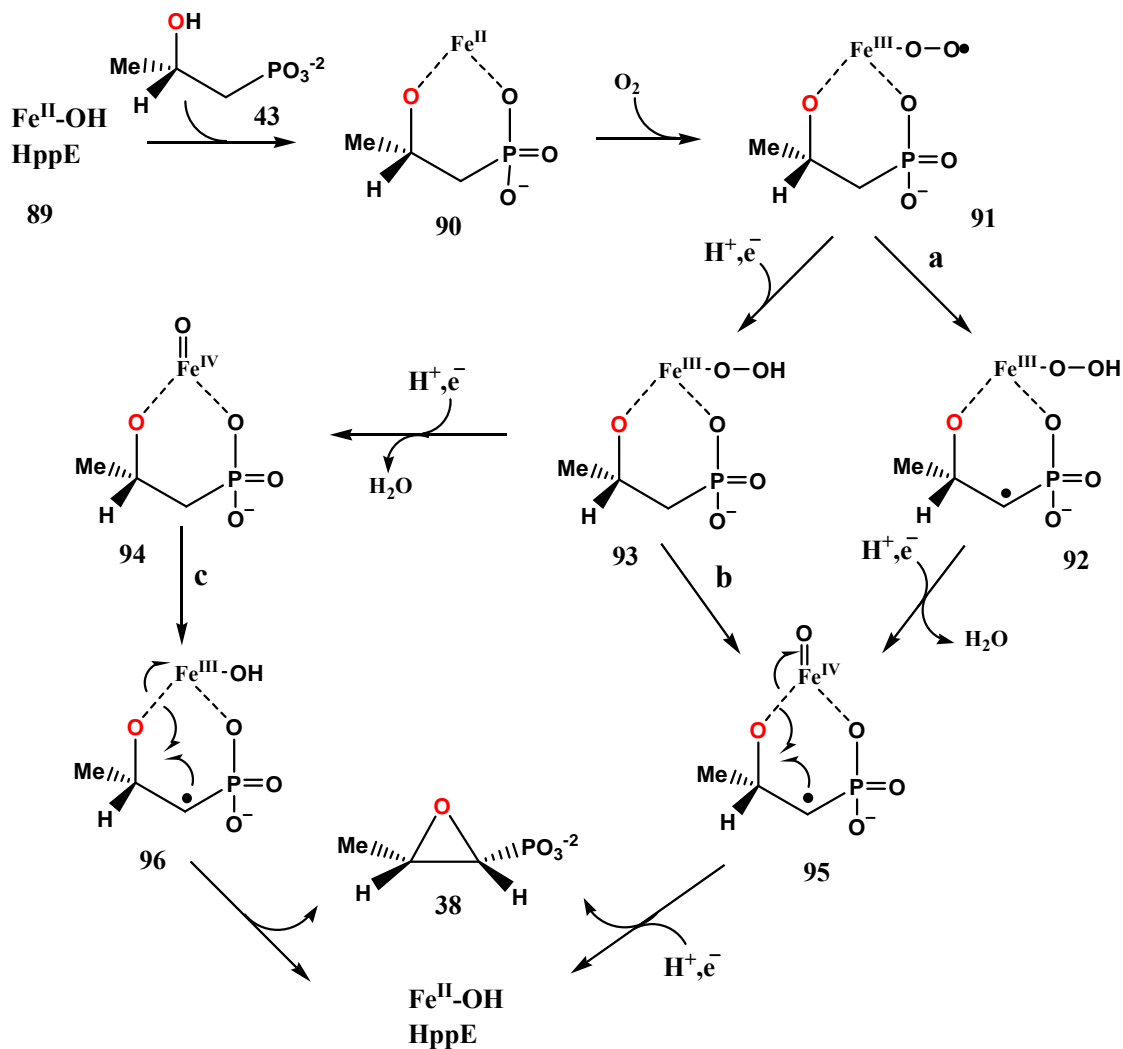
Figure 1-29:   Proposed mechanisms for HppE with (*S*)-HPP (43).

The HppE reaction is stereo- and regiospecific.[69] When HppE reacts with (*S*)-HPP (**43**), the C1 pro-*R* hydrogen atom is abstracted in the course of fosfomycin production. When (*R*)-HPP (**97**) is substituted for (*S*)-HPP (**43**), the C2 hydrogen atom is abstracted and a new ketone product is produced, 2-oxopropylphosphonic acid (**105**). As

depicted in **Figure 1-30**, the proposed mechanisms for the reaction with (*R*)-HPP mirror those proposed for the fosfomycin producing reaction.
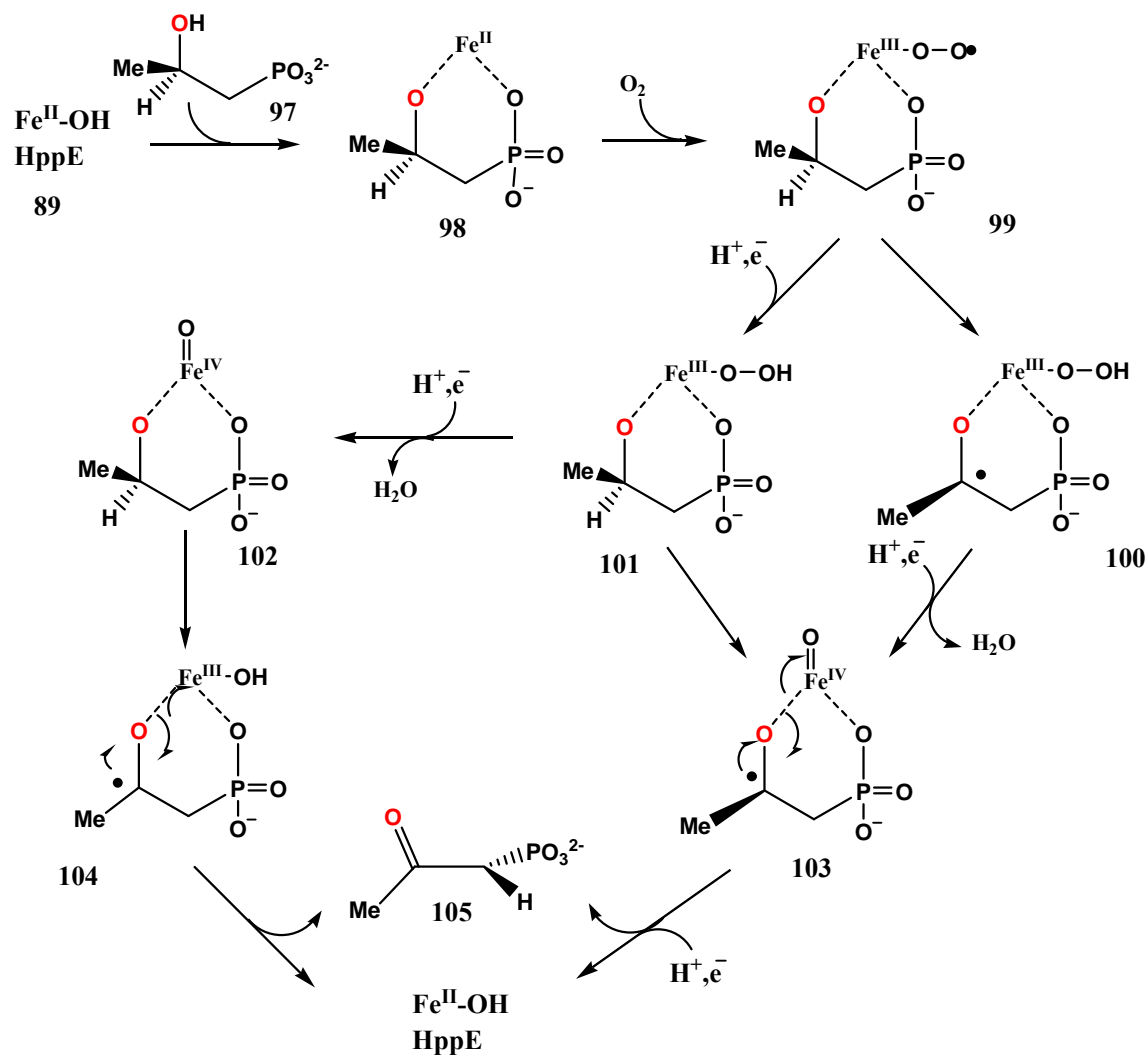
Figure 1-30: Proposed mechanism of HppE with (*R*)-HPP (97).

1.3. THESIS STATEMENT

The focus of this dissertation is the study of two enzymes, DXR and HppE. DXR catalyzes the first committed step in the MEP pathway, which is the

pathway most eubacteria, archeabacteria, algae, and the plastids of plants use for the biosynthesis of isoprenoid. Since mammals utilize the mevalonate pathway and isoprenoids are essential for survival, enzymes in the MEP pathway are excellent antibiotic targets. Every year there are around 300 million new malaria infections and 1-3 million deaths as a result of the disease, which is caused by the parasite *Plasmodium falciparum*. One antibiotic that has promise in the fight against malaria is the natural product fosmidomycin, which has been demonstrated to cure mice infected with malaria.[12] Fosmidomycin's antibiotic activity is due to its ability to bind tightly and inhibit DXR. With a deeper understanding of DXR's catalyzed reaction, it will be possible to design a more sophisticated and potent antibiotic. Chapter 2 describes the design and inhibition analysis of two fluorinated substrate analogues, 3F-DXP and 4F-DXP, and a fluorinated product analogue, FCH_2-MEP. The synthetic schemes for the substrate analogues were designed by Dr. Alexander Wong, and they were synthesized by Dr. Wong with the assistance of Ms. Vidusha Devasthali. In order to complete the investigation, more 3F-DXP was required, which I started and Dr. Gang Dong completed. The product analogue, FCH_2-MEP, was synthesized by Dr. Xiaotao Pu. Chapter 3 described a 2° [^{2}H]-KIE study, which was conducted by the equilibrium perturbation method. The labeled DXP analogues for the study were synthesized by Dr. Xiaotao Pu.

The second enzyme this dissertation examines is HppE, which catalyzes the final step in the biosynthesis of the antibiotic, fosfomycin. Fosfomycin (**38**) is a clinically useful antibiotic[70] for the treatment of limb-threatening diabetic foot infections[71] and lower urinary tract infections. It has been shown to be effective against ciprofloxacin-resistant *E. coli*,[72] as well as methicillin-resistant[73] and vancomycin-resistant[74] strains of *Staphylococcus aureus*. Chemically speaking, HppE is unique

for two reasons. First, HppE's epoxidation differs from Nature's standard method of epoxide formation by alkene oxidation, where the epoxide oxygen is derived from molecular oxygen.[47-49] For HppE, the epoxide is formed through the dehydrogenation of a secondary alcohol; thus the epoxide oxygen is derived from the substrate. Second, HppE is a unique member of the mononuclear non-heme iron-dependent family of enzymes. HppE differs from all other mononuclear non-heme iron-dependent enzymes by requiring NADH and an external electron mediator for turnover but not requiring α-KG, pterin, ascorbate, or an internal iron-sulfur cluster. In Chapter 4, the proposed iron and NADH dependent mechanism of HppE from *Streptomyces wedmorensis* is reevaluated after a study is published on the activity of zinc-reconstituted HppE. This investigation was conducted in collaboration with Dr. Feng Yan. Chapter 5 describes the purification, biochemical and spectroscopic characterization of the HppE from *Pseudomonas syringae* (*Ps*-HppE), and the results of [^{2}H] and [^{18}O]-KIE studies on *Ps*-HppE are also reported. The EPR experiments were conducted in collaboration with Prof. Aimin Liu at the University of Mississippi Medical Center in Jackson, Mississippi. The deuterium labeled compounds for the [^{2}H]-KIE studies were synthesized by Dr. Sung-Ju Moon. The bond dissociation energies were calculated by Dr. Steven O. Mansoorabadi, and the [^{18}O]-KIE studies were conducted in collaboration with Dr. Liviu M. Mirica in the lab of Prof. Judith P. Klinman at the University of California at Berkeley.

1.4. REFERENCES

(1)   Rohdich, F.; Bacher, A.; Eisenreich, W. Perspectives in anti-infective drug design: The late steps in the biosynthesis of the universal terpenoid precursors, isopentenyl diphosphate and dimethylallyl diphosphate. *Bioorg. Chem.*, **2004**, *32*, 292-308.

(2)   Penuelas, J.; Munne-Bosch, S. Isoprenoids: an evolutionary pool for photoprotection. *Trends Plant Sci.*, **2005**, *10*, 166-9.

(3)   Tudzynski, B. Biosynthesis of gibberellins in Gibberella fujikuroi: biomolecular aspects. *Appl. Microbiol. Biotechnol.*, **1999**, *52*, 298-310.

(4)   Fenton, J. W., 2nd; Jeske, W. P.; Catalfamo, J. L.; Brezniak, D. V.; Moon, D. G.; Shen, G. X. Statin drugs and dietary isoprenoids downregulate protein prenylation in signal transduction and are antithrombotic and prothrombolytic agents. *Biochemistry (Mosc)*, **2002**, *67*, 85-91.

(5)   Katsuki, H.; Bloch, K. Studies on the biosynthesis of ergosterol in yeast. Formation of methylated intermediates. *J. Biol. Chem.*, **1967**, *242*, 222-7.

(6)   Lynen, F. Biosynthetic pathways from acetate to natural products. *Pure Appl. Chem.*, **1967**, *14*, 137-67.

(7)   Kuzuyama, T. Mevalonate and nonmevalonate pathways for the biosynthesis of isoprene units. *Biosci. Biotechnol. Biochem.*, **2002**, *66*, 1619-27.

(8)   Watanabe, Y.; Ito, T.; Shiomi, M.; Tsujita, Y.; Kuroda, M.; Arai, M.; Fukami, M.; Tamura, A. Preventive effect of pravastatin sodium, a potent inhibitor of 3-hydroxy-3-methylglutaryl coenzyme A reductase, on coronary atherosclerosis and xanthoma in WHHL rabbits. *Biochim. Biophys. Acta*, **1988**, *960*, 294-302.

(9)   Rohmer, M.; Knani, M.; Simonin, P.; Sutter, B.; Sahm, H. Isoprenoid biosynthesis in bacteria: a novel pathway for the early steps leading to isopentenyl diphosphate. *Biochem. J.*, **1993**, *295 (Pt 2)*, 517-24.

(10)   Schwarz, M. K., ETH, 1994.

(11)   Broers, S. T. J., ETH, 1994.

(12)   Jomaa, H.; Wiesner, J.; Sanderbrand, S.; Altincicek, B.; Weidemeyer, C.; Hintz, M.; Turbachova, I.; Eberl, M.; Zeidler, J.; Lichtenthaler, H. K.; Soldati, D.; Beck, E. Inhibitors of the nonmevalonate pathway of isoprenoid biosynthesis as antimalarial drugs. *Science*, **1999**, *285*, 1573-6.

(13)   Argyrou, A.; Blanchard, J. S. Kinetic and chemical mechanism of *Mycobacterium tuberculosis* 1-deoxy-D-xylulose-5-phosphate isomeroreductase. *Biochemistry*, **2004**, *43*, 4375-84.

(14)   Eisenreich, W.; Bacher, A.; Arigoni, D.; Rohdich, F. Biosynthesis of isoprenoids via the non-mevalonate pathway. *Cell Mol Life Sci*, **2004**, *61*, 1401-26.

(15)   Hill, R. E.; Sayer, B. G.; Spenser, I. D. Biosynthesis of vitamin B6: incorporation of D-1-deoxyxylulose. *J. Am. Chem. Soc.*, **1989**, *111*, 1916-17.

(16)   Himmeldirk, K.; Kennedy, I. A.; Hill, R. E.; Sayer, B. G.; Spenser, I. D. Biosynthesis of vitamins B1 and B6 in *Escherichia coli*: concurrent incorporation of 1-deoxy-D-xylulose into thiamin (B1) and pyridoxol (B6). *Chem. Comm.*, **1996**, *10*, 1187-1188.

(17)   Takahashi, S.; Kuzuyama, T.; Watanabe, H.; Seto, H. A 1-deoxy-D-xylulose 5-phosphate reductoisomerase catalyzing the formation of 2-C-methyl-D-erythritol 4-phosphate in an alternative nonmevalonate pathway for terpenoid biosynthesis. *Proc. Natl. Acad. Sci. U S A*, **1998**, *95*, 9879-84.

(18)   Hoeffler, J. F.; Tritsch, D.; Grosdemange-Billiard, C.; Rohmer, M. Isoprenoid biosynthesis via the methylerythritol phosphate pathway. Mechanistic investigations of the 1-deoxy-D-xylulose 5-phosphate reductoisomerase. *Eur. J. Biochem.*, **2002**, *269*, 4446-57.

(19)   Dumas, R.; Biou, V.; Halgand, F.; Douce, R.; Duggleby, R. G. Enzymology, structure, and dynamics of acetohydroxy acid isomeroreductase. *Acc Chem Res*, **2001**, *34*, 399-408.

(20)   Rohdich, F.; Wungsintaweekul, J.; Fellermeier, M.; Sagner, S.; Herz, S.; Kis, K.; Eisenreich, W.; Bacher, A.; Zenk, M. H. Cytidine 5'-triphosphate-dependent biosynthesis of isoprenoids: YgbP protein of *Escherichia coli* catalyzes the formation of 4-diphosphocytidyl-2-C-methylerythritol. *Proc. Natl. Acad. Sci. U S A*, **1999**, *96*, 11758-63.

(21)   Rohdich, F.; Wungsintaweekul, J.; Luttgen, H.; Fischer, M.; Eisenreich, W.; Schuhr, C. A.; Fellermeier, M.; Schramek, N.; Zenk, M. H.; Bacher, A. Biosynthesis of terpenoids: 4-diphosphocytidyl-2-C-methyl-D-erythritol kinase from tomato. *Proc. Natl. Acad. Sci. U S A*, **2000**, *97*, 8251-6.

(22)   Kuzuyama, T.; Takagi, M.; Kaneda, K.; Watanabe, H.; Dairi, T.; Seto, H. Studies on the nonmevalonate pathway: conversion of 4-(cytidine 5'-diphospho)-2-C-methyl-D-erythritol to its 2-phospho derivative by 4-(cytidine 5'-diphospho)-2-C-methyl-D-erythritol kinase. *Tetrahedron Lett.*, **2000**, *41*, 2925-2928.

(23)   Takagi, M.; Kuzuyama, T.; Kaneda, K.; Watanabe, H.; Dairi, T.; Seto, H. Studies
on the nonmevalonate pathway: formation of 2-C-methyl-D-erythritol 2,4-
cyclodiphosphate from 2-phospho-4-(cytidine 5'-diphospho)-2-C-methyl-D-
erythritol. *Tetrahedron Lett.*, **2000**, *41*, 3395-3398.

(24)   Herz, S.; Wungsintaweekul, J.; Schuhr, C. A.; Hecht, S.; Luttgen, H.; Sagner, S.;
Fellermeier, M.; Eisenreich, W.; Zenk, M. H.; Bacher, A.; Rohdich, F.
Biosynthesis of terpenoids: YgbB protein converts 4-diphosphocytidyl-2C-
methyl-D-erythritol 2-phosphate to 2C-methyl-D-erythritol 2,4-cyclodiphosphate.
Proc. Natl. Acad. Sci. U S A, **2000**, *97*, 2486-90.

(25)   Hecht, S.; Eisenreich, W.; Adam, P.; Amslinger, S.; Kis, K.; Bacher, A.; Arigoni,
D.; Rohdich, F. Studies on the nonmevalonate pathway to terpenes: the role of the
GcpE (IspG) protein. *Proc. Natl. Acad. Sci. U S A*, **2001**, *98*, 14837-42.

(26)   Zepeck, F.; Grawert, T.; Kaiser, J.; Schramek, N.; Eisenreich, W.; Bacher, A.;
Rohdich, F. Biosynthesis of isoprenoids. purification and properties of IspG
protein from Escherichia coli. *J. Org. Chem.*, **2005**, *70*, 9168-74.

(27)   Seemann, M.; Wegner, P.; Schunemann, V.; Bui, B. T.; Wolff, M.; Marquet, A.;
Trautwein, A. X.; Rohmer, M. Isoprenoid biosynthesis in chloroplasts via the
methylerythritol phosphate pathway: the (E)-4-hydroxy-3-methylbut-2-enyl
diphosphate synthase (GcpE) from Arabidopsis thaliana is a [4Fe-4S] protein. *J.
Biol. Inorg. Chem.*, **2005**, *10*, 131-7.

(28)   Brandt, W.; Dessoy, M. A.; Fulhorst, M.; Gao, W.; Zenk, M. H.; Wessjohann, L.
A. A proposed mechanism for the reductive ring opening of the cyclodiphosphate
MEcPP, a crucial transformation in the new DXP/MEP pathway to isoprenoids
based on modeling studies and feeding experiments. *Chembiochem*, **2004**, *5*, 311-
23.

(29)   Rohdich, F.; Hecht, S.; Gartner, K.; Adam, P.; Krieger, C.; Amslinger, S.;
Arigoni, D.; Bacher, A.; Eisenreich, W. Studies on the nonmevalonate terpene
biosynthetic pathway: metabolic role of IspH (LytB) protein. *Proc. Natl. Acad.
Sci. U S A*, **2002**, *99*, 1158-63.

(30)   Altincicek, B.; Duin, E. C.; Reichenberg, A.; Hedderich, R.; Kollas, A. K.; Hintz,
M.; Wagner, S.; Wiesner, J.; Beck, E.; Jomaa, H. LytB protein catalyzes the
terminal step of the 2-C-methyl-D-erythritol-4-phosphate pathway of isoprenoid
biosynthesis. *FEBS Lett.*, **2002**, *532*, 437-40.

(31)   Wolff, M.; Seemann, M.; Tse Sum Bui, B.; Frapart, Y.; Tritsch, D.; Garcia
Estrabot, A.; Rodriguez-Concepcion, M.; Boronat, A.; Marquet, A.; Rohmer, M.
Isoprenoid biosynthesis via the methylerythritol phosphate pathway: the (E)-4-

hydroxy-3-methylbut-2-enyl diphosphate reductase (LytB/IspH) from Escherichia coli is a [4Fe-4S] protein. *FEBS Lett.*, **2003**, *541*, 115-20.

(32)   van Heijenoort, J. In *New Comprehensive Biochemistry*; Ghuysen, J.-M., Hakenbeck, R., Eds.; Elsevier Science B.V.: Amsterdam, 1994; Vol. 27.

(33)   Skarzynski, T.; Kim, D. H.; Lees, W. J.; Walsh, C. T.; Duncan, K. Stereochemical course of enzymatic enolpyruvyl transfer and catalytic conformation of the active site revealed by the crystal structure of the fluorinated analogue of the reaction tetrahedral intermediate bound to the active site of the C115A mutant of MurA. *Biochemistry*, **1998**, *37*, 2572-7.

(34)   Marquardt, J. L.; Brown, E. D.; Lane, W. S.; Haley, T. M.; Ichikawa, Y.; Wong, C. H.; Walsh, C. T. Kinetics, stoichiometry, and identification of the reactive thiolate in the inactivation of UDP-GlcNAc enolpyruvoyl transferase by the antibiotic fosfomycin. *Biochemistry*, **1994**, *33*, 10646-51.

(35)   Shoji, J.; Kato, T.; Hinoo, H.; Hattori, T.; Hirooka, K.; Matsumoto, K.; Tanimoto, T.; Kondo, E. Production of fosfomycin (phosphonomycin) by *Pseudomonas syringae*. *J. Antibiot. (Tokyo)*, **1986**, *39*, 1011-2.

(36)   Hendlin, D.; Stapley, E. O.; Jackson, M.; Wallick, H.; Miller, A. K.; Wolf, F. J.; Miller, T. W.; Chaiet, L.; Kahan, F. M.; Foltz, E. L.; Woodruff, H. B.; Mata, J. M.; Hernandez, S.; Mochales, S. Phosphonomycin, a new antibiotic produced by strains of streptomyces. *Science*, **1969**, *166*, 122-3.

(37)   Hidaka, T.; Goda, M.; Kuzuyama, T.; Takei, N.; Hidaka, M.; Seto, H. Cloning and nucleotide sequence of fosfomycin biosynthetic genes of *Streptomyces wedmorensis*. *Mol. Gen. Genet.*, **1995**, *249*, 274-80.

(38)   Kuzuyama, T.; Seki, T.; Kobayashi, S.; Hidaka, T.; Seto, H. Cloning and expression in *Escherichia coli* of 2-hydroxypropylphosphonic acid epoxidase from the fosfomycin-producing organism, *Pseudomonas syringae* PB-5123. *Biosci. Biotechnol. Biochem.*, **1999**, *63*, 2222-2224.

(39)   Woodyer, R. D.; Shao, Z.; Thomas, P. M.; Kelleher, N. L.; Blodgett, J. A.; Metcalf, W. W.; van der Donk, W. A.; Zhao, H. Heterologous production of fosfomycin and identification of the minimal biosynthetic gene cluster. *Chem. Biol.*, **2006**, *13*, 1171-82.

(40)   Liu, S.; Lu, Z.; Jia, Y.; Dunaway-Mariano, D.; Herzberg, O. Dissociative phosphoryl transfer in PEP mutase catalysis: structure of the enzyme/sulfopyruvate complex and kinetic properties of mutants. *Biochemistry*, **2002**, *41*, 10270-6.

(41)   Hildebrand, R. L. *The Role of Phosphonates in Living Systems*; CRC Press Inc.: Boca Raton, FL, 1983.

(42)   Bowman, E.; McQueney, M.; Barry, R.; Dunaway-Mariano, D. Catalysis and thermodynamics of the phosphoenolpyruvate/phosphonopyruvate rearrangement. Entry into the phosphonate class of naturally occurring organophosphorus compounds. *J. Am. Chem. Soc.*, **1988**, *110*, 5575-6.

(43)   Nakashita, H.; Watanabe, K.; Hara, O.; Hidaka, T.; Seto, H. Studies on the biosynthesis of bialaphos. Biochemical mechanism of C-P bond formation: discovery of phosphonopyruvate decarboxylase which catalyzes the formation of phosphonoacetaldehyde from phosphonopyruvate. *J. Antibiot. (Tokyo)*, **1997**, *50*, 212-9.

(44)   Woodyer, R. D.; Li, G.; Zhao, H.; van der Donk, W. A. New insight into the mechanism of methyl transfer during the biosynthesis of fosfomycin. *Chem. Commun. (Camb)*, **2007**, 359-61.

(45)   Kuzuyama, T.; Hidaka, T.; Kamigiri, K.; Imai, S.; Seto, H. Studies on the biosynthesis of fosfomycin. 4. The biosynthetic origin of the methyl group of fosfomycin. *J. Antibiot. (Tokyo)*, **1992**, *45*, 1812-4.

(46)   Frey, P. A.; Magnusson, O. T. S-Adenosylmethionine: a wolf in sheep's clothing, or a rich man's adenosylcobalamin? *Chem. Rev.*, **2003**, *103*, 2129-48.

(47)   Sono, M.; Roach, M. P.; Coulter, E. D.; Dawson, J. H. Heme-Containing Oxygenases. *Chem. Rev.*, **1996**, *96*, 2841-2888.

(48)   Ortiz de Montellano, P. R. *Cytochrome P450: Structure, Mechanism, and Biochemistry*; 2 ed.; Plenum: New York, 1995.

(49)   Lange, S. J.; Que, L., Jr. Oxygen activating nonheme iron enzymes. *Curr. Opin. Chem. Biol.*, **1998**, *2*, 159-72.

(50)   Shaik, S.; de Visser, S. P.; Ogliaro, F.; Schwarz, H.; Schroder, D. Two-state reactivity mechanisms of hydroxylation and epoxidation by cytochrome P-450 revealed by theory. *Curr. Opin. Chem. Biol.*, **2002**, *6*, 556-67.

(51)   Costas, M.; Mehn, M. P.; Jensen, M. P.; Que, L., Jr. Dioxygen activation at mononuclear nonheme iron active sites: enzymes, models, and intermediates. *Chem. Rev.*, **2004**, *104*, 939-86.

(52)   Liu, P.; Murakami, K.; Seki, T.; He, X.; Yeung, S. M.; Kuzuyama, T.; Seto, H.; Liu, H. Protein purification and function assignment of the epoxidase catalyzing the formation of fosfomycin. *J. Am. Chem. Soc.*, **2001**, *123*, 4619-20.

(53) Liu, P.; Liu, A.; Yan, F.; Wolfe, M. D.; Lipscomb, J. D.; Liu, H. W. Biochemical and spectroscopic studies on (S)-2-hydroxypropylphosphonic acid epoxidase: a novel mononuclear non-heme iron enzyme. *Biochemistry*, **2003**, *42*, 11577-86.

(54) Knapp, M. J.; Rickert, K.; Klinman, J. P. Temperature-dependent isotope effects in soybean lipoxygenase-1: correlating hydrogen tunneling with protein dynamics. *J. Am. Chem. Soc.*, **2002**, *124*, 3865-74.

(55) Glickman, M. H.; Klinman, J. P. Lipoxygenase reaction mechanism: demonstration that hydrogen abstraction from substrate precedes dioxygen binding during catalytic turnover. *Biochemistry*, **1996**, *35*, 12882-92.

(56) Koehntop, K. D.; Emerson, J. P.; Que, L., Jr. The 2-His-1-carboxylate facial triad: a versatile platform for dioxygen activation by mononuclear non-heme iron(II) enzymes. *J. Biol. Inorg. Chem.*, **2005**, *10*, 87-93.

(57) Brown, C. D.; Neidig, M. L.; Neibergall, M. B.; Lipscomb, J. D.; Solomon, E. I. VTVH-MCD and DFT studies of thiolate bonding to [FeNO]7/[FeO2]8 complexes of isopenicillin N synthase: substrate determination of oxidase versus oxygenase activity in nonheme Fe enzymes. *J. Am. Chem. Soc.*, **2007**, *129*, 7427-38.

(58) Ghisla, S.; Entsch, B.; Massey, V.; Husein, M. On the structure of flavin-oxygen intermediates involved in enzymatic reactions. *Eur. J. Biochem.*, **1977**, *76*, 139-48.

(59) Price, J. C.; Barr, E. W.; Tirupati, B.; Bollinger, J. M., Jr.; Krebs, C. The first direct characterization of a high-valent iron intermediate in the reaction of an alpha-ketoglutarate-dependent dioxygenase: a high-spin FeIV complex in taurine/alpha-ketoglutarate dioxygenase (TauD) from Escherichia coli. *Biochemistry*, **2003**, *42*, 7497-508.

(60) Galonic, D. P.; Barr, E. W.; Walsh, C. T.; Bollinger, J. M., Jr.; Krebs, C. Two interconverting Fe(IV) intermediates in aliphatic chlorination by the halogenase CytC3. *Nat. Chem. Biol.*, **2007**, *3*, 113-6.

(61) Eser, B. E.; Barr, E. W.; Frantom, P. A.; Saleh, L.; Bollinger, J. M., Jr.; Krebs, C.; Fitzpatrick, P. F. Direct Spectroscopic Evidence for a High-Spin Fe(IV) Intermediate in Tyrosine Hydroxylase. *J. Am. Chem. Soc.*, **2007**, *129*, 11334-5.

(62) Mirica, L. M.; Klinman, J. P. The nature of O2 activation by the ethylene-forming enzyme 1-aminocyclopropane-1-carboxylic acid oxidase. *Proc. Natl. Acad. Sci.*, **2008**, *105*, 1814-1819.

(63)   Baldwin, J. E.; Adlington, R. M.; Moroney, S. E.; Field, L. D.; Ting, H. H. Stepwise ring closure in penicillin biosynthesis. Initial b-lactam formation. *J. Chem. Soc., Chem. Commun.*, **1984**, *15*, 984-986.

(64)   Baldwin, J. E.; Bradley, M. Isopenicillin N synthase: mechanistic studies. *Chem. Rev.*, **1990**, *90*, 1079-1088.

(65)   Francisco, W. A.; Tian, G.; Fitzpatrick, P. F.; Klinman, J. P. Oxygen-18 Kinetic Isotope Effect Studies of the Tyrosine Hydroxylase Reaction: Evidence of Rate Limiting Oxygen Activation. *J. Am. Chem. Soc.*, **1998**, *120*, 4057 - 4062.

(66)   Adams, D. O.; Yang, S. F. Ethylene biosynthesis: Identification of 1-aminocyclopropane-1-carboxylic acid as an intermediate in the conversion of methionine to ethylene. *Proc. Natl. Acad. Sci.*, **1979**, *76*, 170-174.

(67)   Zhou, J.; Rocklin, A. M.; Lipscomb, J. D.; Que, L., Jr.; Solomon, E. I. Spectroscopic studies of 1-aminocyclopropane-1-carboxylic acid oxidase: molecular mechanism and CO_2 activation in the biosynthesis of ethylene. *J. Am. Chem. Soc.*, **2002**, *124*, 4602-9.

(68)   Solomon, E. I.; Brunold, T. C.; Davis, M. I.; Kemsley, J. N.; Lee, S. K.; Lehnert, N.; Neese, F.; Skulan, A. J.; Yang, Y. S.; Zhou, J. Geometric and electronic structure/function correlations in non-heme iron enzymes. *Chem. Rev.*, **2000**, *100*, 235-350.

(69)   Zhao, Z.; Liu, P.; Murakami, K.; Kuzuyama, T.; Seto, H.; Liu, H. W. Mechanistic studies of HPP epoxidase: configuration of the substrate governs its enzymatic fate. *Angew. Chem. Int. Ed.*, **2002**, *41*, 4529-32.

(70)   Itoh, N.; Kusaka, M.; Hirota, T.; Nomura, A. Microbial production of antibiotic fosfomycin by a stereoselective epoxidation and its formation mechanism. *Applied Microbiology and Biotechnology*, **1995**, *43*, 394-401.

(71)   Stengel, D.; Gorzer, E.; Schintler, M.; Legat, F. J.; Amann, W.; Pieber, T.; Ekkernkamp, A.; Graninger, W. Second-line treatment of limb-threatening diabetic foot infections with intravenous fosfomycin. *J. Chemother.*, **2005**, *17*, 527-35.

(72)   Ko, K. S.; Suh, J. Y.; Peck, K. R.; Lee, M. Y.; Oh, W. S.; Kwon, K. T.; Jung, D. S.; Lee, N. Y.; Song, J. H. In vitro activity of fosfomycin against ciprofloxacin-resistant or extended-spectrum beta-lactamase-producing *Escherichia coli* isolated from urine and blood. *Diagn. Microbiol. Infect. Dis.*, **2007**, *58*, 111-5.

(73)   Nakazawa, H.; Kikuchi, Y.; Honda, T.; Isago, T.; Nozaki, M. Enhancement of antimicrobial effects of various antibiotics against methicillin-resistant

Staphylococcus aureus (MRSA) by combination with fosfomycin. *J. Infect. Chemother.*, **2003**, *9*, 304-9.

(74)   Cassone, M.; Campanile, F.; Pantosti, A.; Venditti, M.; Stefani, S. Identification of a variant "Rome clone" of methicillin-resistant *Staphylococcus aureus* with decreased susceptibility to vancomycin, responsible for an outbreak in an intensive care unit. *Microb. Drug. Resist.*, **2004**, *10*, 43-9.

Chapter 2: Mechanistic Investigations of DXR with Fluorinated Analogues

2.1. INTRODUCTION

Terpenoids are a large family of natural products comprised of over 35,000 distinct compounds.[1] They are widely distributed in nature and are rich in biological activities, including light harvesting pigments,[2] growth hormones,[3] and signal transduction.[4] The terpenoid building block is a 5-carbon unit known as isoprene, which has long been established to be derived from acetate via the mevalonate pathway.[5] However, a new isoprene biosynthetic pathway has recently been discovered in eubacteria, archeabacteria, algae, and in the plastids of plants where the isoprenoid unit is formed independently of mevalonate.[6-8] This non-mevalonate pathway operates in eubacteria, archeabacteria, algae, and the plastids of plants but is absent in mammals.[4-6]

The initial precursors of the pathway are pyruvate and glyceraldehyde-3-phosphate, which condense to form 2-*C*-1-deoxy-d-xylulose-5-phosphate (DXP, **1**).[9,10] DXP is also required for the biosynthesis of the pyridoxal ring of vitamin B_6 and is incorporated into the thiazole ring of vitamin B_1.[11-13] Therefore, the conversion of DXP to methyl-D-erythritol 4-phosphate (MEP, **2**) catalyzed by DXP reductoisomerase (DXR) comprises the first committed step of the non-mevalonate pathway (MEP pathway).[14]
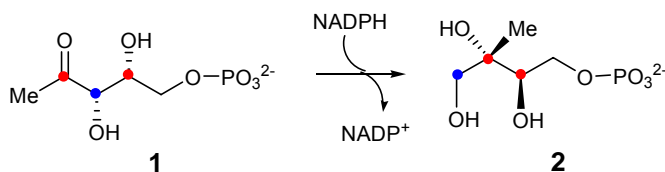
Figure 2-1: Reaction catalyzed by DXR.

Since this pathway is absent in mammals but is essential for many pathogens, including *Plasmodium falciparum*[15] and *Mycobacterium tuberculosis*,[16] all enzymes in this pathway are potential antibacterial targets.[17] This has been demonstrated by the action of the antibiotic fosmidomycin (**3**),[18,19] which inhibits isoprenoid biosynthesis by binding to DXR.[20,21] In clinical trials, fosmidomycin has been shown to clinically and parasitologically cure patients after 7 days of treatment.[22] As the design of a more specific inhibitor for this enzyme depends on a detailed understanding of its mode of action, we have taken effort to investigate the mechanism of the DXR catalyzed reaction.[23]
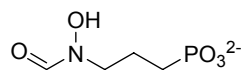
3

Figure 2-2: **Structure of fosmidomycin (3).**

The reaction catalyzed by DXR is the isomerization of DXP (**1**) to methylerythrose phosphate (**4**), followed by the reduction of the aldehyde by NADPH yielding MEP (**2**). As shown in **Figure 2-3**, there are two plausible mechanisms for the rearrangement step catalyzed by DXR. The first mechanism is an α-ketol rearrangement (route A), which is similar to the mechanism catalyzed by ketol acid reductoisomerase, a key enzyme in the biosynthesis of branched chain amino acids.[24] In route A, deprotonation of the C-3 hydroxyl group followed by a 1,2-migration to yield the aldehyde intermediate, methylerythrose phosphate (**4**), is the key step in the mechanism. The second mechanism proceeds through a retroaldolization/aldolization to produce the same intermediate, methylerythrose phosphate (**4**, Scheme 2, route B). Here the enzyme first catalyzes the cleavage of the C3-C4 bond through a retroaldol reaction to yield a three carbon (**5**) and a two carbon phosphate intermediates (**6**); these intermediates then

40

condense through an aldol reaction to form a new C2-C4 bond and the aldehyde intermediate.

A. α-Ketol Rearrangement
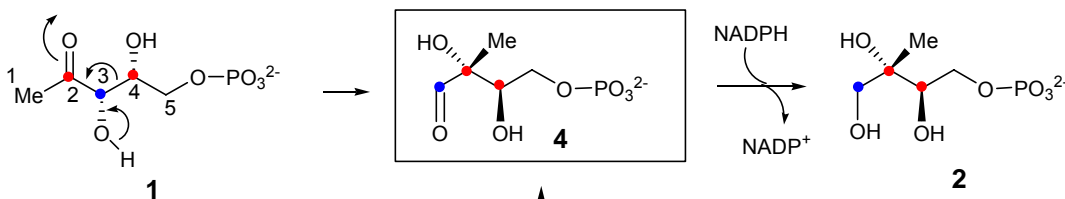
B. Retroaldol/aldol Rearrangement
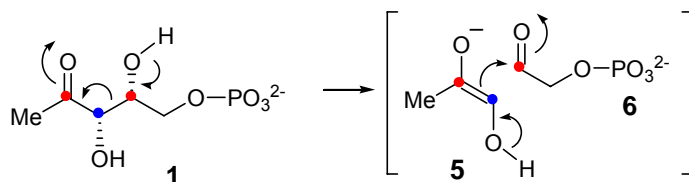
Figure 2-3:   Proposed mechanisms for DXR.

The *Escherichia coli* enzyme, the specific DXR studied herein, has been shown to proceed via an ordered mechanism in which NADPH binds before DXP, and NADP⁺ is released after the discharge of MEP.[25] However, a random mechanism has recently been determined for the *Mycobacterium tuberculosis* enzyme.[16] Due to the significant differences in K_m of the substrates in the forward and reverse reaction, a preferred order of binding exists in the latter case rendering its mechanism effectively similar to that of the *E. coli* enzyme. Early studies have also established that the C-1 *pro-S* hydrogen in MEP (**2**) is derived from H-3 of DXP (**1**),[26,27] and the hydride transfer from NADPH is *pro-S* specific.[16,26,28] In addition, several crystal structures of DXR from various organisms have been determined.[29-34] Despite the advances made thus far in understanding of the catalytic properties of DXR, it remains elusive whether catalysis is best described by route A or route B. In an attempt to gain more insight into this

41

intriguing catalysis, two fluorinated substrate analogues were prepared, 3F-DXP (**7**) and 4F-DXP (**8**), and were examined for their competence as substrates or inhibitors upon incubation with DXR.
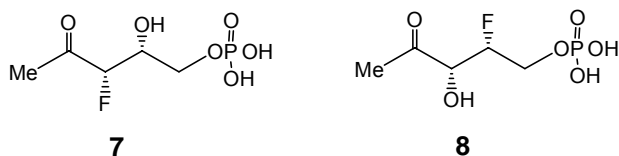
Figure 2-4: **Structures of 3F-DXP (7) and 4F-DXP (8).**

A key difference between the two proposed mechanisms is the involvement of the two hydroxyl groups. The C3-hydroxyl group is essential for catalysis in both rearrangement mechanisms. If this hydroxyl group is replaced by a fluorine (such **7**) no chemistry can take place according to the α-ketol rearrangement. In contrast, this compound can still undergo the initial retroaldol reaction in the retroaldol/aldol rearrangement but will not be able to catalyze the subsequent aldol condensation to form the new C2-C4 bond. Due to the expected endergonic nature of the initial retroaldol reaction, the equilibrium would favor the DXP analogue, resulting in no observable chemistry. The two mechanisms differ significantly in the involvement of the C4-hydroxyl group in the rearrangement reaction. For the α-ketol rearrangement, the C4-hydroxyl group has no direct role in catalysis. Thus, when this hydroxyl group is replaced by a fluorine (**8**), the rearrangement reaction and the following reduction reaction should still proceed to generate the corresponding product. In the retroaldol/aldol rearrangement reaction, the C4-hydroxyl group is crucial for the initial retroaldol reaction. During the cleavage of the C3-C4 bond, the C4-hydroxyl group is believed to be deprotonated in order to neutralize the resulting C4-carbocation. When the

C4-hydroxyl group is removed, the inability to stabilize the resulting C4-carbocation will prevent the reaction from taking place.

To further probe this interesting reaction, we envisioned that a fluoromethyl analogue of MEP, a phosphate mono-((2S,3S)-3-fluoromethyl-2,4-dihydroxy-3-methyl-butyl) ester (FCH$_2$-MEP, **9**), may be a DXR inactivator whose mode of action could also shed light on the catalytic mechanism of DXR. Thus far, all of the inhibitors that have been tested for DXR are either DXP (**1**) or fosmidomycin (**3**) analogues.[25,35-42] Interestingly, while the DXR reaction is reversible, there are no report of MEP (**2**) analogues as inhibitors for this enzyme.[25] There is also no compound known to irreversibly inactivate DXR in a mechanistically relevant manner. To explore this new avenue for elucidating the mechanism of DXR and for controlling its catalyzed reaction, compound **9** was designed as a possible MEP-based suicide inhibitor. If DXR proceeds via the α-ketol rearrangement mechanism (Scheme 2, route A), compound **9** may simply act as a competitive inhibitor against MEP (**2**) when the DXR reaction is run in the reverse direction (**2** → **1**). The primary alcohol would be oxidized by NADP$^+$ to the aldehyde intermediate, and then no further chemistry would be able to take place. In contrast, if a retroaldol/aldol mechanism (Scheme 2, route B) is followed, compound **9** may covalently modify DXR and irreversibly inactivate its activity.

The possible scenarios of inactivation of DXR by **9** are depicted in **Figure 2-5**. When the reaction is run in the DXP (**1**) formation direction, FCH$_2$-MEP (**9**) will be first oxidized to the corresponding aldehyde (**10**), which then proceeds through the same retroaldol mechanism, as MEP would, to cleave the C2-C3 bond. Because the subsequent aldol condensation cannot occur in this case, the resulting 4-C fragment **11** may instead undergo fluoride elimination to yield the Michael acceptor **13**.[43] As shown in path A, this intermediate may trap an active site nucleophile resulting in the inactive,

covalently modified enzyme, **14**.[44]   Alternatively, a 1,4-reduction of **13** by NADPH (generated *in situ*) to give **15** followed by aldol condensation with **12** could generate **16** (path B),[45] which, in equilibrium with **15** and **12**, may be released as the turnover product(s).
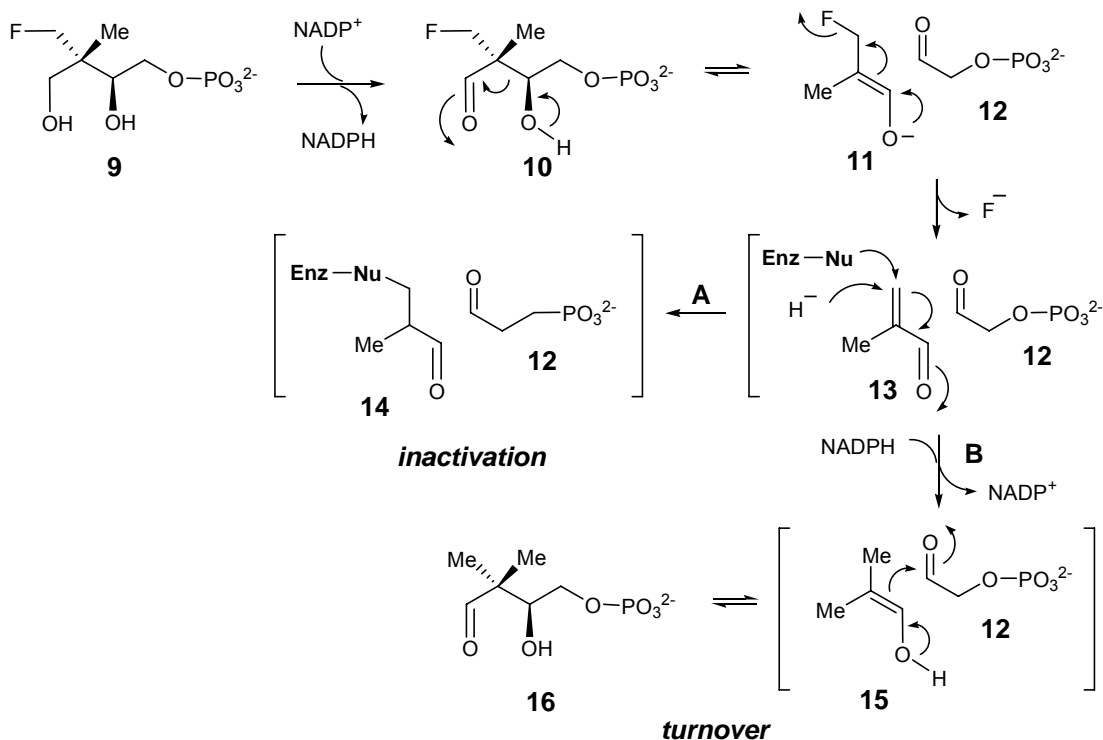
Figure 2-5:   Proposed inactivation mechanism of FCH$_2$-MEP.

Herein, we present our investigation of 3F-DXP (**7**) and 4F-DXP (**8**), which led to the conclusion that both are not substrates of DXR but instead are slow-binding inhibitors. Also reported is the characterization of action of FCH$_2$-MEP (**9**). This compound was found not to be an inactivator of DXR but a weak inhibitor. To investigate the binding of these inhibitors, a FRET binding assay was developed that can be readily modified for high-throughput inhibitor screening.

2.2. MATERIALS AND METHODS

2.2.1. GENERAL. The pET24(+) vector and the overexpression host strain *Escherichia coli* BL21(DE3) were purchased from Novagen Inc. (Madison, WI). Cloned DNA polymerase *Pfu* and GeneClean DNA purification kits were obtained from Stratagene (La Jolla, CA) and Bio 101 Inc. (La Jolla, CA), respectively. Primers used in PCR amplification were customarily prepared by Integrated DNA Technologies, Inc. (Coralville, IA) and used without further purification. Restriction endonucleases were purchased from Invitrogen (Carlsbad, CA). All electrophoretic reagents were obtained from Bio-Rad (Hercules, CA). Culture media were products of Difco (Detroit, MI), and the *Ni*-NTA agarose resin was purchased from Qiagen (Valencia, CA). Fosmidomycin was acquired from Toronto Research Chemicals (North York, ON Canada). All chemicals were purchased from Sigma-Aldrich (St. Louis, MO), or Fisher Scientific (Pittsburgh, PA). DXP and MEP were made through enzymatic synthesis as published,[46,47] except were purified by cellulose chromatography using water and THF as the solvent system. The concentrations of DXP and MEP were determined through a published DXR assay.[25]

2.2.2. CLONING, OVER-EXPRESSION AND PURIFICATION OF DXR. The *E. coli* DXR was cloned into the pET24(+) vector by Ms. Vidusha Devasthali so that the enzyme was expressed with a C-terminal hexa-histidine tag. This resulting plasmid was used to transform *E. coli* BL21(DE3). An overnight culture of the recombinant strain grown in Luria-Bertani (LB) medium supplemented with kanamycin (50 μg/mL) at 37 °C was used to inoculate a 1 L culture of the same medium and antibiotic. These cultures were incubated at 37 °C until the OD_{600} reached 0.45, followed by induction with 1.0 mM isopropyl β-D-thiogalactoside (IPTG) and 3.5 h of additional incubation at 37 °C. The

cells were harvested by centrifugation (6000*g*, 10 min). Purification of this C-terminal His$_6$-tagged protein by *Ni*-NTA agarose resin was performed at 4 °C according to the procedures recommended by the manufacturer, except the elution buffer was 100 mM imidazole. The concentrated purified protein was aliquotted, flash frozen in 30% glycerol, and stored at − 80 °C.

2.2.3. CLONING, OVEREXPRESSION AND PURIFICATION OF DXS.   DXS   was required for the enzymatic synthesis of DXP, and it was amplified from isolated *E. coli* genomic DNA by polymerase chain reaction (PCR) using the forward primer (DXS-1): 5'-GGGAAACATATGAGTTTTGATATTGCC-3', and the reverse primer (DXS-2): 5'-GCGCTC-GAGTGCCAGCCAGGCCTT-3'.   The PCR-amplified DNA fragment was digested with *Nde*I and *Xho*I, and ligated into the *Nde*I/*Xho*I sites of the transcription vector, pET24(+), that had been treated with CIAP to give a recombinant plasmid. This plasmid was used to transform *E. coli* BL21(DE3).   An overnight culture of the recombinant strain grown in Luria-Bertani (LB) medium supplemented with kanamycin (50 μg/mL) at 37 °C was used to inoculate a 1 L culture of the same medium. The culture was incubated at 37 °C until the OD$_{600}$ reached 0.55, followed by induction with 0.5 mM IPTG and 3.5 h of additional incubation at 37 °C.   The cells were harvested by centrifugation (6000*g*, 10 min). Purification of this C-terminal His$_6$-tagged protein by *Ni*-NTA agarose resin was performed at 4 °C according to the procedures recommended by the manufacturer. The concentrated purified protein was aliquotted, flash frozen, and stored at − 80 °C.

2.2.4. ACTIVE SITE TITRATION OF DXR. The   concentration of active DXR was determined via active site titration using NADPH as the titrant. The FRET signal used in

these studies is from an active site tryptophan (Trp212) and the bound NADPH. A 2 mL 100 mM Tris•HCl (pH 7.6) solution containing 2 mM $MgCl_2$ and 3.13 µM DXR (based on Bradford assay) was titrated against a 400 µM NADPH solution. The binding of NADPH to DXR was monitored by the increase in fluorescence of NADPH upon binding to the active site. The titration measurements were conducted with the Fluorolog-3 from Horiba Jobin Yvon (Edison, NJ). The excitation and emission wavelengths were 340 and 458 nm, respectively; and the excitation and emission slit widths were set at 1 and 5 nm, respectively. To correct for the background fluorescence of free NADPH, a control titration without DXR was performed and subtracted from the titration with DXR. This data was then fit, using Grafit 5.0.1, to **Equation 2-1** with F_o, F_∞, E_o and K_D as parameters, where F_o is the starting fluorescence, F_∞ is the final fluorescence, E_o is the total DXR concentration, and S_o is the total NADPH concentration.

Equation 2-1

$$F = F_o + \left(\frac{E_o + S_o + K_D - \sqrt{(E_o + S_o + K_D)^2 - 4E_oS_o}}{2E_o} \right)(F_\infty - F_o)$$

This fit led a DXR concentration of 1.85 ± 0.23 µM, which was then used to determine the stock DXR concentration. This fit also allowed us to deduce a K_D of 0.45 ± 0.15 µM for NADPH, which is very similar to its reported K_m of 0.5 µM.[25]

2.2.5. 3F-DXP AND 4F-DXP INHIBITION STUDY. Enzyme assays were performed at 37 °C following a literature procedure.[25] The reaction mixture contained 200 µL of degassed 100 mM Tris•HCl buffer (pH 7.6), 1 mM $MgCl_2$, 1 mg/mL bovine serum albumin (BSA), 0.15 mM NADPH, 23 nM DXR, and varied concentrations of DXP. The

reaction was initiated by the addition of DXR followed by monitoring the rate of NADPH consumption at 340 nm (ε_{340} = 6.22 mM^{-1}•cm^{-1}). The k_{cat} and K_m for DXP were determined to be 21.3 s^{-1} and 200 µM, respectively, which differ from the literature values of 107 s^{-1} and 115 µM.[25] The low activity is believed to be due to the presence of the C-terminal His$_6$ tag, where the literature values are for the non-tagged enzyme. For the inhibition studies, varied amounts of inhibitor were added to the above reaction mixture minus the DXR, and the resulting solution was incubated at 37 °C in a quartz cuvette for 15 min. The inhibitor concentrations were determined by NMR by comparing the integration of the C-1 methyl signal of 3F-DXP and 4F-DXP to that of a methanol internal standard of known concentration. The rate of NADPH consumption was plotted as the rate of formation of NADP$^+$, and the plot was fitted to **Equation 2-2**, where v_i is the initial velocity, v_{ss} is the steady-state velocity, and k_{obs} is the rate constant going from v_i to v_{ss}.[48]

Equation 2

$$[NADP^+] = \frac{(v_i - v_{ss})}{k_{obs}}\left(1 - e^{-k_{obs}t}\right) + v_{ss}t + C$$

To determine the respective steady-state K_i values, the v_{ss} values from **Equation 2-2** were fit to the equation for competitive inhibition, **Equation 2-3**.

Equation 3

$$v = \frac{V_{max}S}{S + K_{m,s}\left(1 + \dfrac{I}{K_i}\right)}$$

2.2.6. ASSAYS TO INVESTIGATE SLOW-BINDING INHIBITION. Assays were carried out at 24 °C in degassed and N_2 saturated 100 mM Tris•HCl buffer (pH 7.6) containing 2 mM $MgCl_2$, 1 mg/mL BSA, 0.1 mM DTT, 150 μM NADPH, and 975 μM DXP, with varying concentrations of inhibitor (0.0-1.46 mM for 3F-DXP and 0.0-7.8 μM for fosmidomycin). The presence of 0.1 mM DTT in the assay mixture enhanced the linearity of the reaction curve when no inhibitor was present. The reactions were initiated by the addition of enzyme to a final concentration of 25 nM. The reaction was followed by monitoring the rate of NADPH consumption at 340 nm.

The rate of NADPH consumption was plotted as the rate of $NADP^+$ formation, and the plot was fitted to **Equation 2-2**.[48] To obtain the rates constants for the initial inhibition simulations, the plot of k_{obs} versus inhibitor concentration was fitted to **Equation 2-4** for a one-step binding model and to **Equation 2-5** for a two-step binding model, where I is the concentration of inhibitor, S is the concentration of DXP, K_i is the inhibition constant for the initial binding complex, $K_{m,s}$ is the K_m for DXP, and k_6 and k_{-6} are the rate constants of the forward and reverse reactions associated with the step of inhibitor binding to the NADPH•DXR complex (see kinetic model below).

Equation 2-4

$$k_{obs} = k_{-6} + \frac{k_6 I}{\left(1 + \dfrac{S}{K_{m,s}}\right)}$$

Equation 2-5

$$k_{obs} = k_{-6} + \frac{\left(\dfrac{k_6 I}{K_i}\right)}{\left(1 + \dfrac{S}{K_{m,s}} + \dfrac{I}{K_i}\right)}$$

49

Using the information deduced from graphical analysis of the inhibition behavior of 3F-DXP and fosmidomycin, their slow binding nature was further studied by the global simulations of the progress curves to a one-step and a two-step binding mechanism. The initial simulations were performed using the Z-lab program on the family of progress curves recorded at different inhibitor concentrations to deduce the starting rate constants. These rate constants were then used to globally fit the family of progress curves to determine the errors in the rate constants using Dynafit, and to evaluate which binding model yields a better fit.[49] The kinetic mechanism in **Figure 2-6** was used for the simulations, except for the omission of the seventh step, a conformational change, when the one-step binding model was considered. Both the ordered substrate binding mechanism with NADPH binding before DXP, similar to that of the *E. coli* DXR,[25] and a random substrate binding mechanism, analogous to that concluded for the *M. tuberculosis* enzyme,[16] were used for the simulations. The simulations produced similar results irrespective to whether substrate binding is ordered or random; thus for simplification, only the simulations based on an order substrate binding mechanism is described herein.

$$\text{DXR} + \text{NADPH} \underset{k_{-1}}{\overset{k_1}{\rightleftharpoons}} \text{DXR} \bullet \text{NADPH} \qquad \textbf{(1)}$$

$$\text{DXR} \bullet \text{NADPH} + \text{DXP} \underset{k_{-2}}{\overset{k_2}{\rightleftharpoons}} \text{DXR} \bullet \text{NADPH} \bullet \text{DXP} \qquad \textbf{(2)}$$

$$\text{DXR} \bullet \text{NADPH} \bullet \text{DXP} \underset{k_{-3}}{\overset{k_3}{\rightleftharpoons}} \text{DXR} \bullet \text{NADP} \bullet \text{MEP} \qquad \textbf{(3)}$$

$$\text{DXR} \bullet \text{NADP} \bullet \text{MEP} \underset{k_{-4}}{\overset{k_4}{\rightleftharpoons}} \text{DXR} \bullet \text{NADP} + \text{MEP} \qquad \textbf{(4)}$$

$$\text{DXR} \bullet \text{NADP} \underset{k_{-5}}{\overset{k_5}{\rightleftharpoons}} \text{DXR} + \text{NADP} \qquad \textbf{(5)}$$

$$\text{DXR} \bullet \text{NADPH} + \text{I} \underset{k_{-6}}{\overset{k_6}{\rightleftharpoons}} \text{DXR} \bullet \text{NADPH} \bullet \text{I} \qquad \textbf{(6)}$$

$$\text{DXR} \bullet \text{NADPH} \bullet \text{I} \underset{k_{-7}}{\overset{k_7}{\rightleftharpoons}} \text{DXR} \bullet \text{NADPH} \bullet \text{I*} \qquad \textbf{(7)}$$
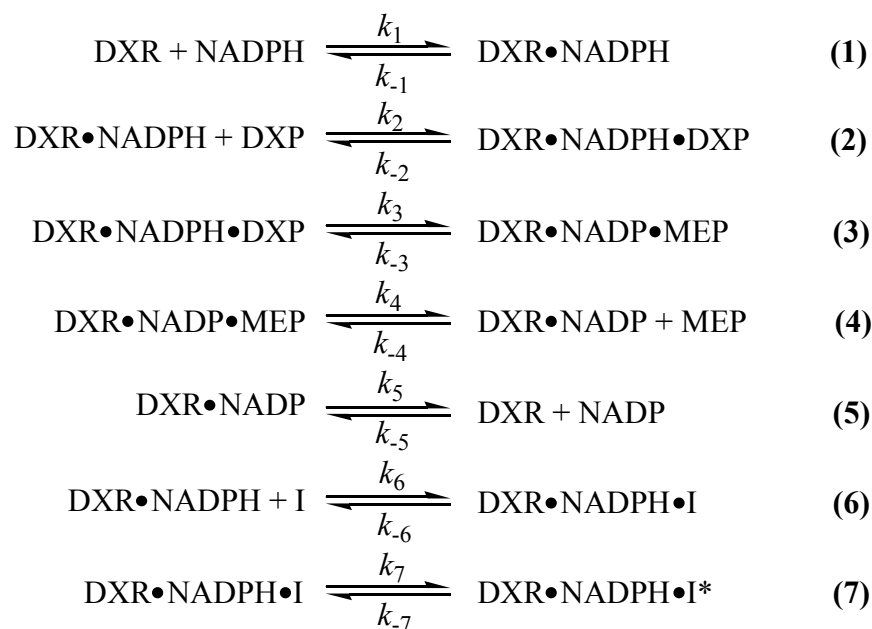
Figure 2- 6: **Kinetic mechanism used for computer simulations.**

In the simulations, it was assumed that substrate binding and product release are not significantly rate-limiting. The rate constants for steps 1 through 5 were fixed in the simulations, and the rate constants for steps 6 and 7 were allowed to float. Since the rate constants for steps 1 through 5 are not explicitly known, their values were approximated based on experimentally determined parameters. The ratio of rate constants for substrate and product binding/dissociation were set to their determined K_d (step 1, 0.5 µM) or K_m (step 2, 200 µM; step 4, 200 µM; step 5, 25 µM) values for steps 1, 2, 4 and 5. The forward and reverse rate constants for step 3 were set to the determined k_{cat} values for the forward (8.15 s^{-1}) and reverse reactions (6.47 s^{-1}) at 24°C. The concentration of DXP was fixed at 975 µM. The concentrations of DXR and NADPH were allowed to locally float.

2.2.7. FCH$_2$-MEP INACTIVATION ANALYSIS. To test if FCH$_2$-MEP could inactivate DXR, 500 nM DXR was incubated at room temperature for 16 h in 100 mM

Tris•HCl buffer (pH 7.6) containing 2 mM MgCl$_2$, 1 mg/mL BSA, 300 μM NADP$^+$, and 1.8 mM FCH$_2$-MEP. An identical solution mixture without FCH$_2$-MEP was incubated for 16 h as a control. An aliquot (10 μL) of each incubation mixture was assayed for activity by adding it to a solution (190 μL) of 150 μM NADPH, 285 μM DXP, 2 mM MgCl$_2$, and 1 mg/mL BSA in 100 mM Tris•HCl buffer, pH 7.6. The concentration of MEP was determined as previously described.

2.2.8. TEST FOR FLUORIDE ELIMINATION BY ^{19}F NMR. To determine if DXR could catalyze the elimination of a fluoride ion from FCH$_2$-MEP (**9**), 10 mM FCH$_2$-MEP was mixed in a NMR tube with 2 mM MgCl$_2$, and 10 mM NADP$^+$ in 100 mM Tris•HCl buffer in D$_2$O (pD 7.8). The ^{19}F NMR spectrum of this sample was recorded. DXR was then added to the mixture to a final concentration of 60 μM, and the solution was incubated at room temperature for 15 h. The ^{19}F NMR spectrum of this sample was recorded at the end of incubation.

2.2.9. TEST OXIDATION OF FCH$_2$-MEP BY NADP$^+$. To determine if DXR can carry out the initial oxidation of the primary hydroxyl group of FCH$_2$-MEP (**9**) to generate the aldehyde intermediate (**10**), the formation of NADPH upon mixing FCH$_2$-MEP, NADP$^+$, MgCl$_2$ and DXR was investigated. A solution of 8.5 mM FCH$_2$-MEP, 1 mM NADP$^+$, 2 mM MgCl$_2$ and 1 mg/mL BSA in 100 mM Tris•HCl buffer pH 7.6 was placed in a cuvette, and the absorbance of the solution at 340 nm was determined. DXR, with a final concentration of 77 μM, was then added to the cuvette, and the solution was monitored at 340 nm for the production of NADPH.

2.2.10. FCH$_2$-MEP INHIBITION STUDIES. The assays were run at 25 °C in degassed and N$_2$ saturated 100 mM Tris•HCl buffer (pH 7.6) containing 2 mM MgCl$_2$, 1 mg/mL BSA, and 400 µM NADP$^+$, 96 µM MEP, and at varying concentrations of FCH$_2$-MEP (**9**, 0-2.9 mM).   The reactions were initiated by the addition of enzyme to a final concentration of 50 nM. All reactions were monitored by following the rate of production of NADPH at 340 nm. The concentrations of MEP and DXR were determined as previously described.

2.2.11. FRET BINDING ASSAY.   The FRET signal used in these studies is the same signal in the active site titration studies. For the FRET titration assays, the excitation wavelength was set at 280 nm, and the emission was set to 444 nm with slit widths of 1 and 3 nm, respectively. Temperature was set to 25 °C by using an electronic temperature controller. The ligands were titrated into a 2 mL solution of 5 µM DXR, 10 µM NADPH and 2 mM MgCl$_2$ in 100 mM Tris•HCl pH 7.6. The solution was stirred during the entire titration with a micro stirbar. The data for the ligands that produced a change in the FRET signal upon binding was fit to the **Equation 2-1** to determine the respective K_d.

For the stopped-flow experiment, one syringe was loaded with 50 µM DXR, 10 µM NADPH and 2 mM MgCl$_2$ in degassed and N$_2$ saturated 100 mM Tris•HCl buffer (pH 7.6), and the other syringe was loaded with 365 µM DXP and 2 mM MgCl$_2$ in the same Tris buffer. The excitation wavelength was set at 280 nm, and a cutoff filter was used to block the emissions of wavelengths shorter than 360 nm. The slit widths were 3 nm for both excitation and emission. The temperature was set to 24 °C.

2.2.12. SYNTHESIS OF FLUORINATED ANALOGUES.   The 3F-DXP (**7**) and 4F-DXP (**8**) were first synthesized by Dr. Alex Wong, who was assisted by Ms. Vidusha

Devasthali, and their schemes are displayed in **Figures 2-7** and **2-8**, respectively. For the slow-binding experiments, more 3F-DXP was needed, so I repeated the first two-thirds of the synthesis, and Dr. Gang Dong completed the 3F-DXP synthesis. The synthesis of FCH$_2$-MEP (**9**) was completed by Dr. Xiaotao Pu and was synthesized as described in **Figure 2-9**.
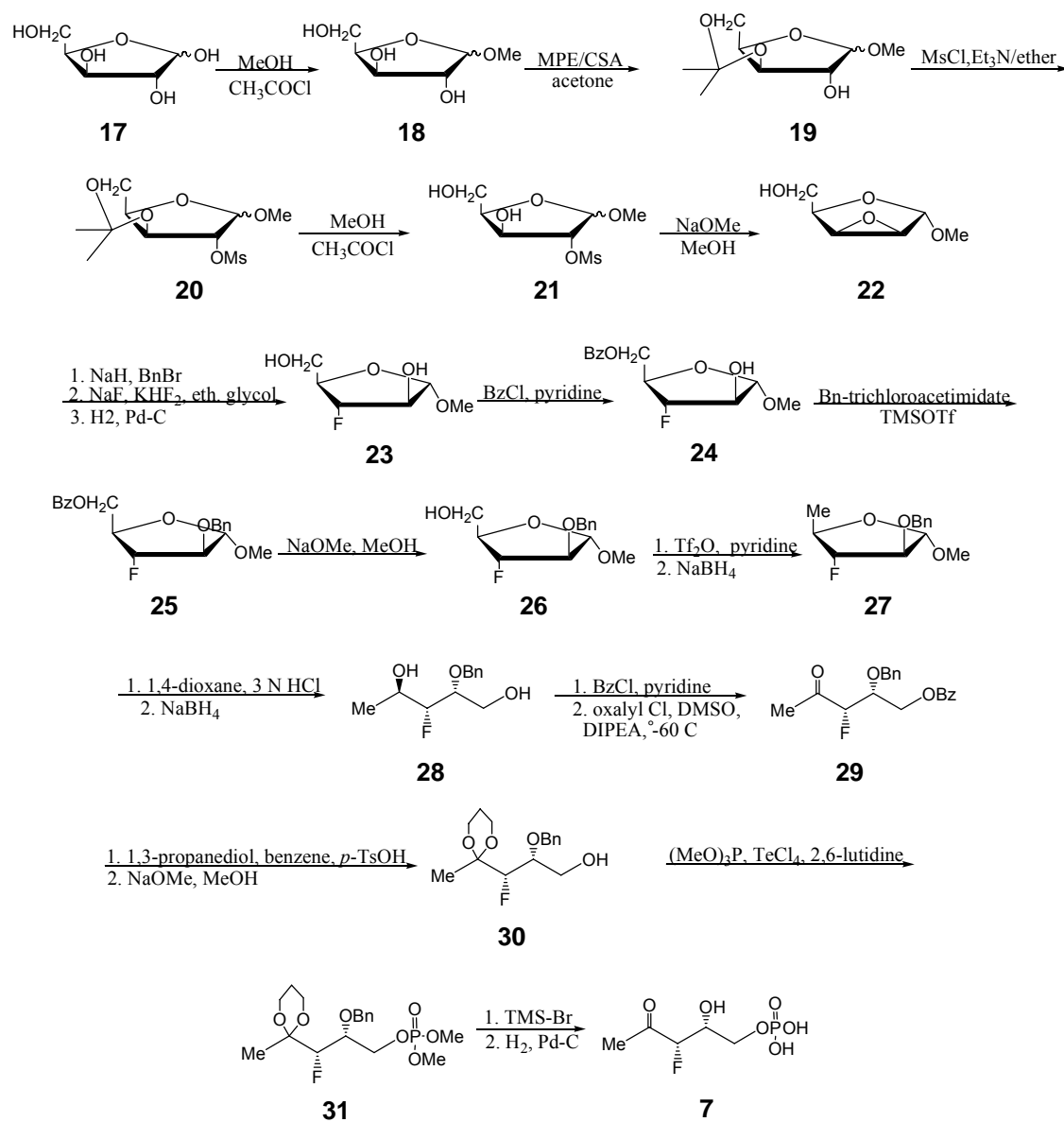
Figure 2-7: Synthetic scheme for 3F-DXP (**7**).
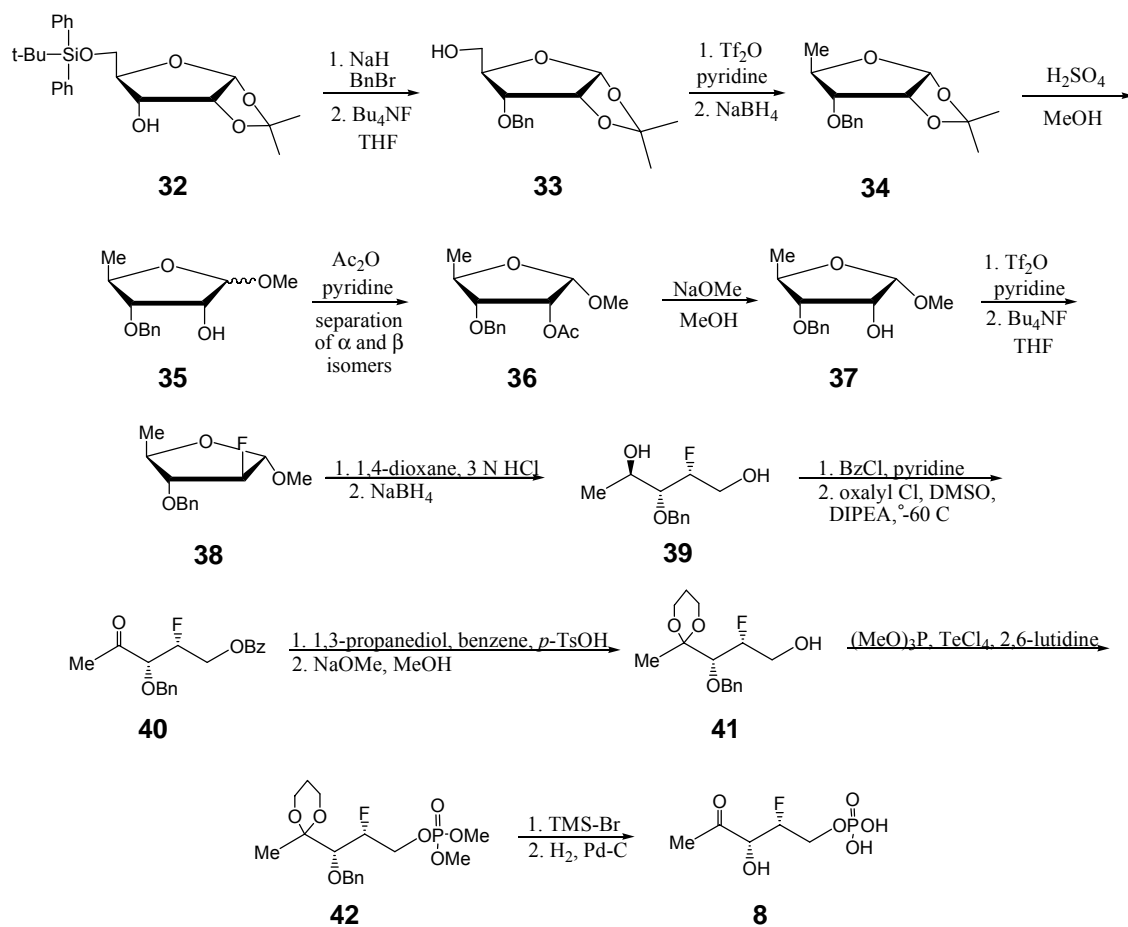
Figure 2-8: Synthetic scheme for 4F-DXP (8).
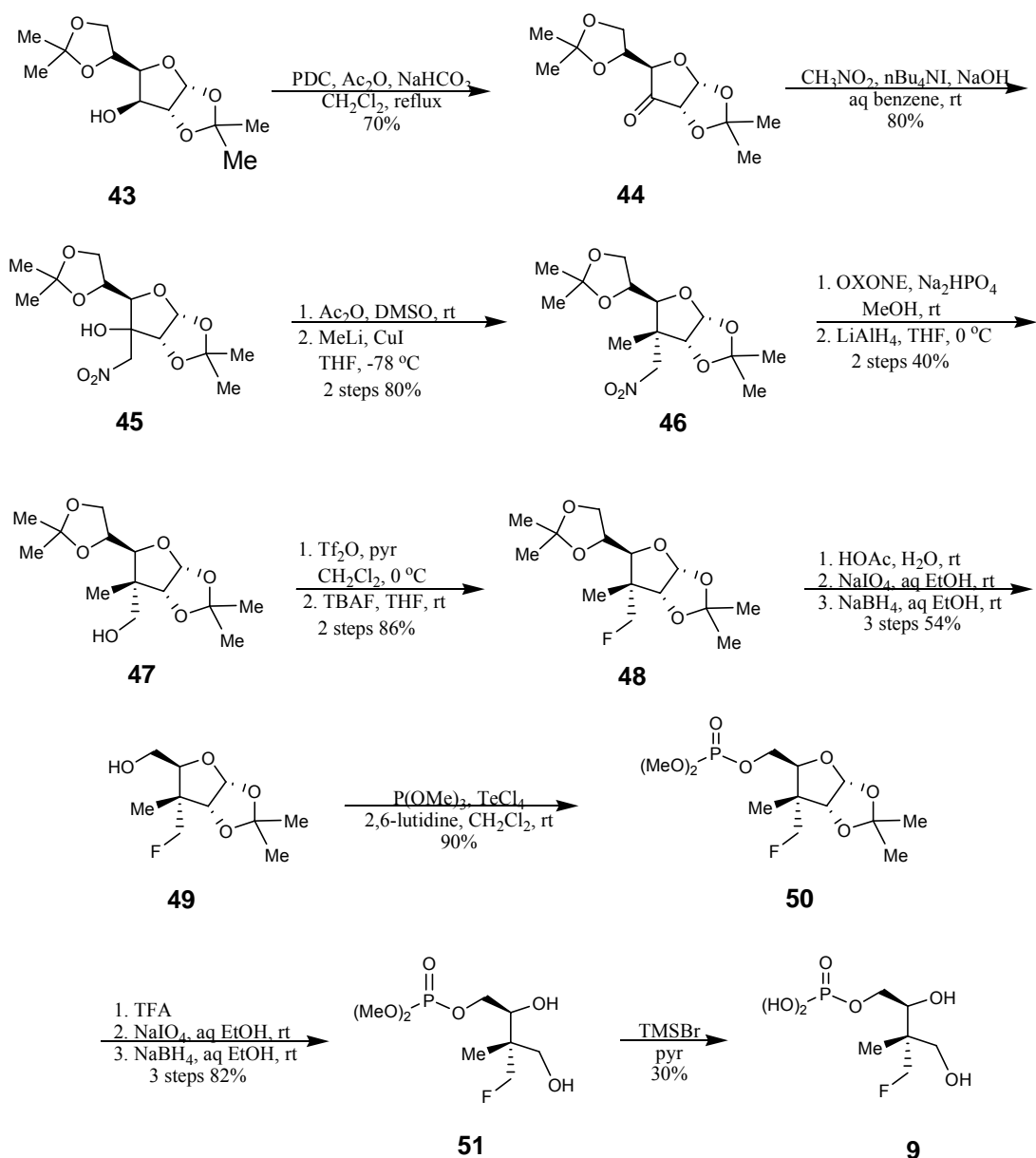
Figure 2-9: Synthetic scheme for FCH₂-MEP (9).

2.3. RESULTS AND DISCUSSION

2.3.1. ANALYSIS OF 3F-DXP AND 4F-DXP AS POSSIBLE SUBSTRATES OF DXR.

When 3F-DXP (0 to 5 mM) was incubated with 150 nM DXR in the presence 2mM MgCl₂ and 150 μM NADPH in 100 mM Tris pH 7.6, no turnover was observed

based on the lack of NADPH oxidation.[23] Under the same conditions, 4F-DXP was tested as a possible substrate of DXR, and it too failed to be turned-over by DXR.[23] Therefore, the substitution of either the C3-hydroxyl group or the C4-hydroxyl of DXP with fluorine results in the loss of activity with respect to DXR.

These observations are consistent with two independent studies, in which 3-deoxy-DXP and 4-deoxy-DXP were examined as possible substrates of *E. coli* DXR.[50,51] It was determined that both are not substrates but mixed-type inhibitors for DXR with K_is of 800 μM and 120 μM, respectively.[50] Since the K_M for DXP was determined in that study to be 97 μM, the K_i for 4-deoxy-DXP is similar in magnitude to the K_M for DXP, yet the K_i for 3-deoxy-DXP is eight-fold higher than the K_M for DXP. The high K_i for 3-deoxy-DXP and the fact that both analogues exhibit mixed-type inhibition, not standard competitive inhibition, raised questions regarding how these analogues bind to DXR. If the removal of a hydroxyl groups prevents proper binding, one may not be able to draw any conclusions to the mechanism of DXR based on these studies. Interestingly, a separate analysis of 3-deoxy-DXP and 4-deoxy-DXP with DXR from *Synechocystis* PCC6803 indicated that both analogues are competitive inhibitors with K_is of 150 and 30 μM, respectively.[51] The K_i for 3-deoxy-DXP is roughly equal to their measured K_M for DXP, while the K_i for 4-deoxy-DXP is roughly six-fold lower than DXP's K_M. This implies that for the DXR from *Synechocystis* PCC6803, both hydroxyl groups are not important for binding but are crucial for chemistry. This conclusion is in favor of the retroaldol/aldol mechanisms over the α-ketol mechanism for the rearrangement reaction catalyzed by DXR. To determine how the substitution of fluorine for each hydroxyl group affects binding, the ability of mode of inhibition of 3F-DXP and 4F-DXP was determined.

2.3.2. Inhibition Analysis of 3F-DXP and 4F-DXP.
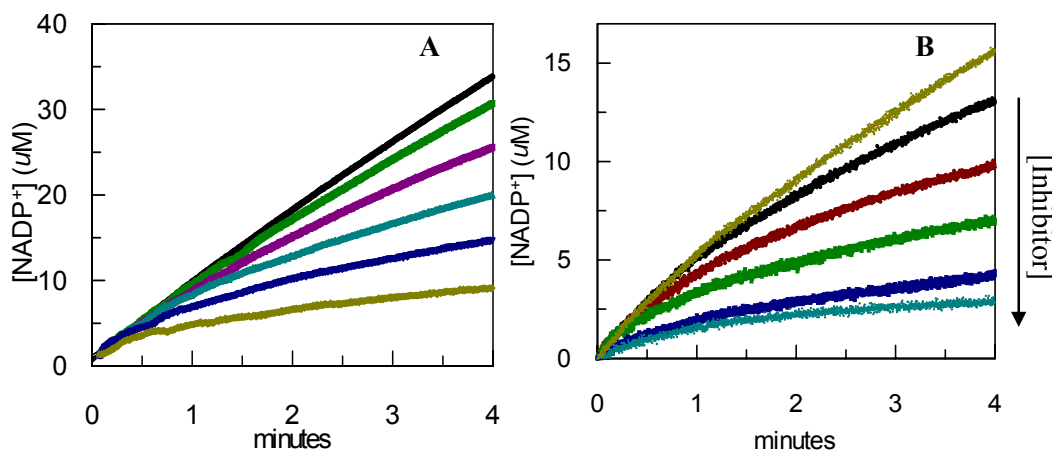
Figure 2-10: Non-linear progress curves with 3F-DXP (A) and 4F-DXP (B).

As seen in **Figure 2-10**, both 3F-DXP and 4F-DXP are inhibitors of DXR. Interestingly, these nonlinear progress curves are characteristic of slow-binding inhibition.[52] For slow-binding inhibitors, the nonlinear progress curves result from initial weak inhibition which slowly converts to strong, steady-state level of inhibition.

When the mode of inhibition for 3F-DXP was analyzed for the steady-state phase (v_{ss} determined from **Equation 2-2**) of the reaction curve, it was determined from the Dixon plot in **Figure 2-11** to exhibit competitive inhibition. To determine the K_i of 3F-DXP, the v_{ss} versus [3F-DXP] curves for each DXP concentration were fitted separately to the standard equation for competitive inhibitors, **Equation 2-3**, which yielded a K_i of 126 ± 21 μM. The pattern for 4F-DXP appears to be the same, but due to its moderate instability, there was too much noise between the curves to determine for sure. When the steady-state phase for each DXP concentration was analyzed separately, and assuming competitive inhibition, a K_i of 224 ± 65 μM was determined for 4F-DXP; due to the moderate instability of 4F-DXP, this value represents the upper limit of the true K_i.
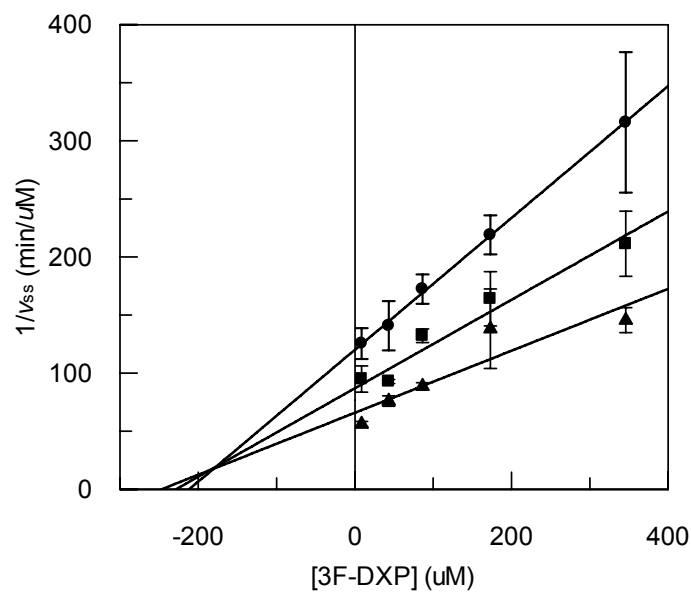
Figure 2-11: Dixon plot of 3F-DXP steady-state phase of inhibition (▲) 100 µM DXP, (■) 75 µM DXP, (●) 50 µM DXP.
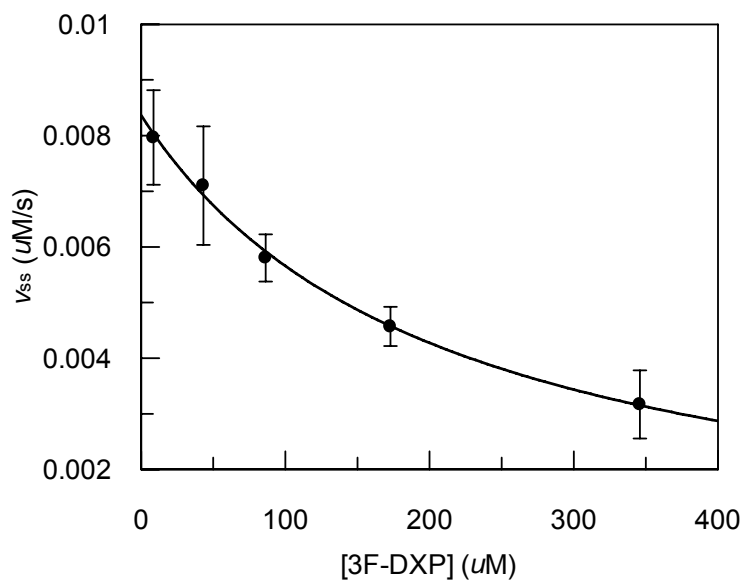
Figure 2-12: 3F-DXP steady-state phase of inhibition fit to Equation 2-3, with DXP at 50 µM.
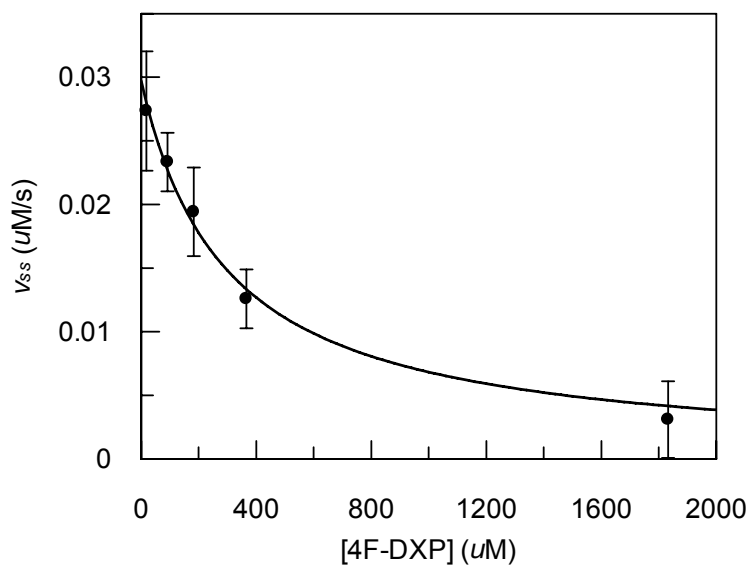
Figure 2-13: **4F-DXP steady-state phase of inhibition fit to Equation 2-3, with DXP at 75 μM.**
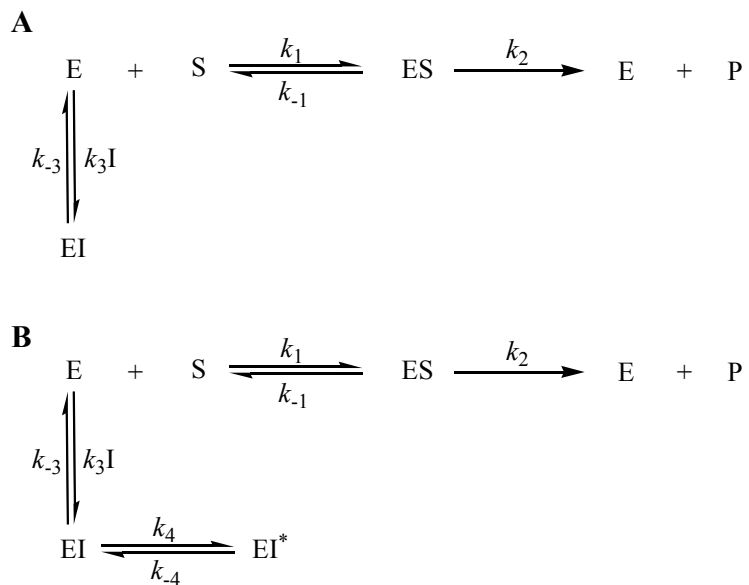
Figure 2-14: **Kinetic mechanisms for slow-binding inhibition.**

As depicted in **Figure 2-14**, there are two possible kinetic mechanism for an inhibitor to display slow-binding inhibition. In mechanism **A**, the inhibitor binds in a

single step, with the rate to equilibrium steady-state inhibition being equal to the sum of $k_3[I]$ and k_{-3}. Therefore, if the inhibitor has a slow on and off rate, it will exhibit slow-binding inhibition. In mechanism **B**, the inhibitor binds weakly in a rapid equilibrium to form E•I. The enzyme-inhibitor complex then undergoes a slow but favorable conformational change to E•I*, which results in tighter inhibition.

To distinguish between the two possible kinetic mechanisms for slow-binding inhibition as shown in **Figure 2-14**, the inhibition experiment for 3F-DXP was repeated at saturating DXP and NADPH to ensure a linear reaction curve over the time scale of the assay. This experiment was not conducted on 4F-DXP due to its moderate instability. To determine how the slow-binding nature of 3F-DXP relates to the previously studied slow-binding inhibitor, fosmidomycin,[25,53,54] these experiments were conducted on fosmidomycin as well. The progress curves were fit to **Equation 2-2**, and the k_{obs} was plotted versus the concentration of inhibitor. If the slow-binding inhibition is the result of a one-step binding mechanism with a slow on and off rates, as shown in **Figure 2-14 A**, then the plot of k_{obs} versus inhibitor concentration should yield a linear relationship. If the inhibitors bind in a two-step mechanism as depicted in **Figure 2-14 B**, there will be a hyperbolic relationship between k_{obs} and inhibitor concentration. For fosmidomycin, the relationship was linear (see **Figure 2-15**), which implies a one-step binding mechanism. However, for 3F-DXP, it was not possible to discriminate between the two possible models. Due to moderate error, the data could be fit to both a linear and a curved line.
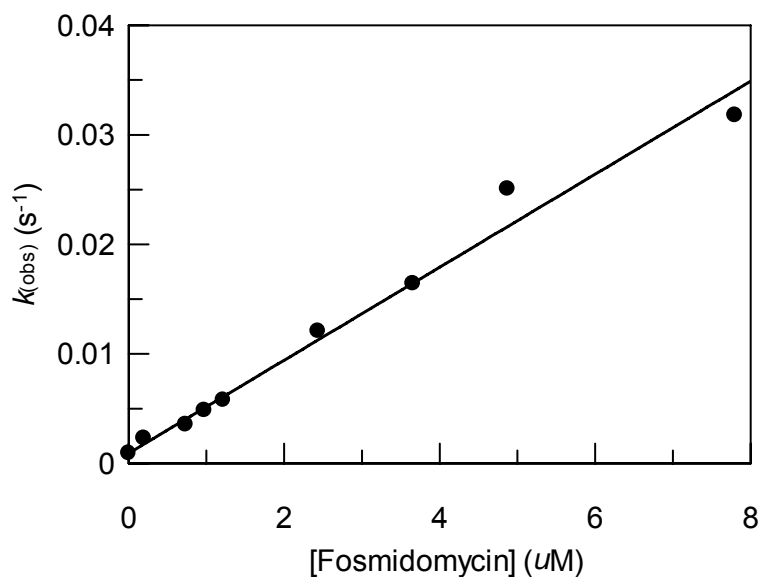
Figure 2-15: Plot of k_{obs} from Equation 2-2 versus [fosmidomycin] and fit to Equation 2-4.

The slow-binding nature of 3F-DXP and fosmidomycin was further explored through global kinetic computer simulations of the progress curves, see **Figure 2-16 and 2-17**. The resulting rate constants and K_i's of the simulations are reported in **Table 2-1**.

Table 2-1: Summary of numerical results from computer simulations.

	One-Step			Two-Step					
	k_6 ($\mu M^{-1}s^{-1}$)	k_{-6} (s^{-1})	K_i	k_6 ($\mu M^{-1}s^{-1}$)	k_{-6} (s^{-1})	K_i	k_7 (s^{-1})	k_{-7} (s^{-1})	K_i^*
3F-DXP	4.84e-5 ± 8e-7	3.88e-3 ± 8e-5	81 ± 2 µM	0.8 ± 30	9000 ± 3e5	11 ± 560 mM	0.5 ± 0.6	3.81e-3 ± 9e-5	80 ± 4000 µM
Fosmidomycin	5.99e-2 ± 8e-4	2.33e-3 ± 5e-5	39 ± 1 nM	6 ± 35	330 ± 110	55 ± 300 µM	3 ± 17	2.4e-3 ± 1e-4	40 ± 290 nM
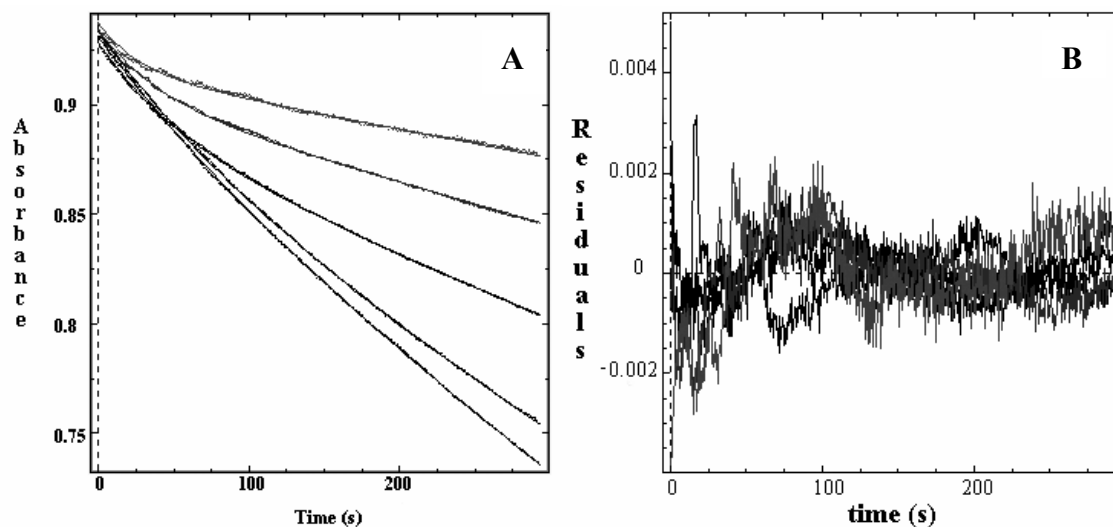
Figure 2-16: **A) Progress curves for 3F-DXP inhibition with corresponding simulation curves from one-step binding mechanism, and B) plot of residuals.**

These simulations concluded that a one-step binding mechanism yielded a better fit to the family of progress curves for both 3F-DXP and fosmidomycin. If 3F-DXP and fosmidomycin both bind in a two-step mechanism, their initial weak K_is should be 11 mM and 55 μM, respectively. With these initial K_i values, the plots of k_{obs} versus inhibitor concentration for both inhibitors will appear linear in the experimental concentration range for both binding mechanisms. Therefore, the plot of k_{obs} versus inhibitor concentration can not be used to distinguish a one-step binding mechanism from a two-step binding mechanism for these two inhibitors. It is through the global fit of the progress curves that these two inhibition mechanisms are distinguished.

63
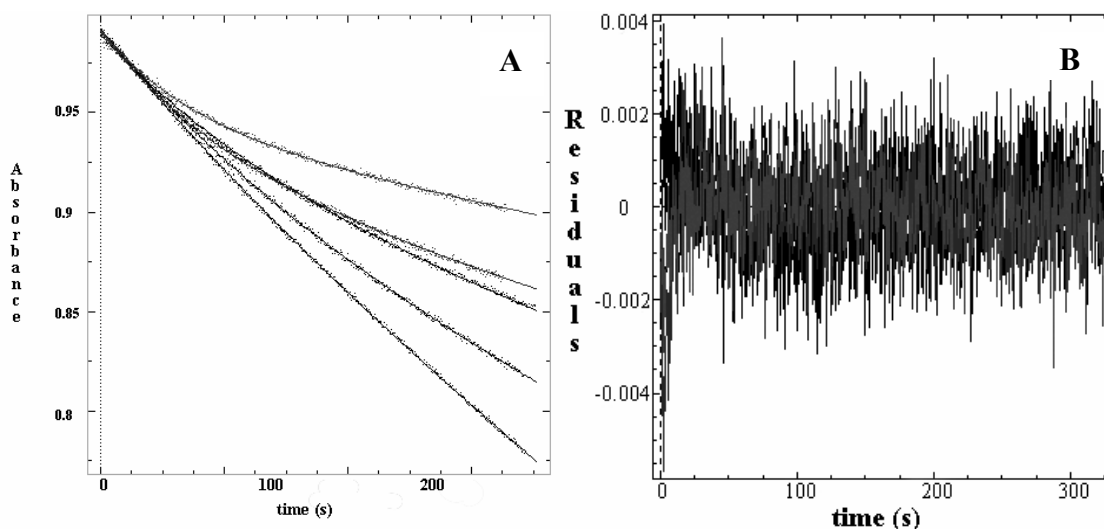
Figure 2-17: **A) Progress curves for fosmidomycin inhibition with corresponding simulation curves from one-step binding mechanism, and B) plot of residuals.**

2.3.3. Analysis of FCH$_2$-MEP as a DXR Inactivator.

To test if FCH$_2$-MEP (**9**) could inactivate DXR, FCH$_2$-MEP was incubated with DXR, NADP$^+$, and MgCl$_2$ overnight at room temperature.[55] An identical incubation without **9** was run in parallel as a control. An aliquot of each incubation mixture was assayed for activity by adding it to a solution containing NADPH, DXP, and MgCl$_2$. No loss in activity was observed as compared to the control. Evidently, this compound is not an irreversible inactivator for DXR.

To determine if DXR could catalyze the elimination of a fluoride ion from FCH$_2$-MEP, FCH$_2$-MEP was mixed in a NMR tube with MgCl$_2$ and NADP$^+$, and the ^{19}F NMR spectrum of this sample was recorded.[55] DXR was then added to this mixture, and the solution was incubated at room temperature overnight. The ^{19}F NMR spectrum of this sample was again recorded, and no new peak in the ^{19}F NMR spectrum was detected. It was determined that no fluoride elimination was not due to DXR's inability to catalyze the retroaldol reaction on **10**, but due to its inability to oxidize FCH$_2$-MEP to **10** using

64

NADP$^+$.[55] This is evident by the lack of NADPH production upon mixing FCH$_2$-MEP with DXR, NADP$^+$ and MgCl$_2$.

The fact that FCH$_2$-MEP is neither a suicide inhibitor nor a substrate for DXR renders it unfit to distinguish the two proposed rearrangement mechanisms for DXR. The inability of DXR to catalyze the initial oxidation of FCH$_2$-MEP, which is a prerequisite for both rearrangement mechanisms, may be ascribed to the increased steric bulk of the fluoromethyl group that may impede the required preorganization of FCH$_2$-MEP in the active site for the oxidation to occur. Interestingly, incubation of FCH$_2$-MEP in the presence of MEP revealed that it is a weak inhibitor against DXR. As shown in **Figure 2-18**, when the reaction was run in the reverse direction with MEP (96 μM, which is roughly half its K_m value) as the substrate, the addition of excess FCH$_2$-MEP (2.9 mM) led to 45% inhibition of the reaction.
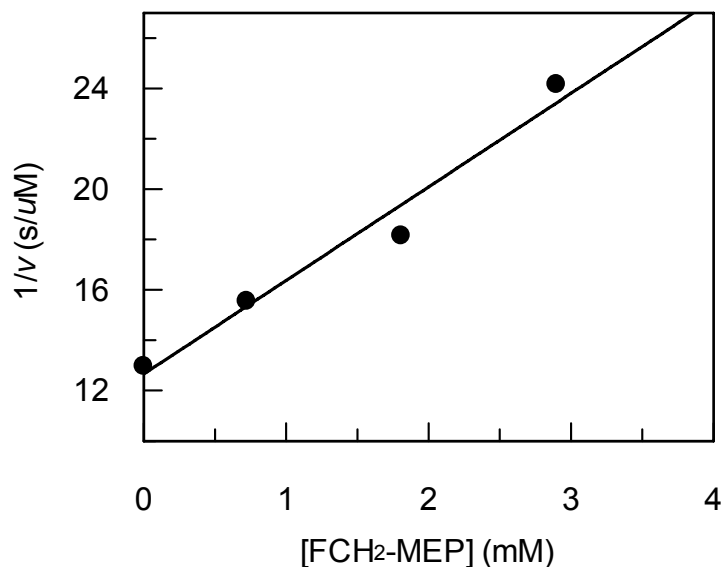
Figure 2-18: Dixon plot showing the inhibition by FCH$_2$-MEP on the formation of DXP catalyzed by DXR. The incubtion mixture contained 40 nM DXR, 400 μM NADP$^+$, 2 mM MgCl$_2$, and 96 μM MEP in 100 mM Tris•HCl buffer, pH 7.6.

2.3.4. FRET Binding Analysis. To explore the binding of the fluorinated analogues to DXR, a binding assay was developed by following the change of the FRET signal from Trp212 and the bound NADPH. To confirm that a FRET signal exists for the DXR•NADPH•Mg^{2+} complex, a fluorescence scan of an NADPH and MgCl$_2$ solution was conducted while exciting at 280 nm. DXR was added to the solution and the scan was repeated, which produced the FRET signal displayed in **Figure 2-19**.
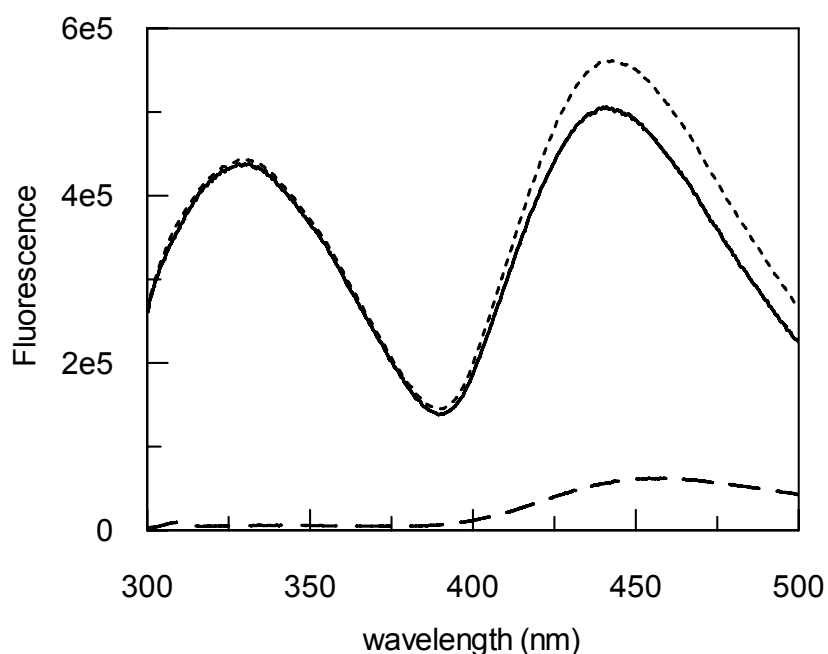
Figure 2-19: **FRET Scans - Dashed line: 2 mM MgCl$_2$, 55 µM NADPH in 100 mM Tris pH 7.6; Dotted line: the same solution but with 50 µM DXR; Solid line: difference spectrum showing the FRET peak at 440 nm.**

When MEP, 4F-DXP and fosmidomycin were titrated into a solution of DXR, NADPH and MgCl$_2$, an increase in the FRET signal was observed, see **Figure 2-20**. This change in FRET signal upon the addition of MEP, 4F-DXP and fosmidomycin was used to determine their respective K_d's to the DXR•NADPH complex, and these values are listed in **Table 2-2**. However, when 3F-DXP, FCH$_2$-MEP or DMAPP (DMAPP is an

66

inhibitor of DXR in the low mM range) was titrated into a solution of DXR, NADPH and MgCl$_2$, no change in the FRET signal was observed.

Table 2-2:   **Summary of analytical results from fitting to Equations 2-1 and 2-3.**

	K_i	K_d
3F-DXP	126 ± 21 µM	ND
4F-DXP	224 ± 65 µM	200 ±12 µM
Fosmidomycin	23 ±10 nM	28 ± 4 nM
DXP	130 ± 40 µM	ND
MEP	165 ± 28 µM	132 ± 6 µM
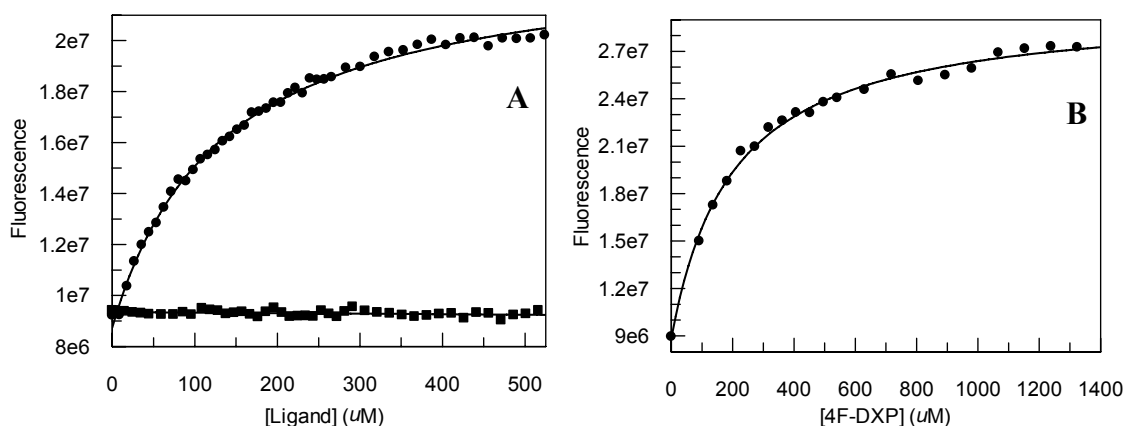
Figure 2-20:   **FRET titration of A: (●) MEP and (■) 3F-DXP; B: 4F-DXP.**

When 3F-DXP, FCH$_2$-MEP or DMAPP was added to a solution of DXR, NADPH, MEP and MgCl$_2$, a decrease in the FRET signal is observed due to competitive binding against MEP for the active site. To determine if DXP induces an increase in the FRET signal upon binding to the active site, the binding assay was adaptive for analysis via stopped-flow under single-turnover conditions. A solution of DXP and MgCl$_2$ was mixed with a solution of DXR, NADPH and MgCl$_2$, and an initial increase in the FRET signal was observed followed by the loss of the FRET signal due to the oxidation of NADPH during catalysis.

67

The fact that 3F-DXP, FCH_2-MEP and DMAPP do not induce a change in the FRET signal while the other compounds tested here do, implies that these three compounds do not bind to the active site of DXR. Since 3F-DXP is a slow-binding inhibitor, and closely resembles DXP and 4F-DXP, it is reasonable to assume that it binds to the active site. Similarly, FCH_2-MEP and DMAPP are related to the compounds that produce a change in the FRET signal upon binding. Since they can compete with MEP for the binding site and have been shown to be inhibitors for DXR, they should also bind to the active site of DXR. From the crystal structure studies, it is clear that fosmidomycin binds to the active site magnesium ion in a bidentate manner through the hydroxamate moiety. It is believed that DXP also binds in an analogous bidentate form involving the C2 carbonyl and the C3 hydroxyl group.[56,57] When the compounds that produced a change in the FRET signal upon binding were compared to those that are innert, it became apparent that all the compounds that produced a change contained both functional groups required for bidentate binding to the magnesium ion, as shown in **Figure 2-21**. The compounds that failed to produce a change in the FRET signal are missing either one or both of the functional groups required for bidentate binding. Since 3F-DXP binds in a slow one-step mechanism, likely due to a slow conformational change that occurs concurrently with inhibitor binding, and does not produce a change in the FRET signal, the change in FRET signal observed for DXP, 4F-DXP, MEP and fosmidomycin unlikely arises from a conformational change. The reason for the increase in the FRET signal is believed to be due to the desolvation of the active site triggered by the elimination of the two water molecules bound to the magnesium when the substrate/inhibitor binds to the magnesium.
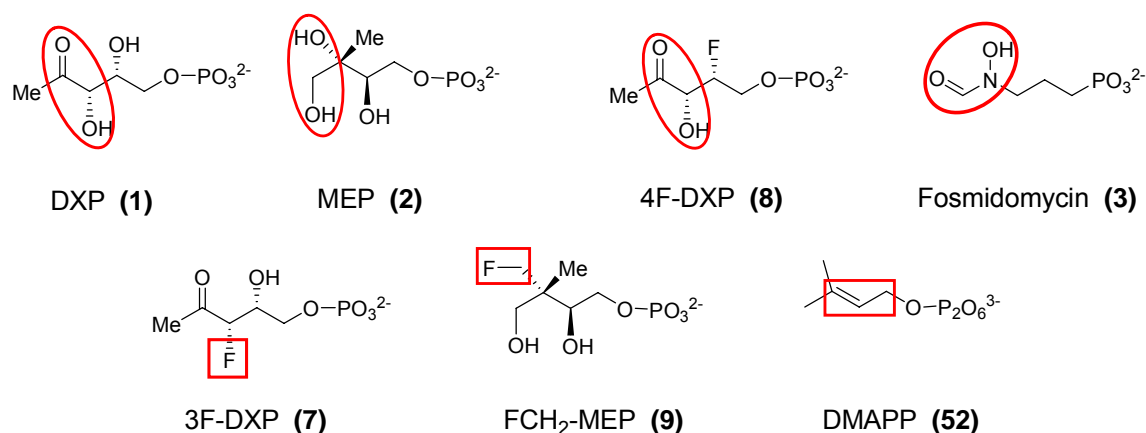
Figure 2-21: Structures of the compounds whose binding to DXR•NADPH•Mg^{2+} was analyzed by FRET assay. The compounds that produce an increase in the FRET signal upon binding have their proposed Mg^{2+} ligands circled. The compounds that do not produce a change in the FRET signal upon bindng have the missing Mg^{2+} ligand boxed.

2.4. CONCLUSION

To discriminate between the α-ketol mechanism and the retroaldol/aldol mechanism for the rearrangement reaction catalyzed by DXR, 3F-DXP and 4F-DXP were synthesized and analyzed as possible substrates. It was determined that neither analogue is a substrate and that both are inhibitors with K_i's similar to the K_M of DXP. These results are in agreement with the analysis from the study on 3-deoxy-DXP and 4-deoxy-DXP, which concluded that both hydroxyl groups are important for catalysis yet not crucial for binding.[37] Interestingly, in that same study, the authors report that 4-epi-DXP is also not a substrate and has a K_i similar to the K_M of DXP; thus the stereochemistry of at least the C4 hydroxyl group is also important for catalysis and not binding. The ability of both 4F-DXP and DXP to produce the same increase in the FRET signal upon binding implies that both bind in the same manner. This further supports the conclusion that the importance of the C4-hydroxyl group is for chemistry and not for proper binding, and the

69

reaction favors the retroaldol/aldol rearrangement mechanism over the α-ketol rearrangement mechanism.

When the study with 3F-DXP and 4F-DXP was first conducted, they were both found to be noncompetitive inhibitors of DXR.[23] After reexamining the data, it was determined that 3F-DXP and 4F-DXP in fact slow-binding inhibitors for DXR. The overlooking of the slow-binding inhibition resulted from using the initial weak binding phase to determine the initial velocity at low inhibitor concentrations, and using the final steady-state phase to determine the initial velocity at high inhibitor concentrations. It is possible that a similar situation also occurred in the determination of 3-deoxy-DXP and 4-deoxy-DXP as mixed type inhibitors for DXR that was also cloned from *E. coli*.[40] However, when 3-deoxy-DXP and 4-deoxy-DXP were analyzed against DXR cloned from *Synechocystis* PCC6803, no slow-binding inhibition was reported and both behaved as competitive inhibitors.[37]

Based on the global analysis, both 3F-DXP and fosmidomycin are slow-binding inhibitors due to their respective slow on and off rates, not due to a slow conformational change following an initial rapid binding. From crystal structure data, it is known that a conformation change does occur for the ternary DXR•NADPH•DXP/inhibitor enzyme complex, in which residues 206-216 move to enclose the active site upon forming the ternary complex.[57] It is likely that this conformational change happens in a concerted manner along with DXP/inhibitor binding, which produces the slow on and off rates.[58] The requirements for slow-binding inhibition are not completely clear. Among the compounds investigated here, only 3F-DXP, 4F-DXP and fosmidomycin exhibited slow-binding inhibition; FCH$_2$-MEP, DXP, MEP and DMAPP did not. According to these results, two possible requirements for slow-binding inhibition become apparent. One is the absence of either the 3-OH group or the 4-OH group but not both. These hydroxyl

groups form hydrogen bonds with active site residues,[57] which can provide part of the driving force for the binding/conformational change. Thus, removal of one hydrogen bond donor/acceptor could raise the energy barrier for this conformational change that accompanies binding, resulting in slow-binding inhibition. Removal of both hydrogen bond donor/acceptors could increase the energy barrier high enough to prevent the conformational change from occurring. Consistent with this notion, fosmidomycin and 4F-DXP are both missing the 4-OH group, and 3F-DXP is missing the 3-OH group. Mercklé et al. also reported that N-acetyl-1-amino-3-phosphonopropane, which lacks both 3-OH and 4-OH groups, does not show slow-binding inhibition.[54] FCH_2-MEP is only missing the 3-OH group, yet it is not slow-binding inhibitor. This can be explained by its violation of the second possible requirement for slow-binding inhibition, no steric hindrance. The increased steric bulk of the fluoromethylene group than the hydroxyl group prevents FCH_2-MEP from proper binding to facilitate the conformational change. This can help account for the weak inhibition of FCH_2-MEP, which is only effective in the mM range. The size restrictions imposed on binding is also evident from the lack of turnover of Et-DXP (($2R$,$3S$)-2,3-dihydroxy-4-oxohexyl dihydrogen phosphate), where the methyl group in DXP was replaced by an ethyl moiety.[41] However, Et-DXP can still bind to and weakly inhibit DXR with an IC_{50} of 6.2 mM, but no slow-binding inhibition was reported for Et-DXP. The impact of steric hindrance on binding and the absence of slow-binding inhibition is also evident for the carbamate fosmidomycin analogues designed by Mercklé et al. to rigidify the slow-binding inhibitor.[54] Even though these analogues were well designed, they only showed inhibition in the high μM to low mM concentration range, and none of the analogues exhibited slow-binding inhibition. This is believed to be due to the increase in steric bulkiness resulting from the modifications of fosmidomycin to increase its rigidity.

In an attempt to further differentiate between the two proposed mechanisms, FCH$_2$-MEP was synthesized and analyzed as a possible mechanism-based inhibitor. Although this analogue was unable to inactivate DXR as originally proposed, it was determined to be a weak inhibitor of DXR. It is possible that the cytidylated form of FCH$_2$-MEP (equivalent to CDP-ME), which could be made synthetically or possibly by IspD, could be a viable inhibitor for IspE, which is also an excellent antibiotic drug target (see **Figure 1-4**). The inability of DXR to oxidize FCH$_2$-MEP to the aldehyde intermediate and the weak inhibition of FCH$_2$-MEP towards DXR are most likely due to the steric hindrance caused by the substitution of a fluoromethylene group for a hydroxyl group.

To investigate the binding of the fluorinated analogues, the FRET binding assay was developed. The high sensitivity and simplicity of this binding assay make it ideal for high-throughput screening purpose. A high-throughput screening assay for binding has previously been developed for DXR; however, this assay requires washing steps, streptavidin coated plates, biotinylated DXR, europium-conjugated streptavidin and a biotinylated peptide to serve as the competing DXR ligand.[59] With the FRET assay described herein, a screening system can be envisioned requiring no washing steps and only native DXR, NADPH, MgCl$_2$ and possibly MEP as a competing ligand.

The results presented in this chapter provide a useful guide for the design of future inhibitors of DXR, which must consider the size restriction imposed by the active-site of DXR. However, due to the difficulty in rationally designing an inhibitor that does not violate DXR's strict size exclusion, a high-throughput screening of chemical libraries might be the most productive approach for future search of inhibitors for this attractive antibiotic target.

2.5. REFERENCES

(1)   Rohdich, F.; Bacher, A.; Eisenreich, W. Perspectives in anti-infective drug design: The late steps in the biosynthesis of the universal terpenoid precursors, isopentenyl diphosphate and dimethylallyl diphosphate. *Bioorg. Chem.*, **2004**, *32*, 292-308.

(2)   Penuelas, J.; Munne-Bosch, S. Isoprenoids: an evolutionary pool for photoprotection. *Trends Plant Sci.*, **2005**, *10*, 166-9.

(3)   Tudzynski, B. Biosynthesis of gibberellins in Gibberella fujikuroi: biomolecular aspects. *Appl. Microbiol. Biotechnol.*, **1999**, *52*, 298-310.

(4)   Fenton, J. W., 2nd; Jeske, W. P.; Catalfamo, J. L.; Brezniak, D. V.; Moon, D. G.; Shen, G. X. Statin drugs and dietary isoprenoids downregulate protein prenylation in signal transduction and are antithrombotic and prothrombolytic agents. *Biochemistry (Mosc)*, **2002**, *67*, 85-91.

(5)   Bochar, D. A.; Freisen, J. A.; Stauffacher, C. V.; Rodwell, V. W. In *Comprehesive Chemistry of Natural Products*; Cane, D. E., Ed.; Elsevier Science B.V.: Amsterdam, 1999; Vol. 2.

(6)   Eisenreich, W.; Schwarz, M.; Cartayrade, A.; Arigoni, D.; Zenk, M. H.; Bacher, A. The deoxyxylulose phosphate pathway of terpenoid biosynthesis in plants and microorganisms. *Chem. Biol.*, **1998**, *5*, R221-33.

(7)   Rohmer, M. The discovery of a mevalonate-independent pathway for isoprenoid biosynthesis in bacteria, algae and higher plants. *Nat. Prod. Rep.*, **1999**, *16*, 565-74.

(8)   Kuzuyama, T.; Seto, H. Diversity of the biosynthesis of the isoprene units. *Nat. Prod. Rep.*, **2003**, *20*, 171-83.

(9)   Sprenger, G. A.; Schorken, U.; Wiegert, T.; Grolle, S.; de Graaf, A. A.; Taylor, S. V.; Begley, T. P.; Bringer-Meyer, S.; Sahm, H. Identification of a thiamin-dependent synthase in Escherichia coli required for the formation of the 1-deoxy-D-xylulose 5-phosphate precursor to isoprenoids, thiamin, and pyridoxol. *Proc. Natl. Acad. Sci. U S A*, **1997**, *94*, 12857-62.

(10)   Lois, L. M.; Campos, N.; Putra, S. R.; Danielsen, K.; Rohmer, M.; Boronat, A. Cloning and characterization of a gene from Escherichia coli encoding a transketolase-like enzyme that catalyzes the synthesis of D-1-deoxyxylulose 5-phosphate, a common precursor for isoprenoid, thiamin, and pyridoxol biosynthesis. *Proc. Natl. Acad. Sci. U S A*, **1998**, *95*, 2105-10.

(11) Hill, R. E.; Sayer, B. G.; Spenser, I. D. Biosynthesis of vitamin B6: incorporation of D-1-deoxyxylulose. *J. Am. Chem. Soc.*, **1989**, *111*, 1916-17.

(12) White, R. H. Stable isotope studies on the biosynthesis of the thiazole moiety of thiamin in *Escherichia coli. Biochemistry*, **1978**, *17*, 3833-40.

(13) David, S.; Estramareix, B.; Fischer, J. C.; Therisod, M. 1-Deoxy-D-threo-2-pentulose: the precursor of the five-carbon chain of the thiazole of thiamine. *J. Am. Chem. Soc.*, **1981**, *103*, 7341-2.

(14) Takahashi, S.; Kuzuyama, T.; Watanabe, H.; Seto, H. A 1-deoxy-D-xylulose 5-phosphate reductoisomerase catalyzing the formation of 2-C-methyl-D-erythritol 4-phosphate in an alternative nonmevalonate pathway for terpenoid biosynthesis. *Proc. Natl. Acad. Sci. U S A*, **1998**, *95*, 9879-84.

(15) Jomaa, H.; Wiesner, J.; Sanderbrand, S.; Altincicek, B.; Weidemeyer, C.; Hintz, M.; Turbachova, I.; Eberl, M.; Zeidler, J.; Lichtenthaler, H. K.; Soldati, D.; Beck, E. Inhibitors of the nonmevalonate pathway of isoprenoid biosynthesis as antimalarial drugs. *Science*, **1999**, *285*, 1573-6.

(16) Argyrou, A.; Blanchard, J. S. Kinetic and chemical mechanism of *Mycobacterium tuberculosis* 1-deoxy-D-xylulose-5-phosphate isomeroreductase. *Biochemistry*, **2004**, *43*, 4375-84.

(17) Eisenreich, W.; Bacher, A.; Arigoni, D.; Rohdich, F. Biosynthesis of isoprenoids via the non-mevalonate pathway. *Cell Mol. Life Sci.*, **2004**, *61*, 1401-26.

(18) Okuhara, M.; Kuroda, Y.; Goto, T.; Okamoto, M.; Terano, H.; Kohsaka, M.; Aoki, H.; Imanaka, H. Studies on new phosphonic acid antibiotics. III. Isolation and characterization of FR-31564, FR-32863 and FR-33289. *J. Antibiot. (Tokyo)*, **1980**, *33*, 24-8.

(19) Kuroda, Y.; Okuhara, M.; Goto, T.; Okamoto, M.; Terano, H.; Kohsaka, M.; Aoki, H.; Imanaka, H. Studies on new phosphonic acid antibiotics. IV. Structure determination of FR-33289, FR-31564 and FR-32863. *J. Antibiot. (Tokyo)*, **1980**, *33*, 29-35.

(20) Shigi, Y. Inhibition of bacterial isoprenoid synthesis by fosmidomycin, a phosphonic acid-containing antibiotic. *J. Antimicrob. Chemother.*, **1989**, *24*, 131-45.

(21) Kuzuyama, T.; Shimizu, T.; Takahashi, S.; Seto, H. Fosmidomycin, a specific inhibitor of 1-deoxy-D-xylulose 5-phosphate reductoisomerase in the nonmevalonate pathway for terpenoid biosynthesis. *Tetrahedron Lett.*, **1998**, *39*, 7913-7916.

(22)   Lell, B.; Ruangweerayut, R.; Wiesner, J.; Missinou, M. A.; Schindler, A.; Baranek, T.; Hintz, M.; Hutchinson, D.; Jomaa, H.; Kremsner, P. G. Fosmidomycin, a novel chemotherapeutic agent for malaria. *Antimicrob. Agents Chemother.*, **2003**, *47*, 735-8.

(23)   Wong, A.; Munos, J. W.; Devasthali, V.; Johnson, K. A.; Liu, H. W. Study of 1-deoxy-D-xylulose-5-phosphate reductoisomerase: synthesis and evaluation of fluorinated substrate analogues. *Org. Lett.*, **2004**, *6*, 3625-8.

(24)   Dumas, R.; Biou, V.; Halgand, F.; Douce, R.; Duggleby, R. G. Enzymology, structure, and dynamics of acetohydroxy acid isomeroreductase. *Acc. Chem. Res.*, **2001**, *34*, 399-408.

(25)   Koppisch, A. T.; Fox, D. T.; Blagg, B. S.; Poulter, C. D. E. coli MEP synthase: steady-state kinetic analysis and substrate binding. *Biochemistry*, **2002**, *41*, 236-43.

(26)   Proteau, P. J.; Woo, Y. H.; Williamson, R. T.; Phaosiri, C. Stereochemistry of the reduction step mediated by recombinant 1-deoxy-D-xylulose 5-phosphate isomeroreductase. *Org. Lett.*, **1999**, *1*, 921-3.

(27)   Arigoni, D.; Giner, J.-L.; Sagner, S.; Wungsintaweekul, J.; Zenk, M. H.; Kis, K.; Bacher, A.; Eisenreich, W. Stereochemical course of the reduction step in the formation of 2-C-methylerythritol from the terpene precursor 1-deoxyxylulose in higher plants. *Chem. Comm.*, **1999**, *12*, 1127-1128.

(28)   Radykewicz, T.; Rohdich, F.; Wungsintaweekul, J.; Herz, S.; Kis, K.; Eisenreich, W.; Bacher, A.; Zenk, M. H.; Arigoni, D. Biosynthesis of terpenoids: 1-deoxy-D-xylulose-5-phosphate reductoisomerase from *Escherichia coli* is a class B dehydrogenase. *FEBS Lett.*, **2000**, *465*, 157-60.

(29)   Ricagno, S.; Grolle, S.; Bringer-Meyer, S.; Sahm, H.; Lindqvist, Y.; Schneider, G. Crystal structure of 1-deoxy-d-xylulose-5-phosphate reductoisomerase from Zymomonas mobilis at 1.9-A resolution. *Biochim. Biophys. Acta*, **2004**, *1698*, 37-44.

(30)   Mac Sweeney, A.; Lange, R.; Fernandes, R. P.; Schulz, H.; Dale, G. E.; Douangamath, A.; Proteau, P. J.; Oefner, C. The crystal structure of E.coli 1-deoxy-D-xylulose-5-phosphate reductoisomerase in a ternary complex with the antimalarial compound fosmidomycin and NADPH reveals a tight-binding closed enzyme conformation. *J. Mol. Biol.*, **2005**, *345*, 115-27.

(31)   Reuter, K.; Sanderbrand, S.; Jomaa, H.; Wiesner, J.; Steinbrecher, I.; Beck, E.; Hintz, M.; Klebe, G.; Stubbs, M. T. Crystal structure of 1-deoxy-D-xylulose-5-

phosphate reductoisomerase, a crucial enzyme in the non-mevalonate pathway of isoprenoid biosynthesis. *J. Biol. Chem.*, **2002**, *277*, 5378-84.

(32)   Yajima, S. H., Kodai; Sanders, John M.; Yin, Fenglin; Ohsawa, Kanju; Wiesner, Jochen; Jomaa, Hassan; Oldfield, Eric. Crystallographic Structures of Two Bisphosphonate:1-Deoxyxylulose-5-Phosphate Reductoisomerase Complexes. *J. Am. Chem. Soc.*, **2004**, *126*, 10824-10825.

(33)   Yajima, S.; Nonaka, T.; Kuzuyama, T.; Seto, H.; Ohsawa, K. Crystal structure of 1-deoxy-D-xylulose 5-phosphate reductoisomerase complexed with cofactors: implications of a flexible loop movement upon substrate binding. *J. Biochem.*, **2002**, *131*, 313-7.

(34)   Steinbacher, S.; Kaiser, J.; Eisenreich, W.; Huber, R.; Bacher, A.; Rohdich, F. Structural basis of fosmidomycin action revealed by the complex with 2-C-methyl-D-erythritol 4-phosphate synthase (IspC). Implications for the catalytic mechanism and anti-malaria drug development. *J. Biol. Chem.*, **2003**, *278*, 18401-7.

(35)   Yajima, S. H., Kodai; Sanders, John M.; Yin, Fenglin; Ohsawa, Kanju; Wiesner, Jochen; Jomaa, Hassan; Oldfield, Eric. Crystallographic Structures of Two Bisphosphonate:1-Deoxyxylulose-5-Phosphate Reductoisomerase Complexes. *J. Am. Chem.l Soc.*, **2004**, *126*, 10824-10825.

(36)   Wong, A.; Munos, J. W.; Devasthali, V.; Johnson, K. A.; Liu, H. W. Study of 1-deoxy-D-xylulose-5-phosphate reductoisomerase: synthesis and evaluation of fluorinated substrate analogues. *Org. Lett.*, **2004**, *6*, 3625-8.

(37)   Phaosiri, C.; Proteau, P. J. Substrate analogs for the investigation of deoxyxylulose 5-phosphate reductoisomerase inhibition: synthesis and evaluation. *Bioorg Med Chem Lett*, **2004**, *14*, 5309-12.

(38)   Fox, D. T.; Poulter, C. D. Mechanistic studies with 2-C-methyl-D-erythritol 4-phosphate synthase from *Escherichia coli*. *Biochemistry*, **2005**, *44*, 8360-8.

(39)   Walker, J. R.; Poulter, C. D. Synthesis and evaluation of 1-deoxy-D-xylulose 5-phosphate analogues as chelation-based inhibitors of methylerythritol phosphate synthase. *J. Org. Chem.*, **2005**, *70*, 9955-9.

(40)   Hoeffler, J. F.; Tritsch, D.; Grosdemange-Billiard, C.; Rohmer, M. Isoprenoid biosynthesis via the methylerythritol phosphate pathway. Mechanistic investigations of the 1-deoxy-D-xylulose 5-phosphate reductoisomerase. *Eur. J. Biochem.*, **2002**, *269*, 4446-57.

(41)   Fox, D. T.; Poulter, C. D. Synthesis and evaluation of 1-deoxy-D-xylulose 5-phosphoric acid analogues as alternate substrates for methylerythritol phosphate synthase. *J. Org. Chem.*, **2005**, *70*, 1978-85.

(42)   Meyer, O.; Grosdemange-Billiard, C.; Tritsch, D.; Rohmer, M. Isoprenoid biosynthesis via the MEP pathway. Synthesis of (3,4)-3,4-dihydroxy-5-oxohexylphosphonic acid, an isosteric analogue of 1-deoxy-D-xylulose 5-phosphate, the substrate of the 1-deoxy-D-xylulose 5-phosphate reducto-isomerase. *Org. Biomol. Chem.*, **2003**, *1*, 4367-72.

(43)   Pongdee, R.; Liu, H. W. Elucidation of enzyme mechanisms using fluorinated substrate analogues. *Bioorg. Chem.*, **2004**, *32*, 393-437.

(44)   Chang, C.-W. T. C., Xuemei H.; Liu, Hung-wen CDP-6-deoxy-6,6-difluoro-D-glucose: A Mechanism-Based Inhibitor for CDP-D-glucose 4,6-Dehydratase. *J. Am. Chem. Soc.*, **1998**, *120*, 9698-9699.

(45)   Parikh, S.; Moynihan, D. P.; Xiao, G.; Tonge, P. J. Roles of tyrosine 158 and lysine 165 in the catalytic mechanism of InhA, the enoyl-ACP reductase from Mycobacterium tuberculosis. *Biochemistry*, **1999**, *38*, 13623-34.

(46)   Taylor, S. V., Vu, L.D., Begley, T.P., Schorken, U., Grolle, S., Sprenger, G.A., Bringer-Meyer, S., Sahm, H. Chemical and Enzymatic Synthesis of 1-Deoxy-D-xylulose-5-phosphate. *J. Org. Chem.*, **1998**, *63*, 2375-2377.

(47)   Hecht, S., Wungsintaweekul, J., Rohdich, F., Kis, K., Radykewicz, T., Schuhr, C.A., Eisenreich, W., Richter, G., and Bacher, A. Biosynthesis of Terpenoids: Efficient Multistep Biotransformation Procedures Affording Isotope-Labeled 2C-Methyl-D-erythritol 4-Phosphate Using Recombinant 2C-Methyl-D-erythritol 4-Phosphate Synthase. *J. Org. Chem.*, **2001**, *66*, 7770-7775.

(48)   Sculley, M. J.; Morrison, J. F.; Cleland, W. W. Slow-binding inhibition: the general case. *Biochim. Biophys. Acta*, **1996**, *1298*, 78-86.

(49)   Kuzmic, P. Program DYNAFIT for the analysis of enzyme kinetic data: application to HIV proteinase. *Anal. Biochem.*, **1996**, *237*, 260-73.

(50)   Hoeffler, J. F.; Tritsch, D.; Grosdemange-Billiard, C.; Rohmer, M. Isoprenoid biosynthesis via the methylerythritol phosphate pathway. Mechanistic investigations of the 1-deoxy-D-xylulose 5-phosphate reductoisomerase. *Eur. J. Biochem.*, **2002**, *269*, 4446-57.

(51)   Phaosiri, C.; Proteau, P. J. Substrate analogs for the investigation of deoxyxylulose 5-phosphate reductoisomerase inhibition: synthesis and evaluation. *Bioorg. Med. Chem. Lett.*, **2004**, *14*, 5309-12.

(52)   Sculley, M. J.; Morrison, J. F.; Cleland, W. W. Slow-binding inhibition: the general case. *Biochim. Biophys. Acta*, **1996**, *1298*, 78-86.

(53)   Kuntz, L.; Tritsch, D.; Grosdemange-Billiard, C.; Hemmerlin, A.; Willem, A.; Bach, T. J.; Rohmer, M. Isoprenoid biosynthesis as a target for antibacterial and antiparasitic drugs: phosphonohydroxamic acids as inhibitors of deoxyxylulose phosphate reducto-isomerase. *Biochem. J.*, **2005**, *386*, 127-35.

(54)   Merckle, L.; de Andres-Gomez, A.; Dick, B.; Cox, R. J.; Godfrey, C. R. A fragment-based approach to understanding inhibition of 1-deoxy-D-xylulose-5-phosphate reductoisomerase. *Chembiochem*, **2005**, *6*, 1866-74.

(55)   Munos, J. W.; Pu, X.; Liu, H. W. Synthesis and Analysis of a Fluorinated Product Analogue for the Mechanistic Analysis of 1-Deoxy-D-xylulose 5-phosphate Reductoisomerase. *Bioorg. Med. Chem. Lett.*, **2008**, in press.

(56)   Steinbacher, S.; Kaiser, J.; Eisenreich, W.; Huber, R.; Bacher, A.; Rohdich, F. Structural basis of fosmidomycin action revealed by the complex with 2-C-methyl-D-erythritol 4-phosphate synthase (IspC). Implications for the catalytic mechanism and anti-malaria drug development. *J. Biol. Chem.*, **2003**, *278*, 18401-7.

(57)   Mac Sweeney, A.; Lange, R.; Fernandes, R. P.; Schulz, H.; Dale, G. E.; Douangamath, A.; Proteau, P. J.; Oefner, C. The crystal structure of E.coli 1-deoxy-D-xylulose-5-phosphate reductoisomerase in a ternary complex with the antimalarial compound fosmidomycin and NADPH reveals a tight-binding closed enzyme conformation. *J. Mol. Biol.*, **2005**, *345*, 115-27.

(58)   Williams, J. W.; Morrison, J. F. The kinetics of reversible tight-binding inhibition. *Methods Enzymol.*, **1979**, *63*, 437-67.

(59)   Gottlin, E. B.; Benson, R. E.; Conary, S.; Antonio, B.; Duke, K.; Payne, E. S.; Ashraf, S. S.; Christensen, D. J. High-throughput screen for inhibitors of 1-deoxy-d-xylulose 5-phosphate reductoisomerase by surrogate ligand competition. *J. Biomol. Screen.*, **2003**, *8*, 332-9.

Chapter 3: Secondary Kinetic Isotope Effect Study on DXR

3.1. INTRODUCTION

Terpenoids are a large family of natural products comprised of over 35,000 distinct compounds.[1] They are widely distributed in nature and are rich in biological activities, including light harvesting pigments,[2] growth hormones,[3] and molecules involved in signal transduction.[4] The terpenoid building block is a 5-carbon unit known as isoprene, which has long been established to be derived from acetate via the mevalonate pathway.[5] However, a new isoprene biosynthetic pathway has recently been discovered in eubacteria, archeabacteria, algae, and in the plastids of plants where the isoprenoid unit is formed independently of mevalonate.[6-8] Since this pathway is absent in mammals but is essential for many pathogens, including *Plasmodium falciparum*[9] and *Mycobacterium tuberculosis*,[10] all enzymes in this pathway are potential antibacterial targets.[11]

The first committed step of the nonmevalonate pathway is catalyzed by DXR, which catalyzes the rearrangement and NADPH mediated reduction of DXP (**1**) to MEP (**3**). Since MEP is the first metabolite specific to this pathway, this pathway is also known as the MEP pathway. There are two proposed mechanisms for the rearrangement reaction, a concerted α-ketol rearrangement and a stepwise retroaldol/aldol rearrangement. In the α-ketol rearrangement, deprotonation of the C-3 hydroxyl group followed by a 1,2-migration to yield the aldehyde intermediate, methylerythrose phosphate (**2**), which is subsequently reduced by NADPH. In the retroaldol/aldol rearrangement mechanism, DXR first cleaves the C3-C4 bond of **1** through a retroaldol mechanism to yield a three carbon (**4**) and a two carbon phosphate intermediates (**5**);

these intermediates then condense through an aldol reaction to form a new C-C bond (between C2 and C4 of **1**) and the same aldehyde intermediate (**2**).

A. *α-Ketol Rearrangement*

B. *Retroaldol/aldol Rearrangement*
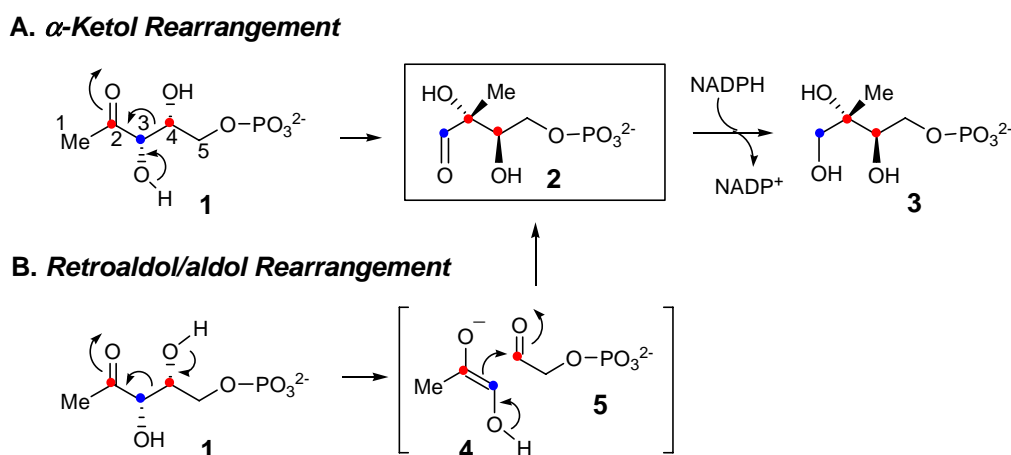
Figure 3-1:   **Proposed Mechanisms for DXR.**

A key difference between these two proposed mechanisms is the chemistry that occurs at C3 versus C4. In Chapter 2, it was described how the hydroxyl groups at C3 and C4 were separately replaced with a fluorine atom to probe the involvement of each hydroxyl group in the rearrangement reaction.[12] Neither of these fluoro analogues is a substrate for DXR, but both are slow-binding inhibitors.[12,13] These results are consistent with the retroaldol/aldol mechanism, since both hydroxyl groups are involved in the rearrangement reaction. If the reaction proceeds with the α-ketol rearrangement mechanism, which only utilizes the C3-hydroxyl group, the 4-fluoro-analogue should be a substrate.

To further investigate this important reaction, we designed and synthesized 3[^{2}H]-DXP (**6**) and 4[^{2}H]-DXP (**7**) to study the secondary kinetic isotope effect experiment (2° KIE) of the DXR reaction. The results may provide insight to distinguish between the two proposed rearrangement mechanisms. A KIE of a is observed when there is a

difference in the zero-point energies (ZPE) of a C-H bond and the corresponding C-D bond in the reactant state versus in the transition state. Differences in mass moments of inertia (MMI) and excited vibrational states (EXC) also contribute to the KIE. However, for deuterium KIE's, the difference in ZPE dominates the KIE. If the reaction under investigation involves the cleavage of the C-H/D bond, a 1° KIE greater than unity is predicted. If bond cleavage occurs next the labeled C-H bond in the reaction, a 2° KIE may be observed. If the KIE is greater than unity, it is a normal KIE, and if the resulting KIE is less than unity, it is known as an inverse KIE. Secondary KIE's can be further devided into α and β effects. An α effect occurs when the H/D is bonded to the carbon center where the reaction takes place, and in a β effect, the H/D is attached to a carbon adjacent to the carbon center where the reaction occurs. The isotope effect study described herein is a 2° α-KIE.
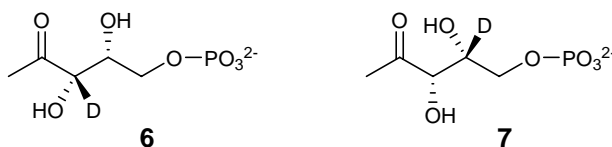
Figure 3-2:   **Structures of 3[^{2}H]-DXP (6) and 4[^{2}H]-DXP (7).**

As stated above, a KIE arises predominantly from the difference in the ZPE of a C-H bond and a C-D bond in the reactant state versus in the transition state. For a 2° α-KIE, this difference is mostly due to changes in the hybridization state between the substrate and transition state. When a carbon atom changes from sp^3 to sp^2 hybridization, a number of vibrational modes (stretches, in-plane and out-of-plane bending) change. The changes in streches and in-plane bending are too small to create a significant isotope effect. However, the out-of-plane bending vibration for a sp^3 carbon is 1350 cm^{-1}, while that for a sp^2 carbon is 800 cm^{-1}. This difference is large enough to produce a significant

81

isotope effect. The larger force constant for the out-of-plane bending vibration of the sp^3 centered C-H/D bond implies a stiffer bond vibration and thus a more narrow potential energy well.   As seen in **Figure 3-3**, the narrower energy well produces a larger difference in the ZPEs between the sp^3 C-H/D bonds than the difference between the sp^2 C-H/D bonds. This difference determines the magnitude of the observed isotope effect.
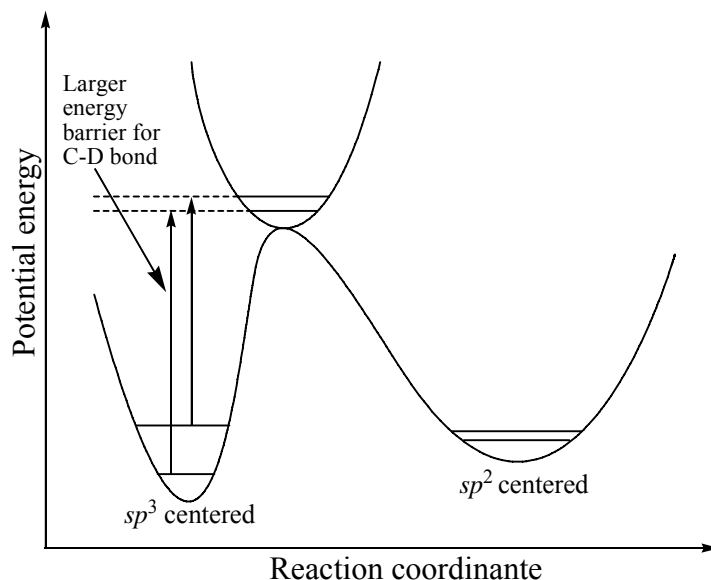
Figure 3-3:　　**Reaction coordinate diagram displaying the origin of the normal 2° KIE for a sp^3 carbon that rehybridizes to a sp^2 centered carbon.**

The hybridization state of the transition state lies between the hybridization state of the substrate and product. If a carbon rehybridizes from sp^3 to sp^2, the transition state will have an s-character greater than an sp^3 center but less than an sp^2 center.   The amount of rehybridization that has occurred in the transition state is determined by whether the transition state occurs early or late. Either way, the transition state will have a smaller force constant than the sp^3 reactant state; thus it will have a smaller difference between the C-H/D ZPEs. This smaller difference in the ZPEs at the transition state will increase the activation energy of the deuterium labeled reaction, resulting in a normal 2°

KIE. Whether the transition state is early or late will impact the size of the intrinsic isotope effect. If a reaction has an early transition state, it will be more reactant-like than product-like; thus little rehybridization would have occurred for that stage of the reaction. This will produce a small difference in the C-H/D ZPEs between the reactant state and transition state, which will give a small, normal intrinsic isotope effect. The later the transition state of the reaction, the larger the difference of the C-H/D ZPEs between the reactant state and transition state will be, and thus the larger the intrinsic isotope effect will be, with a theoretical maximum value of 1.4.[14] A reaction undergoing a rehybridization from sp^2 to sp^3 will have the opposite scenario and will produce an inverse KIE.
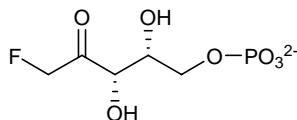
8

Figure 3-4:   Structure of 1F-DXP (8).

In a report from Fox *et al.*, 1F-DXP (**8**) was synthesized and analyzed as a possible substrate. The fluorine addition to the methyl group is expected to accelerate the retroaldol reaction by stabilizing the negative charge on the resulting three carbon intermediate. Indeed, the k_{cat} for 1F-DXP was determined to be roughly twice that of DXP.[15] To investigate whether the reduction step is rate-limiting, the 1° KIE was examined with 4S-[^{2}H]-NADPH and DXP under single-turnover conditions. A KIE of 1.02 ± 0.02 was determined. The experiment was repeated with 1F-DXP substituted for DXP, and a 1° KIE of 1.34 ± 0.01 was determined. The KIE of unity with DXP implies that the hydride transfer step is not rate-limiting; however, the hydride-transfer step becomes partially rate-limiting when 1F-DXP (**8**) is substituted for DXP (**1**). For the

83

hydride-transfer step to become partially rate-limiting, the step that is rate-limiting in the DXR reaction would have to become faster with a rate comparable to that of the hydride-transfer step. Since the addition of the fluorine at C1 is expected to accelerate the retroaldol reaction, the rearrangement step must be rate-limiting when DXP (**1**) is used as the substrate. Thus, an observed 2° KIE should result only from the rearrangement reaction, specifically from the retroaldol reaction.

In the α-ketol rearrangement, the C3 rehybridizes from sp^3 to sp^2, while the C4 remains sp^3 through out the reaction coordinate. Therefore, if DXR utilizes the α-ketol rearrangement mechanism, $3[^2H]$-DXP should produce a normal 2° KIE, and $4[^2H]$-DXP should have a 2° KIE of unity.[16] In the retroaldol/aldol rearrangement reaction, the C3 rehybridizes from sp^3 to sp^2 in the retroaldol reaction and remains sp^2 through out the aldol condensation reaction. The C4 changes from sp^3 to sp^2 in the retroaldol reaction and changes back to sp^3 in the aldol condensation reaction; however, it is believed that the retroaldol reaction will be significantly more rate-limiting than the aldol condensation reaction. Thus if DXR follows the retroaldol/aldol rearrangement mechanism, $3[^2H]$-DXP and $4[^2H]$-DXP should both produce a normal 2° KIE.[16]

3.2. MATERIALS AND METHODS

3.2.1. GENERAL.   The pET24(+) vector was purchased from Novagen (Madison, WI). Cloned DNA polymerase *Pfu* was obtained from Stratagene (La Jolla, CA). Primers used in PCR amplification were customarily prepared by Integrated DNA Technologies (Coralville, IA) and used without further purification. All electrophoretic reagents were obtained from Bio-Rad (Hercules, CA), and culture media were products of Difco (Detroit, MI). All other chemicals were purchased from Sigma-Aldrich (St. Louis, MO) or Fisher Scientific (Pittsburgh, PA). DXP and MEP were made through

enzymatic synthesis as published,[17,18] except were purified by cellulose chromatography using water and THF as the solvent system. The concentrations of DXP, 3[^{2}H]-DXP, 4[^{2}H]-DXP and MEP were determined according to a literature proceedure.[19]

3.2.2. REMOVAL OF HIS-TAG, OVER-EXPRESSION AND PURIFICATION OF DXR.

The DXR used in this work is the native (non-tagged) form of the enzyme; in the studies described in Chapter 2, a C-terminal His-tagged DXR.[12,13,20] The C-terminal His-tag was removed by inserting a stop codon after the dxr sequence and before the coding sequence for the His-tag. This was performed by site-directed mutagenesis using the QuickChange site-directed mutagenesis kit from Stratagene (La Jolla, CA). The oligonucleotides used for mutagenesis were customarily synthesized by Integrated DNA Technology (Coralville, IA). The mutagenesis primers used were dxrn1 (5'GGTGATGCGTCTCGCAAGCTGACTCGAGCACC) and dxrn2 (5'GGTGGTGGTGGTGCTCGAGTCAGCTTGCGAGA). The constructed mutant plasmids were amplified in *E. coli* strain DH5α and purified with QIAprep spin miniprep kit (Qiagen, Valencia, CA). Once the mutation was verified by DNA sequencing performed by the core facility in the Institute for Cellular and Molecular Biology of the University of Texas at Austin, the mutant plasmids were used to transform *E. coli* BL21 Star™ (DE3) (Invitrogen, Carlsbad, CA) for protein expression.

An overnight culture of the recombinant strain grown in LB media supplemented with kanamycin (50 μg/mL) at 37 ^{o}C was used to inoculate six 1 L cultures of the same medium and antibiotic. These cultures were grown at 37 ^{o}C until the OD$_{600}$ reached 0.65, followed by induction with 0.1 mM IPTG and 3.5 h of additional incubation at 37 ^{o}C. The cells were harvested by centrifugation (7000g, 8 min). DXR was purified according to a literature procedure.[19] The purified protein was concentrated, mixed with glycerol to

a final concentration of 30%, aliquotted, flash frozen, and stored at −80 °C. The concentration of DXR was determined by the method of fluorescence active-site titration with NADPH as described in Chapter 2.[12]

3.2.3. SYNTHESIS OF 3[^{2}H]-DXP AND 4[^{2}H]-DXP.

The deuterium labeled DXP, 3[^{2}H]-DXP (**6**) and 4[^{2}H]-DXP (**7**), were synthesized according to the synthetic schemes depicted in **Figures 3-5** and **3-6**, respectively, by Dr. Xiaotao Pu.
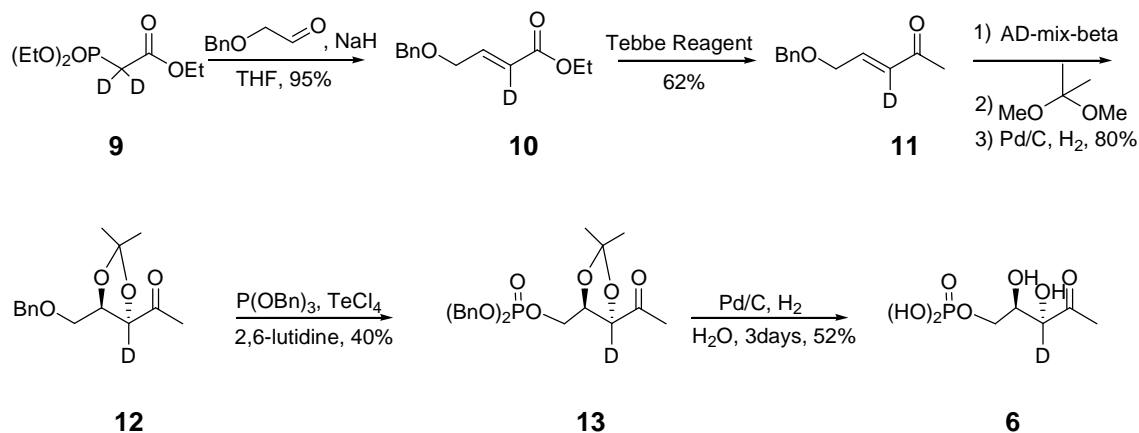
Figure 3-5: Synthetic scheme of 3[^{2}H]-DXP (**6**).
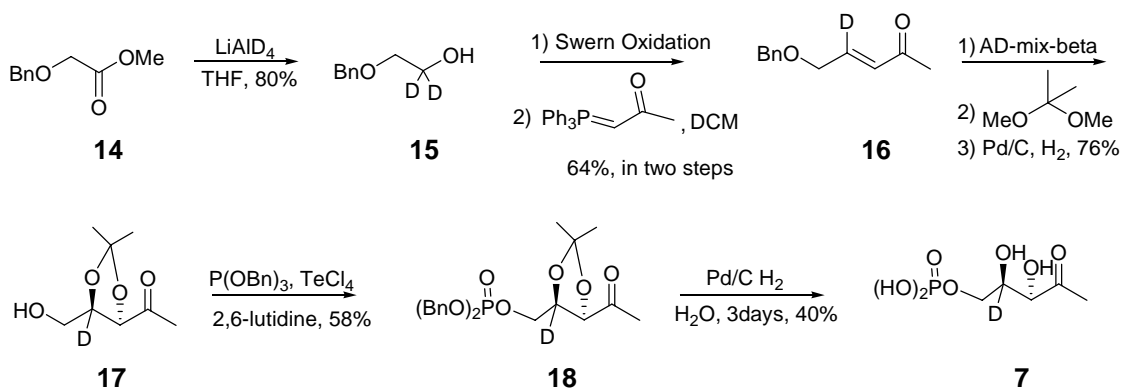
Figure 3-6: Synthetic scheme of 4[^{2}H]-DXP (**7**).

3.2.4. DETERMINING K_{CAT} AND K_M FOR DXP, 3[^{2}H]-DXP AND 4[^{2}H]-DXP.

Enzyme assays were performed in duplicate and according to a literature procedure.[19] The reactions were carried out at 24 °C. The reaction mixture contained 100 µL of degassed and N_2 saturated 100 mM Tris•HCl buffer (pH 7.6), 2 mM $MgCl_2$, 1 mg/mL BSA, 0.15 mM NADPH, 30 nM DXR, and varied (20 µM-2328 µM) concentrations of DXP, 3[^{2}H]-DXP and 4[^{2}H]-DXP. The reaction was initiated by the addition of DXR and was monitored by the consumption of NADPH at 340 nm. The kinetic parameters of k_{cat} and K_m were determined using Grafit 5.0.1.

3.2.5. DETERMINING K_{EQ} FOR THE DXR REACTION USING DXP, 3[^{2}H]-DXP AND 4[^{2}H]-DXP.

The equilibrium constant for the reaction with DXP, 3[^{2}H]-DXP and 4[^{2}H]-DXP was determined by measuring the change in [NADPH] from before the addition of DXR to after the addition of DXR till the reaction mixture reached equilibrium. The assays were carried out at a fixed concentrations of $MgCl_2$ (2 mM), NADPH (75 µM), DXP (67 µM), 3[^{2}H]-DXP (57 µM), 4[^{2}H]-DXP (70 µM), and at varying concentrations of $NADP^+$ (0-1.7 mM) in 500 µL of 100 mM Tris pH 7.6 that was degassed and N_2 saturated. To drive the reaction to equilibrium, DXR was added to a final concentration of 1.7 µM. The assays were carried out at 24 °C in duplicate. To determine the K_{eq} for each reaction the data was fit to **Equation 3-1** using Grafit 5.0.1, where $[NADPH]_o$, $[DXP]_o$, and $[NADP^+]_o$ are the respective starting concentrations before the addition of DXR. In the equation, [X] is the difference between $[NADPH]_o$ and the concentration of NADPH once equilibrium is reached. In the data fitting, K_{eq} was set as a parameter, and $[NADPH]_o$ and $[DXP]_o$ were set as constants.

87

Equation 3-1

$$[NADP^+]_o = \frac{K_{eq}[NADPH]_o[DXP]_o - K_{eq}([NADPH]_o + [DXP]_o)[X] + (K_{eq} - 1)[X]^2}{[X]}$$

3.2.6. EQUILIBRIUM PERTURBATION EXPERIMENT. The equilibrium perturbation experiments were conducted according to literature procedures.[21-23] The concentrations used in the experiment were based on a similar study on alcohol dehydrogenase.[23] The perturbations were carried out in triplicate and at 24 °C. A stock solution containing $MgCl_2$, NADPH, 3/4[^{2}H]-DXP, MEP and $NADP^+$ was made, and a 1 mL aliquot of this stock solution was diluted to 3 mL for each perturbation experiment. The final concentrations for the 3[^{2}H]-DXP perturbation experiments were 165 μM NADPH, 1 mM 3[^{2}H]-DXP, 1.1 mM MEP, 3.1 mM $NADP^+$ and 2 mM $MgCl_2$. For the 4[^{2}H]-DXP perturbation experiments, the final concentrations were 148.5 μM NADPH, 900 μM 4[^{2}H]-DXP, 990 μM MEP, 2.79 mM $NADP^+$ and 1.8 mM $MgCl_2$. Before the addition of enzyme, the sample in the cuvette was incubated in the UV/Vis cell holder, which is connected to a water circulator to allow the temperature of the sample to equilibrate and to ensure the sample produce an acceptable baseline reading. The concentration of DXR in each perturbation experiment varied from 300-450 nM.

3.2.7. KINETIC SIMULATIONS OF EQUILIBRIUM PERTURBATION EXPERIMENTS.
The *E. coli* DXR has been shown to have an ordered substrate binding mechanism, with NADPH binding before DXP.[19] In contrast, studies of *M. tuberculosis* DXR concluded that it binds substrate in random order, but with a preference to bind NADPH before DXP.[10] In computer simulations described here, the ordered substrate binding mechanism was used. It was assumed that product release is also ordered with MEP dissociating before $NADP^+$. A fully random kinetic mechanism was tested by

88

simulation but did not produce significantly different results. Therefore, for simplification, only the ordered mechanism is considered herein. The kinetic mechanism used in the simulation is shown in **Figure 3-7**.

$$\text{DXR} + \text{NADPH} \underset{k_{-1}}{\overset{k_1}{\rightleftharpoons}} \text{DXR} \bullet \text{NADPH} \qquad \textbf{(1)}$$

$$\text{DXR} \bullet \text{NADPH} + \text{DXP} \underset{k_{-2}}{\overset{k_2}{\rightleftharpoons}} \text{DXR} \bullet \text{NADPH} \bullet \text{DXP} \qquad \textbf{(2)}$$

$$\text{DXR} \bullet \text{NADPH} \bullet \text{DXP} \underset{k_{-3}}{\overset{k_3}{\rightleftharpoons}} \text{DXR} \bullet \text{NADP} \bullet \text{MEP} \qquad \textbf{(3)}$$

$$\text{DXR} \bullet \text{NADP} \bullet \text{MEP} \underset{k_{-4}}{\overset{k_4}{\rightleftharpoons}} \text{DXR} \bullet \text{NADP} + \text{MEP} \qquad \textbf{(4)}$$

$$\text{DXR} \bullet \text{NADP} \underset{k_{-5}}{\overset{k_5}{\rightleftharpoons}} \text{DXR} + \text{NADP} \qquad \textbf{(5)}$$

$$\text{DXR} \bullet \text{NADPH} + \text{d-DXP} \underset{k_{-6}}{\overset{k_6}{\rightleftharpoons}} \text{DXR} \bullet \text{NADPH} \bullet \text{d-DXP} \qquad \textbf{(6)}$$

$$\text{DXR} \bullet \text{NADPH} \bullet \text{d-DXP} \underset{k_{-7}}{\overset{k_7}{\rightleftharpoons}} \text{DXR} \bullet \text{NADP} \bullet \text{d-MEP} \qquad \textbf{(7)}$$

$$\text{DXR} \bullet \text{NADP} \bullet \text{d-MEP} \underset{k_{-8}}{\overset{k_8}{\rightleftharpoons}} \text{DXR} \bullet \text{NADP} + \text{d-MEP} \qquad \textbf{(8)}$$
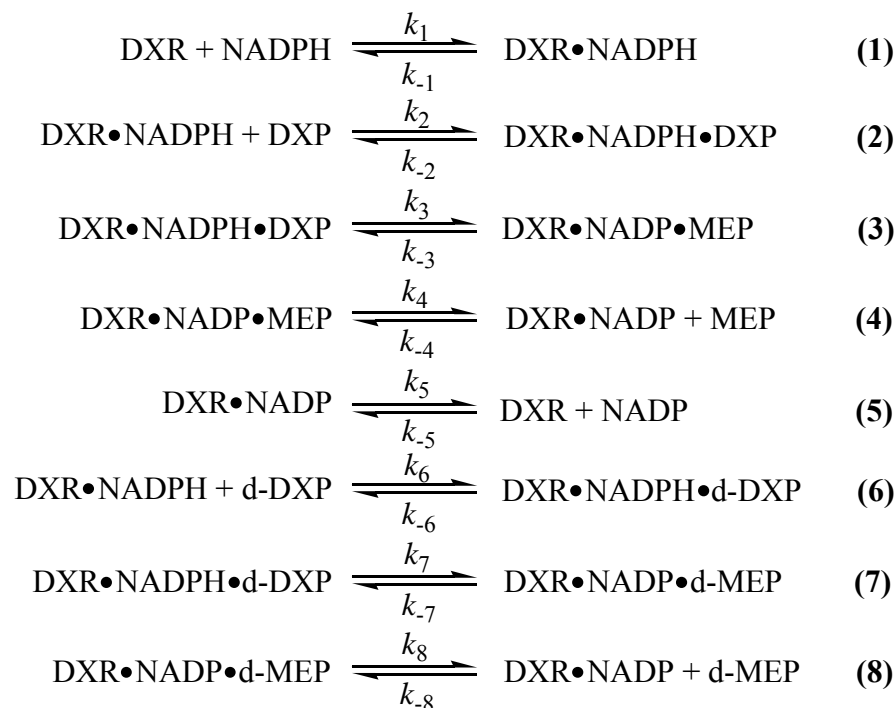
Figure 3-7:   Kinetic scheme used for computer simulations.

In the simulations, all the rate constants were allowed to float but with a few restrictions. One restriction is that there is no isotope effect on binding. The simulation was carried out by having the rate constant for binding of DXP and [^{2}H]-DXP set equal to each other so that they floated together. This condition was also applied to true for the dissociation of DXP and [^{2}H]-DXP and for the binding/dissociation of MEP and [^{2}H]-MEP. The K_d of 750 nM for NADPH to DXR was previously determined in the active site titration experiment. In the simulations, the rate constants for NADPH binding and dissociation were floated together so that the equilibrium for binding equaled the K_d

value for NADPH. Since the K_ds for DXP, MEP and NADP$^+$ are not known, their rate constants for binding and dissociation were allowed to float independent of each other. To further restrict the simulation, the ratio of the equilibrium for chemistry of the unlabeled reaction, Step 3, and that for the labeled reaction, Step 7, was set to their respective equilibrium isotope effect (See **Table 3-3**). This was performed by fixing the ratio of chemistry for the unlabeled reaction, Step 3, to the ratio of the k_{cat} for the forward and reverse reactions. The ratio for chemistry in the labeled reaction was then fixed so that the equilibrium isotope effect equaled the experimentally determined value.

The binding and dissociation rates for all compounds and the equilibrium binding values for DXP, MEP or NADP$^+$ derived from computer simulations are not to be considered as accurate. The values obtained by simulations depend on the initial starting values. All of the starting binding rates were set less than the diffusion controlled limit to ensure that the returned values were also under the limit. If different values for the binding and dissociation rates were used to start the simulation, the program would give different rates and equilibrium values at the end. If the K_d for DXP was lowered, then the K_d for either NADP$^+$ or MEP would also lower so that the starting reactant concentrations entered into the program were at equilibrium. In the simulations, the exact equilibrium binding value for each reactant is not important, only the relationship among the four reactants is important. The binding and dissociation rates did affect the KIE values but not in a significant manner. Depending on the starting binding and dissociation rates, the KIE for 3[^{2}H]-DXP ranged from 1.02 to 1.05 and the KIE for 4[^{2}H]-DXP ranged from 1.09 to 1.14. The simulation results from **Table 3-2** were used to calculate the KIEs reported in **Table 3-3**.

3.3. RESULTS AND DISCUSSION

3.3.1. NON-COMPETITIVE KIE ANALYSIS.   The k_{cat} and K_M for DXP, 3[^{2}H]-DXP and 4[^{2}H]-DXP were determined under identical conditions and according to the procedure described above. These values and their corresponding (non-competitive) $^dk_{cat}$'s and $^dk_{cat}/K_M$'s are reported in **Table 3-1**. While this investigation was underway, a similar study was reported by Wong *et al.*, and their reported KIEs are also listed in **Table 3-1** for comparison.[24] Our $^dk_{cat}$ values are in support of the retroaldol/aldol mechanism; however, the $^dk_{cat}/K_m$ values do not completely agree with expected results for either mechanism. The normal C4 KIE is consistent with the retroaldol/aldol mechanism and derives from the initial retroaldol cleavage reaction where the C4 carbon rehybridizes from sp^3 to sp^2. The inverse C3 KIE could only arise for both proposed mechanisms from the sp^2 to sp^3 rehybridization of C3 carbon when the rearranged aldehyde intermediate is reduced by NADPH. This would result if the reduction step is rate-limiting, which is inconsistent with the findings of Fox *et al.*[15] If the reduction step is rate-limiting, the C4 KIE should be close to unity.

In the study carried out by Wong *et al.*,[24] the reported KIE's were determined in a similar non-competitive manner. Their data was interpreted in favor of the retroaldol/aldol rearrangement mechanism; however, there are a few problems with their KIE values as well. First, both values for $^dV_{max}$ are smaller than the theoretical minimum for a 2° KIE of ~0.71. Second, the $^dV_{max}$ and $^dV_{max}/K_M$ KIE's for C3 and C4 are inverse. As discussed in the previous paragraph, a C3 inverse KIE is possible only if the reduction step is rate-limiting. However, this has been determined not to be the rate-limiting step.[15] Also, if the reduction step is the rate-limiting step of the DXR reaction, the C4 KIE should be close to unity. Again, this is not true. The reported C4 KIE for both $^dV_{max}$ and $^dV_{max}/K_M$ is inverse, which could only result from the aldol condensation in the proposed

91

retroaldol/aldol mechanism and is impossible for the α-ketol rearrangement mechanism. Thus, if the data are correct, the aldol condensation reaction sould be the rate-limiting step for DXR, even though the retroaldol cleavage is more likely the rate-limiting step for the retroaldol/aldol rearrangement mechanism. Again, the C3 KIE should have a value close to unity, if the aldol condensation is the rate-limiting step. Clearly the latter is inconsistent with what was observed.

Table 3-1:   Summary of non-competitive KIE measurements.

Substrate	k_{cat} (s^{-1})	K_M (μM)	$^d k_{cat}$	$^d k_{cat}/K_M$	$^d V_{max}$ [a]	$^d V_{max}/K_M$ [a]
DXP	16.1 ± 0.7	166 ± 20	--	--	--	--
3[^{2}H]-DXP	13.2 ± 0.7	116 ± 20	1.21 ± 0.08	0.85 ± 0.19	0.56	0.92
4[^{2}H]-DXP	13.7 ± 0.5	154 ± 17	1.17 ± 0.05	1.12 ± 0.17	0.62	0.86

(a) KIE results from study by Wong *et al.*[24]

After close inspection of the data obtained by our assays, it became apparent that not all of the progress curves for the 3[^{2}H]-DXP and 4[^{2}H]-DXP assays were linear, see **Figure 3-8**. This is different from what was found when the enzymatically synthesized DXP was used in the assays. The nonlinear progress curves are characteristic of a slow-binding inhibitor,[25] and slow-binding inhibitors for DXR have been reported and discussed in Chapter 2.[13,19] The presumed slow-binding inhibitor is likely the DXP enantiomer resulting from the dihydroxylation step in the synthesis of both labeled substrates.[26] This is supported by the observation that DXP with the stereochemistry of its C4-hydroxyl group inverted is not a substrate for DXR.[27] This observation raised concerns about the validity of these KIE values and our method to accurately determine them.
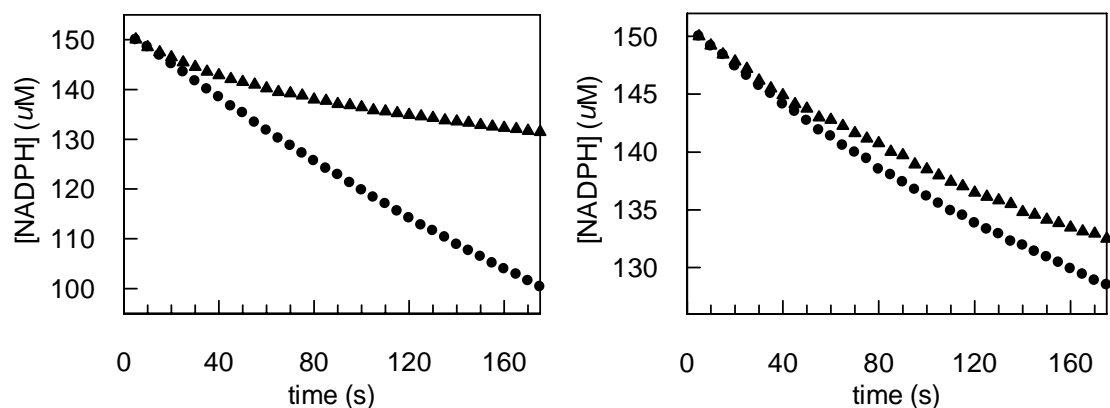
Figure 3-8: Steady-state progress curves for DXP, 3[^{2}H]-DXP and 4[^{2}H]-DXP in determining $^dk_{cat}$ and $^dk_{cat}/K_m$ for 3[^{2}H]-DXP and 4[^{2}H]-DXP. Reaction conditions A) 100 mM Tris pH 7.6, 2 mM MgCl$_2$, 150 μM NADPH, 30 nM DXR, and 118 μM DXP (●) or 116 μM 3[^{2}H]-DXP (▲); B) 100 mM Tris pH 7.6, 2 mM MgCl$_2$, 150 μM NADPH, 30 nM DXR, and 2295 μM DXP (●) or 2328 μM 4[^{2}H]-DXP (▲).

3.3.2. EQUILIBRIUM PERTURBATION EXPERIMENTS. In order to avoid any complications due to the contamination of an inhibitor, we decided to employ the equilibrium perturbation method to determine the KIE. Since this is a competitive technique, the contaminant will not have an effect on the size of the KIE.[21,22] DXR is an excellent system for this method due its reaction being freely reversible and the easiness to follow the course of the reaction by monitoring the formation/consumption of NADPH at 340 nm. The experiment is initiated by adding DXR to a solution of NADPH, 3/4[^{2}H]-DXP, NADP$^+$ and MEP at chemical equilibrium but not isotopic equilibrium. If there is a normal KIE (labeled substrate being slower than unlabeled substrate), there will be a temporary increase in the concentration of NADPH due to the forward reaction being slower than the reverse reaction. If there is an inverse isotope effect, then there will be a temporary decrease in the concentration of NADPH due to the forward reaction being faster than the reverse reaction. To determine the concentrations of NADPH, 3/4[^{2}H]-DXP, NADP$^+$ and MEP required for the mixture to be at chemical equilibrium at the

93

beginning of the perturbation experiment and to aid in the simulations to determine the KIE's, the equilibrium constants for the reaction with DXP, $3[^2H]$-DXP and $4[^2H]$-DXP and the corresponding equilibrium isotope effects were determined from the data in **Figure 3-9** and are reported in **Table 3-3**.
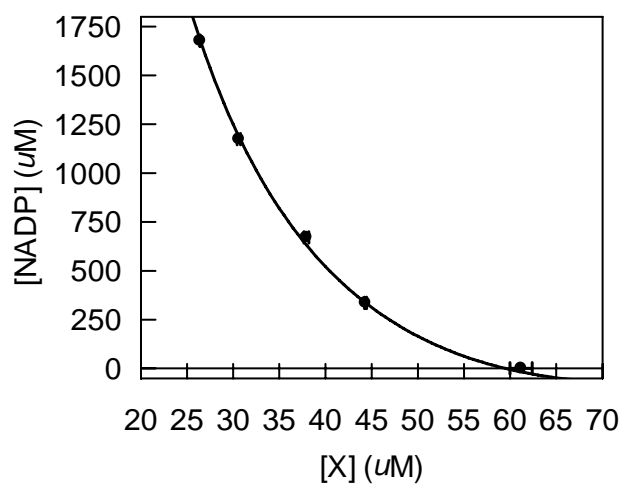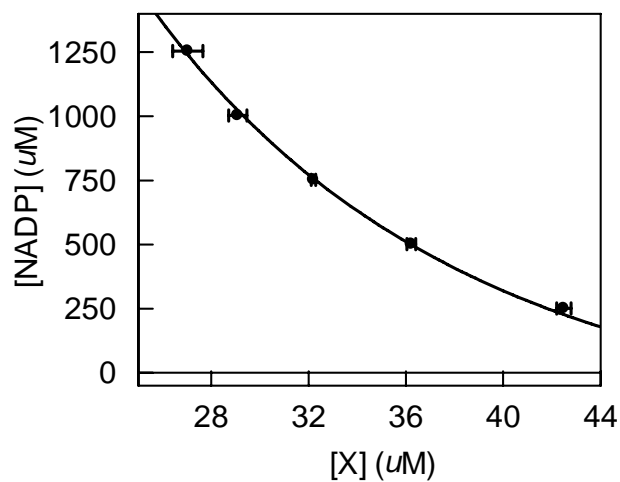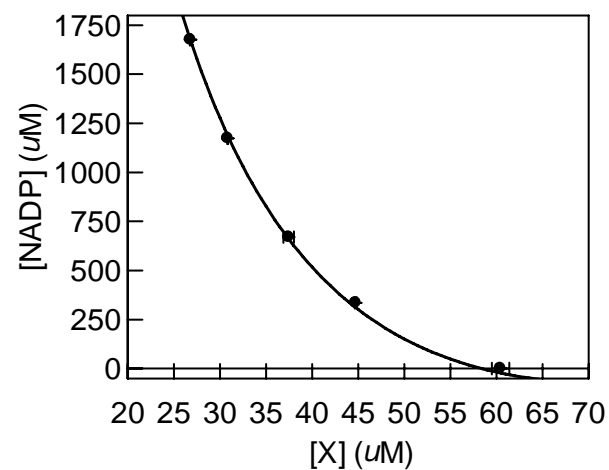
Figure 3-9: Curves for determining K_{eq} for the reaction with A) DXP, B) 3[^{2}H]-DXP, and C) 4[^{2}H]-DXP. [X] is from Equation 3-1, and represents the change in [NADPH] upon addition of DXR.

For $3[^2H]$-DXP and $4[^2H]$-DXP a temporary increase in the concentration of NADPH was observed before returning to equilibrium, corresponding to a normal 2° KIE for both compounds, see **Figure 3-10**. To solve for the KIEs, an equation was derived based on Cleland's methodology; however, to solve the differential equation, we had to assume that NADPH is in large excess of $3/4[^2H]$-DXP and MEP. Reaction conditions where this assumption is valid would produce a perturbation smaller than the detection limit of a UV/Vis instrument. To avoid this problem, conditions were used that produced a measurable perturbation in our experiment and the KIE was determined using a kinetic simulation software, as opposed to the FORTRAN program developed by Cleland.[28]
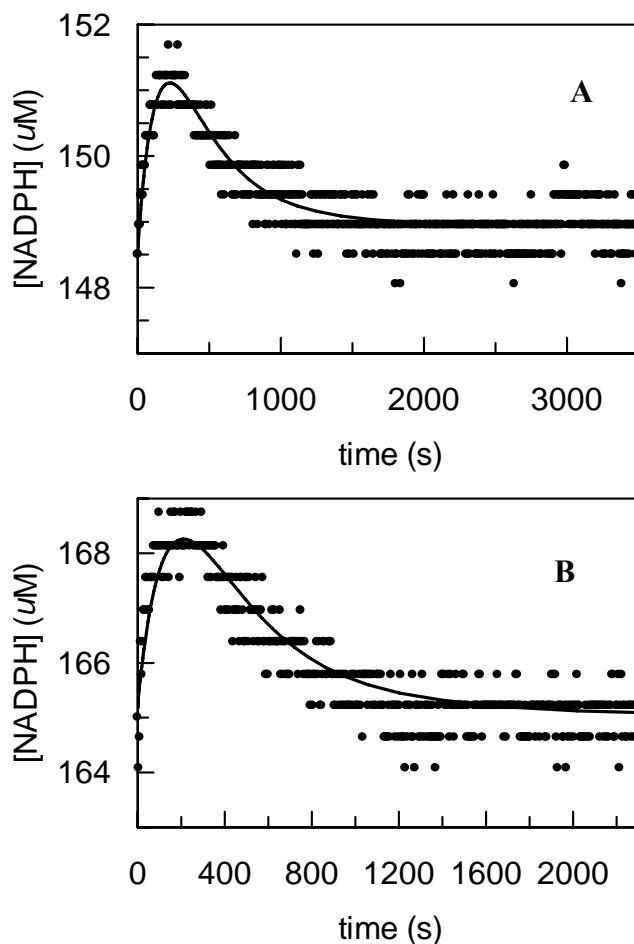
Figure 3-10: **Data from equilibrium perturbation experiment and the respective curve fit from computer simulations: A) 165 µM NADPH, 1 mM 3[^{2}H]-DXP, 1.1 mM MEP, 3.1 mM NADP$^+$ and 2 mM MgCl$_2$; B) 148.5 µM NADPH, 900 µM 4[^{2}H]-DXP, 990 µM MEP, 2.79 mM NADP$^+$ and 1.8 mM MgCl$_2$.**

The data was fit by computer simulation as described in the experimental section, and the resulting rate constants are listed in **Table 3-2**, and the corresponding KIE's are listed in **Table 3-3**. The normal KIE values for both compounds strongly favor the retroaldol/aldol rearrangement mechanism over the α-ketol rearrangement mechanism. These values are smaller than the 2° KIE values determined for muscle aldolase, suggesting either a step other than chemistry is partially rate-limiting, or the retroaldol reaction has an early transition state where little rehybridization has occurred. The size

97

of the KIE for 4[^{2}H]-DXP is slightly larger than 3[^{2}H]-DXP. This would result from the C3 having less *s*-character in the transition state than C4, which could result from the negative charge on C3 not fully delocalized on to the C2-carbonyl in the transition state.

Table 3-2:   **Results from computer simulations.**

	3[^{2}H]-DXP [(b)]		4[^{2}H]-DXP [(b)]	
	Float All	Fix Binding	Float All	Fix Binding
k_1	73 ± 3	73	72 ± 4	72
k_{-1}	55 ± 2	55	54 ± 3	54
k_2	2.15 ± 0.06	2.15	6.9 ± 0.3	6.9
k_{-2}	463 ± 13	463	946 ± 40	946
k_3	19.2 ± 0.5	19.6 ± 0.2	19.8 ± 0.5	19.8 ± 0.3
k_{-3}	9.1 ± 0.2	9.4 ± 0.1	9.4 ± 0.2	9.4 ± 0.1
k_4	2410 ± 130	2410	1660 ± 90	1660
k_{-4}	11.8 ± 0.4	11.8	5.9 ± 0.3	5.9
k_5	127 ± 5	127	91 ± 4	91
k_{-5}	16.5 ± 0.7	16.5	25 ± 1	25
k_6	2.15 ± 0.06	2.15	6.9 ± 0.3	6.9
k_{-6}	463 ± 13	463	946 ± 40	946
k_7	18.4 ± 0.4	18.9 ± 0.2	17.8 ± 0.4	17.8 ± 0.2
k_{-7}	8.4 ± 0.2	8.6 ± 0.1	9.4 ± 0.2	9.4 ± 0.1
k_8	2410 ± 130	2410	1660 ± 90	1660
k_{-8}	11.8 ± 0.4	11.8	5.9 ± 0.3	5.9

(b) All second order rate constants are given in $\mu M^{-1}s^{-1}$, and all first order rate constants are given in s^{-1}.

Table 3-3:   **Summary of K_{eq} and KIE data from equilibrium perturbation experiments.**

Substrate	K_{eq}	$^dK_{eq}$	$^dk_{chem}$ [(c)]
DXP	22.0 ± 0.3	--	--
3[^{2}H]-DXP	22.7 ± 0.2	0.97 ± 0.02	1.04 ± 0.02 (0.04)
4[^{2}H]-DXP	19.8 ± 0.2	1.11 ± 0.02	1.11 ± 0.02 (0.04)

(c) This is the KIE determined by the equilibrium perturbation experiment, and this value is determined by the ratio of k_3 to k_7, (See **Figure 3-7**). The error reported is from the simulations when the binding rates are fixed on the values obtained from initially allowing them to float, and the error is the parenthesis is the error for when all the rate constants are allowed to float. See supplementary section for a more complete description of the computer simulations.

3.4 CONCLUSION

In conclusion, the normal 2° KIE's observed for 3[^{2}H]-DXP and 4[^{2}H]-DXP are the first direct evidence that strongly favor the retroaldol/aldol rearrangement mechanism utilized by DXR to catalyze the rearrangement of DXP to the aldehyde intermediate. With this information in hand, it is now possible to design inhibitors by focusing only on the retroaldol/aldol mechanism and not the α-ketol rearrangement mechanism.

3.5 REFERENCES

(1)   Rohdich, F.; Bacher, A.; Eisenreich, W. Perspectives in anti-infective drug design: The late steps in the biosynthesis of the universal terpenoid precursors, isopentenyl diphosphate and dimethylallyl diphosphate. *Bioorg. Chem.*, **2004**, *32*, 292-308.

(2)   Penuelas, J.; Munne-Bosch, S. Isoprenoids: an evolutionary pool for photoprotection. *Trends Plant Sci.*, **2005**, *10*, 166-9.

(3)   Tudzynski, B. Biosynthesis of gibberellins in Gibberella fujikuroi: biomolecular aspects. *Appl. Microbiol. Biotechnol.*, **1999**, *52*, 298-310.

(4)   Fenton, J. W., 2nd; Jeske, W. P.; Catalfamo, J. L.; Brezniak, D. V.; Moon, D. G.; Shen, G. X. Statin drugs and dietary isoprenoids downregulate protein prenylation in signal transduction and are antithrombotic and prothrombolytic agents. *Biochemistry (Mosc)*, **2002**, *67*, 85-91.

(5)   Bochar, D. A.; Freisen, J. A.; Stauffacher, C. V.; Rodwell, V. W. In *Comprehesive Chemistry of Natural Products*; Cane, D. E., Ed.; Elsevier Science B.V.: Amsterdam, 1999; Vol. 2.

(6)   Eisenreich, W.; Schwarz, M.; Cartayrade, A.; Arigoni, D.; Zenk, M. H.; Bacher, A. The deoxyxylulose phosphate pathway of terpenoid biosynthesis in plants and microorganisms. *Chem. Biol.*, **1998**, *5*, R221-33.

(7)   Rohmer, M. The discovery of a mevalonate-independent pathway for isoprenoid biosynthesis in bacteria, algae and higher plants. *Nat. Prod. Rep.*, **1999**, *16*, 565-74.

(8)   Kuzuyama, T.; Seto, H. Diversity of the biosynthesis of the isoprene units. *Nat. Prod. Rep.*, **2003**, *20*, 171-83.

(9)   Jomaa, H.; Wiesner, J.; Sanderbrand, S.; Altincicek, B.; Weidemeyer, C.; Hintz, M.; Turbachova, I.; Eberl, M.; Zeidler, J.; Lichtenthaler, H. K.; Soldati, D.; Beck, E. Inhibitors of the nonmevalonate pathway of isoprenoid biosynthesis as antimalarial drugs. *Science*, **1999**, *285*, 1573-6.

(10)   Argyrou, A.; Blanchard, J. S. Kinetic and chemical mechanism of *Mycobacterium tuberculosis* 1-deoxy-D-xylulose-5-phosphate isomeroreductase. *Biochemistry*, **2004**, *43*, 4375-84.

(11)   Eisenreich, W.; Bacher, A.; Arigoni, D.; Rohdich, F. Biosynthesis of isoprenoids via the non-mevalonate pathway. *Cell. Mol. Life Sci.*, **2004**, *61*, 1401-26.

(12)   Wong, A.; Munos, J. W.; Devasthali, V.; Johnson, K. A.; Liu, H. W. Study of 1-deoxy-D-xylulose-5-phosphate reductoisomerase: synthesis and evaluation of fluorinated substrate analogues. *Org. Lett.*, **2004**, *6*, 3625-8.

(13)   Munos, J. W.; Dong, G.; Johnson, K. A.; Liu, H. W. *Manuscript in preparation*.

(14)   Anslyn, E. V.; Dougherty, D. A. *Modern Physical Organic Chemistry*; University Science Books: Sausalito, 2006.

(15)   Fox, D. T.; Poulter, C. D. Mechanistic studies with 2-C-methyl-D-erythritol 4-phosphate synthase from Escherichia coli. *Biochemistry*, **2005**, *44*, 8360-8.

(16)   Jencks, W. P. *Catalysis in Chemistry and Enzymology*; DoverPublications, Inc.: New York, 1975.

(17)   Taylor, S. V., Vu, L.D., Begley, T.P., Schorken, U., Grolle, S., Sprenger, G.A., Bringer-Meyer, S., Sahm, H. Chemical and Enzymatic Synthesis of 1-Deoxy-D-xylulose-5-phosphate. *J. Org. Chem.*, **1998**, *63*, 2375-2377.

(18)   Hecht, S., Wungsintaweekul, J., Rohdich, F., Kis, K., Radykewicz, T., Schuhr, C.A., Eisenreich, W., Richter, G., and Bacher, A. Biosynthesis of Terpenoids: Efficient Multistep Biotransformation Procedures Affording Isotope-Labeled 2C-Methyl-D-erythritol 4-Phosphate Using Recombinant 2C-Methyl-D-erythritol 4-Phosphate Synthase. *J. Org. Chem.*, **2001**, *66*, 7770-7775.

(19)   Koppisch, A. T.; Fox, D. T.; Blagg, B. S.; Poulter, C. D. E. coli MEP synthase: steady-state kinetic analysis and substrate binding. *Biochemistry*, **2002**, *41*, 236-43.

(20)   Munos, J. W.; Pu, X.; Liu, H. W. Synthesis and Analysis of a Fluorinated Product Analogue for the Mechanistic Analysis of 1-Deoxy-D-xylulose 5-phosphate Reductoisomerase. *Bioorg. Med. Chem. Lett.*, **2008**, in press.

(21)   Schimerlik, M. I.; Rife, J. E.; Cleland, W. W. Equilibrium perturbation by isotope substitution. *Biochemistry*, **1975**, *14*, 5347-54.

(22)   Cleland, W. W. In *Isotope effects on enzyme-catalyzed reactions : proceedings of the Sixth Annual Harry Steenbock Symposium*; Cleland, W. W., O'Leary, M. H., Northrop, D. B., Eds.; University Park Press: Madison, WI, 1976.

(23)   Cook, P. F.; Oppenheimer, N. J.; Cleland, W. W. Secondary deuterium and nitrogen-15 isotope effects in enzyme-catalyzed reactions. Chemical mechanism of liver alcohol dehydrogenase. *Biochemistry*, **1981**, *20*, 1817-25.

(24)   Wong, U.; Cox, R. J. The chemical mechanism of D-1-deoxyxylulose-5-phosphate reductoisomerase from Escherichia coli. *Angew. Chem. Int. Ed. Engl.*, **2007**, *46*, 4926-9.

(25)   Sculley, M. J.; Morrison, J. F.; Cleland, W. W. Slow-binding inhibition: the general case. *Biochim. Biophys. Acta*, **1996**, *1298*, 78-86.

(26)   Sharpless, K. B.; Amberg, W.; Bennani, Y. L.; Crispino, G. A.; Hartung, J.; Jeong, K. S.; Kwong, H. L.; Morikawa, K.; Wang, Z. M.; Xu, D.; Zhang, X.-L. The osmium-catalyzed asymmetric dihydroxylation: a new ligand class and a process improvement. *J. Org. Chem.*, **1992**, *57*, 2768-2771.

(27)   Phaosiri, C.; Proteau, P. J. Substrate analogs for the investigation of deoxyxylulose 5-phosphate reductoisomerase inhibition: synthesis and evaluation. *Bioorg. Med. Chem. Lett.*, **2004**, *14*, 5309-12.

(28)   Cleland, W. W. Measurement of isotope effects by the equilibrium perturbation technique. *Methods Enzymol.*, **1980**, *64*, 104-25.

Chapter 4: Reconfirmation HppE is an Iron and NAD(P)H Dependent Epoxidase

4.1. INTRODUCTION

Fosfomycin (**2**) is a clinically useful antibiotic[1] for the treatment of lower urinary tract infections[2] and limb-threatening diabetic foot infections.[3] It is also effective against methicillin-resistant[4] and vancomycin-resistant[5] strains of *Staphylococcus aureus*. The antimicrobial activity of fosfomycin has been attributed to the inactivation of UDP-GlcNAc-3-O-enolpyruvyltransferase (MurA), which catalyzes the first committed step in the biosynthesis of peptidoglycan, the main component of the cell wall.[6,7]
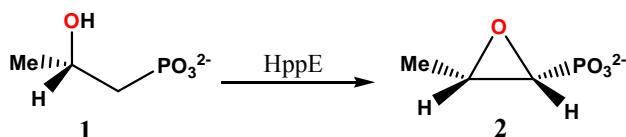
Figure 4-1:   Reaction catalyzed by HppE.

Fosfomycin (**2**) is a natural product that is made by several species of *Pseudomonas* and *Streptomyces*,[8,9] and it is biosynthetically derived from (*S*)-2-hydroxypropylphosphonic acid [**1**, (*S*)-HPP].[10,11] The conversion of (*S*)-HPP (**1**) to fosfomycin (**2**) is catalyzed by HPP epoxidase (HppE), see **Figure 4-1**.[12,13] A mononuclear non-heme iron in the HppE active site is essential for enzyme activity.[14] Coordination of the iron in the enzyme from *Streptomyces wedmorensis*, which is the source of the HppE used in this study, is by His138, Glu142, and His180. The 2-H-1-D/E facial triad, was first implied by sequence alignment[15] and site-directed mutagenesis studies,[16] and it was later confirmed by the X-ray crystal structure of this enzyme.[17] Earlier research also demonstrated that molecular oxygen is essential for the reaction.[13,14]

103

However, no oxygen atoms from O_2 are incorporated into the fosfomycin product.[11,13,14] Instead, the oxygen atom of the epoxy ring in **2** is derived from the secondary hydroxyl group of (*S*)-HPP (**1**). Thus, the conversion of **1** to **2** by HppE is effectively a dehydrogenation reaction, not an oxygenation reaction.

This unusual epoxidation reaction is NAD(P)H-dependent and involves four-electron redox chemistry with full reduction of dioxygen to water.[13,14] In this process, two electrons are generated through epoxide ring formation, and the other two electrons are supplied by NAD(P)H. The use of NAD(P)H as a source of reducing equivalents distinguishes HppE from most other mononuclear non-heme iron-dependent oxygenases, where the source of electrons is either the substrate or a cosubstrate such as α-ketoglutarate, ascorbate, or tetrahydropterin.[18-21]

Despite the unusual chemistry of its physiological reaction, HppE can also function as a typical oxygenase. In particular, it can self-hydroxylate an active site tyrosine to form 3,4-dihydroxyphenylalanine (DOPA).[22] The modified residue has been identified as Tyr105, on the basis of its proximity to the iron center (8.7 Å)[17] and the results of site-directed mutagenesis.[22] The chelation of DOPA105 with the active site ferric ion gives HppE a green color. This green chromophore has been assigned, on the basis of UV-vis and resonance Raman spectral analyses, to a catecholate-to-Fe(III) charge transfer complex.[22]

Unlike the self-hydroxylation reactions observed for other non-heme iron-dependent enzymes, such as the ribonucleotide reductase (RNR) R2 F208Y mutant,[23] taurine dioxygenase (TauD),[24] and 2,4-dichlorophenoxyacetic acid dioxygenase (TfdA),[25] where the newly introduced oxygen atom in DOPA is derived from H_2O, the oxygen atom incorporated into DOPA105 of HppE originates from dioxygen.[22] The discovery of such oxygenase activity for HppE is significant because the same reactive intermediate

responsible for self-hydroxylation may also participate in the reaction cycle for the formation of fosfomycin.
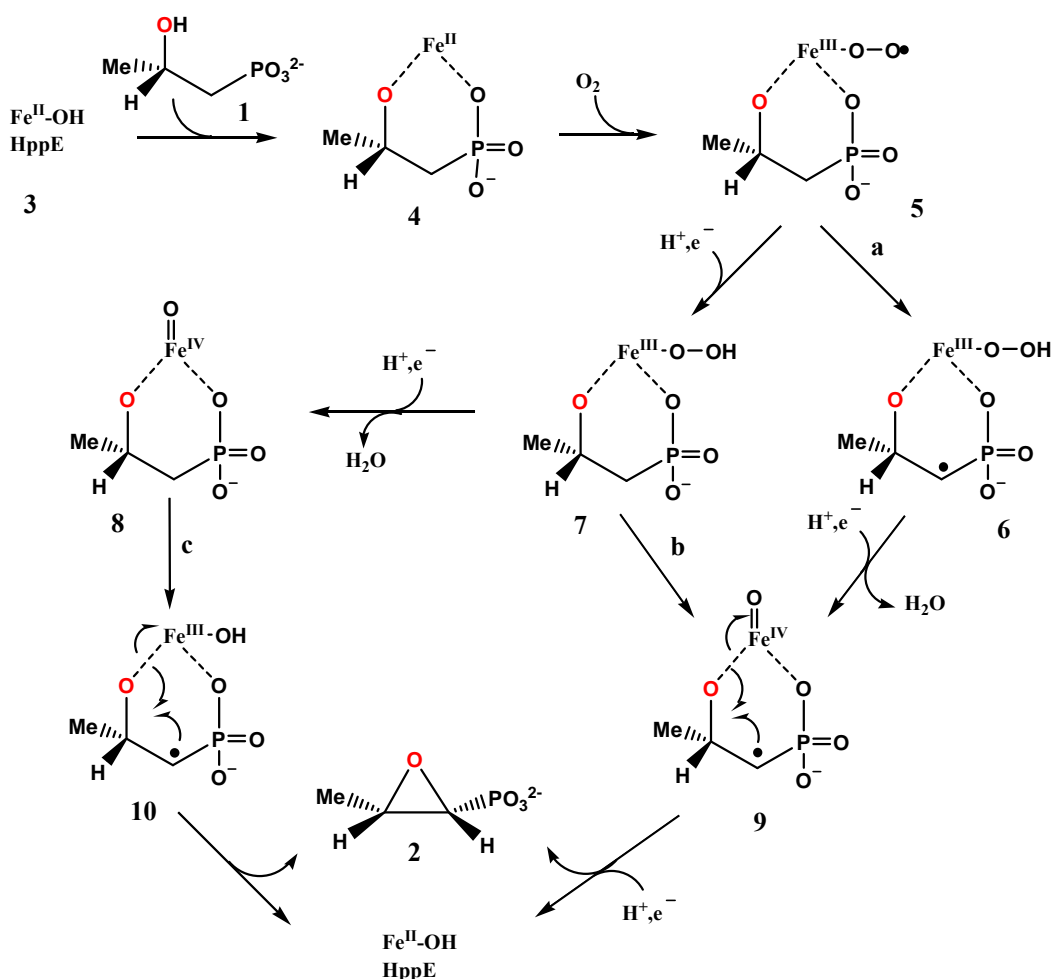
Figure 4-2: **Proposed NAD(P)H and Iron dependent mechanisms for HppE.**

The mechanism of HppE-catalyzed HPP epoxidation likely invokes an Fe^{III}-OOH intermediate (**7**) derived from the one-electron reduction of an initial Fe(II)-O_2 adduct. As shown in **Figure 4-2**, this peroxo intermediate (**7**) may either directly abstract a hydrogen atom from C-1 of (*S*)-HPP (**1**) to generate a transient substrate radical intermediate (**9**) or be converted to a high-valent iron-oxo species (such as **8**) that carries

out the oxidation (**8** →**10**). A direct attack by the iron-superoxide complex (**5**) to generate radical **6** is also possible. Evidence for the involvement of an iron-superoxide species in the myoinositol oxygenase reaction has been reported.[26] The subsequent cyclization to yield fosfomycin (**2**) and concomitant reduction of the metal center is reminiscent of oxygen rebound in the hydroxylation of alkanes by cytochrome P450[27] and non-heme iron oxygenases (see **Figure 4-3**).[28,29]
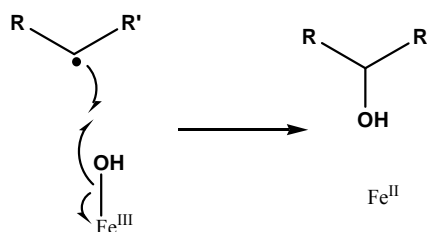
Figure 4-3:   **Oxygen rebound mechanism.**

In a recent study, McLuskey *et al.* found that purified recombinant HppE, also from *Streptomyces wedmorensis,* is active when reconstituted with Fe^{2+} or Zn^{2+}.[30] They also determined that HppE exhibits modest affinity for FMN which is required for activity. Since Zn^{2+} is redox inert, these findings suggested that the previously proposed mechanism, which relies on metal ion redox chemistry (**Figure 4-2**), is incorrect. Hence, McLuskey *et al.* proposed a new mechanism in which the active site-bound divalent metal ion (Fe^{2+} or Zn^{2+}) serves as a Lewis acid to activate the C-2 hydroxyl group, and the epoxide ring is formed by the attack of the 2-hydroxyl group at C-1 coupled with the transfer of the C-1 hydrogen as a hydride ion to the bound oxidized FMN (**11**). This "nucleophilic displacement-hydride transfer" mechanism is depicted in **Figure 4-4**.
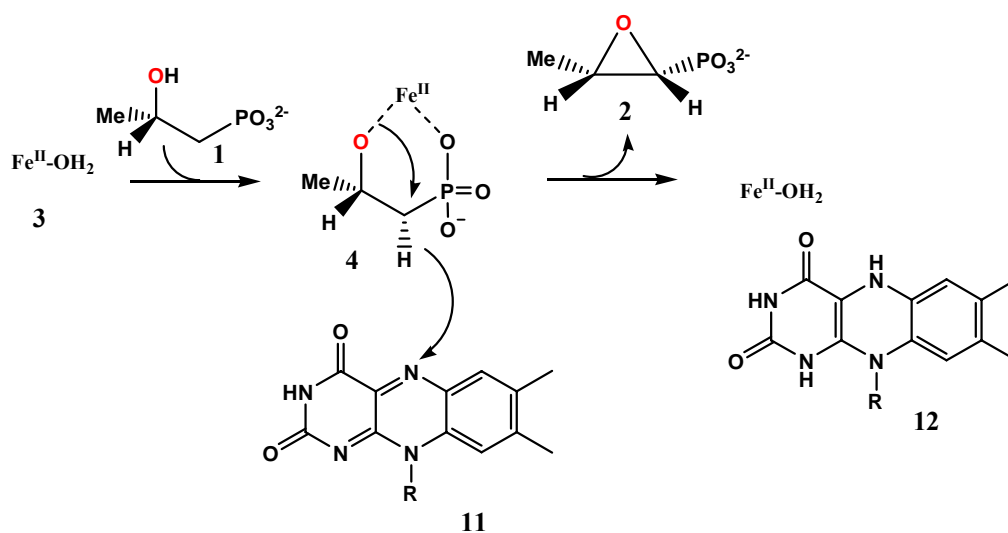
Figure 4-4: Proposed nucleophilic displacement-hydride transfer mechanism for HppE.

To resolve the mechanistic discrepancies, we characterized the Zn^{2+}-reconstituted HppE and re-evaluated the NADH dependence of HppE activity. We also compared the efficiency of various enzyme activity assays and determined the binding affinity of HppE for several flavin derivatives. The results support an exclusive role for iron in HppE catalysis. We also found that FMN is unlikely a hydride acceptor, but an artificial electron mediator for the *in vitro* HppE activity. It serves the role of accepting a hydride from NADH and then passes electrons on to reduce the iron center of HppE. On the basis of these lines of evidence, we conclude that the "iron redox chemistry" mechanism (**Figure 4-2**) stands as the more likely mechanism for the HppE-catalyzed reaction.

4.2.   MATERIALS AND METHODS

4.2.1. GENERAL. Enzyme E3 (AscD, CDP-6-deoxy-L-*threo*-D-*glycero*-4-hexulose-3-dehydrase reductase) used in the assay was purified from the *Escherichia coli* JM105/pOPI culture based on a procedure published earlier.[31]   Culture medium

ingredients were purchased from Difco (Detroit, MI). Biochemicals, including the fosfomycin disodium salt standard (**2**), were purchased from Sigma-Aldrich Chemical Co. (St. Louis, MO). The substrate, (*S*)-2-hydroxypropylphosphonic acid [(*S*)-HPP, **1**], was chemically synthesized according to a literature procedure.[13,14] All other reagents and solvents were purchased from commercial sources and were used without further purification unless otherwise noted. Protein concentrations were determined by the procedure of Bradford using bovine serum albumin as the standard.[32]

4.2.2. PURIFICATION OF HPPE WITH AND WITHOUT BOUND METALS. Recombinant HppE from *Streptomyces wedmorensis* was overproduced from *E. coli* BL21(DE3)/pPL1001, and the metal-free HppE (apo-HppE) was purified according to the published procedure.[14] An overnight culture of *E. coli* BL21(DE3)/pPL1001 grown at 37 °C in LB medium supplemented with kanamycin (50 μg/mL) was used, in a 200-fold dilution, to inoculate 6 L of the same medium. When the OD_{600} reached 0.6, the incubation temperature was lowered to 18 °C and IPTG was added to a final concentration of 0.1 mM to induce gene expression. After incubation for an additional 15 h at 18 °C, cells were harvested by centrifugation (8000*g*, 5 min) at 4 °C, washed with Tris·HCl buffer (20 mM, pH 7.5), collected again by centrifugation (8000*g*, 5 min), and stored at -80 °C for future use. The typical yield was 6 g of wet cells per liter of culture.

All purification operations were carried out at 4 °C except for the FPLC step, and all buffers were degassed and saturated with nitrogen before use. Thawed cells were resuspended in a 5-fold (w/v) excess of lysis buffer (20 mM Tris·HCl, pH 7.5, 0.1 mM DTT; 1 mM EDTA was included to remove trace amounts of iron ion when necessary) and subjected to 5 × 40 s ultrasonic bursts, with a 1 min cooling interval between each blast. Cellular debris was removed by centrifugation at 15000*g* for 20 min. The

supernatant was fractionated by ammonium sulfate, and the 30-65% ammonium sulfate precipitate was collected. The protein pellet was resuspended in a minimal amount of Tris·HCl buffer (20 mM, pH 7.5). The resulting protein solution was dialyzed against 1 L of the same buffer for 4 h with two buffer changes.

The dialysate was applied to a DEAE-Sepharose CL-6B column (2.5 × 24 cm) pre-equilibrated with 20 mM Tris·HCl, pH 7.5. After loading, the column was washed with 500 mL of the wash buffer (20 mM Tris·HCl, pH 7.5, 0.15 M KCl). The elution was then continued with a linear gradient of KCl from 0.15 to 0.35 M in 20 mM Tris·HCl buffer, pH 7.5 (2 L total volume). The flow rate was 2 mL/min, and fractions of 15 mL were collected throughout the gradient elution. The fractions containing the desired HPP epoxidase, as determined by SDS-PAGE, were pooled, concentrated to about 10 mL by ultrafiltration on an Amicon concentrator using a YM 10 membrane (Millipore, Bedford, MA), and desalted by dialyzing against 1 L of 20 mM Tris·HCl buffer, pH 7.5 for 3 h with two buffer changes.

The protein from the last step was further purified at room temperature by FPLC equipped with a Mono Q HR 10/10 (GE Healthcare, Piscataway, NJ) using the solvent systems A (20 mM Tris·HCl buffer, pH 7.5) and B (A plus 0.6 M NaCl). The elution profile included a linear gradient of 0 to 60% B from 0 to 25 min, followed by a linear gradient of 60 to 100% B from 25 to 26 min, and concluded with a 5 min wash at 100% B. The flow rate was 3 mL/min, and the detector was set at 280 nm. A sharp peak with a retention time of about 19 min was collected, concentrated by ultrafiltration as described before, desalted with 20 mM Tris·HCl buffer (pH 7.5), and stored at -80 °C.

4.2.3. BIOAUTOGRAPHY ASSAY. The conversion of (*S*)-HPP (**1**) to fosfomycin (**2**) by HppE was monitored by a previously developed bioautography assay, which is based on

the ability of fosfomycin to inhibit the biosynthesis of the bacterial cell wall.[14] A typical assay mixture (200 μL) contained 20 mM (*S*)-HPP (**1**), 90 μM apo-HppE, 90 μM FMN, 22.5 mM NADH, and 150 μM metal ions in 20 mM Tris-HCl buffer (pH 7.5). The reaction was carried out at room temperature for 2 h. Meanwhile, 20 mL of LB agar medium was autoclaved, cooled to 40-45 °C, mixed with 1 mL of *E. coli* K12 strain HW8235 precultivated in LB medium, and poured into a Petri dish. After the agar solidified, sterilized paper disks (10 mm in diameter) were placed on the top of the agar. Each reaction mixture was divided into two portions, one of which was filtered through a Y-10 membrane to remove HppE. Subsequently, an aliquot of 20 μL was applied to the paper disk, and the plate was incubated at 37 °C for 12-16 h. The amount of fosfomycin produced in the reaction mixture was estimated by measuring the diameter of the inhibition zone and comparing it with that of a fosfomycin standard (10 μL of a 5 mg/mL solution). To test the proposed hydride transfer mechanism, a separate set of reaction mixtures containing 20 mM (*S*)-HPP (**1**), 90 μM apo-HppE, 900 μM FMN, and 150 μM metal ions in 200 μL of 20 mM Tris-HCl buffer (pH 7.5) was prepared and incubated at room temperature for 2 h. The subsequent treatment was the same as that described above. These experiments were conducted by Dr. Fang Yan.

4.2.4. ^{31}P NMR SPECTROSCOPY ASSAY.   To directly determine the percentage of conversion of (*S*)-HPP (**1**) to fosfomycin (**2**) catalyzed by HppE, a ^{31}P NMR spectroscopy assay developed previously was used.[13,14] A typical assay mixture (200 μL) contained 20 mM (*S*)-HPP (**1**), 90 μM apo-HppE, 90 μM FMN, 22.5 mM NADH, and 150 μM metal ions in 20 mM Tris-HCl buffer (pH 7.5).   The reaction was carried out at room temperature for 2 h, followed by rapid freezing with liquid nitrogen. The frozen sample was thawed immediately before ^{31}P NMR analysis. The amount of fosfomycin produced

110

was determined on the basis of the integration of the appropriate ^{31}P NMR peaks. To test the newly proposed "hydride transfer" mechanism, the assay conditions were modified to include 20 mM (*S*)-HPP (**1**), 90 μM apo-HppE, 900 μM FMN, and 150 μM metal ions in 200 μL of 20 mM Tris-HCl buffer (pH 7.5). The incubation was allowed to proceed at room temperature for 2 h and then flash-frozen with liquid nitrogen. The frozen sample was thawed immediately before NMR analysis. These experiments were conducted by Dr. Fang Yan.

4.2.5. NADH STOICHIOMETRY. The NADH dependence of the conversion of (*S*)-HPP to fosfomycin was also studied. The reaction mixture (100 μL) contained 4.5 mM (*S*)-HPP (**1**), 78 μM apo-HppE, 120 M Fe(NH$_4$)$_2$(SO$_4$)$_2$, 156 μM FMN, and various amounts of NADH (0-0.9 mM). The incubation was carried out at room temperature for 2 h, and the reaction was quenched by the addition of EDTA to a final concentration of 100 mM, followed by freezing with liquid nitrogen. Product formation was assessed by ^{31}P NMR spectroscopy. The percentage of conversion was calculated on the basis of the integration of the corresponding peaks [fosfomycin vs the sum of fosfomycin and (*S*)-HPP] from the spectra. These experiments were conducted by Dr. Fang Yan.

4.2.6. BINDING AFFINITY OF FLAVIN DERIVATIVES. The binding affinity between HppE and various flavin derivatives (**11a-c**) was determined by the change in fluorescence intensity of flavin resulting from binding to HppE. Since flavin fluorescence is linear only up to ~5 μM, HppE was titrated into the flavin solution [1 μM flavin in 2 mL of 20 mM Tris-HCl buffer (pH 7.5)], as opposed to the standard method of titrating the ligand into the enzyme solution. The excitation and emission wavelengths were 450 and 525 nm, respectively, and the excitation and emission slit widths were set

at 1 and 3 nm, respectively. The titrations were carried out at 25 °C. The fluorescence data were adjusted so that the y-axis represented the net decrease in fluorescence. These data were then fit, using Grafit 5.0.1, to Equation **2-1** with F_o, F, and K_D as parameters, where F_o is the initial fluorescence, F_∞ is the final fluorescence, E_o is the total HppE concentration, and S_o is the total ligand concentration.[33]

Equation 4-1

$$F = F_o + \left(\frac{E_o + S_o + K_D - \sqrt{(E_o + S_o + K_D)^2 - 4E_oS_o}}{2E_o} \right)(F_\infty - F_o)$$

4.2.7. HPLC ACTIVITY ASSAY.   Enzyme assays were carried out in 50 µL of 20 mM Tris-HCl buffer (pH 7.5) in triplicate. The reactions were initiated by the addition of a mixture of apo-HppE, $Fe(NH_4)_2(SO_4)_2$, and an electron mediator (flavin cofactors (**11a-c**), benzyl viologen (**15**), methyl viologen (**16**) or E_3) to a mixture of (*S*)-HPP (**1**) and NADH. The final concentrations were as follows: 50 µM HppE, 50 µM Fe^{2+}, 75 µM flavin cofactors/benzyl viologen/E_3, 10 mM (*S*)-HPP (**1**), and 15 mM NADH.   The reactions were quenched by the addition of 2 M acetic acid (50 µL), and then the mixtures centrifuged through a Nanosep centrifugal device with a 10K Omega Membrane (Pall Life Sciences, Ann Arbor, MI) to remove protein. The samples (77 µL each) were analyzed with a HPLC system equipped with a Dionex CarboPac PA-1 (4 × 250 mm) column. The fosfomycin product was eluted with a gradient of water as solvent A and 500 mM NH_4OAc as solvent B where the following gradient was used: 5% B for 2 min, from 5 to 25% B over 30 min, from 25 to 100% B over 1 min, 100% B for 9 min, from 100 to 5% B over 2 min, and then 5% B for 13 min. The flow rate was 1 mL/min. The detector used is the Corona charged aerosol detector (CAD) (ESA, Inc., Chelmsford,

MA), which is designed to detect nonvolatile compounds. The amount of fosfomycin produced was determined by peak integration and then converted into micromoles on the basis of a calibration curve.

4.3. RESULTS AND DISCUSSION

4.3.1. ENZYME ACTIVITY DETERMINED BY BIOAUTOGRAPHY ASSAY.

Two assay methods had been developed in our early work to determine the activity of HppE.[13,14] One is the bioautography assay, in which a paper disk soaked with the assay mixture is placed in direct contact with a lawn of *E. coli* K12 HW8235 grown on nutrient (LB) agar. When fosfomycin is produced in the assay mixture, an inhibition zone is visible after incubation for a few hours. Using this bioautography assay led to the identification of Fe(II) and NAD(P)H as two essential components for HppE activity.[13,14] While this assay is convenient and sensitive, the same incubation mixture with all of the components mentioned above included failed to produce enough fosfomycin that can be discerned by NMR analysis.[13] It was later found by a ^{31}P NMR assay that the addition of FMN or FAD greatly enhanced the production of fosfomycin.[13,14] Because this NMR method allows direct detection of fosfomycin production in the assay mixture, it has been the assay of choice in our subsequent studies. However, since the conclusions of McLuskey *et al*. about HppE activity and mechanism were based mainly on the bioautography results,[30] we decided to re-examine the assay conditions using both Fe(II)- and Zn(II)-reconstituted HppE. It should be pointed that FMN was introduced into the bioautography assay carried out by McLuskey *et al*. but was not included in our original bioautography assay.[13,14]

As shown in **Figure 4-5**, fosfomycin production was detected in the incubation mixture containing Zn(II)-HppE (disk 1) and Fe(II)-HppE (disk 4) complexes with excess

113

FMN and (*S*)-HPP (**1**). The addition of NADH to the assay mixture led to more fosfomycin formation in both cases as indicated by the enlarged diameter of inhibition zones (**Figure 4-5B**, disks 1 and 4). These results are in agreement with those of McLuskey *et al.* [30] showing that the Zn(II)-HppE complex is catalytically active but less active than the Fe(II)-HppE complex. However, we were troubled by the positive response given by the metal-free apo-HppE sample, which was performed as a negative control (disk 3 in **Figure 4-5A,B**). The fact that the Fe(II)-HppE complex was active in the absence of NADH was also puzzling (**Figure 4-5A**, disk 4).
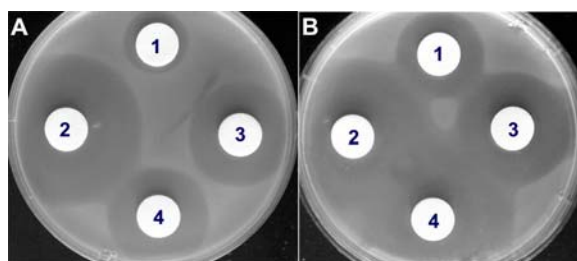
Figure 4-5: Bioautography assay results of unfiltered reaction samples. (A) (1) Apo-HppE, Zn(II), FMN, and (*S*)-HPP, (2) fosfomycin standard, (3) apo-HppE, FMN, and (*S*)-HPP, and (4) apo-HppE, Fe(II), FMN, and (*S*)-HPP. (B) (1) Apo-HppE, Zn(II), FMN, (*S*)-HPP, and NADH, (2) fosfomycin standard, (3) apo-HppE, FMN, (*S*)-HPP, and NADH, and (4) apo-HppE, Fe(II), FMN, (*S*)-HPP, and NADH.

Since HppE was not removed prior to application of the reaction mixture to the disk, it should still be catalytically active when exposed to the nutrient rich agar media where metal ions are plentiful. This "postincubation activation/activity" may be partially responsible for the positive response exhibited by the Zn(II)-HppE and apo-HppE samples. To eliminate this potential complication, the reaction mixture was passed through a membrane with a molecular mass cutoff of 10 kDa. After this treatment, the inhibition results should reflect the total amount of fosfomycin produced in the assay solution under defined reaction conditions because no HppE is available to make

additional fosfomycin during the overnight incubation on the plate. As expected, no inhibition by the reaction mixture containing the Zn(II)-HppE sample was discernible (**Figure 4-6A,B**, disk 1), whereas the inhibitory effect of the Fe(II)-HppE sample remained very apparent (**Figure 4-6B**, disk 3). The addition of more FMN to the reaction mixture containing the Zn(II)-HppE complex (up to 200-fold more than the HppE concentration) showed no effect on the autobiography results (data not shown). It is thus evident that the Zn(II)-HppE sample is not active and Zn(II) cannot substitute for Fe(II) in reconstituting a catalytically active HppE. The activity observed for the unfiltered samples shown in **Figure 4-5** must be an artifact and may be attributed to the ability of HppE on the disk to elicit iron from the LB agar to make fosfomycin.
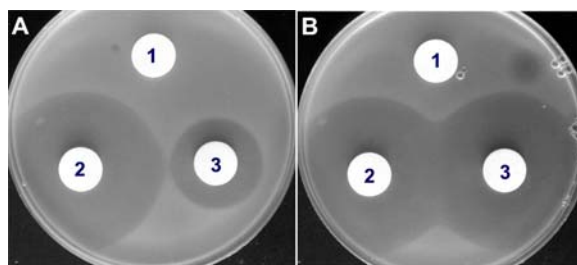
Figure 4-6: Bioautography assay results of filtered reaction samples. (A) (1) Apo-HppE, Zn(II), FMN, and (*S*)-HPP, (2) fosfomycin standard, and (3) apo-HppE, Fe(II), FMN, and (*S*)-HPP. (B) (1) Apo-HppE, Zn(II), FMN, (*S*)-HPP, and NADH, (2) fosfomycin standard, and (3) apo-HppE, Fe(II), FMN, (*S*)-HPP, and NADH.

While the observations described above clearly ruled out a role for Zn(II) in the HppE-catalyzed reaction, the inhibitory effect exhibited by the mixture containing Fe(II) and FMN but no NADH was unexpected (**Figure 4-5A**, disk 4, and **Figure 4-6A**, disk 3). We speculated that the photoreducible properties of FMN could play a role. This speculation was substantiated by the subsequent two parallel reactions, one carried out in the dark and another in sunlight. As for the reaction in the dark without NADH, no

detectable level of fosfomycin was produced when the incubation mixture was filtered prior to being applied to the disk (**Figure 4-7**, disk 3). In sharp contrast, the same reaction performed in sunlight gave a large inhibition zone (**Figure 4-7**, disk 2). Thus, photoreduction of FMN is clearly the cause of the complication. Taken together, enzyme activity determined by the bioautography assay should be analyzed with caution, since the readout could be misleading if the assay conditions are not properly controlled.
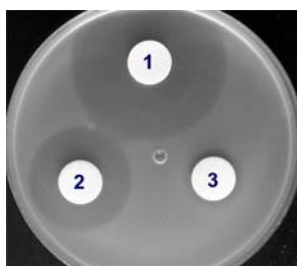
Figure 4-7: **Bioautography assay results of filtered reaction samples carried out in dark and in sunlight: (1) fosfomycin standard, (2) apo-HppE, Fe(II), FMN, and (*S*)-HPP in sunlight, and (3) apo-HppE, Fe(II), FMN, and (*S*)-HPP in the dark.**

4.3.2. ENZYME ACTIVITY DETERMINED BY NMR SPECTROSCOPY. The HppE reactions conducted under various conditions as described above were also subjected to ^{31}P NMR analysis. In agreement with our previous observation, only the incubation mixture containing the Fe(II)-HppE complex in the presence of FMN and NADH produced NMR-discernible amounts of fosfomycin from (*S*)-HPP (**1**). The detection limit of fosfomycin is estimated to be 1 mM on the basis of ^{31}P NMR peak integration and is equivalent to 5% conversion of (*S*)-HPP (20 mM, total amount used) under our assay conditions. The fact that no fosfomycin formation was detected when the Zn(II)-HppE complex was used strongly suggested an exclusive role for iron in HppE catalysis. In an earlier study, the apo-HppE was reconstituted with various redox active metal ions to examine their effects on enzyme activity using the same NMR assay. Among the

divalent metal ions that were examined [Fe(II), Co(II), Ni(II), Cu(II), and Mn(II)], only Fe(II) could reconstitute HppE activity.[14] Thus, HppE is believed to be iron-dependent. Clearly, the direct detection of product formation by NMR spectroscopy is a much more reliable activity assay.

4.3.3. ENZYME ACTIVITY DETERMINED BY THE HPLC ASSAY.

Although ^{31}P NMR spectroscopy is a highly reliable method of measuring fosfomycin production, it is not amenable to microanalysis due to its low sensitivity. To overcome this shortcoming, an HPLC assay coupled with a charged aerosol detector (CAD) to detect nonvolatile compounds in the eluent was developed. This HPLC assay allowed us to quantitatively analyze the conversion of (*S*)-HPP (**1**) to fosfomycin (**2**), both nonchromophoric, under different incubation conditions. As illustrated in **Figure 4-8**, baseline resolution of **1** and **2** was achieved using a Dionex CarboPac PA-1 (4 × 250 mm) column.
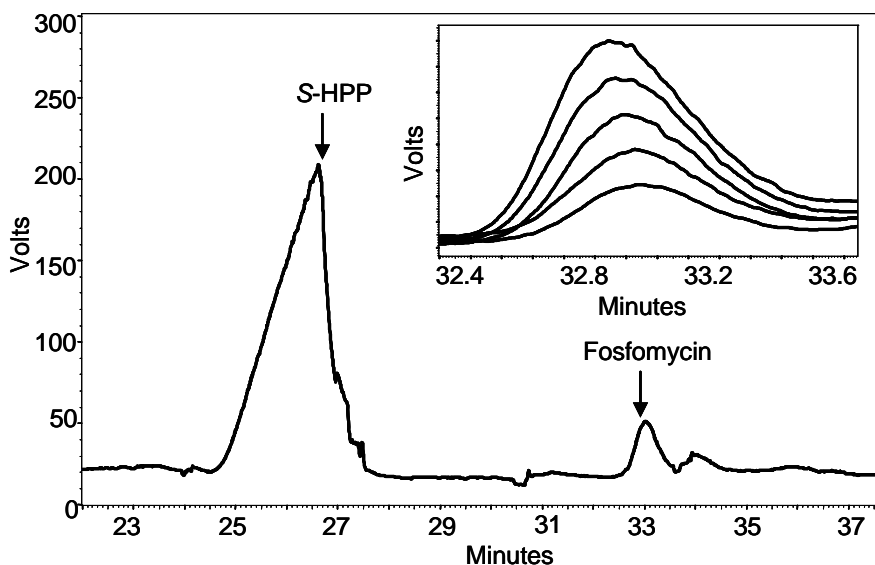
Figure 4-8:   **HPLC chromatogram of the HppE-catalyzed conversion of (*S*)-HPP (1) to fosfomycin (2). The inset shows the increase in the fosfomycin peak after 10, 20, 40, 60, and 80 min (from bottom to top).**

117

4.3.4. NADH DEPENDENCE OF HPPE ACTIVITY. A fundamental distinction between the iron-redox mechanism and the nucleophilic displacement-hydride transfer mechanism is the NADH dependence of the reaction. As depicted in **Figure 4-2**, in the iron-redox mechanism, NADH plays an essential role by supplying two electrons to prime the iron center for oxygen activation and to reduce an iron-oxygen species during catalysis. In contrast, no NADH is needed for the nucleophilic displacement-hydride transfer mechanism (**Figure 4-4**) since the transferred hydride is derived from (*S*)-HPP (**1**) and not from NADH. Although the activity assay results have clearly implicated NADH as the source of reducing equivalents, further analysis was performed to determine the stoichiometry of NADH required per catalytic turnover to better quantify the NADH dependence. As expected, a direct correlation between the percentage of conversion and the NADH/(*S*)-HPP ratio was found (see **Figure 4-9**). Our data also established that 1 equiv of NADH is consumed per conversion of 1 equiv of (*S*)-HPP to fosfomycin. The direct involvement of NADH in the HppE reaction supports the iron-redox mechanism and is not consistent with a nucleophilic displacement-hydride transfer mechanism.
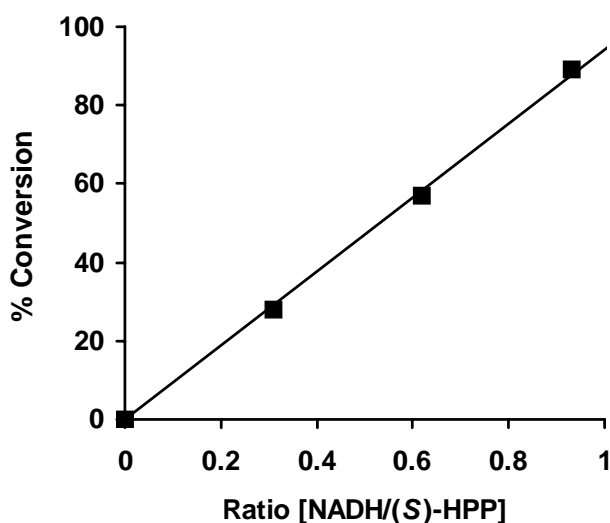
Figure 4-9:   The NADH-dependence of the conversion of (*S*)-HPP (**1**) to fosfomycin (**2**) catalyzed by HppE.

118

4.3.5. BINDING OF FLAVIN COFACTORS. While no flavin cofactor was found in the purified HppE, FMN had been shown to be an important component in the HppE activity assay.[13,14] It serves as an electron mediator in the iron-redox mechanism and has been proposed to be the hydride acceptor in the nucleophilic displacement-hydride transfer mechanism.[30] Since the translated sequence of HppE lacks an ADP βαβ-binding fold characteristic of flavin-dependent enzymes and reconstitution failed to incorporate FMN in the active site, FMN has not been considered to be a true coenzyme of HppE.[13] Instead, it is believed to function as a surrogate in the iron-redox mechanism for an electron transfer protein involved in the catalysis in vivo. Interestingly, a K_d of 10 μM for dissociation of FMN from HppE was determined by McLuskey *et al.*,[30] which was cited as an indication of a specific binding of FMN in HppE in support of the proposed nucleophilic displacement-hydride transfer mechanism.
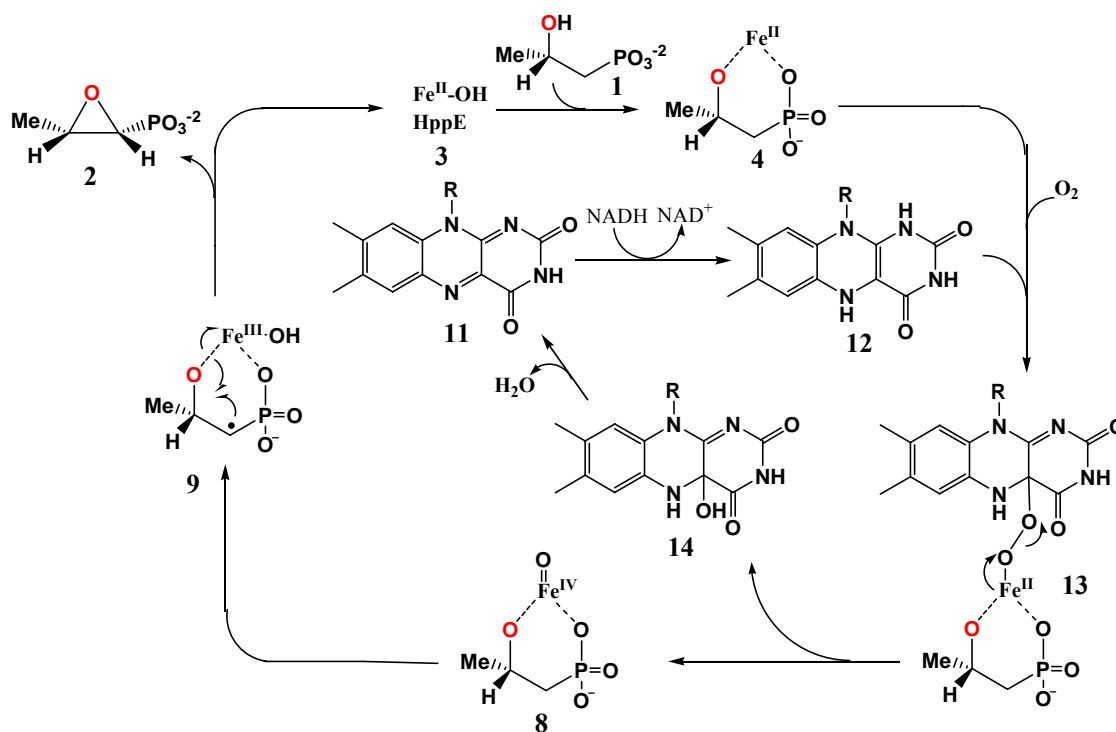
Figure 4-10: **Proposed pterin-dependent hydroxylase-like mechanism for HppE**

119

If FMN is indeed a coenzyme of HppE, a non-heme iron pterin-dependent hydroxylase-like mechanism found for aromatic amino acid hydroxylase (see **Figure 4-10**), where a Fe-O-O-pterin intermediate (**13**) is involved, may also need to be considered.[19,20]   In this mechanism, the reduced flavin (**12**), acting as a tetrahydrobiopterin mimic, may react with Fe(II)-activated dioxygen to form a Fe-O-O-flavin intermediate (**13**). Subsequent heterolytic breakdown of the O-O bond leads to the generation of the reactive Fe(IV)-oxo intermediate (**8**). This iron-oxo species, capable of hydroxylating the substrate in the aromatic amino acid hydroxylase reaction, may be used to abstract the C-1 hydrogen of (*S*)-HPP (**1**) in the HppE reaction (**8** →**9**). To gain more insight into flavin binding, the affinities of HppE for a series of flavin analogues were determined.

Table 4-1:   **Binding affinity of HppE for flavin derivatives.**

	Apo-HppE	Zn(II)-HppE	Fe(II)-HppE
Riboflavin (**11a**)	N.B. [a]	N.B.	N.B.
FMN (**11b**)	N.B.	$3.2 \pm 0.9 \ \mu M$	$5.3 \pm 0.9 \ \mu M$
FAD (**11c**)	N.B.	$300 \pm 700 \ \mu M$	$50 \pm 10 \ \mu M$
FMN + (*S*)-HPP	-	N.B.	N.B.

[a]N.B., no binding. This is based on an estimated upper detection limit of a K_d equal to 1 mM.

In this study, the K_d constants were determined by the change in the fluorescence intensity of flavin resulting from binding to HppE (see **Figures 4-11** and **4-12**), and the K_d's determined are listed in **Table 4-1**. The K_d values for binding of FMN (**11b**) to the Zn(II)-HppE and Fe(II)-HppE complexes are 3.2 ± 0.9 and $5.3 \pm 0.9 \ \mu M$, respectively, similar to the reported values measured by isothermal titration calorimetry.[30] However, when metal ions were absent (apo-HppE) or substrate, (*S*)-HPP (**1**), was present, no binding interaction between FMN and protein was detected (**Table 4-1**).   These

observations suggest that the binding of substrate and the binding of FMN are mutually exclusive and do not support specific binding of FMN to HppE. Interestingly, riboflavin (**11a**), which is an effective FMN (**11b**) substitute (see **Table 4-2**), shows no affinity for the Zn(II)-HppE or Fe(II)-HppE complex (**Table 4-1**). Since the epoxidation reaction catalyzed by HppE proceeds at a comparable rate using FMN (**11b**) or riboflavin (**11a**) (**Table 4-2**) and if HppE binds FMN in a specific manner, one would expect a similar specific binding of riboflavin. Taken together, the measured binding interactions are unlikely catalytically relevant and may result from binding of the phosphate of FMN to the metal center. This would explain why the presence of substrate, which is known to bind to the active site metal,[17] can block FMN binding and why riboflavin, which has no phosphate group, cannot bind to the enzyme. The probability of a flavoenzyme not having a defined flavin binding pocket is low. The fact that no flavin was found in the crystal structure of HppE also suggests that a specific flavin binding site in HppE is not present.[17,30]
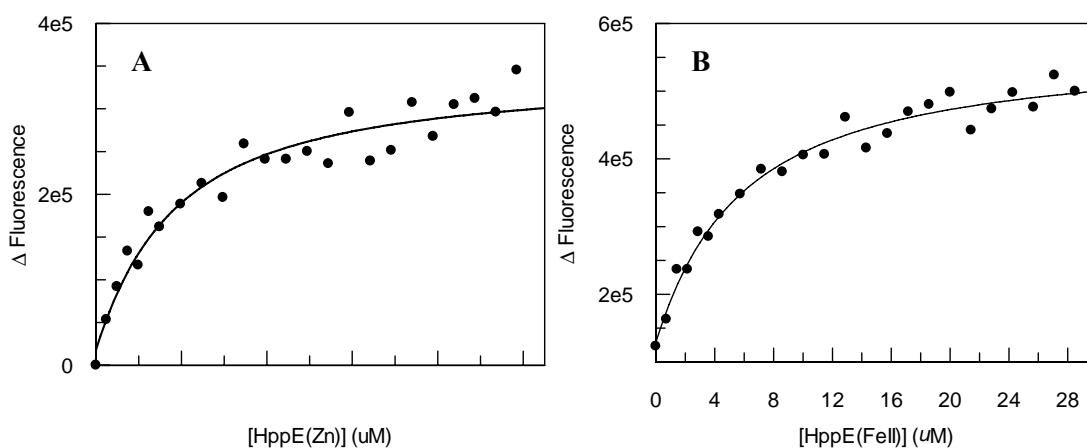
Figure 4-11: To examine FMN (**11b**) binding, A) HppE(Zn^{2+}) and B) HppE(Fe^{2+}) were titrated into a 1 μM solution of FMN in 20 mM Tris pH 7.5.
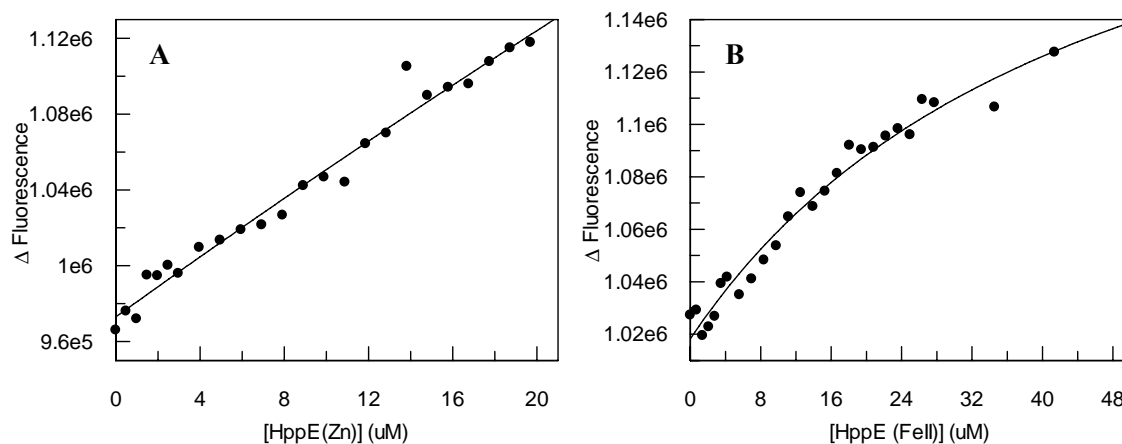
Figure 4-12: To examine FAD (**11c**) binding, A) HppE(Zn^{2+}) and B) HppE(Fe^{2+}) were titrated into a 1 μM solution of FAD in 20 mM Tris pH 7.5.

4.3.6. ELECTRON MEDIATORS. Using our newly developed HPLC assay, we determined the rates for fosfomycin formation with FMN (**11b**) and other electron mediators (**Figure 4-11**), including FAD (**11c**), riboflavin (**11a**), benzyl viologen (**15**), methyl viologen (**16**) and an electron transfer protein, E$_3$. As listed in **Table 4-2**, the rates of these reactions are within the same order of magnitude, suggesting that these compounds and/or proteins are all competent to enhance HppE reaction. As discussed above, riboflavin does not bind to HppE, yet it is as effective as FMN which binds to the Fe(II)-HppE complex with a K_d of 5.3 ± 0.9 μM (**Table 4-1**). This observation is at odds with the expectation of a flavin-dependent hydride transfer mechanism, because the lack of riboflavin binding should result in a significant reduction in enzyme activity. Interestingly, HppE remains active, albeit slightly slower, when FMN (**11b**) is replaced with benzyl viologen (**15**). This finding again supports an electron mediator role of FMN in catalysis because benzyl viologen is a well-known electron carrier and is not expected to bind to the putative FMN binding site due to lack of structural similarity with FMN. The reduced rate seen for benzyl viologen may be due to its $E_m°$ value of -370 mV which

122

is lower than the midpoint potential of -211 mV for free FMN.[34,35] In agreement with this analysis, replacing FMN with methyl viologen (**16**), which has a much lower $E_m°$ (-448 mV),[34] failed to reconstitute HppE activity.

Table 4-2: Rates of HppE-catalyzed epoxidation using different electron mediators.

	Riboflavin (**11a**)	FMN (**11b**)	FAD (**11c**)	E_3	Benzyl viologen (**15**)	Methyl viologen (**16**)
k (min^{-1})	0.41 ± 0.03	0.44 ± 0.05	0.22 ± 0.03	1.3 ± 0.2	0.13 ± 0.01	N.A.^{b}

b) N.A. stands for no activity detected
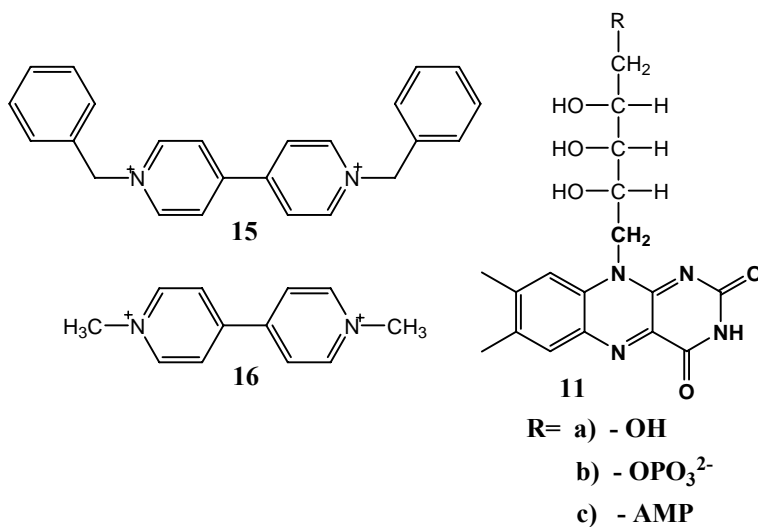
Figure 4-13: Structure of the electron mediators analyzed.

The results obtained with E_3, an NADH-dependent [2Fe-2S]-containing flavoenzyme from *Yersinia pseudotuberculosis*,[36,37] provide further support for the assigned electron mediator role of FMN in HppE catalysis. E_3, along with E_1 (CDP-6-deoxy-L-*threo*-D-*glycero*-4-hexulose-3-dehydrase), catalyzes the C-3 deoxygenation reaction in the biosynthesis of 3,6-dideoxyhexoses.[38] During turnover, the reducing equivalents are relayed from the E_3-bound NADH to the active site of E_1 via a chain of redox-active cofactors, including FAD and the iron-sulfur center in E_3.[37] The

involvement of an iron-sulfur cluster, an obligatory one-electron carrier, defines E_3 as an electron transfer protein. No change in function is expected for E_3 in the HppE reaction where the FAD in E_3 is the immediate recipient of hydride from NADH and serves as a two-electron (hydride)/one-electron switch in the subsequent electron relay to reduce the ferric center in HppE. The fact that E_3 is more effective than any flavin analogues that were tested (**Table 4-2**) implies that the physiological electron mediator is likely a protein reductase. However, since no reductase gene exists in the two known fosfomycin biosynthetic gene clusters of *Streptomyces wedmorensis*[12] and *Pseudomonas syringae*,[39] the electron transfer in the HppE reaction may not be mediated by a specific reductase but may rely on a promiscuous reductase within the cell.

4.4. CONCLUSION

Literature precedence for epoxide formation via a nucleophilic substitution mechanism comes from the halohydrin dehalogenase reaction in which the leaving group is a chloride (or a bromide) anion that is intramolecularly displaced by a vicinal hydroxyl group to yield the corresponding epoxide.[40] A similar mechanism has recently been proposed for HppE where a divalent metal ion [Zn(II) or Fe(II)] acts as a Lewis acid and enhances the nucleophilicity of the attacking 2-hydroxyl group, and an active site-bound flavin coenzyme (FMN) receives the departing hydride to complete this energetically challenging epoxidation reaction (**Figure 4-4**).[30] However, in this study, we have demonstrated that the Zn(II)-reconstituted HppE is catalytically inactive, and FMN cannot bind to the HppE-substrate binary complex. Both observations fail to support the nucleophilic displacement-hydride transfer mechanism. Likewise, a non-heme iron pterin-dependent hydroxylase-like mechanism (**Figure 4-10**) can be ruled out on the basis of the preclusion of binding of FMN to the HppE-substrate complex and the

124

competence of non-flavin electron mediators in the catalysis. Our results also confirmed that Fe(II) is the only metal ion examined that is effective in reconstituting HppE activity, and NADH is an exogenous electron donor which is necessary for multiple turnovers by the Fe(II)-HppE complex. The requirement of an electron mediator, either an electron transfer protein or a small molecule electron carrier, for HppE activity is also firmly established. All of these results strongly support the iron-redox mechanism (**Figure 4-2**). Clearly, the reaction catalyzed by HppE is beyond the scope encompassed by common biological epoxidation and C-O bond formation reactions. More studies aimed at uncovering details of the mechanism of HppE-catalyzed epoxidation are in progress. Insight gained from study of this unique non-heme iron-dependent enzyme will certainly enhance our understanding of this important and growing enzyme family.

4.5. REFERENCES

(1)   Itoh, N.; Kusaka, M.; Hirota, T.; Nomura, A. Microbial production of antibiotic fosfomycin by a stereoselective epoxidation and its formation mechanism. *App. Microbio. Biotech.*, **1995**, *43*, 394-401.

(2)   Lobel, B. Short term therapy for uncomplicated urinary tract infection today. Clinical outcome upholds the theories. *Int. J. Antimicrob. Agents*, **2003**, *22 Suppl 2*, 85-7.

(3)   Stengel, D.; Gorzer, E.; Schintler, M.; Legat, F. J.; Amann, W.; Pieber, T.; Ekkernkamp, A.; Graninger, W. Second-line treatment of limb-threatening diabetic foot infections with intravenous fosfomycin. *J. Chemother.*, **2005**, *17*, 527-35.

(4)   Nakazawa, H.; Kikuchi, Y.; Honda, T.; Isago, T.; Nozaki, M. Enhancement of antimicrobial effects of various antibiotics against methicillin-resistant Staphylococcus aureus (MRSA) by combination with fosfomycin. *J. Infect. Chemother.*, **2003**, *9*, 304-9.

(5)   Cassone, M.; Campanile, F.; Pantosti, A.; Venditti, M.; Stefani, S. Identification of a variant "Rome clone" of methicillin-resistant Staphylococcus aureus with decreased susceptibility to vancomycin, responsible for an outbreak in an intensive care unit. *Microb. Drug. Resist.*, **2004**, *10*, 43-9.

(6)   Marquardt, J. L.; Brown, E. D.; Lane, W. S.; Haley, T. M.; Ichikawa, Y.; Wong, C. H.; Walsh, C. T. Kinetics, stoichiometry, and identification of the reactive thiolate in the inactivation of UDP-GlcNAc enolpyruvoyl transferase by the antibiotic fosfomycin. *Biochemistry*, **1994**, *33*, 10646-51.

(7)   Brown, E. D.; Vivas, E. I.; Walsh, C. T.; Kolter, R. MurA (MurZ), the enzyme that catalyzes the first committed step in peptidoglycan biosynthesis, is essential in *Escherichia coli*. *J. Bacteriol.*, **1995**, *177*, 4194-7.

(8)   Shoji, J.; Kato, T.; Hinoo, H.; Hattori, T.; Hirooka, K.; Matsumoto, K.; Tanimoto, T.; Kondo, E. Production of fosfomycin (phosphonomycin) by *Pseudomonas syringae*. *J. Antibiot. (Tokyo)*, **1986**, *39*, 1011-2.

(9)   Hendlin, D.; Stapley, E. O.; Jackson, M.; Wallick, H.; Miller, A. K.; Wolf, F. J.; Miller, T. W.; Chaiet, L.; Kahan, F. M.; Foltz, E. L.; Woodruff, H. B.; Mata, J. M.; Hernandez, S.; Mochales, S. Phosphonomycin, a new antibiotic produced by strains of streptomyces. *Science*, **1969**, *166*, 122-3.

(10)   Seto, H.; Hidaka, T.; Kuzuyama, T.; Shibahara, S.; Usui, T.; Sakanaka, O.; Imai, S. Studies on the biosynthesis of fosfomycin. 2. Conversion of 2-hydroxypropyl-

phosphonic acid to fosfomycin by blocked mutants of Streptomyces wedmorensis. *J. Antibiot. (Tokyo)*, **1991**, *44*, 1286-8.

(11)   Hammerschmidt, F. Biosynthesis of natural products with a phosphorus-carbon bond. Part 8. On the origin of the oxirane oxygen atom of fosformycin in *Streptomyces fradiae*. *J. Chem. S., Perkin Trans.*, **1991**, *8*, 1993-1996.

(12)   Hidaka, T.; Goda, M.; Kuzuyama, T.; Takei, N.; Hidaka, M.; Seto, H. Cloning and nucleotide sequence of fosfomycin biosynthetic genes of *Streptomyces wedmorensis*. *Mol. Gen. Genet.*, **1995**, *249*, 274-80.

(13)   Liu, P.; Murakami, K.; Seki, T.; He, X.; Yeung, S. M.; Kuzuyama, T.; Seto, H.; Liu, H. Protein purification and function assignment of the epoxidase catalyzing the formation of fosfomycin. *J. Am. Chem. Soc.*, **2001**, *123*, 4619-20.

(14)   Liu, P.; Liu, A.; Yan, F.; Wolfe, M. D.; Lipscomb, J. D.; Liu, H. W. Biochemical and spectroscopic studies on (S)-2-hydroxypropylphosphonic acid epoxidase: a novel mononuclear non-heme iron enzyme. *Biochemistry*, **2003**, *42*, 11577-86.

(15)   Dunwell, J. M.; Culham, A.; Carter, C. E.; Sosa-Aguirre, C. R.; Goodenough, P. W. Evolution of functional diversity in the cupin superfamily. *Trends Biochem. Sci.*, **2001**, *26*, 740-6.

(16)   Yan, F.; Li, T.; Lipscomb, J. D.; Liu, A.; Liu, H. W. Site-directed mutagenesis and spectroscopic studies of the iron-binding site of (S)-2-hydroxypropylphosphonic acid epoxidase. *Arch. Biochem. Biophys.*, **2005**, *442*, 82-91.

(17)   Higgins, L. J.; Yan, F.; Liu, P.; Liu, H. W.; Drennan, C. L. Structural insight into antibiotic fosfomycin biosynthesis by a mononuclear iron enzyme. *Nature*, **2005**, *437*, 838-44.

(18)   Prescott, A. G.; Lloyd, M. D. The iron(II) and 2-oxoacid-dependent dioxygenases and their role in metabolism. *Nat. Prod. Rep.*, **2000**, *17*, 367-83.

(19)   Kappock, T. J.; Caradonna, J. P. Pterin-Dependent Amino Acid Hydroxylases. *Chem. Rev.*, **1996**, *96*, 2659-2756.

(20)   Fitzpatrick, P. F. Tetrahydropterin-dependent amino acid hydroxylases. *Annu. Rev. Biochem.*, **1999**, *68*, 355-81.

(21)   Rocklin, A. M.; Tierney, D. L.; Kofman, V.; Brunhuber, N. M.; Hoffman, B. M.; Christoffersen, R. E.; Reich, N. O.; Lipscomb, J. D.; Que, L., Jr. Role of the nonheme Fe(II) center in the biosynthesis of the plant hormone ethylene. *Proc. Natl. Acad. Sci.*, **1999**, *96*, 7905-9.

(22)   Liu, P.; Mehn, M. P.; Yan, F.; Zhao, Z.; Que, L., Jr.; Liu, H. W. Oxygenase activity in the self-hydroxylation of (s)-2-hydroxypropylphosphonic acid epoxidase involved in fosfomycin biosynthesis. *J. Am. Chem. Soc.*, **2004**, *126*, 10306-12.

(23)   Ling, J.; Sahlin, M.; Sjoberg, B. M.; Loehr, T. M.; Sanders-Loehr, J. Dioxygen is the source of the mu-oxo bridge in iron ribonucleotide reductase. *J. Biol. Chem.*, **1994**, *269*, 5595-601.

(24)   Ryle, M. J.; Liu, A.; Muthukumaran, R. B.; Ho, R. Y.; Koehntop, K. D.; McCracken, J.; Que, L., Jr.; Hausinger, R. P. O2- and alpha-ketoglutarate-dependent tyrosyl radical formation in TauD, an alpha-keto acid-dependent non-heme iron dioxygenase. *Biochemistry*, **2003**, *42*, 1854-62.

(25)   Liu, A.; Ho, R. Y.; Que, L., Jr.; Ryle, M. J.; Phinney, B. S.; Hausinger, R. P. Alternative reactivity of an alpha-ketoglutarate-dependent iron(II) oxygenase: enzyme self-hydroxylation. *J. Am. Chem. Soc.*, **2001**, *123*, 5126-7.

(26)   Xing, G.; Diao, Y.; Hoffart, L. M.; Barr, E. W.; Prabhu, K. S.; Arner, R. J.; Reddy, C. C.; Krebs, C.; Bollinger, J. M., Jr. Evidence for C-H cleavage by an iron-superoxide complex in the glycol cleavage reaction catalyzed by myo-inositol oxygenase. *Proc. Natl. Acad. Sci.*, **2006**, *103*, 6130-5.

(27)   Ortiz de Montellano, P. R. *Cytochrome P450: Structure, Mechanism, and Biochemistry*; 2 ed.; Plenum: New York, 1995.

(28)   Solomon, E. I.; Brunold, T. C.; Davis, M. I.; Kemsley, J. N.; Lee, S. K.; Lehnert, N.; Neese, F.; Skulan, A. J.; Yang, Y. S.; Zhou, J. Geometric and electronic structure/function correlations in non-heme iron enzymes. *Chem. Rev.*, **2000**, *100*, 235-350.

(29)   Costas, M.; Mehn, M. P.; Jensen, M. P.; Que, L., Jr. Dioxygen activation at mononuclear nonheme iron active sites: enzymes, models, and intermediates. *Chem. Rev.*, **2004**, *104*, 939-86.

(30)   McLuskey, K.; Cameron, S.; Hammerschmidt, F.; Hunter, W. N. Structure and reactivity of hydroxypropylphosphonic acid epoxidase in fosfomycin biosynthesis by a cation- and flavin-dependent mechanism. *Proc. Natl. Acad. Sci.*, **2005**, *102*, 14221-6.

(31)   Miller, V. P.; Thorson, J. S.; Ploux, O.; Lo, S. F.; Liu, H. W. Cofactor characterization and mechanistic studies of CDP-6-deoxy-delta 3,4-glucoseen reductase: exploration into a novel enzymatic C-O bond cleavage event. *Biochemistry*, **1993**, *32*, 11934-42.

(32)   Bradford, M. M. A rapid and sensitive method for the quantitation of microgram quantities of protein utilizing the principle of protein-dye binding. *Anal. Biochem.*, **1976**, *72*, 248-54.

(33)   Anderson, K. S.; Sikorski, J. A.; Johnson, K. A. Evaluation of 5-enolpyruvoylshikimate-3-phosphate synthase substrate and inhibitor binding by stopped-flow and equilibrium fluorescence measurements. *Biochemistry*, **1988**, *27*, 1604-10.

(34)   Wardman, P. Reduction potentials of one-electron couples involving free radicals in aqueous solution. *J. Phys. Chem. Ref. Data*, **1989**, *18*, 1637-1755.

(35)   Clark, W. M.; Lowe, H. J. Studies on oxidation-reduction. XXIV. Oxidation-reduction potentials of flavin adenine dinucleotide. *J. Biol. Chem.*, **1956**, *221*, 983-92.

(36)   Gassner, G. T.; Johnson, D. A.; Liu, H. W.; Ballou, D. P. Kinetics of the reductive half-reaction of the iron-sulfur flavoenzyme CDP-6-deoxy-L-threo-D-glycero-4-hexulose-3-dehydrase reductase. *Biochemistry*, **1996**, *35*, 7752-61.

(37)   Johnson, D. A.; Gassner, G. T.; Bandarian, V.; Ruzicka, F. J.; Ballou, D. P.; Reed, G. H.; Liu, H. W. Kinetic characterization of an organic radical in the ascarylose biosynthetic pathway. *Biochemistry*, **1996**, *35*, 15846-56.

(38)   He, X.; Liu, H. W. Mechanisms of enzymatic C-O bond cleavages in deoxyhexose biosynthesis. *Curr. Opin. Chem. Biol.*, **2002**, *6*, 590-7.

(39)   Kuzuyama, T.; Seki, T.; Kobayashi, S.; Hidaka, T.; Seto, H. Cloning and expression in Escherichia coli of 2-hydroxypropylphosphonic acid epoxidase from the fosfomycin-producing organism, *Pseudomonas syringae* PB-5123. *Biosci. Biotechnol. Biochem.*, **1999**, *63*, 2222-2224.

(40)   Tang, L.; Lutje Spelberg, J. H.; Fraaije, M. W.; Janssen, D. B. Kinetic mechanism and enantioselectivity of halohydrin dehalogenase from *Agrobacterium radiobacter*. *Biochemistry*, **2003**, *42*, 5378-5386.

CHAPTER 5:   PURIFICATION, CHARACTERIZATION AND A

KINETIC ISOTOPE EFFECT ANALYSIS OF THE HPPE FROM

PSEUDOMONAS SYRINGAE

5.1.   INTRODUCTION

Fosfomycin (**6**) is a clinically useful antibiotic[1] for the treatment of limb-threatening diabetic foot infections[2] and lower urinary tract infections.[3]   It has been shown to be effective against ciprofloxacin-resistant *E. coli*,[4] as well as methicillin-resistant[5] and vancomycin-resistant[6] strains of *Staphylococcus aureus*. The antimicrobial activity of fosfomycin results from the inactivation of UDP-Glc*N*Ac-3-*O*-enolpyruvyltransferase (MurA), which catalyzes the first committed step in the biosynthesis of peptidoglycan, the main component of the cell wall.[7,8]

Fosfomycin belongs to a steadily growing family of natural products containing a C-P bond.[9]   Members of this family, such as fosfomycin,[10] fosmidomycin,[11] and bialaphos,[12] are all derived from phosphoenolpyruvate (**1,** PEP). The C-P bonds in these compounds are formed through an intramolecular rearrangement reaction catalyzed by PEP mutase resulting in the conversion of PEP (**1**) to phosphopyruvate (**2,** PnPy) (**Figure 1**).[13-15]   Since the equilibrium between PEP and PnPy highly favors PEP, the decarboxylation catalyzed by the second enzyme, Fom2 (PnPy decarboxylase), provides the driving force to shift the equilibrium in favor of C-P bond formation.[16] The next two steps in the biosynthesis have not been explicitly demonstrated, but it is believed to be the reduction of the aldehyde (**3**) to generate hydroxyethylphosphonic acid (**4**), followed by a methyl transfer reaction to generate (*S*)-2-hydroxypropylphosphonic acid (**5**, (*S*)-HPP).[17]

The final step of the pathway is the conversion of (S)-HPP (**5**) to fosfomycin (**6**) catalyzed by (S)-HPP epoxidase (HppE).
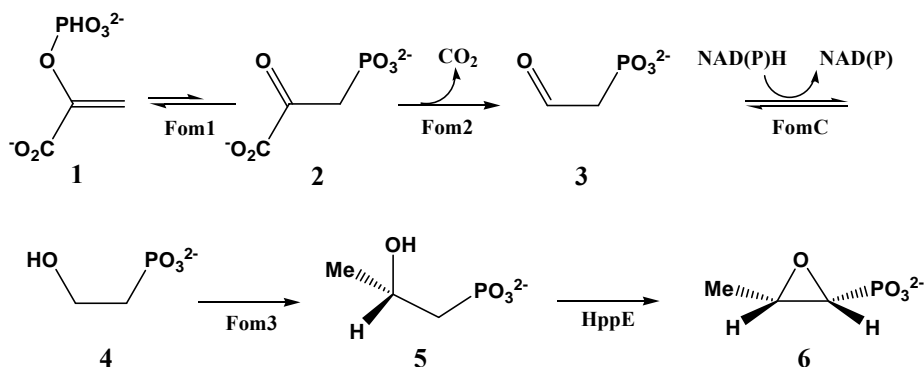
Figure 5-1: Fosfomycin biosynthetic pathway.

Previous investigations of HppE from *Streptomyces wedmorensis* (*Sw*-HppE) revealed that this enzyme is a mononuclear non-heme iron-containing catalyst, and unlike most other enzymes in the same class, its activity is α-ketoglutarate-independent.[18] For activity, HppE does require NADH, FMN and O_2.[19] In nature, most epoxide rings are generated via oxidation of the corresponding alkenes by either heme-dependent cytochrome P450s[20,21] or non-heme iron-dependent monooxygenases.[22] However, isotope labeling experiments with *Sw*-HppE revealed that no oxygen atoms from O_2 are incorporated into fosfomycin, and instead, the oxygen atom of the epoxy ring in **6** is derived from the secondary hydroxyl group of (S)-HPP (**5**).[18,19] Thus the conversion of **5** to **6** by *Sw*-HppE is effectively a dehydrogenation reaction, not an oxygenation reaction.

The mechanism of HppE epoxidation (**Figure 5-2**) has been proposed to parallel alkane hydroxylation catalyzed by cytochrome P450[21] and non-heme iron-dependent oxygenases.[23,24] The reaction likely begins with hydrogen abstraction from the C-1 position by an activated oxygen species. In a manner similar to the oxygen rebound mechanism for cytochrome P450s, the C-1 centered radical intermediate can then cyclize

to form fosfomycin and the reduced iron center. The reactive oxygen species can be one of three species. The reactive species can be Fe(III)-superoxide (**9**), which forms upon dioxygen binding to the ferrous iron center, similar to what has been proposed for isopenicillin N synthase (IPNS).[25,26] The Fe(III)-superoxide species can be reduced by one electron and protonated to form Fe(III)-hydroperoxide (**11**), which can also abstract the C-1 hydrogen atom. The Fe(III)-hydroperoxide species can be further reduced by a second single electron transfer with concurrent cleavage of the O-O bond to form Fe(IV)-oxo (**12**), as proposed for α-ketoglutarate dependent TauD[27] and for tyrosine hydroxylase[28], which can later abstract the hydrogen atom.
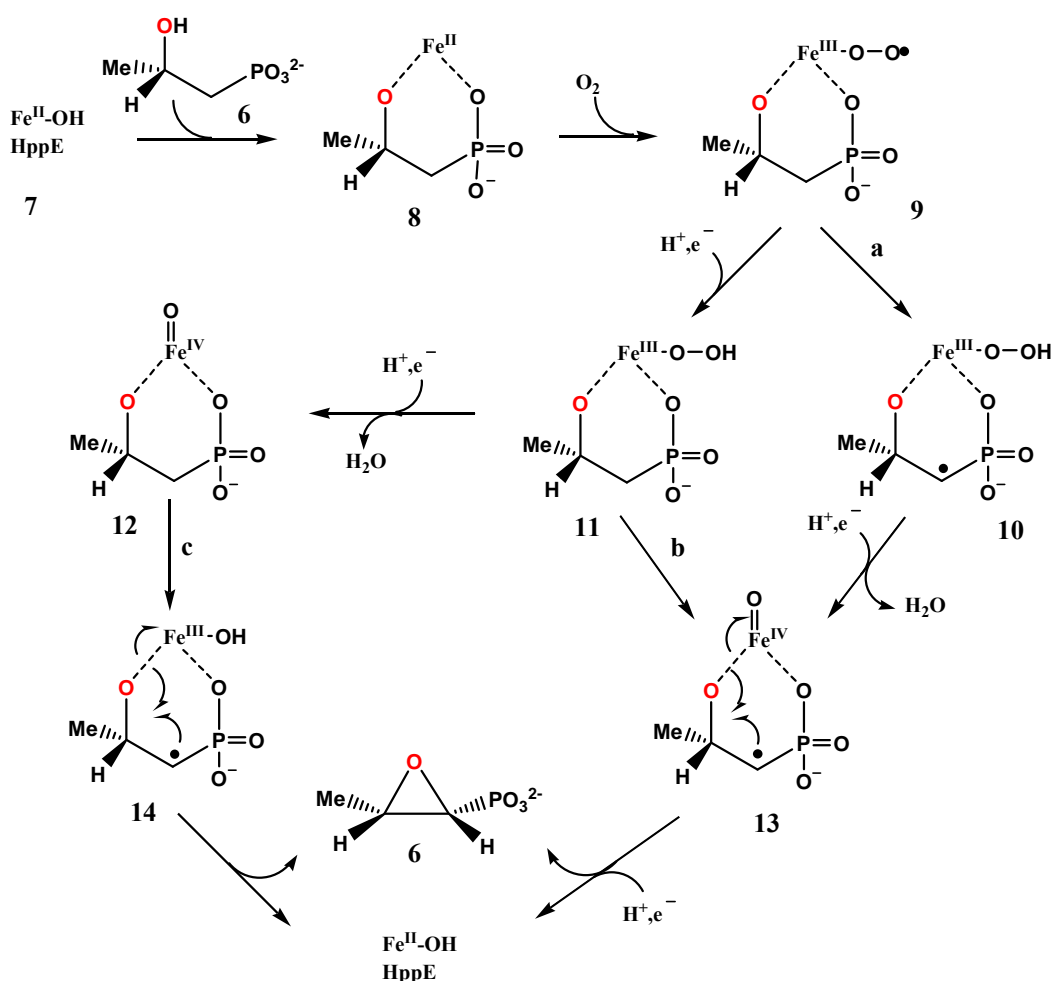
Figure 5-2:   **Proposed NAD(P)H and Iron dependent mechanisms for HppE.**

Clearly, *Sw*-HppE is unique with respect to all other mononuclear non-heme iron-dependent enzymes regarding the required components for activity, and it is also unique among epoxidase enzymes in that the net transformation is a dehydrogenation reaction and not an oxygen insertion across a carbon-carbon double bond. Interestingly, an homologous enzyme has been identified in the fosfomycin producing *Pseudomonas syringae* PB-5123.[29] This HppE (*Ps*-HppE) has not been investigated to determine if it is a functional mimic of *Sw*-HppE, acting as an iron-dependent enzyme and catalyzing the analogous epoxidation reaction. Reported herein is an account of the biochemical and

spectroscopic characterization of the *Ps*-HppE enzyme and the implications of its mode of action.

In order to obtain a more intimate understanding of how *Ps*-HppE, and presumably *Sw*-HppE, activates molecular oxygen and possibly to determine the identity of the reactive oxygen species, an [^{18}O]-KIE analysis was conducted in collaboration with Prof. Judith P. Klinman at the University of California at Berkeley. The ^{18}O in the experiments is from the natural abundance in air, which is ~0.2%.[30] Due to the low level of abundance, the isotope effect determined is for $^{16,16}O_2$ versus $^{16,18}O_2$.[30,31] As described in Chapter 3, a KIE arises from differences in the zero-point energies (ZPE), mass moments of inertia (MMI) and excited vibrational states (EXC) between the reactant state and the transition state. This is also true for an equilibrium isotope effect (EIE), except the difference is then between the reactant state and the product state. Unlike the deuterium KIE, the [^{18}O]-KIE and EIE is not necessarily dominated by differences in ZPE. However, for the single electron reduction of molecular oxygen to superoxide (see **Table 5-1**)[30] the difference in ZPE does dominate the EIE, and a reaction coordinate diagram depicting the EIE (see **Figure 5-3**) can be drawn as in Chapter 3.

Table 5-1: Calculated EIEs for the reduction of molecular oxygen.[30]

Reaction	ΔBO	ZPE	EXC	MMI	$^{18}K_{calc}$
$O_2 \overset{1e^-}{\rightleftharpoons} O_2^{\bullet-}$	0.5	1.03309	.99921	1.00004	1.03309
$O_2 \overset{2e^-}{\rightleftharpoons} O_2^{2-}$	1	1.05147	0.99761	1.00063	1.04962
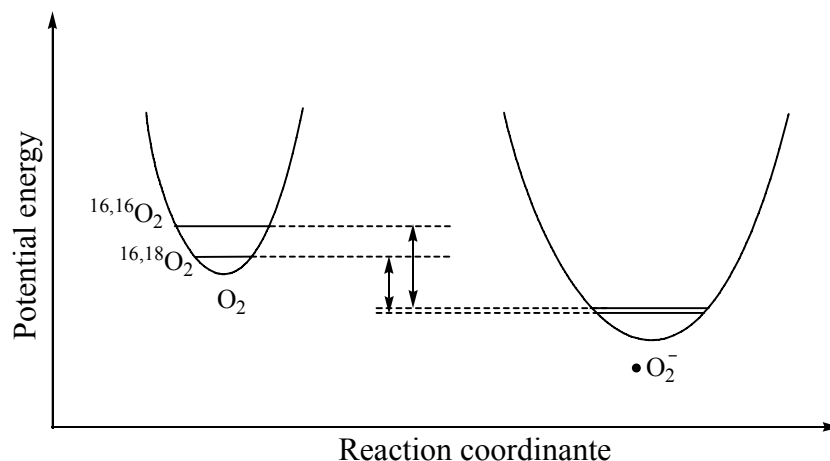
Figure 5-3: **Reaction coordinate diagram displaying the origin of the ^{18}O KIE for the single electron reduction of molecular oxygen to superoxide.**

The 2° [^{2}H]-KIE in Chapter 3 was described as arising from changes in the hybridization state of the carbon center. This rehybridization results is a difference in the frequency for the out-of-plane bending vibration of the reacting carbon center in the reactant state versus in the transition state, which in turn produces an isotope effect. For ^{18}O isotope effects, it is most easily to envision them arising from changes in bond order; however, this is not always true when metal ions or protons are involved.[30] For the single electron reduction of dioxygen to superoxide, there is a decrease in bond order of 0.5 (see **Table 5-1**). As seen in **Figure 5-4**, this results because the additional electron enters one of the π* molecular orbitals, which is an antibonding orbital. Such a decrease in bond order weakens the O-O bond, which in turn decreases the O-O stretching frequency (see **Table 5-2**).

Table 5-2: Vibration frequencies of molecular oxygen and reduced forms.[31]

Molecule	$v_{16,16}$ (cm^{-1})	$v_{16,18}$ (cm^{-1})
O_2	1556.3	1512.5
$\cdot O_2^-$	1064.8	1034.8
O_2^{2-}	800	777
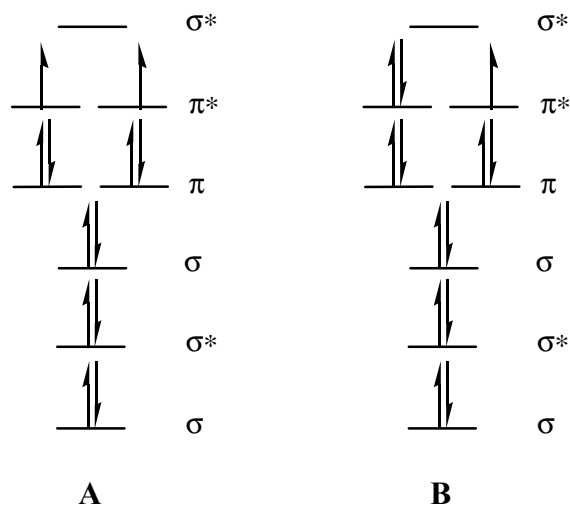
Figure 5-4: Molecular orbital diagram for A) O_2 and B) $\cdot O_2^-$

Using either calculated or experimentally determined frequencies for all the stretching and bending vibrations, the isotope effect from the difference in ZPE, EXC and MMI can be calculated. The product of the three terms is the EIE (see **Equation 5-1**). These frequencies are not easy to obtain for the transition state, so it is not typically calculated.[32] Instead, the EIE is calculated and is used as an upper boundary for the KIE, assuming a negligible isotope effect contribution from the reaction coordinate frequency.[30,32,33] To probe the identity of the oxygen species that forms in the rate-limiting step of the enzymatic reaction, the experimentally determined KIE can be compared to a list of calculated EIEs of possible oxygen intermediates. Due to the [^{18}O]-

136

KIEs being determined by competition between $^{16,16}O_2$ and $^{16,18}O_2$, the experimental $[^{18}O]$-KIEs are on k_{cat}/K_M. KIEs on k_{cat}/K_M only take in to account the enzymatic steps up to and including the first irreversible step; therefore, any steps after the first irreversible step will not affect the $[^{18}O]$-KIE.

Equation 5-1

$$EIE = ZPE \times EXC \times MMI$$

In the proposed HppE mechanism in **Figure 5-2**, the first irreversible step differs based on the reactive oxygen species used to abstract the C-1 hydrogen atom. If Fe(III)-superoxide (**9**) is the reactive species, then the first irreversible step will be the electron transfer from reduced FMN to the active site iron (**10→13**). If the reactive species is either Fe(III)-hydroperoxide (**11**) or Fe(IV)-oxo (**12**), then the first irreversible step will also be the electron transfer from reduced FMN to the active site iron (**9→11**). For all three possible reactive species, the resulting $[^{18}O]$-KIE will be too similar to discriminate between the three. The mechanisms differ in if the hydrogen atom abstraction occurs before or after the first irreversible step. For the reaction with Fe(III)-superoxide (**9**) as the reactive species, hydrogen atom abstraction (**9→10**) occurs before the first irreversible step, and with Fe(III)-hydroperoxide (**11**) or Fe(IV)-oxo (**12**) as the reactive species, abstraction occurs after the first irreversible step (**11→13** and **12→14**, respectively). If the hydrogen that is abstracted is replaced with deuterium, there will be a 1° $[^{2}H]$-KIE on its abstraction. If the $[^{18}O]$-KIE is determined with the deuterium labeled (*S*)-HPP, it may or may not affect the $[^{18}O]$-KIE value, depending on whether or not hydrogen atom abstraction occurs before or after the first irreversible step. Therefore, if Fe(III)-hydroperoxide or Fe(IV)-oxo is the reactive species, then the $[^{2}H]$-KIE will have no effect on the $[^{18}O]$-KIE, but if Fe(III)-superoxide (**9**) is the reactive species, then

abstraction ($\mathbf{9} \rightarrow \mathbf{10}$) will occur before the first irreversible step and could possibly affect the [^{18}O]-KIE.

5.2. MATERIALS AND METHODS

5.2.1. GENERAL. Protein concentrations were determined by the procedure of Bradford using bovine serum albumin as the standard.[34] The NMR spectra were acquired on a Varian Unity 300 spectrometer, and chemical shifts (δ in ppm) are given relative to those for Me$_4$Si (for ^{1}H and ^{13}C) and aqueous 85% H$_3$PO$_4$ (external, for ^{31}P), with coupling constants reported in hertz (Hz). The UV-vis absorption spectra were recorded on the Agilent 8453A Diode Array Spectrophotometer. The HPLC assays were conducted with the Beckman Coulter System Gold 125 Solvent Module coupled with the System Gold 508 Autosampler. The Corona charged aerosol detector (CAD) from ESA (Chelmsford, MA) was used as the HPLC detector.

5.2.2. MATERIALS. Culture medium ingredients were purchased from Difco (Detroit, MI). DNA minipreps were performed using QIA Spin Miniprep Kit from Qiagen (Valencia, CA). All oligonucleotide primers for PCR amplification of the desired inserts were customly prepared by Integrated DNA Technologies (Coralville, IA) and used without further purification. Restriction endonucleases were acquired from New England Biolabs (Ipswich, MA). The pET24b(+) vector and the overexpression host strain *Escherichia coli* BL21(DE3) were obtained from Novagen Inc. (Madison, WI). All electrophoresis materials were products of Gibco BRL or Bio-Rad (Hercules, CA). All chemicals were analytical grade or the highest quality commercially available. Biochemicals, including fosfomycin disodium salt (**6**) standard, were purchased from Sigma-Aldrich (St. Louis, MO), unless noted otherwise. The natural substrate, (*S*)-2-

138

hydroxypropylphosphonic acid (**5**, (*S*)-HPP) and its enantiomer (**7**, (*R*)-HPP) were chemically synthesized according to reported proceedures.[18,19,35]

5.2.3. SYNTHESIS OF DEUTERIUM LABELED HPP ANALOGUES.

The deuterium labeled HPP analogues, (*R*)-2-[²H]-HPP (**20**), (1*R*,2*S*)-1-[²H]-HPP (**31**) and (*S*)-1,1-[²H]₂-HPP (**35**), were synthesized by Dr. Sung-Ju Moon and according to **Figures 5-5**, **5-6** and **5-7**, respectively.
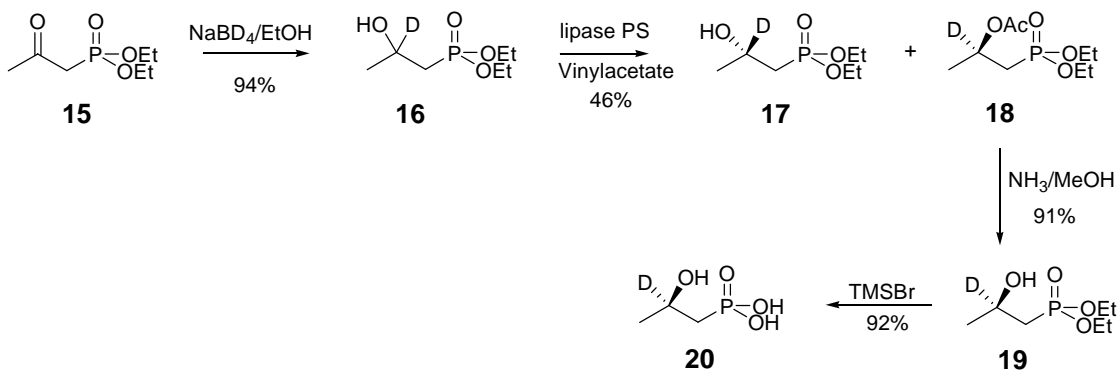
Figure 5-5: Synthetic scheme for (*R*)-2-[²H]-HPP (**20**).
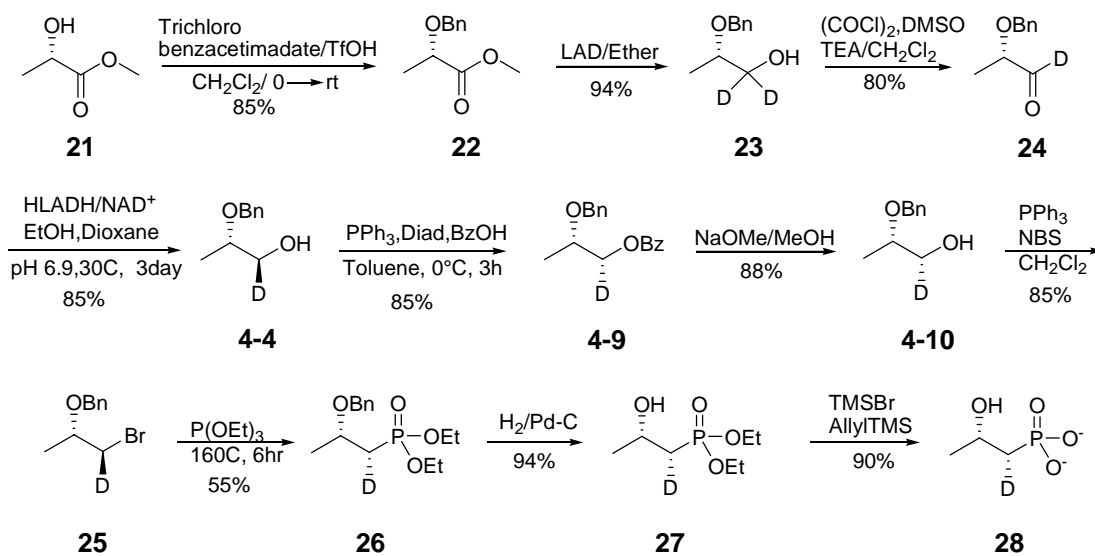
Figure 5-6: Synthetic scheme for (1*R*,2*S*)-1-[²H]-HPP (**28**).

139
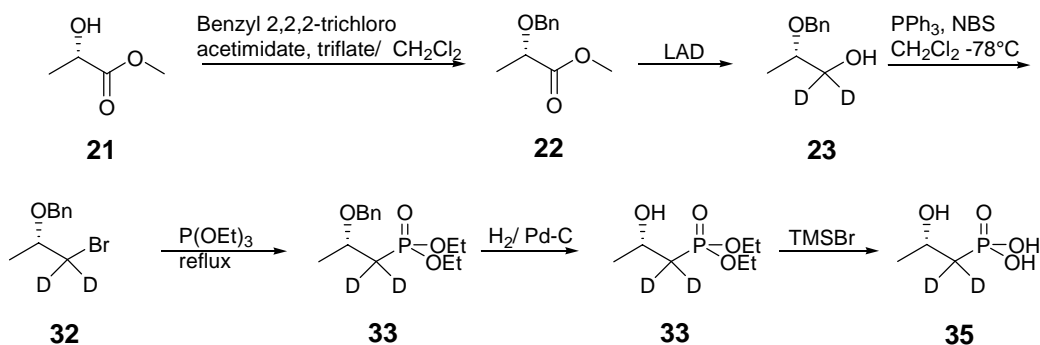
Figure 5-7: Synthetic scheme for (S)-1,1-[²H]₂-HPP (35).

5.2.4. CONSTRUCTION OF EXPRESSION PLASMID FOR THE *Ps*-HPPE GENE. A clone of the *Ps*-HppE gene (*orf3*) in pUC118 was generously provided by Dr. Tomohisa Kuzuyama, the University of Tokyo. The *Ps*-HppE gene was PCR amplified from this plasmid and ligated into pET24b(+) to generate pLH01. The resulting plasmid was used to transform *Escherichia coli* BL21(DE3). The general methods and protocols for recombinant DNA manipulations were as described by Sambrook *et al.*[36] This was conducted by Dr. Lin Hong.

5.2.5. GROWTH OF *E. COLI* BL21(DE3)/PLH01 CELLS. An overnight culture of *E. coli* BL21(DE3)/pLH01 grown at 37 °C in Luria-Bertani (LB) medium supplemented with kanamycin (50 μg/mL) was used, in a 250-fold dilution, to inoculate 6 L of the same medium. The culture grew at 37 °C until the OD_{600} reached 0.6. The incubation temperature was then lowered to 18 °C, and isopropyl β-D-thiogalactoside (IPTG) was added to a final concentration of 0.5 mM. After incubation for an additional 16 h at 18 °C, cells were harvested by centrifugation (7000*g*, 8 min) at 4 °C and washed with the lysis buffer (20 mM Tris·HCl, pH 7.5, 0.1 mM DTT, 10 mM EDTA). The washed cells were again centrifuged (7000*g*, 8 min) and stored at -80 °C until future use.

140

5.2.6. PURIFICATION OF RECOMBINANT APO-*PS*-HPPE. All purification operations were carried out at 4 °C except for the fast protein liquid chromatography (FPLC) step. All buffers were degassed and saturated with nitrogen before use. Thawed cells were resuspended in a 5-fold (w/v) excess of lysis buffer (see above) and subjected to 14 × 30 s ultrasonic bursts, with a 50 s cooling interval between each blast. Cellular debris was removed by centrifugation at 17000g for 25 min. The supernatant was fractionated by ammonium sulfate, and the 10-65% ammonium sulfate precipitate was collected. The protein pellet was resuspended in a minimal amount of buffer A (20 mM Tris·HCl, pH 7.5, 0.1 mM DTT, 0.1 mM EDTA). The resulting protein solution was dialyzed against 1 L of the same buffer for 3 h with two buffer changes.

The dialysate was applied to a DEAE-Sepharose CL-6B column (6 × 18 cm) pre-equilibrated with buffer A. After loading, the column was washed with 300 mL of buffer A containing 180 mM NaCl. The elution was then continued with a linear gradient of NaCl from 180 to 300 mM in the same buffer (2 L total volume). The flow rate was 1.5 mL/min, and fractions of 20 mL were collected throughout the gradient elution. The fractions containing HppE, as determined by SDS-PAGE, were pooled, concentrated to about 15 mL by ultrafiltration on an Amicon concentrator using a YM 10 membrane (Millipore, Bedford, MA), and desalted by dialyzing against 1 L of buffer A for 1 h, followed by 1 L of 20 mM Tris·HCl buffer (pH 7.5) for 2 h with one buffer change. The concentrated protein from the last step was further purified at room temperature by FPLC equipped with a Mono Q HR 16/10 column (GE Healthcare, Piscataway, NJ) using the solvent systems B (20 mM Tris·HCl buffer, pH 7.5) and C (B plus 0.6 M NaCl). The elution profile included a linear gradient of 0 to 35% C over 40 mL, followed by a linear gradient of 35 to 60% C over 160 mL, and concluded with a 40 mL wash at 100% C. The flow rate was 7 mL/min, and the detector was set at 280 nm. A peak with a retention

time of approximately 19 min was collected, concentrated by ultrafiltration as described before, and dialyzed against 1 L of 20 mM Tris·HCl buffer (pH 7.5) for 3 h with two buffer changes. The purified protein was then aliquoted, flash frozen, and stored at -80 °C.

5.2.7. MOLECULAR MASS DETERMINATION. The molecular mass of *Ps*-HppE was determined by size exclusion chromatography performed on a FPLC Superdex 200 HR 10/300 column (GE Healthcare, Piscataway, NJ) with an eluent of 20 mM Tris·HCl, 0.15 M NaCl, pH 7.5, at a flow rate of 1 mL/min. Calibration of the column was achieved using the following protein standards (Aldrich): cytochrome C (14.2 kDa), carbonic anhydrase (29 kDa), bovine serum albumin (66 kDa), alcohol dehydrogenase (150 kDa), and β-amylase (200 kDa). The void volume (V_0) of the column was measured using blue dextran (2000 kDa). A linear fit to a plot of the Log molecular weight versus V_e/V_0 was used to estimate the native molecular mass (M_r) of the protein sample.[37] This experiment was conducted by Dr. Svetlana Borisova.

5.2.8. NBT STAINING OF *Ps*-HPPE. Detection of the presence of quinoid structure in the protein was performed according to a published procedure.[38,39] The wild-type HppE and its mutants were subjected to 15% SDS-PAGE and transblotted onto a nitro-cellulose membrane at 100 V for 1 h using a transfer buffer (25 mM Tris base, 192 mM glycine, 20% methanol). Detection of the presence of quinoid structure was performed according to a procedure of Paz *et al.*[38] by immersing the membrane in a solution of 0.24 mM nitroblue tetrazolium and 2 M potassium glycinate, pH 10, for 45 min. After the membrane was rinsed with H_2O, the stained bands were recorded.

5.2.9. ENZYME ACTIVITY ASSAYS. The enzyme activity was determined by an HPLC assay, which was conducted as previously described in Chapter 4. Due to the slower rate of turnover of *Ps*-HppE compared to that of *Sw*-HppE, the concentrations of *Ps*-HppE, iron, and FMN used in the assays were doubled. The final concentration of each reagent in a 50 μL assay was 100 μM *Ps*-HppE, 100 μM Fe(NH$_4$)$_2$(SO$_4$)$_2$, 150 μM FMN, 10 mM HPP, and 16 mM NADH in 20 mM Tris•HCl buffer (pH 7.5). To compare the activity of *Ps*-HppE to *Sw*-HppE, the assays were carried out on the same day and with the same stock of reagents for *Sw*-HppE. The final concentrations in the 50 μL *Sw*-HppE reactions were 50 μM *Sw*-HppE, 50 μM Fe(NH$_4$)$_2$(SO$_4$)$_2$, 75 μM FMN, 10 mM HPP, and 16 mM NADH in 20 mM Tris•HCl buffer (pH 7.5). The amount of product formed was normalized by dividing by the concentration of HppE, which was then plotted versus time to determine k_{obs}. With the assumption that substrate is saturating, k_{obs} is k_{cat}. Over the time scale used in all assays, the product formation was linear with respect to time.

5.2.10. PRIMARY [²H] KINETIC ISOTOPE EFFECT. The catalytic rate of HppE increases with increasing concentration of FMN. To determine the ratio of FMN:*Ps*-HppE where the increase in rate plateaus, the reaction with (*R*)-HPP (**38**) was conducted at increasing ratios of FMN:*Ps*-HPP by varying the concentration of FMN at a fixed concentration of *Ps*-HppE. The final concentrations in the 50 μL reactions were 100 μM *Ps*-HppE, 100 μM Fe(NH$_4$)$_2$(SO$_4$)$_2$, 0.01-12.9 mM FMN, 10 mM (*R*)-HPP, and 16 mM NADH in 20 mM Tris•HCl buffer (pH 7.5). At each ratio, each reaction was incubated at room temperature for 20 min before being quenched with 50 μL of 2 M acetic acid and analyzed by HPLC as previously described. The concentration of ketone (**39**) formed was plotted versus the FMN:*Ps*-HppE ratio to determine the saturating ratio. It was

assumed that the saturating FMN:*Ps*-HppE ratio for the (*R*)-HPP (**38**) reaction is the same as the (*S*)-HPP (**5**) reaction. To determine the 1° [^{2}H]-KIE for hydrogen atom abstraction, the k_{obs} was measured by the HPLC assay for (*S*)-HPP (**5**), (1*R*,2*S*)-1-[^{2}H]-HPP (**31**), (*S*)-1,1-[^{2}H]$_2$-HPP (**35**), (*R*)-HPP (**38**) and (*R*)-2-[^{2}H]-HPP (**20**) at specified ratios of FMN to *Ps*-HppE. The final concentrations in the 50 μL reactions to determine the KIE were 100 μM *Ps*-HppE, 100 μM Fe(NH$_4$)$_2$(SO$_4$)$_2$, 0.11-5 mM FMN, 10 mM HPP, and 16 mM NADH in 20 mM Tris•HCl buffer (pH 7.5).

5.2.11. NMR CHARACTERIZATION OF THE *PS*-HPPE'S PRODUCTS. ^{1}H and ^{31}P NMR's were used to characterize the products of the reaction catalyzed by *Ps*-HppE with (*S*)-HPP (**5**) and (*R*)-HPP (**38**) as the substrates. The conditions used were 150 μM *Ps*-HppE, 150 μM Fe(NH$_4$)$_2$(SO$_4$)$_2$, 370 μM FMN, 40 mM (*S*)-HPP (**5**) or (*R*)-HPP (**38**), and 40 mM NADH in 200 μL of 20 mM Tris•HCl buffer (pH 7.5). The reactions were incubated at room temperature for 15 h. The samples were then lyophilized to dryness and redissolved in 600 μL of D$_2$O. Spectral data of fosfomycin (**6**):^{1}H NMR (300 MHz, D$_2$O) δ 3.11 (1H, m, *J* = 5.4, 2-H), 2.66 (1H, d, *J* = 5.3, 18.6, 1-H), 1.33 (3H, d, *J* = 5.4, 3-H); ^{31}P NMR (D$_2$O, 121 MHz) δ 10.9 (s). Spectral data for 2-oxopropylphosphonic acid (**39**): ^{1}H NMR (300 MHz, D$_2$O) δ 2.81 (2H, d, *J* = 21.0 Hz), 2.16 ppm (3H, s); ^{31}P NMR (D$_2$O) δ 11.1 (s).

5.2.12. EFFECTS OF METAL IONS ON THE ACTIVITY OF *PS*-HPPE. A systematic investigation to determine the metal ion(s) requirement for the activity of *Ps*-HppE was performed by including different redox-active metals, such as iron (Fe(NH$_4$)$_2$(SO$_4$)$_2$), copper (CuSO$_4$), cobalt (CoCl$_2$), and manganese (MnCl$_2$), and the non-redox active metal, zinc (ZnSO$_4$), in the reaction mixture, and assessing their effects on enzyme

activity. A typical 50 μL reaction mixture contained 16 mM NADH, 10 mM (*S*)-HPP (**5**), 100 μM *Ps*-HppE, 150 μM FMN, and 100 μM of the investigate metal in 20 mM Tris·HCl buffer (pH 7.5). After incubating at room temperature for 1.5 h, the reaction was quenched with 2 M acetic acid, and the relative activity of each sample was determined by the HPLC assay described above. To further assess the metal ion requirement for the enzyme activity, the effect of the metal chelator, EDTA, on the catalysis of *Ps*-HppE was also examined. In this case, the activity assay with *Ps*-HppE reconstituted with ferrous iron was repeated in the presence of 5 mM EDTA.

5.2.13. THE DEPENDENCE OF *PS*-HPPE ACTIVITY ON OXYGEN. In a sealed vessel, an assay mixture (1 mL) containing 200 μM *Ps*-HppE and 200 μM Fe(NH$_4$)$_2$(SO$_4$)$_2$ in 20 mM Tris·HCl, pH 7.5, was made anaerobic by 15 repeated cycles of subjecting the mixture to vacuum and purging with argon. The mixture was kept under argon for 20 min followed by another 15 cycles of vacuum and argon purging to ensure anaerobic conditions. In a separate sealed vessel, a solution of 32 mM NADH, 300 μM FMN, and 20 mM (*S*)-HPP (**5**) in the same buffer was made anaerobic by the same procedure. The vessels were transferred to an anaerobic glove box, where 25 μL of each mixture was combined to start the assay. The final concentrations of the reagents in 50 μL were 100 μM *Ps*-HppE, 100 μM Fe(NH$_4$)$_2$(SO$_4$)$_2$, 150 μM FMN, 10 mM (*S*)-HPP, and 16 mM NADH. After incubating for 1.5 h at room temperature, the reaction was quenched with 50 μL of 2 M acetic acid. The activity was then analyzed by the HPLC assay described above.

5.2.14. DFT CALCULATIONS OF BOND DISSOCIATION ENERGIES. To gain insight into the distinct regiospecificity observed in the reactions of HppE with (*R*)- and

145

(*S*)-HPP (**38** and **5**, respectively), electronic structure calculations were performed to estimate the bond dissociation enthalpies of the C_1-H and C_2-H bonds of HPP. All calculations were performed using Gaussian98.[40]   Geometry optimizations were performed using Becke-style 3-Parameter Density Functional Theory (DFT) with the Lee-Yang-Parr correlation functional (B3LYP) and Pople's diffuse polarized triple-ζ 6-311+G(d,p) basis set with the Opt = Tight and Int = Ultrafine keywords. The initial geometry of the heavy atoms of the substrate was taken from the crystal structure of Fe^{2+}-HppE in complex with (*S*)-HPP (**5**) (PDB accession number 1ZZ8).[41]   Vibration frequency calculations were then performed on the optimized geometries based on the same B3LYP/6-311+G(d,p) scheme at 25 °C and 1.0 Atm, using a scale factor of 0.9877 to correct the zero-point vibrational energies.[42]   These calculations were performed by Dr. Steven O. Mansoorabadi.

5.2.15. EPR SPECTROSCOPY.   EPR first derivative spectra of *Ps*-HppE were collected at X-band microwave frequency with 100-kHz field modulation using a Bruker (Billerica, MA) EMX spectrometer with a 4119HS high-sensitivity resonator. Sample temperature was maintained with an ITC503S temperature controller, an ESR910 liquid helium cryostat, and LLT650/13 liquid helium transfer tube (Oxford Instruments, Concord, MA). The EPR parameters were obtained by simulation of the experimental spectra using an EPR program written by Dr. Frank Neese[43] and were further verified in Bruker SimFonia. The as-isolated *Ps*-HppE was made anaerobic by repeated cycles of evacuation and flushing with argon. A molar equivalent of $Fe(NH_4)_2(SO_4)_2$ from an anaerobic stock solution was added to *Ps*-HppE to reconstitute it under anaerobic conditions. For the sample with (*S*)-HPP bound, ten molar equivalents of anaerobic (*S*)-HPP (**5**) were incubated with the ferrous reconstituted *Ps*-HppE in the EPR tube. Nitric

146

oxide gas was passed over NaOH pellets to remove any acid impurities and then introduced into the substrate-bound enzyme samples through a gas-tight Hamilton syringe under argon. The samples were frozen by slow immersion in liquid nitrogen for later EPR analysis. Spin quantification was performed by double integration of the EPR spectra recorded under nonsaturating conditions at 20 K for comparison with a Cu-EDTA standard (0.5 mM). The EPR samples were prepared by myself, and Dr. Aimin Liu helped with the analysis of the signal.

5.2.16. [^{18}O] KINETIC ISOTOPE EFFECTS MEASUREMENTS. [^{18}O]-KIEs were measured competitively as described previously.[31,44] The ^{18}O/^{16}O ratios were measured using isotopic ratio mass spectrometry (Laboratory for Environmental and Sedimentary Geochemistry, Department of Earth and Planetary Science, UC Berkeley, CA). The [^{18}O]-KIEs were obtained by fitting the ^{18}O/^{16}O ratio of ratios versus fractional conversion according to **Equation 5-2**, where R_f is the ^{18}O/^{16}O isotopic ratio at f fractional conversion, and R_0 is the isotopic ratio prior to the enzymatic reaction. All KIEs are reported with errors of $\pm$ 1σ from the nonlinear regression fit to **Equation 5-2**.

Equation 5-2

$$\frac{R_f}{R_0} = (1-f)^{1/(^{18}OKIE)-1}$$

The [^{18}O]-KIE experiments were carried out in 20 mM Tris-HCl buffer (pH 7.5), in the presence of 1 mM (*S*)-HPP (**5**) or (*S*)-1,1-[^{2}H]$_2$-HPP (**35**), 1.5 mM NADH, and 0.4–0.6 mM O$_2$. Reactions were initiated by the addition of 3 µL of apo-*Ps*-HppE reconstituted with equimolar Fe(NH$_4$)$_2$(SO$_4$)$_2$, followed by the addition of FMN to minimize the background oxygen consumption. Final concentrations were typically 8–12

147

μM HppE and 9–13 μM FMN. The fractional conversions used for the $[^{18}O]$-KIE measurements were between 20 and 60%. The amount of O_2 consumed was corrected for the background O_2 consumption due to FMN, NADH and/or Fe(II) in the absence of enzyme. In all experiments, the O_2 consumed in non-enzymatic reactions accounted for less than 10% of the total O_2 consumed. The $[^{18}O]$-KIE was also measured for the background oxygen consumption (at 11 μM FMN and 1.5 mM NADH), for comparison with the enzymatic reaction. The $[^{18}O]$-KIE experiments were conducted by Dr. Liviu Mirica in the lab of Prof. Judith Klinman at the University of California at Berkeley.

5.2.17. CALCULATION OF ^{18}O EQUILIBIUM ISOTOPE EFFECTS. The $[^{18}O]$-EIEs for the reactions with O_2 were determined as the product of three terms, ZPE, EXC and MMI, see **Equation 5-1**.[45,46] All three terms are related to vibrational frequencies (v) of ^{18}O– and ^{16}O–containing reactants (R $\equiv O_2$) and products (P), as shown in **Equations 5-3**, **5-4** and **5-5**, where the asterisk denotes the ^{18}O-containing reactants or products, T is temperature in K, h is Planck's constant, and k is Boltzmann's constant.[31] Experimentally determined frequencies for Fe(III)-OO•, Fe(III)-OOH,[47,48] and Fe(IV)=O species[49] were used for calculation of the $[^{18}O]$-EIE (**Table 5-3**). For the asymmetric Fe(III)-O_2• and Fe(III)-OOH, species, the ^{18}O label can be at either the central or terminal position. The populations of the two isotopic products are expected to be close to each other, hence the $[^{18}O]$-EIE was calculated using the formula: $[^{18}O]$-EIE$_{calc}$ = 2/(^{18,16}K–1 + ^{16,18}K–1). The $[^{18}O]$-EIE calculations were conducted by Dr. Liviu Mirica in the lab of Prof. Judith Klinman at the University of California at Berkeley.

Equation 5-3

$$ZPE = \frac{\displaystyle\prod_{j}^{3N-6}\frac{\exp^{(h\nu_j^{P*}/2kT)}}{\exp^{(h\nu_j^{P}/2kT)}}}{\displaystyle\prod_{j}^{3N-5}\frac{\exp^{(h\nu_j^{R*}/2kT)}}{\exp^{(h\nu_j^{R}/2kT)}}}$$

Equation 5-4

$$EXC = \frac{\displaystyle\prod_{j}^{3N-6}\frac{1-\exp^{-(h\nu_j^{P*}/kT)}}{1-\exp^{(h\nu_j^{P}/kT)}}}{\displaystyle\prod_{j}^{3N-5}\frac{1-\exp^{(h\nu_j^{R*}/kT)}}{1-\exp^{(h\nu_j^{R}/kT)}}}$$

Equation 5-5

$$MMI = \frac{\displaystyle\prod_{j}^{3N-6}(\nu_j^{P}/\nu_j^{P*})}{\displaystyle\prod_{j}^{3N-5}(\nu_j^{R}/\nu_j^{R*})}$$

Table 5-3:   Vibrational frequencies (cm^{-1}) of O_2, H_2O, and Fe/O_2 species.

Molecule	Mode	Frequency (cm^{-1})			
		$\nu_{16-16}{}^a$	$\nu_{18-18}{}^a$	$\nu_{18-16}{}^a$	$\nu_{16-18}{}^a$
O_2	O–O^b	1556	1467	1512	1512
H_2O	H–O^b	3824	-^{c}	3824	-
	H–O^b	3939	-	3922	-
	H-O-H^b	1654	-	1644	-
Fe(III)-OO•	Fe–O^d	555	526	526	555
	O–O^d	1136	1066	1100^e	1100^e
Fe(III)-OOH	Fe–O^f	621	599	599	621
	O–O^f	844	796	820^e	820^e
	O–H^b	3539	-	3527	3539
	O-O-H^b	1205	1199	1199	1204
Fe(IV)=O	Fe–O^g	821	-	787	-

a) Frequencies ν_{x-x} represent the modes for the species derived from $^{x,x}O_2$, the first label corresponding to the O atom closest to the metal center; b) Ref 31; c) Not applicable; d) Ref 50; e) ν_{18-16} was calculated as follows: $\nu_{18-16} = (\nu_{16-16}\,\nu_{18-18})^{1/2}$; f) Ref 48; g) Ref 49.

5.3.   RESULTS AND DISCUSSION

5.3.1.   CLONING, OVEREXPRESSION, AND PURIFICATION OF *PS*-HPPE.   The

gene, *orf3*, coding for *Ps*-HppE which catalyzes the last step of fosfomycin biosynthesis in *Pseudomonas syringae* PB-5123, was amplified by PCR and cloned into the expression vector pET24b(+). The resulting construct, pLH01, was used to transform *E. coli* BL21(DE3) cells. The induction of *orf3* expression by IPTG was conducted at 18 °C to minimize the formation of inclusion bodies.

As shown in SDS-PAGE (**Figure 5-5**), the desired protein was isolated in nearly homogeneous form after ammonium sulfate fractionation and two anion exchange chromatographic steps (DEAE-Sepharose and MonoQ). The subunit molecular mass of 21 kDa, assessed by SDS-PAGE, correlates well with the predicted value of 21,315 Da calculated from the deduced amino acid sequence. As determined by size exclusion chromatography, the purified recombinant *Ps*-HppE has a mass of 73 kDa in solution.

When *Sw*-HppE, which has a mass of 21,210 Da as a monomer, was analyzed under the same conditions, it yielded a mass of 95 kDa. Based on the results of X-ray crystallography, *Sw*-HppE has been determined to exist as a homotetramer.[41] Since the observed mass for *Sw*-HppE is 11 kDa higher than the predicted mass for a homotetramer, and the *Ps*-HppE is 10 kDa higher than the predicted mass for a homotrimer, *Ps*-HppE likely exists as a homotrimer instead of homotetramer. Determination of the crystal structure for *Ps*-HppE is in progress, and the results will reveal if *Ps*-HppE is indeed a homotrimer.
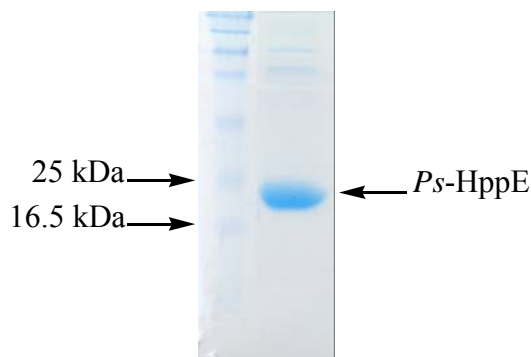
Figure 5-8: **SDS-PAGE gel of as-purified (apo) *Ps*-HppE.**

5.3.2. SEQUENCE ANALYSIS. The epoxidation reaction catalyzed by *Ps*-HppE is identical to that catalyzed by *Sw*-HppE and is the final step in the biosynthesis of fosfomycin. Interestingly, amino acid sequence alignment showed that the two enzymes share only 27% identity (**Figure 5-6**). However, the residues that have been determined to be crucial for *Sw*-HppE are conserved in *Ps*-HppE. These include Lys21, Tyr92, Tyr93, Tyr95, His128, Glu132, and His171 (the numbering given is based on the *Ps*-HppE sequence). His128, Glu132, and His171 are assigned to be the ligands responsible for iron binding in *Ps*-HppE, since the corresponding residues; His138, Glu142, and His180; in *Sw*-HppE have been determined to be the metal binding residues.[41,51] The

proposed role for Lys21 in *Ps*-HppE is to stabilize the negative charge on the iron-peroxo intermediate generated during oxygen activation. A similar function has been assigned to its counterpart, Lys23, in *Sw*-HppE based on the crystal structure as well as the mutagenesis results.[41] The three conserved tyrosine residues; Tyr92, Tyr93, and Tyr95; are proposed to be part of a relay for shuttling electrons derived from NADH from the protein surface to reduce the active site iron. This is based on the observation from the crystal structure of *Sw*-HppE, which undergoes a significant conformational change upon (*S*)-HPP binding. It was noted that the three conserved tyrosine residues in the enzyme-substrate complex align themselves in a row constituting a pathway extending from the surface of the protein to the active site.[41]

```
Sw-HppE      1    MSNTKTASTGFAELLKDRREQVKMDHAALASLLGETPETVAAWENGEGGELTLTQLGRIA
Ps-HppE      1    M-DVRTLAVGKAHLEA-LLATRKMT---LEHLQDVRHDATQVYFDG------LEHLQNVA
Consensus             T   G A L         KM    L  L              G       L  L   A

Sw-HppE     61    HVLGTSIGALTP-PAGNDLDDGVIIQMPDERPILKGVRDNVDYYVYNCLVRTKRAPSLVP
Ps-HppE     50    QYLAIPLSEFFVGQTQSDLDDGVKIARRNGGFKREEIRGGVHYYTYEHLVTTNQDPGLMA
Consensus          L              DLDDGV I              R  V YY Y  LV T    P L

Sw-HppE    120    LVVDVLTDNPDDAKFNSGHAGNEFLFVLEGEIHMKWG-DKENPKEALLPTGASMFVEEHV
Ps-HppE    110    LRLDLHSDDEQPLRLNGGHGSREIVYVTRGAVRVRWVGDNDELKEDVLNEGDSIFILPNV
Consensus        L  D   D       N GH    E   V  G       W  D     KE  L  G S F      V

Sw-HppE    179    PHAFTAAKGTGSAKLIAVNF-
Ps-HppE    170    PHSFTNHVGGAKSEIIAINYG
Consensus        PH FT   G      IA N
```

Figure 5-9: **Protein sequence alignment of *Ps*-HppE and *Sw*-HppE.**

5.3.3. RECONSTITUTION OF EPOXIDASE ACTIVITY. As described above, *Ps*-HppE and *Sw*-HppE catalyze the same reaction, and the residues important for catalysis are conserved in both enzymes. Thus, it is very likely that *Ps*-HppE utilizes the same chemistry as *Sw*-HppE to catalyze the epoxide formation. To verify this contention, the as-purified *Ps*-HppE was reconstituted using the same procedures developed for *Sw*-HppE with ferrous iron and assayed under aerobic conditions in the presence of FMN,

NADH and (S)-HPP.[19]   Formation of the product, fosfomycin (6), was detected by HPLC, and its chemical identity verified by ^{1}H and ^{31}P NMR.   If either iron, FMN or NADH was omitted from the reaction mixture, no product formation was discernible by HPLC.   Our results showed that NADH is essential and is consistent with its role to provide two of the four electrons needed for oxygen activation and the conversion of molecular oxygen to water (**Figure 5-2**).   FMN is also required.   This requirement may be ascribed to its role as an electron mediator in the reduction of the metal center by NADH.   Since oxygen is used to activate the iron center, when the incubation was carried out under an anaerobic environment, no epoxidase activity could be detected by the HPLC-based enzyme assay.

It was reported in a recent publication that *Sw*-HppE was not strictly iron-dependent, because the zinc reconstituted enzyme retained reduced but measurable activity.[52]   Since zinc ion is redox-inert, a new mechanism that does not involve the reductive activation of molecular oxygen was proposed.   In this mechanism (**Figure 5-7**), the divalent metal ion acts as a Lewis acid to activate the C-2 hydroxyl group, which attacks C-1 with concurrent transfer of the pro-*R* hydrogen as a hydride to FMN.   It was later determined that the observed activity with the zinc *Sw*-HppE was an artifact.[53]   This "nucleophilic displacement-hydride transfer" mechanism could also be ruled out for *Ps*-HppE, since no epoxidase activity could be detected with zinc reconstituted *Ps*-HppE. To explore if other redox active metals could substitute iron in the epoxidase assay, the catalytic property of *Ps*-HppE reconstituted with cobalt, copper and manganese was investigated.   No turnover could be detected using *Ps*-HppE carrying any of these metals. The fact that the addition of 5 mM EDTA abolished the activity of the iron reconstituted *Ps*-HppE further confirm the importance of iron in the catalysis.

153
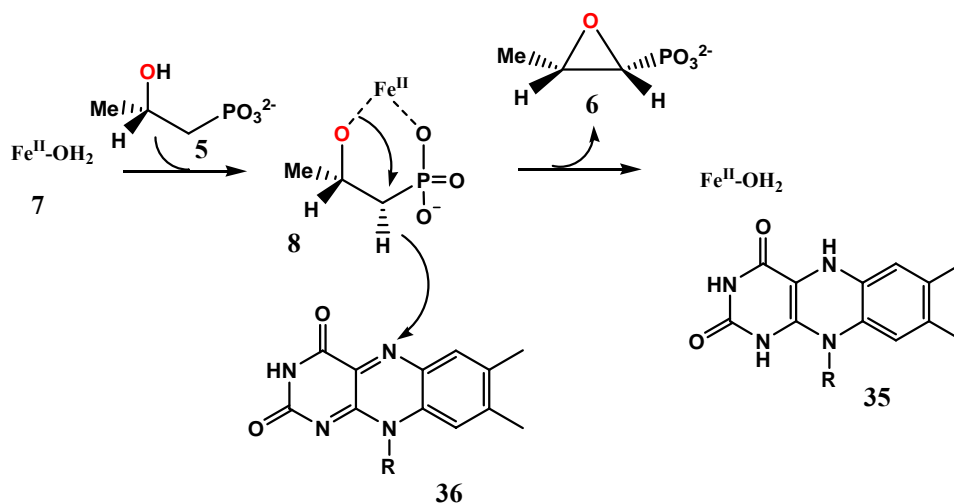
Figure 5-10: **Proposed nucleophilic displacement-hydride transfer mechanism for HppE.**

When using (R)-HPP (**38**) as the substrate, *Sw*-HppE catalyzed the conversion of the C-2 hydroxyl group to a ketone to yield 2-oxopropylphosphonic acid (**39**) as the product (**Figure 5-8**).[54] Further investigation indicated that the stereochemistry at the C-2 position of HPP determines the regiospecificity of the initial hydrogen atom abstraction. In the mechanism depicted in **Figure 5-2**, when (S)-HPP binds to *Sw*-HppE, the C-1 pro-*R* hydrogen atom is abstracted, which leads to the production of fosfomycin. However, when (R)-HPP binds to *Sw*-HppE, it is believed that the C-2 hydrogen atom is abstracted, which leads to the formation of 2-oxopropylphosphonic acid (**39**). It was investigated if *Ps*-HppE utilizes this method to control the regiospecificity of the initial hydrogen atom abstraction. When the above activity assays for *Ps*-HppE where conducted using (R)-HPP as the substrate, the product 2-oxopropylphosphonic acid (**39**) was formed. This was verified by ^{1}H and ^{31}P NMR spectroscopy.

154
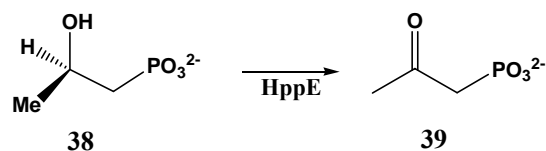
Figure 5-11: The HppE catalyzed reaction with (*R*)-HPP as the substrate.

5.3.4. ACTIVITY FOR (*S*)-HPP AND (*R*)-HPP. To determine how the activity of *Ps*-HppE compares to *Sw*-HppE, the rate of catalysis was determined separately using (*S*)-HPP (**5**) and (*R*)-HPP (**38**) at saturating concentration. To determine the optimal substrate concentration for the assay, the amount of product formation was measured after 20 min incubation using 5, 10, 15 and 20 mM substrate. Since all four substrate concentrations resulted in the same amount of product formation, 10 mM substrate was set as the saturating concentration. Due to the reduced activity of *Ps*-HppE with respect to *Sw*-HppE, the concentrations of *Ps*-HppE, Fe(NH$_4$)$_2$SO$_4$ and FMN were doubled. The ratio of 1:1:1.5 for HppE to Fe(NH$_4$)$_2$SO$_4$ to FMN was held constant for all assays.

Table 5-4: Rate constants for reactions at 1.5:1 FMN to HppE ratio.

Substrate	*Ps*-HppE	*Sw*-HppE
(*S*)-HPP (**5**) k_{obs} (min^{-1})	0.17 ± 0.02	0.31 ± 0.06
(*R*)-HPP (**38**) k_{obs} (min^{-1})	0.33 ± 0.04	0.58 ± 0.02

As seen in **Table 5-4**, the observed rate constants for both enzymes with both substrates are of similar magnitudes. Two observations are worthy of comments. The first is that the *Sw*-HppE is roughly 1.8 times faster than *Ps*-HppE for both (*S*)-HPP and (*R*)-HPP. It appears that *Sw*-HppE is a more effective epoxidase. Secondly, the reaction rate for (*R*)-HPP (**38**) is 1.9 times faster than that for (*S*)-HPP (**5**) using either *Sw*-HppE or *Ps*-HppE.

155

To determine how rate-limiting hydrogen atom abstraction is for the (S)-HPP (**5**) and (R)-HPP (**38**) reactions, the 1° [^{2}H]-KIE was determined for both. It has previously been demonstrated that the C-1 pro-R hydrogen atom is abstracted in the conversion of (S)-HPP to fosfomycin,[55] and for the turnover of (R)-HPP to **39**, it is the C-2 hydrogen atom that is abstracted.[54] When the [^{2}H]-KIE was determined for the (S)-HPP reaction, using (S)-1,1-[^{2}H]$_2$-HPP (**35**) as the labeled substrate and at a FMN to Ps-HppE ratio of 1.1:1, a [^{2}H]-KIE of 1.10 ± 0.04 was measured. Since this [^{2}H]-KIE was determined with (S)-1,1-[^{2}H]$_2$-HPP (**35**), it results from the 1° [^{2}H]-KIE on hydrogen atom abstraction and from the 2° [^{2}H]-KIE on radical formation (sp^3 to sp^2) and ring-closure (sp^2 to sp^3). The 2° [^{2}H]-KIE on radical formation will be small and normal, while the 2° [^{2}H]-KIE on ring-closure will be small and inverse. Since ring-closure is not expected to be significantly rate-limiting, the impact of the inverse isotope effect should be small. Either way, due to the difference in magnitude of a 1° [^{2}H]-KIE versus a 2° [^{2}H]-KIE; the measured [^{2}H]-KIE will be dominated by the 1° [^{2}H]-KIE. The 1° [^{2}H]-KIE for the (R)-HPP (**38**) reaction was determined with (R)-2-[^{2}H]-HPP (**20**) as the labeled substrate and at an FMN to Ps-HppE ratio of 1.5:1. The measured 1° [^{2}H]-KIE was 1.07 ± 0.07. The observed [^{2}H]-KIEs for both reactions are smaller than is expected for a 1° [^{2}H]-KIE; therefore, a step other than hydrogen atom abstraction is rate-limiting, presumably electron transfer to the active site iron.

It is known that the rate of reaction increases with increasing FMN, presumably due to an increased rate in electron transfer to the active site iron. In order to reduce the commitments to catalysis, which could have masked the previous 1° [^{2}H]-KIEs, the [^{2}H]-KIEs were re-measured at an FMN:Ps-HppE ratio where the rate enhancement of FMN is saturated. To determine this saturating FMN:Ps-HppE ratio, the (R)-HPP reaction was conducted at varying ratios of FMN:Ps-HppE. At each ratio, the reaction incubated for

20 min before being quenched and analyzed by HPLC. The amount of product (**39**) formed was plotted versus the respective FMN:*Ps*-HppE ratio. From the plot in **Figure 5-12**, an FMN to *Ps*-HppE ratio of 50:1 was chosen. It was assumed that this ratio is saturating for the (*S*)-HPP reaction as well. For the (*S*)-HPP [^{2}H]-KIE measurement at this FMN ratio, (1*R*,2*S*)-1-[^{2}H]-HPP (**31**) was used as the labeled substrate; therefore there is no 2° [^{2}H]-KIE to complicate the analysis. From the results in **Table 5-5**, it is evident that hydrogen atom abstraction does become more rate-limiting for the (*S*)-HPP. The measured 1° [^{2}H]-KIE is smaller than what would be expected for an intrinsic 1° [^{2}H]-KIE. Thus the hydrogen abstraction step is believed to be partially rate-limiting, and electron transfer may still be the predominant rate-limiting step. For the (*R*)-HPP reaction, there is again no significant [^{2}H]-KIE, so the abstraction is still not significantly rate-limiting.
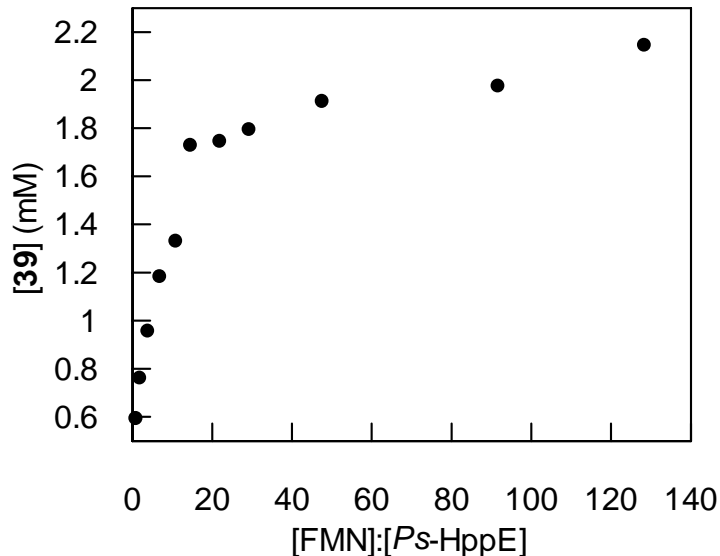
Figure 5-12: Plot of the product (**39**) from the reaction of (*R*)-HPP (**38**) with *Ps*-HppE at varying ratios of FMN to *Ps*-HppE.

157

Table 5-5:   Summary of 1° [²H]-KIE results at a different FMN to *Ps*-HppE ratios.

Substrate	FMN:*Ps*-HppE (50:1)		FMN:*Ps*-HppE (1.5:1)		FMN:*Ps*-HppE (1.1:1)	
	k_{obs}	$^d k_{obs}$	k_{obs}	$^d k_{obs}$	k_{obs}	$^d k_{obs}$
(*S*)-HPP (**5**)	0.46 ± 0.04	--	ND	--	0.199 ± 0.002	--
(1*R*,2*S*)-1-[²H]-HPP (**31**)	0.31 ± 0.03	1.5 ± 0.2	ND	ND	ND	ND
(*S*)-1,1-[²H]₂-HPP (**35**)	ND	ND	ND	ND	0.18 ± 0.007	1.10 ± 0.04
(*R*)-HPP (**38**)	1.12 ± 0.1	--	0.45 ± 0.03	--	ND	--
(*R*)-2-[²H]-HPP (**20**)	1.12 ± 0.1	1.08 ± 0.14	0.42 ± 0.01	1.07 ± 0.07	ND	ND

The reduced rate for the *Ps*-HppE reaction with (*S*)-HPP compared to with (*R*)-HPP reaction and the small but significant 1° [²H]-KIE for (*S*)-HPP versus the KIE of unity for (*R*)-HPP implies that hydrogen atom abstraction is slower and more rate-limiting for (*S*)-HPP than (*R*)-HPP. There are two possible explanations for the difference in rates for C-2 hydrogen atom abstraction in the (*R*)-HPP reaction versus C-1 hydrogen atom abstraction in the (*S*)-HPP reaction. It is possible that the C-2 hydrogen for bound (*R*)-HPP is closer to the reactive oxygen species than the C-1 hydrogen for the bound (*S*)-HPP, thus reducing the barrier for abstraction.[56] The rate difference is likely due to the difference in the energetics of the hydrogen being abstracted and the stability of the resulting substrate radical. Based on DFT calculations, the bond dissociation energies (BDE) for the C-1 hydrogen and the C-2 hydrogen are 96.5 and 89.0 kcal/mol, respectively. Thus, the thermodynamic energy barrier for hydrogen atom abstraction in the (*R*)-HPP reaction is 7.5 kcal/mol lower than in the (*S*)-HPP reaction. This may account for the observed rate difference of the two substrates.

5.3.5. EPR CHARACTERIZATION OF *PS*-HPPE. EPR spectra of *Ps*-HppE-Fe(II) nitrosyl complexes, in the presence and absence of substrate, are shown in **Figure 5-13.** The corresponding EPR spectra of *Sw*-HppE-Fe(II) are also shown in this figure in dashed traces for comparison. In the absence of (*S*)-HPP (**5**), the EPR spectrum of the *Ps*-HppE-NO complex consists of two sets of axial EPR signals of the Fe-nitrosyl complexes in an 88:12 ratio. The major axial species exhibits an isotropic resonance component at g = 3.96 and a V-shaped resonance at 2.00 (not shown). This is typical for an S = 3/2 non-heme $\{Fe-NO\}^7$ species with an E/D value of 0.01 and $D > 0$. The minor species is also an S = 3/2 $\{Fe-NO\}^7$ complex, but less axial, with principal g values of 4.30, 3.69, and 2.00 (*E/D* value of 0.05). In contrast, an apparent heterogeneity is observed for *Sw*-HppE, with two similar species present in a 3:7 ratio.[19] Thus, the Fe(II) center in *Ps*-HppE appears to be more uniform than that in *Sw*-HppE.
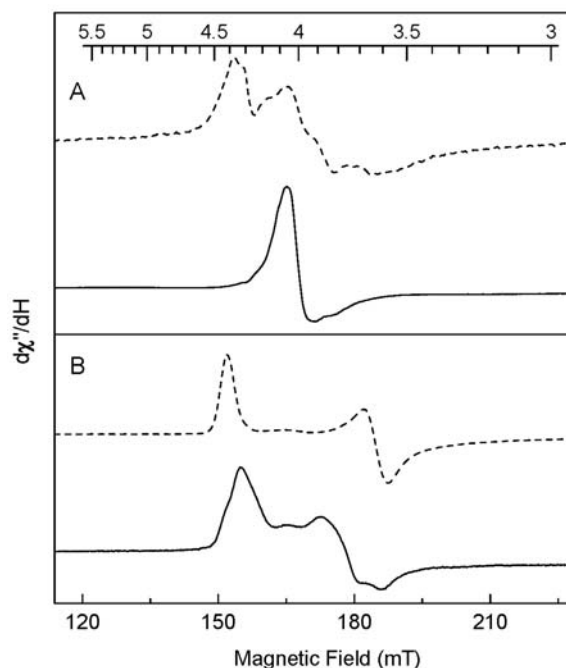
Figure 5-13: EPR spectra of reduced HppE-Fe(II) nitrosyl complexes at 4 K: (A) 250 μM *Ps*-HppE (solid trace) or *Sw*-HppE (dashed trace) in the presence of NO; (B) the ternary complex of substrate-HppE- NO (*Ps*-HppE, solid trace; *Sw*-HppE, dashed trace). Substrate was present in 10-fold excess. The spectrum shown also contains a minor species (ca. 5%) due to a denatured protein-bound Fe-NO complex (g = 4.07) which was previously characterized.[19] Instrumental conditions: microwave power, 0.5 mW; modulation amplitude, 5 G; time constant, 0.02 s; and sweep rate: 50 G/s. The *g*-scale is plotted on the top of the spectra.

Although the ferrous center of *Sw*-HppE can react with NO and form two spectroscopically distinguishable complexes, we have previously found that only a uniform substrate-Fe-NO complex of *Sw*-HppE (g = 4.42, 3.63, and 1.97, *E/D* = 0.066) is formed in the presence of substrate (*S*)-HPP (**5**).[19] These results suggested that the substrate likely binds to the active site iron center first, and as such organizes the center to bind NO, an O_2 analogue, only in one conformation. In contrast, in the presence of (*S*)-HPP, the EPR spectrum of the nitrosyl complex of *Ps*-HppE-Fe(II) presents apparent heterogeneity. Two sets of EPR signals are observed (in a 3:7 ratio); both can be

160

attributed to the substrate-enzyme-NO ternary complexes. This is opposite to the prior *Sw*-HppE result. The minor ternary complex (30%) observed for *Ps*-HppE exhibits the same EPR parameters as those previously observed for *Sw*-HppE (g = 4.42, 3.63, and 1.97, E/D = 0.066). The major ternary complex (70%) having g = 4.33, 3.74, and 2.00, E/D = 0.059, is less rhombic.

The above results indicate that substrate and NO could bind to the ferrous center of the reduced *Ps*-HppE enzyme to form a stable complex. But the heterogeneity EPR signals observed for the ternary complex of *Ps*-HppE suggest that substrate binding to the active site Fe(II) ion may lead to two different conformations.   Our recent isotope labeling study showed that the uniform EPR signal for the ternary complex of *Sw*-HppE is a result of the substrate coordination to the Fe(II) ion in a bidentate fashion.[57] This same species is also seen in the *Ps*-HppE ternary complex, albeit it represents only 30% of the total iron.   The remaining 70% of the ternary complex may be in a form of monodentate coordination of substrate onto the metal center. This is an intermediate step towards the bidentate binding to the active site Fe ion.

5.3.6. POST-TRANSLATIONAL HYDROXYLATION OF *PS*-HPPE. The   reconstituted ferrous form of *Ps*-HppE is colorless. However, when the protein is exposed to air, it slowly turns green in color. The optical spectrum of this green protein exhibits a broad band around 600-750 nm having a λ_{max} at 672 nm with a molar absorption coefficient of approximately 409 (M of Fe)$^{-1}$·cm^{-1} (**Figure 5-14**). A similar peak formed with a λ_{max} at 680 nm and a molar extinction coefficient of 450 (M of Fe)$^{-1}$·cm^{-1} was previously observed when the reconstituted ferrous form of *Sw*-HppE was exposed to air.[19] Further investigation showed that the color change in *Sw*-HppE is due to a post-translational hydroxylation of Tyr105 to DOPA.[39] The green chromophore arises from a ligand to

161

metal charge transfer transition of a bidentate catecholate-iron (III) complex formed between the active-site iron center and the modified tyrosine. A similar post-translationally hydroxylate ion of Tyr95 (the Tyr105 equivalent in *Ps*-HppE) to DOPA, may also occur when ferrous reconstituted Ps-HppE is exposed to air leading to the formation of the bidentate catecholate-iron (III) complex.
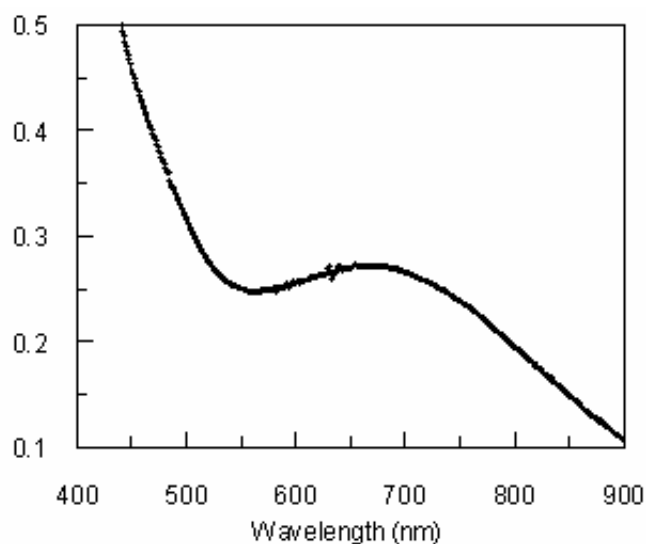
Figure 5-14: **Electronic absorption spectrum of as-purified *Ps*-HppE that has been reconstituted with 1.1 equivalents of Fe(NH$_4$)$_2$(SO$_4$)$_2$.**

To verify the occurrence of the catecholate residue, the isolated *Ps*-HppE was subjected to the Paz's quinone staining reagents including glycine and nitroblue tetrazolium (NBT).[38] If a quinone is present, it can oxidize the glycine in solution. The reduced quinone then reacts with dioxygen to generate superoxide, which oxidizes NBT to generate a blue-purple compound. As shown in **Figure 5-15**, the stain produced a positive result indicating the presence of quinone in *Ps*-HppE. It is therefore highly likely that Tyr95 is post-translationally hydroxylated to DOPA. The significance of this modification in HppE is currently under investigation.
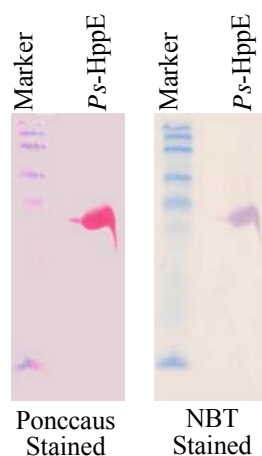
Figure 5-15: As-purified *Ps*-HppE was run on SDS-PAGE gel and transfered electrophoritically to nitrocellulose membrane. The membrane is then temporarily stained for proteins with Ponccaus (left) and then NBT stained (right) to detect the presence of quinone.

5.3.7. [¹⁸O]-KIE Analysis of Ps-HppE.
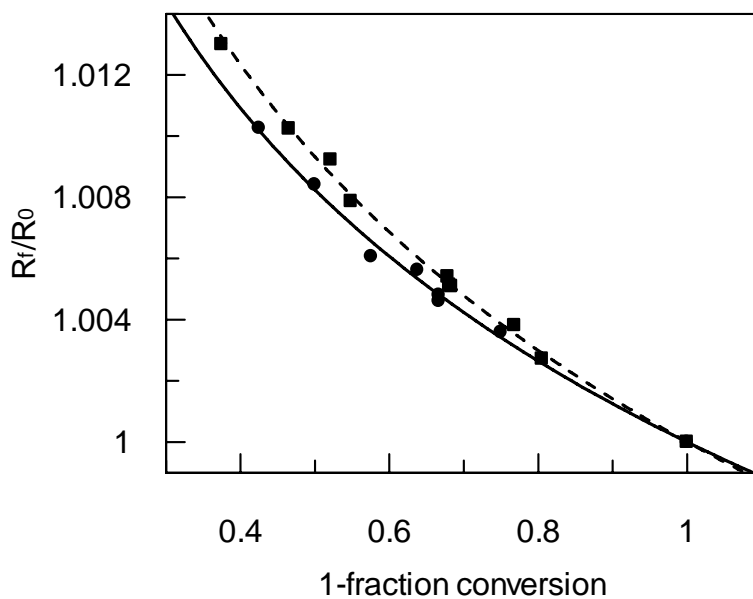
Figure 5-16: Isotope fractionation plots for (*S*)-HPP (5) (●) and (*S*)-1,1-[²H]₂-HPP (35) (■). The fits for obtaining [¹⁸O]-KIEs are shown in solid for (*S*)-HPP (5) and dashed for (*S*)-1,1-[²H]₂-HPP (35). Conditions: *Ps*-HppE: 10 μM HppE, 0.4–0.6 mM O₂, 1 mM (*S*)-HPP or (*S*)-1,1-[²H]₂-HPP, 11 μM FMN, 1.5 mM NADH, 20 mM Tris-HCl (pH 7.5), 25 ºC.

163

The [^{18}O]-KIE was determined from the data in **Figure 5-16** for the *Ps*-HppE reaction with (*S*)-HPP and separately with (*S*)-1,1-[^{2}H]$_2$-HPP (**35**), and these values are reported in **Table 5-6**. As described above, the values in **Table 5-6** are [^{18}O]-KIEs on $k_{cat}/K_M(O_2)$, which reflect changes in the oxygen bond order that occur in all steps from initial O_2 binding up to and including the first irreversible step.[44] To help interpret the measured [^{18}O]-KIEs, [^{18}O]-EIEs were calculated from vibrational frequencies from **Table 5-3** of the reactants and possible oxygen products, following the formalism developed by Bigeleisen and Mayer.[45] These calculated [^{18}O]-EIEs (see **Table 5-7**) can be used as upper limits for the measured [^{18}O]-KIEs,[30,32,33] allowing a direct comparison between model reactions and experimental values.

Table 5-6: **Summary of experimental [^{18}O]-KIEs**

Substrate	[^{18}O]-KIE
(*S*)-HPP (**5**)	1.0120 ± 0.0002
(*S*)-1,1-[^{2}H]$_2$-HPP (**35**)	1.0136 ± 0.0002

Table 5-7: Calculated [^{18}O]-EIEs using vibrational frequencies.

Reaction	ZPE	EXC	MMI	[^{18}O]-EIE$_{calc}$	[^{18}O]-EIE$_{net}$^{a}
Fe(II) + O_2 $\rightleftharpoons$ Fe(III)-$O_2^{\bullet}$					
Fe-^{18}O-^{16}O$\bullet$	0.9493	0.9887	1.0590	0.9939	
Fe-^{16}O-^{18}O$\bullet$	1.0193	0.9994	1.0037	1.0224	**1.0080**
Fe(II)+ O_2 $\xrightarrow{e^-, H^+}$ Fe(III)-OOH					
Fe^{III}-^{18}O^{16}OH	0.9947	0.9921	1.0370	1.0234	
Fe^{III}-^{16}O^{18}OH	1.0044	0.9979	1.0087	1.0110	**1.0172**
Fe(II) + O_2 $\xrightarrow{2e^-, 2H^+}$ Fe(IV)=O + H$_2$O					
Fe^{IV}=^{18}O, H$_2$^{16}O	1.0239	0.9967	1.0138	1.0347	
Fe^{IV}=^{16}O, H$_2$^{18}O	1.0414	1.0001	0.9820	1.0228	**1.0287**

^{a} The net ^{18}O EIE was calculated using the formula: $^{18}EIE_{net} = 2/(^{18,16}EIE^{-1} + {}^{16,18}EIE^{-1})$.[31]

Comparing the measured $[^{18}O]$-KIE for (S)-HPP (**5**) of 1.0120 ± 0.0002 with the calculated $[^{18}O]$-EIEs, the oxygen product formed in the rate-limiting step appears to be Fe(III)-hydroperoxide, which would be either species **10** or **11** in **Figure 5-2**. The $[^{18}O]$-KIE is slightly lower than the calculated $[^{18}O]$-EIE for Fe(III)-hydroperoxide of 1.0172; however, it is similar to the experimentally determined $[^{18}O]$-EIE of 1.0113 ± 0.0005 for Hr, which does form a Fe(III)-OOH as its product.[31] From the $[^{18}O]$-KIE measured with (S)-1,1-$[^{2}H]_2$-HPP (**35**) as the substrate (1.0136 ± 0.0002), it can be concluded that the $[^{18}O]$-KIE is mechanistic in origin. If the $[^{18}O]$-KIE was dominated by O_2 binding, the $[^{18}O]$-KIE would not change when measured with a deuterated substrate. The fact that the $[^{18}O]$-KIE did increase when (S)-1,1-$[^{2}H]_2$-HPP (**35**) was the substrate also implies that the step giving rise to the $[^{18}O]$-KIE becomes more rate-limiting with the deuterated substrate. The change in $[^{18}O]$-KIE with (S)-1,1-$[^{2}H]_2$-HPP (**35**) as the substrate also requires that hydrogen atom abstraction occurs before or in the first irreversible step. The first irreversible step is believed to be the first electron transfer from reduced FMN to the active site iron. If Fe(III)-superoxide (**9**) (**path a** in **Figure 5-2**) is the reactive species, the first irreversible step will be **10→13**, and if either Fe(III)-hydroperoxide (**11**) or Fe(IV)-oxo (**12**) (**paths b** and **c** in **Figure 5-2**, respectively), then the first irreversible step will be **9→11**. If the reactive species was either Fe(III)-hydroperoxide (**11**) or Fe(IV)-oxo (**12**) is the reactive species, hydrogen atom abstraction will occur after the first irreversible step; thus there would be no change in the $[^{18}O]$-KIE when using the deuterated substrate. Of the different mechanisms depicted in **Figure 5-2**, only in **path a**, where Fe(III)-superoxide (**9**) is the reactive species, does hydrogen atom abstraction occur before or in the first irreversible step. Therefore, based on the increase in the $[^{18}O]$-KIE when using the deuterated substrate, (S)-1,1-$[^{2}H]_2$-HPP (**35**), versus (S)-HPP; the

165

reactive oxygen species in the *Ps*-HppE reaction, and presumably the *Sw*-HppE reaction, is Fe(III)-superoxide (**9**).

Superoxide has been proposed as the reactive oxygen species in the copper-dependent enzymes, dopamine β-monooxygenase (DβM)[58] and peptidylglycine α-amidating monooxygenase (PHM),[59] in the binuclear non-heme iron dependent, *myo*-inositol oxygenase (MIOX),[60] and in the mononuclear non-heme iron-dependent, isopenicillin *N*-synthase (IPNS).[25]   The mechanism of IPNS is displayed in **Figure 5-17**. The IPNS reaction begins with the binding of the substrate, δ-(L-α-aminoadipoyl)-L-cysteinyl-D-valine (ACV, see **41**).[25,61]   The binding of the thiolate group of ACV to the active site iron produces a five-coordinate iron, which leaves the sixth site open for oxygen binding. Dioxygen now binds to the ferrous iron at the available coordination site, where it is reduced by an inner-sphere electron transfer from iron(II) to yield Fe(III)-superoxide (**42**). The reactive species for the first oxidative ring closure, formation of the β-lactam ring, is believed to be this Fe(III)-superoxide (**42**); however, it has not been experimentally verified. The Fe(III)-superoxide (**42**) is believed to abstract a hydrogen atom from the cysteine β-carbon to form the substrate radical and Fe(III)-hydroperoxide (**43**). The substrate is then further oxidized by a second single electron transfer to the iron to form the thioketone and Fe(II)-hydroperoxide (**44**).   The O-O bond of the peroxide is then cleaved heterolytically to generate Fe(IV)-oxo (**45**), which abstracts the unactivated hydrogen atom from the valine β-carbon. Similar in fashion to the oxygen rebound mechanism of cytochrome P450 and the ring-closure reaction proposed for HppE (**Figure 5-2**), the resulting substrate radical attacks the thiolate to close the thiazolidine ring with concurrent homolytic cleavage of the Fe-S bond.
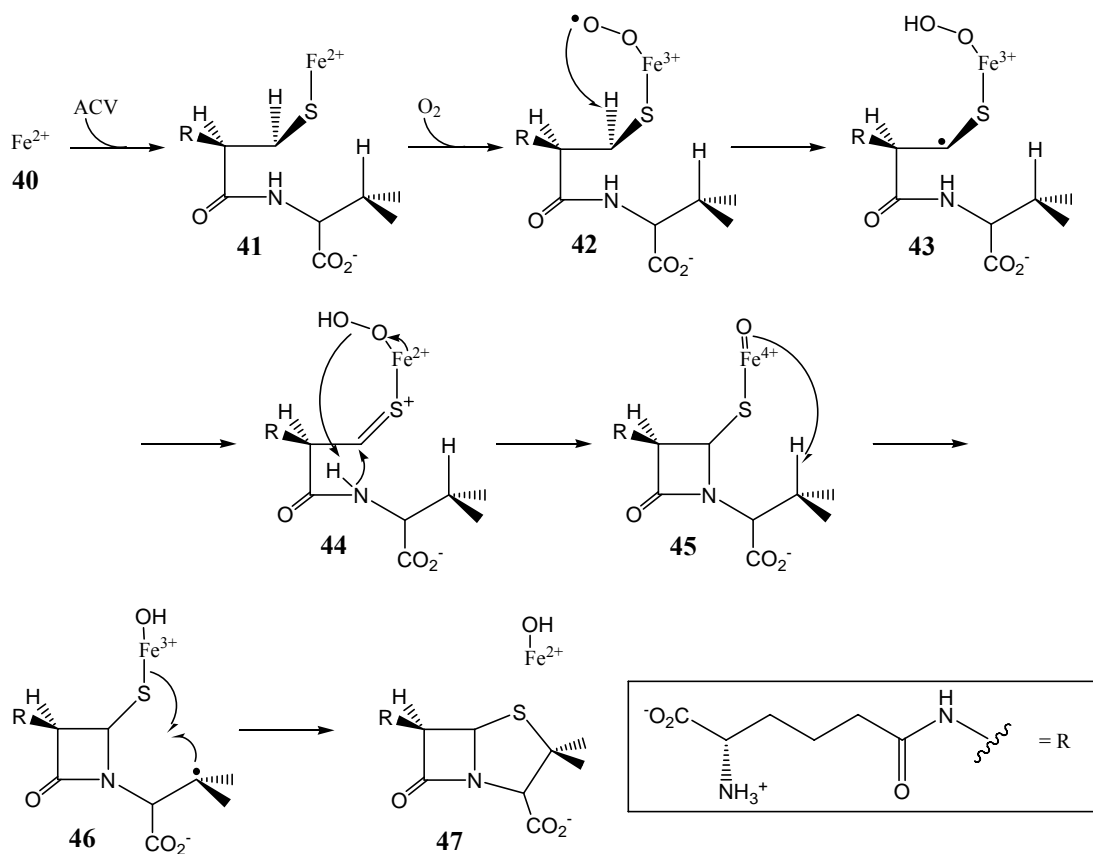
Figure 5-17: Proposed mechanism of isopenicillin *N*-synthase (IPNS).

Fe(III)-superoxide (**42**) has not been experimentally verified as the reactive species for IPNS, as it has for MIOX[60] and DβM.[58] Through the use of semi-empirical density functional theory (DFT) calculations that were guided by variable-temperature, variable-field magnetic circular dichroism (VTVH-MCD) experiments, the labs of Profs. Lipscomb and Solomon were able to determine Fe(III)-superoxide (**42**) to be an energetically accessible reactive species for the IPNS reaction.[26] The formation of an Fe(III)-superoxide species is not typically a favored reaction. In other mononuclear non-heme iron-dependent enzymes, this is overcome by distal oxygen inserting itself into either the substrate, as in extradiol catechol dioxygenases, or co-substrate, as in the α-KG- and pterin-dependent enzymes. They determined that the charge donation from the

thiolate of ACV stabilizes the oxidation Fe(II) to Fe(III), which allows the IPNS-ACV complex to form a now energetically favorable Fe(III)-superoxide complex (**42**).

It is possible that HppE utilizes a similar strategy to stabilize the HppE-Fe(III)-superoxide complex (**9**) from charge donation. From EPR and X-ray crystallography results with Sw-HppE, it is known that (*S*)-HPP (**5**) binds the iron in a bidentate manner (**8**) through the hydroxyl group and a phosphonate oxygen.[41,57] Thus, there could be stabilizing charge donation from the C-2 oxygen, assuming it is deprotonated when bound to iron, and/or from the phosphonate oxygen. It is also possible that the positively charged Lys21 (Lys23 in *Sw*-HppE) stabilizes the negative charge that develops on oxygen in the superoxide complex. Thus HppE could stabilize the Fe(III)-superoxide species (**9**) in a push-pull type manner. This Fe(III)-superoxide stabilizing mechanism will also prevent the formation of a reactive oxygen species that could possibly damage the enzyme if the substrate is not present. Compared to other metaloenzymes where a metal-superoxide is believed to be the reactive species that abstracts a hydrogen atom from the substrate, the BDEs of the abstracted hydrogen atom in those cases are all lower than the BDE of the hydrogen atom that is abstracted in the (*S*)-HPP (**5**) reaction (see **Table 5-8**). The closest in energy is the β-C-H bond in the IPNS reaction, the only other mononuclear non-heme iron enzyme proposed to utilize metal-superoxide as the reactive species. Thus the C-1 hydrogen of (*S*)-HPP (**5**) has the highest thermodynamic energy barrier for a hydrogen atom that is abstracted by a metal-superoxide in an enzyme catalyzed reaction.

Table 5-8: **Summary of BDEs of the different hydrogen atoms abstracted by a metal-superoxide.**

Enzyme	BDE of H-atom abstracted (kcal/mol)
HppE ((*S*)-HPP, **5**)	96.5
HppE ((*R*)-HPP, **38**)	89.0
DβM	85[a]
PHM	87[b]
MIOX	91[c]
IPNS (β-C-H bond)	93[d]

a) Ref. 62; b) Ref. 63; c) Ref. 64; d) Ref. 65.

5.4 CONCLUSION

In this study, the newly isolated *Ps*-HppE was established to be an iron dependent enzyme, which catalyzes the same reactions and requires the same components; iron, FMN, NADH, and O_2; as *Sw*-HppE. As implicated by the EPR results, dioxygen is activated in the reaction with the aid of ferrous iron, to a reactive species in order to abstract a hydrogen atom from the substrate. To complete the oxygen activation cycle, four electrons are consumed. Two of the electrons are supplied by the substrate, and the remaining two are provided by NADH. Due to the fact that reduction of iron requires single electron transfer and NADH is incapable of single electron transfer, FMN is needed to mediate the two single electron transfers from NADH to reduce the active site iron. Since no suitable reductase gene can be found in the *S. wedmorensis* and *P. syringae* fosfomycin biosynthetic gene clusters, a promiscuous reductase may serve the role as electron mediator *in vivo*.

On the basis of sequence comparison with *Sw*-HppE, *Ps*-HppE utilizes two histidines and one glutamate residue as ligands to bind the active site iron. Thus, *Ps*-HppE is a new member of the growing superfamily of non-heme iron-dependent enzymes that contain the 2-His-1-carboxylate facial triad to bind and activate iron. This family of enzymes have proven to be remarkably versatile in the types of reactions they catalyze.[20]

According to Koehntop *et al.*, this superfamily of enzymes can be devided into five classes: extradiol cleaving catechol dioxygenases, Rieske dioxygenases, α-ketoglutarate-dependent enzymes, pterin-dependent enzymes, and "other" oxidases.[66] The fifth family of enzymes is described as a "catch all" for the unique enzymes that can not be included in one of the other four families. The "other" family includes IPNS, 1-aminocyclopropane-1-carboxylic acid oxidase and *Sw*-HppE. From the results reported herein, *Ps*-HppE has been demonstrated to require the same components for activity and catalyze the same unique reaction as *Sw*-HppE. *Ps*-HppE is therefore a second example of a member in the superfamily of enzymes that utilize the 2-His-1-carboxlyate facial triad that catalyzes this unusual epoxidation reaction, and it can be further subdivided as a member of the "other" division in this superfamily.

Based on the comparison of the measured $[^{18}O]$-KIE to the calculated $[^{18}O]$-EIEs, *Ps*-HppE forms Fe(III)-hydroperoxide (**10**) in the rate-limiting step (looking up to and including the first irreversible step). When the $[^{18}O]$-KIE was measured using a deuterated (*S*)-HPP that would produce a 1° $[^2H]$-KIE on hydrogen atom abstraction, the $[^{18}O]$-KIE increased. Since the $[^{18}O]$-KIE only takes into account the steps up to and including the first irreversible step, the hydrogen atom abstraction must occur before or be part of the first irreversible step to have an effect on the $[^{18}O]$-KIE. When the proposed mechanisms for the different possible reactive oxygen species (see **Figure 5-2**) were examined for when hydrogen atom abstraction occurred in relation to the first irreversible step, only in the mechanism with Fe(III)-superoxide (**9**) as the reactive species did hydrogen atom abstraction occur before or in the first irreversible step. Therefore, the reactive oxygen species that abstract the C-1-hydrogen of (*S*)-HPP (**5**), and presumably the C-2 hydrogen of (*R*)-HPP (**38**), in the HppE reaction is Fe(III)-superoxide

(**9**). This is the first experimental evidence of Fe(III)-superoxide as the reactive oxygen species in a mononuclear non-heme iron-dependent enzyme.

The method of C-O bond formation catalyzed by *Sw*-HppE was believed to be unique among Nature; however, with the characterization reported herein of *Ps*-HppE, it is evident that there is another example. In these two reactions, an important factor is believed to be the coordination of the reacting oxygen to the active site iron. There are two α-KG dependent enzymes, hyoscyamine 6β-hydroxylase (H6H)[67] and clavaminic acid synthase (CAS),[68] that catalyze similar C-O bond formations (see **Figure 5-18**); however, for the standard oxygen activation mechanism in α-KG dependent enzymes,[24] there is no available coordination site for the reacting oxygen. It will be interesting to determine if the chemistry utilized by *Sw*-HppE and *Ps*-HppE for C-O bond formation is more widely used, and if it has been adapted for the α-KG dependent enzymes, H6H and CAS.
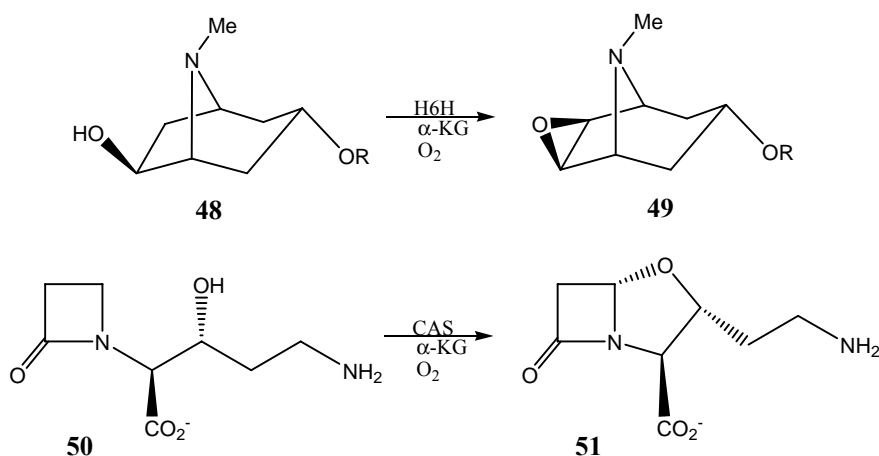
Figure 5-18:   **Reactions catalyzed by the α-KG-dependent H6H and CAS.**

171

5.5 REFERENCES

(1) Itoh, N.; Kusaka, M.; Hirota, T.; Nomura, A. Microbial production of antibiotic fosfomycin by a stereoselective epoxidation and its formation mechanism. *App. Microbio. Biotech.*, **1995**, *43*, 394-401.

(2) Stengel, D.; Gorzer, E.; Schintler, M.; Legat, F. J.; Amann, W.; Pieber, T.; Ekkernkamp, A.; Graninger, W. Second-line treatment of limb-threatening diabetic foot infections with intravenous fosfomycin. *J. Chemother.*, **2005**, *17*, 527-35.

(3) Lobel, B. Short term therapy for uncomplicated urinary tract infection today. Clinical outcome upholds the theories. *Int. J. Antimicrob. Agents*, **2003**, *22 Suppl 2*, 85-7.

(4) Ko, K. S.; Suh, J. Y.; Peck, K. R.; Lee, M. Y.; Oh, W. S.; Kwon, K. T.; Jung, D. S.; Lee, N. Y.; Song, J. H. In vitro activity of fosfomycin against ciprofloxacin-resistant or extended-spectrum beta-lactamase-producing *Escherichia coli* isolated from urine and blood. *Diagn. Microbiol. Infect. Dis.*, **2007**, *58*, 111-5.

(5) Nakazawa, H.; Kikuchi, Y.; Honda, T.; Isago, T.; Nozaki, M. Enhancement of antimicrobial effects of various antibiotics against methicillin-resistant Staphylococcus aureus (MRSA) by combination with fosfomycin. *J. Infect. Chemother.*, **2003**, *9*, 304-9.

(6) Cassone, M.; Campanile, F.; Pantosti, A.; Venditti, M.; Stefani, S. Identification of a variant "Rome clone" of methicillin-resistant *Staphylococcus aureus* with decreased susceptibility to vancomycin, responsible for an outbreak in an intensive care unit. *Microb. Drug. Resist.*, **2004**, *10*, 43-9.

(7) Marquardt, J. L.; Brown, E. D.; Lane, W. S.; Haley, T. M.; Ichikawa, Y.; Wong, C. H.; Walsh, C. T. Kinetics, stoichiometry, and identification of the reactive thiolate in the inactivation of UDP-GlcNAc enolpyruvoyl transferase by the antibiotic fosfomycin. *Biochemistry*, **1994**, *33*, 10646-51.

(8) Brown, E. D.; Vivas, E. I.; Walsh, C. T.; Kolter, R. MurA (MurZ), the enzyme that catalyzes the first committed step in peptidoglycan biosynthesis, is essential in *Escherichia coli*. *J. Bacteriol.*, **1995**, *177*, 4194-7.

(9) Seto, H.; Kuzuyama, T. Bioactive natural products with carbon-phosphorus bonds and their biosynthesis. *Nat. Prod. Rep.*, **1999**, *16*, 589-96.

(10) Hidaka, T.; Iwakura, H.; Imai, S.; Seto, H. Studies on the biosynthesis of fosfomycin. 3. Detection of phosphoenol-pyruvate phosphomutase activity in a fosfomycin high-producing strain of *Streptomyces wedmorensis* and

characterization of its blocked mutant NP-7. *J. Antibiot. (Tokyo)*, **1992**, *45*, 1008-10.

(11)   Jomaa, H.; Wiesner, J.; Sanderbrand, S.; Altincicek, B.; Weidemeyer, C.; Hintz, M.; Turbachova, I.; Eberl, M.; Zeidler, J.; Lichtenthaler, H. K.; Soldati, D.; Beck, E. Inhibitors of the nonmevalonate pathway of isoprenoid biosynthesis as antimalarial drugs. *Science*, **1999**, *285*, 1573-6.

(12)   Hidaka, T.; Mori, M.; Imai, S.; Hara, O.; Nagaoka, K.; Seto, H. Studies on the biosynthesis of bialaphos (SF-1293). 9. Biochemical mechanism of C-P bond formation in bialaphos: discovery of phosphoenolpyruvate phosphomutase which catalyzes the formation of phosphonopyruvate from phosphoenolpyruvate. *J. Antibiot. (Tokyo)*, **1989**, *42*, 491-4.

(13)   Seidel, H. M.; Freeman, S.; Seto, H.; Knowles, J. R. Phosphonate biosynthesis: isolation of the enzyme responsible for the formation of a carbon-phosphorus bond. *Nature*, **1988**, *335*, 457-8.

(14)   Kim, J.; Dunaway-Mariano, D. Phosphoenolpyruvate mutase catalysis of phosphoryl transfer in phosphoenolpyruvate: kinetics and mechanism of phosphorus-carbon bond formation. *Biochemistry*, **1996**, *35*, 4628-35.

(15)   Liu, S.; Lu, Z.; Jia, Y.; Dunaway-Mariano, D.; Herzberg, O. Dissociative phosphoryl transfer in PEP mutase catalysis: structure of the enzyme/sulfopyruvate complex and kinetic properties of mutants. *Biochemistry*, **2002**, *41*, 10270-6.

(16)   Nakashita, H.; Watanabe, K.; Hara, O.; Hidaka, T.; Seto, H. Studies on the biosynthesis of bialaphos. Biochemical mechanism of C-P bond formation: discovery of phosphonopyruvate decarboxylase which catalyzes the formation of phosphonoacetaldehyde from phosphonopyruvate. *J. Antibiot. (Tokyo)*, **1997**, *50*, 212-9.

(17)   Woodyer, R. D.; Li, G.; Zhao, H.; van der Donk, W. A. New insight into the mechanism of methyl transfer during the biosynthesis of fosfomycin. *Chem. Commun. (Camb)*, **2007**, 359-61.

(18)   Liu, P.; Murakami, K.; Seki, T.; He, X.; Yeung, S. M.; Kuzuyama, T.; Seto, H.; Liu, H. Protein purification and function assignment of the epoxidase catalyzing the formation of fosfomycin. *J. Am. Chem. Soc.*, **2001**, *123*, 4619-20.

(19)   Liu, P.; Liu, A.; Yan, F.; Wolfe, M. D.; Lipscomb, J. D.; Liu, H. W. Biochemical and spectroscopic studies on (S)-2-hydroxypropylphosphonic acid epoxidase: a novel mononuclear non-heme iron enzyme. *Biochemistry*, **2003**, *42*, 11577-86.

(20)   Sono, M.; Roach, M. P.; Coulter, E. D.; Dawson, J. H. Heme-Containing Oxygenases. *Chem. Rev.*, **1996**, *96*, 2841-2888.

(21)   Ortiz de Montellano, P. R. *Cytochrome P450: Structure, Mechanism, and Biochemistry*; 2 ed.; Plenum: New York, 1995.

(22)   Lange, S. J.; Que, L., Jr. Oxygen activating nonheme iron enzymes. *Curr. Opin. Chem. Biol.*, **1998**, *2*, 159-72.

(23)   Solomon, E. I.; Brunold, T. C.; Davis, M. I.; Kemsley, J. N.; Lee, S. K.; Lehnert, N.; Neese, F.; Skulan, A. J.; Yang, Y. S.; Zhou, J. Geometric and electronic structure/function correlations in non-heme iron enzymes. *Chem. Rev.*, **2000**, *100*, 235-350.

(24)   Costas, M.; Mehn, M. P.; Jensen, M. P.; Que, L., Jr. Dioxygen activation at mononuclear nonheme iron active sites: enzymes, models, and intermediates. *Chem. Rev.*, **2004**, *104*, 939-86.

(25)   Baldwin, J. E.; Bradley, M. Isopenicillin N synthase: mechanistic studies. *Chem. Rev.*, **1990**, *90*, 1079-1088.

(26)   Brown, C. D.; Neidig, M. L.; Neibergall, M. B.; Lipscomb, J. D.; Solomon, E. I. VTVH-MCD and DFT studies of thiolate bonding to [FeNO]7/[FeO2]8 complexes of isopenicillin N synthase: substrate determination of oxidase versus oxygenase activity in nonheme Fe enzymes. *J. Am. Chem. Soc.*, **2007**, *129*, 7427-38.

(27)   Price, J. C.; Barr, E. W.; Tirupati, B.; Bollinger, J. M., Jr.; Krebs, C. The first direct characterization of a high-valent iron intermediate in the reaction of an alpha-ketoglutarate-dependent dioxygenase: a high-spin FeIV complex in taurine/alpha-ketoglutarate dioxygenase (TauD) from *Escherichia coli*. *Biochemistry*, **2003**, *42*, 7497-508.

(28)   Eser, B. E.; Barr, E. W.; Frantom, P. A.; Saleh, L.; Bollinger, J. M., Jr.; Krebs, C.; Fitzpatrick, P. F. Direct Spectroscopic Evidence for a High-Spin Fe(IV) Intermediate in Tyrosine Hydroxylase. *J. Am. Chem. Soc.*, **2007**, *129*, 11334-5.

(29)   Kuzuyama, T.; Seki, T.; Kobayashi, S.; Hidaka, T.; Seto, H. Cloning and expression in Escherichia coli of 2-hydroxypropylphosphonic acid epoxidase from the fosfomycin-producing organism, *Pseudomonas syringae* PB-5123. *Biosci. Biotechnol. Biochem.*, **1999**, *63*, 2222-2224.

(30)   Roth, J. P.; Klinman, J. P. In *Isotope Effects in Chemistry and Biology*; Kohen, A., Limbach, H.-H., Eds.; CRC Press LLC: Boca Raton, FL, 2006.

(31)   Tian, G. K., Judith P. Discrimination between 16O and 18O in oxygen binding to
         the reversible oxygen carriers hemoglobin, myoglobin, hemerythrin, and
         hemocyanin: a new probe for oxygen binding and reductive activation by
         proteins. *J. Am. Chem. Soc.*, **1993**, *115*, 8891-7.

(32)   Roth, J. P. Advances in studying bioinorganic reaction mechanisms: isotopic
         probes of activated oxygen intermediates in metalloenzymes. *Curr. Opin. Chem.
         Biol.*, **2007**, *11*, 142-50.

(33)   Lanci, M. P.; Brinkley, D. W.; Stone, K. L.; Smirnov, V. V.; Roth, J. P. Structures
         of transition states in metal-mediated O2-activation reactions. *Angew. Chem. Int.
         Ed.*, **2005**, *44*, 7273-6.

(34)   Bradford, M. M. A rapid and sensitive method for the quantitation of microgram
         quantities of protein utilizing the principle of protein-dye binding. *Anal.
         Biochem.*, **1976**, *72*, 248-54.

(35)   Hammerschmidt, F. Labelled representatives of a possible intermediate of
         fosfomycin biosynthesis in Streptomyces fradiae: preparation of (R,S)-(2-
         hydroxypropyl)-,(R,S)-, (R)- and (S)-(2-hydroxy-[1,1-2H2]propyl)- and (R,S)-(2-
         [18O]hydroxypropyl)phosphonic acid. *Monatshefte fuer Chemie*, **1991**, *122*, 389-
         98.

(36)   Sambrook, J.; Fritsch, E. F.; Maniatis, T. *Molecular Cloning: A Laboratory
         Manual*; Cold Spring Harbor Laboratory Press: Cold Spring Harbor, NY, 1989.

(37)   Andrews, P. Estimation of the molecular weights of proteins by Sephadex gel-
         filtration. *Biochem. J.*, **1964**, *91*, 222-33.

(38)   Paz, M. A.; Fluckiger, R.; Boak, A.; Kagan, H. M.; Gallop, P. M. Specific
         detection of quinoproteins by redox-cycling staining. *J. Biol. Chem.*, **1991**, *266*,
         689-92.

(39)   Liu, P.; Mehn, M. P.; Yan, F.; Zhao, Z.; Que, L., Jr.; Liu, H. W. Oxygenase
         activity in the self-hydroxylation of (s)-2-hydroxypropylphosphonic acid
         epoxidase involved in fosfomycin biosynthesis. *J. Am. Chem. Soc.*, **2004**, *126*,
         10306-12.

(40)   Frisch, M. J.; Trucks, G. W.; Schlegel, H. B.; Scuseria, G. E.; Robb, M. A.;
         Cheeseman, J. R.; Zakrzewski, V. G.; Montgomery, J. A., Jr.; Stratmann, R. E.;
         Burant, J. C.; Dapprich, S.; Millam, J. M.; Daniels, A. D.; Kudin, K. N.; Strain,
         M. C.; Farkas, O.; Tomasi, J.; Barone, V.; Cossi, M.; Cammi, R.; Mennucci, B.;
         Pomelli, C.; Adamo, C.; Clifford, S.; Ochterski, J.; Petersson, G. A.; Ayala, P. Y.;
         Cui, Q.; Morokuma, K.; Malick, D. K.; Rabuck, A. D.; Raghavachari, K.;
         Foresman, J. B.; Cioslowski, J.; Ortiz, J. V.; Baboul, A. G.; Stefanov, B. B.; Liu,

175

G.; Liashenko, A.; Piskorz, P.; Komaromi, I.; Gomperts, R.; Martin, R. L.; Fox, D. J.; Keith, T.; Al-Laham, M. A.; Peng, C. Y.; Nanayakkara, A.; Gonzalez, C.; Challacombe, M.; Gill, P. M. W.; Johnson, B.; Chen, W.; Wong, M. W.; Andres, J. L.; Head-Gordon, M.; Replogle, E. S.; Pople, J. A.; A.9 ed. ed.; Gaussian, Inc: Pittsburgh, PA, 1998.

(41)   Higgins, L. J.; Yan, F.; Liu, P.; Liu, H. W.; Drennan, C. L. Structural insight into antibiotic fosfomycin biosynthesis by a mononuclear iron enzyme. *Nature*, **2005**, *437*, 838-44.

(42)   Andersson, M. P.; Uvdal, P. New scale factors for harmonic vibrational frequencies using the B3LYP density functional method with the triple-zeta basis set 6-311+G(d,p). *J. Phys. Chem. A*, **2005**, *109*, 2937-41.

(43)   Neese, F.; Zumft, W. G.; Antholine, W. E.; Kroneck, P. M. H. The Purple Mixed-Valence CuA Center in Nitrous-oxide Reductase: EPR of the Copper-63-, Copper-65-, and Both Copper-65- and [15N]Histidine-Enriched Enzyme and a Molecular Orbital Interpretation. *J. Am. Chem. Soc.*, **1996**, *118*, 8692 -8699.

(44)   Tian, G.; Berry, J. A.; Klinman, J. P. Oxygen-18 kinetic isotope effects in the dopamine beta-monooxygenase reaction: evidence for a new chemical mechanism in non-heme metallomonooxygenases. *Biochemistry*, **1994**, *33*, 226-34.

(45)   Bigeleisen, J.; Mayer, M. G. Calculation of equilibrium constants for isotopic exchange reactions. *J. Chem. Phys.*, **1947**, *15*, 261-267.

(46)   Smirnov, V. V.; Brinkley, D. W.; Lanci, M. P.; Karlin, K. D.; Roth, J. P. Probing metal-mediated O2 activation in chemical and biological systems. *J. Mol. Catal. A: Chem.*, **2006**, *251*, 100-107.

(47)   Lehnert, N.; Ho, R. Y.; Que, L., Jr.; Solomon, E. I. Electronic structure of high-spin iron(III)-alkylperoxo complexes and its relation to low-spin analogues: reaction coordinate of O-O bond homolysis. *J. Am. Chem. Soc.*, **2001**, *123*, 12802-16.

(48)   Lehnert, N.; Fujisawa, K.; Solomon, E. I. Electronic structure and reactivity of high-spin iron--alkyl- and--pterinperoxo complexes. *Inorg. Chem.*, **2003**, *42*, 469-81.

(49)   Proshlyakov, D. A.; Henshaw, T. F.; Monterosso, G. R.; Ryle, M. J.; Hausinger, R. P. Direct detection of oxygen intermediates in the non-heme Fe enzyme taurine/alpha-ketoglutarate dioxygenase. *J. Am. Chem. Soc.*, **2004**, *126*, 1022-3.

(50) Das, T. K.; Couture, M.; Ouellet, Y.; Guertin, M.; Rousseau, D. L. Simultaneous observation of the O---O and Fe---O2 stretching modes in oxyhemoglobins. *Proc. Natl. Acad. Sci. U S A*, **2001**, *98*, 479-84.

(51) Yan, F.; Li, T.; Lipscomb, J. D.; Liu, A.; Liu, H. W. Site-directed mutagenesis and spectroscopic studies of the iron-binding site of (S)-2-hydroxypropylphosphonic acid epoxidase. *Arch. Biochem. Biophys.*, **2005**, *442*, 82-91.

(52) McLuskey, K.; Cameron, S.; Hammerschmidt, F.; Hunter, W. N. Structure and reactivity of hydroxypropylphosphonic acid epoxidase in fosfomycin biosynthesis by a cation- and flavin-dependent mechanism. *Proc. Natl. Acad. Sci.*, **2005**, *102*, 14221-6.

(53) Yan, F.; Munos, J. W.; Liu, P.; Liu, H. W. Biosynthesis of fosfomycin, re-examination and re-confirmation of a unique Fe(II)- and NAD(P)H-dependent epoxidation reaction. *Biochemistry*, **2006**, *45*, 11473-81.

(54) Zhao, Z.; Liu, P.; Murakami, K.; Kuzuyama, T.; Seto, H.; Liu, H. W. Mechanistic studies of HPP epoxidase: configuration of the substrate governs its enzymatic fate. *Angew. Chem. Int. Ed.*, **2002**, *41*, 4529-32.

(55) Woschek, A.; Wuggenig, F.; Peti, W.; Hammerschmidt, F. On the transformation of (S)-2-hydroxypropylphosphonic acid into fosfomycin in Streptomyces fradiae--a unique method of epoxide ring formation. *Chembiochem*, **2002**, *3*, 829-35.

(56) Nagel, Z. D.; Klinman, J. P. Tunneling and dynamics in enzymatic hydride transfer. *Chem. Rev.*, **2006**, *106*, 3095-118.

(57) Yan, F.; Moon, S. J.; Liu, P.; Zhao, Z.; Lipscomb, J. D.; Liu, A.; Liu, H. W. Determination of the substrate binding mode to the active site iron of (S)-2-hydroxypropylphosphonic acid epoxidase using 17O-enriched substrates and substrate analogues. *Biochemistry*, **2007**, *46*, 12628-38.

(58) Evans, J. P.; Ahn, K.; Klinman, J. P. Evidence that dioxygen and substrate activation are tightly coupled in dopamine beta-monooxygenase. Implications for the reactive oxygen species. *J. Biol. Chem.*, **2003**, *278*, 49691-8.

(59) Chen, P.; Solomon, E. I. Oxygen activation by the noncoupled binuclear copper site in peptidylglycine alpha-hydroxylating monooxygenase. Reaction mechanism and role of the noncoupled nature of the active site. *J. Am. Chem. Soc.*, **2004**, *126*, 4991-5000.

(60) Xing, G.; Diao, Y.; Hoffart, L. M.; Barr, E. W.; Prabhu, K. S.; Arner, R. J.; Reddy, C. C.; Krebs, C.; Bollinger, J. M., Jr. Evidence for C-H cleavage by an

iron-superoxide complex in the glycol cleavage reaction catalyzed by myo-inositol oxygenase. *Proc. Natl. Acad. Sci.*, **2006**, *103*, 6130-5.

(61)   Baldwin, J. E.; Adlington, R. M.; Moroney, S. E.; Field, L. D.; Ting, H. H. Stepwise ring closure in penicillin biosynthesis. Initial β-lactam formation. *J. Chem. Soc., Chem. Commun.*, **1984**, *15*, 984-986.

(62)   Weast, R. C. *CRC Handbook of Chemistry and Physics*; 51 ed.; The Chemical Rubber Company: Cleveland, OH, 1970.

(63)   Armstrong, D. A.; Yu, D.; Rauk, A. Oxidative damage to the glycyl a-carbon site in proteins: an ab initio study of the C-H bond dissociation energy and the reduction potential of the C-centered radical. *Can. J. Chem.*, **1996**, *74*, 1192-1199.

(64)   Stubbe, J.; van Der Donk, W. A. Protein Radicals in Enzyme Catalysis. *Chem. Rev.*, **1998**, *98*, 705-762.

(65)   Rauk, A.; Yu, D.; Armstrong, D. A. Oxidative Damage to and by Cysteine in Proteins: An ab Initio Study of the Radical Structures, C-H, S-H, and C-C Bond Dissociation Energies, and Transition Structures for H Abstraction by Thiyl Radicals. *J. Am. Chem. Soc.*, **1998**, *120*, 8848-8855.

(66)   Koehntop, K. D.; Emerson, J. P.; Que, L., Jr. The 2-His-1-carboxylate facial triad: a versatile platform for dioxygen activation by mononuclear non-heme iron(II) enzymes. *J. Biol. Inorg. Chem.*, **2005**, *10*, 87-93.

(67)   Hashimoto, T.; Matsuda, J.; Yamada, Y. Two-step epoxidation of hyoscyamine to scopolamine is catalyzed by bifunctional hyoscyamine 6 beta-hydroxylase. *FEBS Lett.*, **1993**, *329*, 35-9.

(68)   Busby, R. W.; Townsend, C. A. A single monomeric iron center in clavaminate synthase catalyzes three nonsuccessive oxidative transformations. *Bioorg. Med. Chem.*, **1996**, *4*, 1059-64.

Vita

Jeffrey (Jeff) W. Munos was born in Houston, TX on March 8, 1979 to Ronald and Martha Munos and is the brother of Stephanie Gleitz. Jeff's education began at Post Elementary School, and after wards he attended Dean Middle School and Cook Junior High School. For high school, Jeff attended Jersey Village High School and graduated in 1997. Jeff was always interested in science. When he was a child, he thoroughly enjoyed watching Mr. Wizard on television. Jeff was fortunate that his high school teachers for advanced biology and chemistry gave him a strong background which enabled him to excel in college, and their depiction of what real science is like, inspired him to go further in science. For college, Jeff wanted to go to a small, more intimate school than the major state universities, so he attended Hendrix College, a small liberal arts school in Conway, AR.

Jeff was interested in chemistry and biology, basically biochemistry. However, due to the small size of Hendrix College, there was no Biochemistry program, so he had to major in either Chemistry or Biology. Jeff chose Biology, but by the end of his freshman year, he had switched to Chemistry. Jeff still took a few biology classes but only ones with a molecular angle. When it came to his chemistry classes, he loved all of them. In Physical Chemistry, he found quantum mechanics, kinetics and the energetics of chemical reactions to be fascinating. Then in Inorganic Chemistry, he was able to apply what he had learned in Physical Chemistry to subjects like ligand field theory. The two classes that he enjoyed the most were Organic Chemistry and Biochemistry. He enjoyed thinking about all the different types of reactions and their proposed mechanisms in Organic Chemistry. He especially thought it was interesting of how the course of the reaction could be altered based on which transition state and/or intermediate was stabilized under the chosen conditions. In Biochemistry, Jeff enjoyed learning about the molecular details of the biology he already knew; however, what interested him the most was the study of enzyme mechanisms. It was the application of everything he found

interesting in Organic Chemistry to a biological subject he had always known of but never truly studied. As Jeff later began to understand enzymes superior catalytic ability and cleanness of regio- and stereospecificity, he was sold. Jeff graduated with distinction from Hendrix College in 2001 with a B.A. in Chemistry and a minor in Biology.

For his senior thesis paper, Jeff chose to write about catalytic antibodies. While writing the paper, he thought the principle behind them and their potential was very exciting. However, upon visiting the University of Texas for a graduate school recruiting trip and talking to Prof. Brent Iverson, he became aware of their apparent limitations in catalysis, and was informed of the more powerful directed evolution approach for enzyme engineering.

After this visitation, Jeff decided to attend the University of Texas for graduate school where he pursued a Ph.D. in Biochemistry.   After completing his rotations and much thought, he decided to join Prof. Hung-wen (Ben) Liu's lab. In Prof. Liu's lab, Jeff could learn directed evolution by working on a project involving the enzyme poly(ADP-ribose) polymerase (PARP), but he would also be surrounded by other lab members working on more chemical and chemical biology research projects. As Jeff began to research directed evolution, he became less interested in it. He realized the chemical knowledge that went into catalytic antibodies was absent in directed evolution research. Around this same time, Jeff needed to chose a project to develop into an original research proposal for his doctoral canidacy exam. For his proposal, he chose to investigate the chemical mechanism of a new dehalogenase, with a little directed evolution thrown in as well. After, completing and passing canidacy, Jeff realized that directed evolution did not satisfy his chemical interest that developed in college, so he decided to switch his research focus to the study of enzyme mechanisms, which he thoroughly enjoyed. The two enzyme mechanisms Jeff focused on while in Prof. Liu's lab were 1-deoxy-D-xylulose 5-phosphate reductoisomerase (DXR) and (*S*)-2-hydroxypropylphosphonic acid epoxidase (HppE). While working in Prof. Liu's lab, Jeff realized another interest of his, enzyme catalysis. Jeff will pursue this second interest of his for his postdoctoral research fellowship in the lab of Prof. Judith P. Klinman at the University of California at

Berkeley, where he would look at the role enzyme dynamics plays in facilitating hydrogen tunneling.

At the time this dissertation was written, Jeff has been a contributing author on five scientific publications, with several other papers in preparation. Jeff has also been the recipient of several awards including the Lewis Award, Continuing Bruton Fellowship, Houston Chemical Association Scholarship, Eakin Summer Fellowship, Welch Fellowship Award, College of Natural Sciences Dean's Excellence Award, and the John E. Stuckey Award for Outstanding Freshman Chemist. In his first two years of graduate school Jeff was a teacher's assistant for General and Organic Chemistry Laboratory (CH 113P), Elementary Organic and Biochemistry Laboratory (CH 114P), Introduction to Chemical Practice (CH 204), and Biochemistry Laboratory (CH 369L).

Permanent address: 914 East Village Ln.

Austin, TX 78758

This dissertation was typed by Jeffrey W. Munos.